

Springer Geochemistry

Vojtěch Janoušek
Jean-François Moyen
Hervé Martin
Vojtěch Erban
Colin Farrow

Geochemical Modelling of Igneous Processes – Principles And Recipes in R Language

Bringing the Power of R
to a Geochemical Community

 Springer

Springer Geochemistry

More information about this series at <http://www.springer.com/series/13486>

Vojtěch Janoušek · Jean-François Moyen
Hervé Martin · Vojtěch Erban
Colin Farrow

Geochemical Modelling of Igneous Processes – Principles And Recipes in R Language

Bringing the Power of R to a Geochemical
Community

 Springer

Vojtěch Janoušek
Czech Geological Survey
Prague
Czech Republic

Vojtěch Erban
Czech Geological Survey
Prague
Czech Republic

Jean-François Moyen
Université Jean-Monnet
Saint-Etienne
France

Colin Farrow
Glasgow
Scotland

Hervé Martin
Université Blaise-Pascal
Clermont-Ferrand
France

Springer Geochemistry
ISBN 978-3-662-46791-6 ISBN 978-3-662-46792-3 (eBook)
DOI 10.1007/978-3-662-46792-3

Library of Congress Control Number: 2015937379

Springer Heidelberg New York Dordrecht London
© Springer-Verlag Berlin Heidelberg 2016

This work is subject to copyright. All rights are reserved by the Publisher, whether the whole or part of the material is concerned, specifically the rights of translation, reprinting, reuse of illustrations, recitation, broadcasting, reproduction on microfilms or in any other physical way, and transmission or information storage and retrieval, electronic adaptation, computer software, or by similar or dissimilar methodology now known or hereafter developed.

The use of general descriptive names, registered names, trademarks, service marks, etc. in this publication does not imply, even in the absence of a specific statement, that such names are exempt from the relevant protective laws and regulations and therefore free for general use.

The publisher, the authors and the editors are safe to assume that the advice and information in this book are believed to be true and accurate at the date of publication. Neither the publisher nor the authors or the editors give a warranty, express or implied, with respect to the material contained herein or for any errors or omissions that may have been made.

Printed on acid-free paper

Springer-Verlag GmbH Berlin Heidelberg is part of Springer Science+Business Media
(www.springer.com)

Preface

*Because I have known the torment of thirst,
I would build a well where others may drink.*

—Ernest Thompson Seton

The goal of generations of igneous geochemists is to use mineralogical and chemical laws in an attempt to explain the geological processes they are investigating. This scientific approach is both simple and rigorous. Initially it consists of highlighting magmatic differentiation trends and determining the possible underlying petrogenetic mechanism(s). Then, the major elements are used to establish the nature and the modal composition of the fractionating mineral assemblage responsible for the differentiation trends; its temporal evolution is also addressed. Finally all these data are fed into models calculating the behaviour of trace elements (and possibly isotopes), in order to account for the chemistry of the investigated igneous rocks and evolution of the parental magma.

Such methodology is very powerful; not only because it is consistent with field geological data but also it is based on several independent methods. Indeed, major elements, trace elements and isotopes are governed by different principles. Thus any model predicting the coherent behaviour of these three independent parts of the dataset would possess a high internal consistency, making the modelled scenario robust.

Everyone, needing to interpret whole-rock geochemical data from igneous rocks, faces the same problem. Regardless of whether he/she has to calculate some simple indexes, more complex norms, plot a diagram for a paper or model effects of some petrogenetic process, he will end up using a computer. He would be certainly delighted to find that several programs exist designed specifically for this purpose. At first glance, most look useful with a plethora of built-in functions, but after a second look, he realizes that they are essentially black boxes, in which he soon loses track of exactly what is happening with his precious data. Worse still, there could be something missing or not quite appropriate to the required task. The code is difficult or impossible to alter (many geochemical programs are commercial). And even when the required diagram is plotted correctly, it may need to be altered extensively before reaching publication quality.

Indeed, graphical and numerical methods remain the alpha and omega of modern igneous geochemistry. The problem is how to implement the necessary diagrams or formulae so that the code can be understood and used by an ordinary

geochemist. We strongly believe that this knowledge can be mediated in the form of simple numerical recipes in a high-level programming language that includes built-in mathematical and statistical functionality, matrix manipulation tools and be capable of generating publication-quality graphics. There are currently available several potentially suitable environments, but only one of them—the R language (www.r-project.org)—has the advantage of being freely available for all the main platforms (MS Windows, Mac OS and various dialects of Linux). Moreover, there already exists an R package *GCDkit* (www.gcdkit.org)¹, containing most of the required geochemical calculation procedures and graphics. Furthermore, the underlying code can be easily viewed, modified or extended.

In the realm of geochemical modelling, there does not exist any prescribed scenario. In fact, the modelling strategy not only depends on the geological problem, but also on the nature of the available data: hence the approach must be adapted and optimized to each individual case. The purpose of this book is to show, using many concrete examples, how a researcher can proceed in developing a realistic model tailored to his questions. It is in this investigative adventure that the authors of this book invite you. Let's embark on a scientific journey in the intimacy of petrogenetic modelling!

Book structure—how to read?

This textbook gives a detailed overview of modelling approaches to petrogenesis of igneous rocks using whole-rock geochemical data. The theoretical chapters are followed by their implementation using R/*GCDkit*, and by numerous exercises, mostly based on real-life problems.

The text is divided into six parts, and three appendices. **Part I** gives a short but comprehensive introduction to R (with, or without *GCDkit*), the implementation of simple geochemical computations, calculation of norms, statistical evaluation of complex data sets, and plotting the most common diagrams. In all cases, the geological and geochemical backgrounds are briefly discussed. Moreover, a refresher on radiogenic isotope data interpretation is presented. For newbies, the fundamentals and syntax of the R language are explained in **Appendix A**, and an introduction to the *GCDkit* system is given in **Appendix B**.

The core of the book (**parts II–IV**) is dedicated to modelling of the main processes in igneous petrogenesis using various types of geochemical data. These include major elements (treated by the concept of mass balance), trace elements (modelling based on solid/liquid partitioning or saturation concepts) and radiogenic isotopic data (either constraining open-system processes such as mixing and assimilation or giving direct information on the source). The principles of forward and reverse numerical techniques are presented and explained, as is the underlying mathematical apparatus; the R code necessary for their implementation is also given. The specific problem of solving sets of linear algebraic equations is outlined in **Appendix C**.

¹ Natively for Windows, but can be run on other platforms with a suitable emulator environment.

Part V provides a practical guide on how to formulate and run a sensible petrogenetic model simulating natural systems. It stresses the fundamental significance of additional information coming, e.g., from field relations, petrology or physics. Above all, the importance of critical thinking is underlined.

The text is supplemented by numerous solved **exercises**. It is crowned by two worked **real-world problems (Part VI)** that illustrate the complex approach to petrogenetic modelling based on the techniques described in this book.

On the other hand, intentionally omitted are most of the more sophisticated statistical methods as these have been dealt with by other, more competent authors. This is also the case for detailed mathematical derivations of laws governing geochemical variations in complex petrogenetic scenarios.

The book is intended for senior undergraduate and postgraduate courses, as well as all potential users of *R/GCDkit* interested in the implementation of graphical, statistical and numerical methods. The prerequisite is a sound knowledge of secondary school maths as well as of basic principles of solid-rock geochemistry.

Electronic supplementary material

Errata, code to the exercises and data sets from this book are available on: <http://book.gcdkit.org>. Moreover, this web site also contains the scripts used to produce many of the figures. However, in the latter case the code is not always simple and easy to comprehend by a beginner. It is supplied purely for the sake of curiosity, and in order to stimulate the interested reader. They are unlikely to work without at least some adaptations. If reading an electronic version of this book, the exercises, dataset icons and relevant figures are clickable.



Most of the exercises in this book are designed to run in an interactive mode. To adopt them for batch use, the contents of any variable should be displayed using the functions `print` or `cat` (see Appendix A, Sect. 3.1).

The code supplied, obviously, will run only if the current R directory is that in which the data file(s) reside. The best is probably to save all the needed files in a directory of your choice and, before starting, set the working directory either from the GUI (*File|Change dir...*), or with a command such as:

```
GCDkit->Rbook.dir<-"C:/user/my_name/Documents/Rbook"2
GCDkit->setwd(Rbook.dir)
```



This text is based on version 2.13 of R for Windows, 4.0 of *GCDkit*. It concentrates on MS Windows implementation of the R language. Plain R will run on other systems, including Linux and Mac OS, but the current *GCDkit* will require a suitable emulation environment, e.g. Wine on Linux. The code, relying on *GCDkit* functions, will be displayed with the namesake prompt, `GCDkit->`.

² Backslash is an escape character in R, so it would need to be preceded by another one, i.e.:

```
"C:\\user\\my_name\\Documents\\Rbook".
```

Acknowledgements

We would like to thank several people without whom this book would have hardly originated. First of all Robert Gentleman and Ross Ihaka, as well as members of the R Development Core Group, for their ideas and sterling efforts in developing the R language. In particular, Friedrich Leisch (Technische Universität, Vienna) provided valuable consultations on the development of R packages.

This book builds on hand-outs used for workshops given in Prague and Helsinki (2011), Stellenbosch, South Africa (2012) and Hyderabad, India (2013) by VJ and JFM. The authors are indebted to many people without whom these events would not materialize, especially Tapani Ramö (Helsinki), Gary Stevens (Stellenbosch) and Santosh Kumar (Nainital, India). VJ is grateful to Graeme Rogers, once supervisor of his PhD. thesis, who has taught him to ask the basic petrogenetic questions, *why and how much*, Francis Albarède for his excellent book and a motivating course of geochemical modelling and Milan Novák (Brno, Czech Republic) with František V. Holub (Prague), who requested, in 2000, a practical course on interpretation of geochemical data in R that is running ever since.

GCDkit originated during a post-doctoral stay of VJ at University of Salzburg (FWF Project 15133–GEO to F. Finger). The work was, over the years, supported by several projects from the Czech Grant Agency (GAČR), Czech Geological Survey (3314, 336200) and Ministry of Education of the Czech Republic (LK11202 to K. Schulmann). The scientific exchanges were facilitated by the French–Czech programme Mobility 7AMB13FR026.

Régis Doucelance (Clermont-Ferrand, France) brought to our attention a great reverse mixing hyperbola example from Martinique, and other papers on mantle geochemistry that escaped our attention. Nice photos were contributed by Gerhard Wörner (Göttingen, Germany), Christian Nicollet (Clermont-Ferrand), Ewa Słaby (Warsaw, Poland) and S. Hidalgo (Quito, Ecuador). Didier Laporte (Clermont-Ferrand) supplied an original version of his figure on wetting angles (Fig. 24.1). Leon Bagas (Crawley, Australia) provided dataset for the anomaly plot.

Oscar Laurent (Liège, Belgium) and Arnaud Villaros (Orléans, France)—in addition to always being pleasant company—are responsible for many good ideas and suggestions, which eventually helped to develop the existing code. We are also grateful to the many students and *GCDkit* users, whose requests, in the course of time, led to more software development, clever ideas and debugging.

We are thankful to people from Springer, Annett Buettner, Ulrike Stricker and Chris Bendall, for their hard work and patience with which they have guided us through the dire straits of preparing and publishing this monograph. The Czech brewing industry was a source of inspiration during late-night coding sessions.

In Prague, St. Etienne, Clermont-Ferrand and Glasgow, Christmas 2014

Vojtěch Janoušek (vojtech.janousek@geology.cz)
 Jean-Francois Moyen (jean.francois.moyen@univ-st-etienne.fr)
 Hervé Martin (h.martin@opgc.univ-bpclermont.fr)
 Vojtěch Erban (vojtech.erban@geology.cz)
 Colin Farrow (colinfarrow537@gmail.com)

Typographic Conventions

Most important are the warning boxes indicating potential pitfalls:



'Warning'

Pointers and additional information opening new prospects (not dealt with in this text) are labelled as:



'Next step'

The *GCDkit* implementation of the given problem is outlined in:





'GCDkit box'

The text is supplemented by a large number of solved exercises, graphically introduced like this:



Exercise 1.2: Fractional crystallization

An associated data file is marked by , and the beginning of a solution to the exercise by .

In the main text, **R code and its output** are set in a non-proportional font, the latter additionally in italics. Plain R code has a simple prompt, the *GCDkit*-specific one is marked as such:

```
> summary(x[, "Sr"])
  Min. 1st Qu.  Median    Mean 3rd Qu.    Max.   NA's
 278.0  392.5   430.0   443.0   537.5   599.0    2.0
```

```
GCDkit-> loadData("sazava.data")
GCDkit-> results <- CIPW(WR)
```

Broken, continuing lines of code have a plus sign as a prompt and are indented:

```
GCDkit-> plot(WR[, "SiO2"),
+           pch="*", col="khaki")
```

In Part VI and Appendix A, commented chunks of R code, often just outlined and not complete, are displayed as “code boxes”:

We create Harker plots (Fig. 25.3) using *Plot|Multiple plots...*, i.e. the command:

```
GCDkit-> multiple("SiO2", "Al2O3, Fe2O3, MgO, CaO, Na2O, K2O")
```

Names for R objects and file names, occurring in the text, are also set in a non-proportional font:

... factor `silica` from the previous exercise ...

Comments in the code start with the hash mark (“#”):

```
# Fig. 4.2.1
```

Names of mathematical variables and **Menu items** are type set in italics, e.g. *Misc|Stop current computation*, indicating an item ‘*Stop current computation*’ of the ‘*Misc*’ menu.

Equations in the text are numbered sequentially, starting with the chapter number:

$$C_L = \frac{C_0}{D + F(1 - D)} \quad (5.1)$$

The same applies to figures, tables, or exercises. Otherwise, the first number of figures or tables is that of the relevant Appendix; the second refers to a sequence there in (Fig. A1.2; Table A3.5).

Matrices are named with a bold italics letter topped by a double bar. When presented in full, they are enclosed in brackets:

$$\overline{\overline{\mathbf{C}}} = \begin{pmatrix} C_{Pl}^{SiO_2} & C_{Opx}^{SiO_2} & \dots & C_n^{SiO_2} \\ C_{Pl}^{TiO_2} & C_{Opx}^{TiO_2} & \dots & C_n^{TiO_2} \\ \vdots & \vdots & \ddots & \vdots \\ C_{Pl}^{P_2O_5} & C_{Opx}^{P_2O_5} & \dots & C_n^{P_2O_5} \end{pmatrix}$$

Vectors are written in a similar way, but their symbol has a single arrow:

$$\overrightarrow{\mathbf{m}} = \begin{pmatrix} m_{Pl} \\ m_{Opx} \\ \vdots \\ m_n \end{pmatrix}$$

Equation systems are linked together by a single curly brace to their left:

$$\left\{ \begin{array}{l} C_S^{SiO_2} = \sum_{i=1}^n (m_i C_i^{SiO_2}) \\ C_S^{TiO_2} = \sum_{i=1}^n (m_i C_i^{TiO_2}) \\ \dots \\ C_S^{P_2O_5} = \sum_{i=1}^n (m_i C_i^{P_2O_5}) \end{array} \right.$$

Variables and Symbols

This book uses, as much as possible, a consistent set of symbols to represent variables of geochemical interest both in the text and in the accompanying R code. The following is a summary of the main symbols used. Often, a series of similar variables exists for a range of elements, minerals or portions of a system: this is indicated by subscripts and superscripts.

General

Symbol	Meaning and definition	R symbol
W	Mass (weight) of a whole system, or a portion thereof (indicated by subscript, see separate table below)	<i>Not used</i> ³
W^α	The mass of an element α in a portion of the system (see subscript)	<i>Not used</i>
F	Melt fraction: $F = W_L/W_0$	ff
F_C	Degree of crystallization: $F_C = 1 - F = W_S/W_0$	fc
C, C^α	Concentration of element α in a system or portion thereof (subscript): $C^\alpha = w^\alpha/W$	c0, cs, cl...
C_i^α	Concentration of element α in mineral i	mins
T	Temperature, normally in K but some equations use °C	tt

³ Some equations discussed in the text are not implemented in the R code.

Mineral proportions in various portions of a system (always summing up to 1)

Symbol	Meaning and definition	R symbol
m_i	... in the whole solid (cumulate or restite)	m
q_i	... in the peritectic assemblage	<i>Not used</i>
p_i	... in the reactants (non-modal melting)	<i>Not used</i>
$m_{0,i}$... in the original solid (non-modal melting)	<i>Not used</i>

Mixing

Symbol	Meaning and definition	R symbol
$f_1, f_2 \dots f_m$	Fraction of end-members 1, 2, ... m involved in mixing	f 1, f 2.. or f [1], f [2] ...
a, b, u, v	Various elements for which mixing is modelled (Sect. 11.3)	<i>Not used</i>
A, B, C, D	Parameters of a mixing hyperbola (Sect. 11.3)	AA, BB, CC, DD

Element partitioning

Symbol	Meaning and definition	R symbol
$K_{D\alpha}^{min/L}$	Partition coefficient of element α between mineral (min) i and liquid: $K_{D\alpha}^{min/L} = \frac{C_{min}^{\alpha}}{C_L^{\alpha}}$	kd, or commonly kd[j, i] or kd[elt, min] assuming elt and min have been de- fined before...
D_{α}	Often just K_D in text, when its meaning (element/mineral) is clear from the context Bulk distribution (solid/liquid) of element α $D_{\alpha} = \frac{C_S^{\alpha}}{C_L^{\alpha}} = \sum_i m_i K_{D\alpha}^{i/L}$	dd dd[elt] dd[j]
$D_{0\alpha}$	Often just D in text when the meaning is unambiguous “Bulk distribution coefficient” for the initial melting assemblage (non-modal melting): $D_{0\alpha} = \sum_{i=1}^n m_{0i} K_{D\alpha}^{i/L}$ (or just D_0 when unambiguous)	<i>Not used</i>
$D_{P\alpha}$	“Bulk distribution coefficient” for the reactants (non-modal melting): $D_{P\alpha} = \sum_{i=1}^n p_i K_{D\alpha}^{i/L}$ (or just D_P when unambiguous)	<i>Not used</i>

AFC

Symbol	Meaning and definition	R symbol
\dot{W}_A	Rate of assimilation	<i>Not used</i>
\dot{W}_C	Rate of fractional crystallization	<i>Not used</i>
r	Rate of assimilation to fractionation: $r = \frac{\dot{W}_A}{\dot{W}_C}$	r
r_C	Critical value of r for AFC, above which assimilation is dominant	r_C
z	Convenience parameter: $z = \frac{r+D-1}{r-1}$	z
S	Slope of a mixing array in a diagram I/c vs. I employed in reverse AFC modelling	<i>Not used</i>
C_0, I_0	Element concentration and isotopic ratio in pristine melt	c_0, i_0
C_A, I_A	Element concentration and isotopic ratio in assimilant	c_a, i_a
C_L, I_L	Element concentration and isotopic ratio in liquid	<i>Not used</i>

Radiogenic isotopes

Symbol	Meaning and definition	R symbol
Ab	Isotopic abundance, e.g. Ab_{87Rb}	<i>Not used</i>
AW	Atomic weight, e.g., AW_{Rb}	<i>Not used</i>
I	Ratio of daughter and stable, unradiogenic isotopes of the same element (e.g., $^{87}\text{Sr}/^{86}\text{Sr}$, $^{143}\text{Nd}/^{144}\text{Nd}$), measured	I
I^X, I^Y	Two such isotopic ratios for two distinct isotopic systems, e.g., Sr and Nd	<i>Not used</i>
R	Ratio of parental isotope/stable, unradiogenic isotope of the daughter element (e.g., $^{87}\text{Rb}/^{86}\text{Sr}$, $^{147}\text{Sm}/^{144}\text{Nd}$)	R
λ	Decay constant	lambda
I_i	Initial isotopic ratio	i_1, i_2, i_m
I_1, I_2, I_M	(subscripts $1, 2, M$ indicate isotopic ratios in mixing)	
X, Y	Isotopic systems if two involved in plotting	e.g., c_{x1}, i_{y1}
b	Slope of an isochron	<i>Not used</i>
α	Parameter controlling the shape of a mixing hyperbola	alpha
q	Curvature of a mixing hyperbola	q
x_0, y_0	Asymptotes of a mixing hyperbola	x_0, y_0

Additional subscripts/superscripts for isotopic ratios

<i>SA</i>	Sample
<i>DM</i>	Depleted Mantle
<i>CC</i>	Average Crust
<i>CHUR</i>	Chondritic Uniform Reservoir
<i>0</i>	Present-day
<i>i</i>	Initial
<i>t</i>	At the time <i>t</i>

Parts of a system (subscript)

Subscript	Meaning	Process
<i>0</i>	Source	[zero] solid source in the case of melting, primitive magma for crystallization
<i>L</i>	Liquid	melt for melting or differentiated liquid for crystallization
<i>L.inst</i>	Instantaneous liquid	fractional melting
<i>L.bulk</i>	Bulk (aggregated) liquid	fractional melting
<i>S</i>	Solid	restite for melting, cumulate for crystallization
<i>S.inst</i>	Instantaneous solid	fractional crystallization
<i>S.bulk</i>	Bulk (aggregated) solid	fractional crystallization
<i>M</i>	Mixture	mixing
<i>P</i>	Reactants	non-modal melting
<i>C</i>	Crystallized phases	AFC
<i>A</i>	Assimilant	AFC
<i>Q</i>	Peritectic assemblage	Melting or crystallization (with slightly different meanings)

Additional sub- and superscripts

Object	Symbol	Numbering
Minerals	A, B...	<i>i</i> = 1 to <i>n</i>
Chemical elements (components)	$\alpha, \beta \dots$	<i>j</i> = 1 to <i>p</i>
End-members in a mixing	1, 2...	<i>k</i> = 1 to <i>m</i>
Step of a stepwise process	<i>t</i>	<i>Not used</i>



It is not always possible to use the same conventions for printed text and R variables. For instance, mixed case variables (both upper and lower case) are dangerous in R, because it is case sensitive. Therefore, we use lower case in (most) R variable names. Furthermore, many single-letter symbols are reserved words: for instance `c`, `D` and `t` refer to common R functions (see Appendix A), whereas `T` and `F` are shorthand notations for logical `TRUE` and `FALSE`. For this reason, the commonly used *F* (melt fraction) and *D* (bulk distribution coefficient) are represented by `ff` and `dd` in our R code. Note also that the suffix used to indicate the source/parental magma is the number 0, not the letter O!

List of Abbreviations

AFC	Assimilation and Fractional Crystallization
ASCII	American Standard Code for Information Interchange
BSE	Back-Scattered Electrons, Mad Cows Disease
CBPC	Central Bohemian Plutonic Complex
CHUR	Chondritic Uniform Reservoir
CL	Cathodoluminescence
DM	Depleted Mantle
ESC	Essential Structural Component
FAQ	Frequently Asked Questions
fO ₂	oxygen fugacity
Ga	10 ⁹ years
GUI	Graphical User Interface
HFSE	High-Field Strength Element(s)
ICP-MS	Inductively Coupled Plasma Mass Spectrometry
INAA	Instrumental Neutron Activation Analysis
ICP-OES	Inductively Coupled Plasma Optical Emission Spectrometry
ka	10 ³ years
LA ICP-MS	Laser-Ablation Inductively Coupled Plasma Mass Spectrometry
LILE	Large Ion Lithophile Element(s)
Ma	10 ⁶ years
MORB	Mid-Ocean Ridge Basalt
MME	Mafic Microgranular Enclave
NB	Nota Bene
ppm	Parts Per Million
REE	Rare Earth Elements; LREE, MREE, HREE: light, medium, heavy REE
SIMS	Secondary Ion Mass Spectrometry
TIMS	Thermal Ionization Mass Spectrometry
TTG	Tonalite–Trondhjemite–Granodiorite association
XRF	X-Ray Fluorescence Spectrometry

Abbreviations of Mineral Names

Symbols for mineral names mostly follow Kretz (1983):

Ab	Albite
All	Allanite
Amp	Amphibole
An	Anorthite
Ap	Apatite
Bt	Biotite
Cpx	Clinopyroxene
Crd	Cordierite
Di	Diopside
En	Enstatite
Fo	Forsterite
Grt	Garnet
Hbl	Hornblende
Ilm	Ilmenite
Kfs	Potassium feldspar
Mnz	Monazite
Ms	Muscovite
Mt	Magnetite
Ol	Olivine
Opx	Orthopyroxene
Phl	Phlogopite
Pl	Plagioclase
Qtz	Quartz
Rt	Rutile
Sil	Sillimanite
Spl	Spinel
Zrn	Zircon

Reference

Kretz R (1983) Symbols for rock-forming minerals. *Amer Miner* 68:277-279.

Contents

1	Introduction	1
1.1	Causes of Whole-Rock Chemical Variation in Igneous Suites	1
1.2	Conventional Software for Igneous Geochemistry.....	3
1.2.1	Spreadsheets	3
1.2.2	Dedicated Programs (PC Compatibles).....	4
1.3	A Revolution? The R Language	4
1.3.1	What is R?.....	4
1.3.2	Geochemical Data Toolkit (<i>GCDkit</i>).....	5
	References.....	6

Part I R/GCDkit at Work

2	Data Manipulation and Simple Calculations	11
2.1	Loading and Manipulating Data	11
2.2	Linking Whole-Rock Chemistry with Mineral Stoichiometry	13
2.2.1	Basic Indexes.....	14
2.2.2	Cationic Parameters.....	16
2.2.3	Normative Calculations and Classification of Igneous Rocks.....	17
2.3	Statistics	18
2.4	Classification and Grouping—Using Factors	19
2.4.1	Statistical Examination of Complex Data Sets.....	20
2.4.2	Conversion of Numeric Vectors to Factors	22
2.4.3	Frequency (Contingency) Tables	23
	References.....	24
3	Classical Plots	27
3.1	Binary Plots	27
3.1.1	Plotting Simple Binary Plots	27
3.1.2	Constant Sum Effect (Closure).....	30
3.2	Harker Plots and Other Basic Multiple Plots.....	31
3.3	Ternary Plots	32
3.4	Classification Plots in <i>GCDkit</i>	34
3.5	Geotectonic Diagrams	35
3.6	Spiderplots.....	36
3.7	Multiple Plots by Groups.....	40
	References.....	41

4	Specialized Plots	45
4.1	Log-Log Binary Plots	45
4.2	Specialized Spiderplots	46
4.2.1	Double-Normalized Spiderplots	47
4.2.2	Spider Boxplots, Spider Box and Percentile Plots.....	47
4.3	Contour Plots	48
4.4	Anomaly Plots.....	49
4.5	Stripplots and Strip Boxplots.....	50
	References.....	51
5	Radiogenic Isotopes	53
5.1	Recalculation of Elemental to Isotopic Ratios.....	53
5.2	Calculation of Initial Ratios or Ages	55
5.3	Epsilon, Delta and Gamma Values.....	57
5.4	Model Ages	60
5.4.1	Single-Stage Nd Model Ages.....	60
5.4.2	Two-Stage Nd Model Ages	61
5.5	Isochron Ages.....	63
	References.....	65

Part II Modelling Major Elements

6	Direct Models	69
6.1	Mass Balance During Crystallization	69
6.1.1	Graphical Solutions	70
6.1.2	Cumulate Composition.....	71
6.1.3	Analytical Formulation.....	72
6.1.4	Generating a Magmatic Series Through Crystallization.....	73
6.2	Partial Melting.....	75
6.3	Peritectic Reactions	76
6.4	Mixing.....	78
6.5	Crystallization and Partial Melting—Are These Just Special Cases of Mixing?.....	79
	Reference.....	80
7	Reverse Models	81
7.1	An Under-Determined Problem.....	81
7.2	Least-Square Solution to Crystallization/Melting Problems	82
7.3	Least-Square Solution to Mixing Problems.....	83
	References.....	83
8	Forward Modelling in R	85
	References.....	92
9	Reverse Modelling in R	93

Part III Modelling Trace Elements

10 Dilute Trace Elements: Partition Coefficients	101
10.1 Crystal Networks and Substitutions	101
10.2 Partition Coefficients.....	101
10.3 Controls on the Values of Partition Coefficients.....	102
10.4 Bulk Distribution Coefficients	103
References.....	104
11 Direct (Dilute) Trace-Element Models	105
11.1 Crystallization	106
11.1.1 Batch Crystallization.....	106
11.1.2 Fractional Crystallization	106
11.1.3 Comparing Different Models.....	109
11.2 Melting.....	110
11.2.1 Batch Melting	110
11.2.2 Fractional Melting	110
11.2.3 Comparing Different Models.....	111
11.2.4 Alternative Formulations of the Melting Equations	111
11.3 Mixing.....	114
11.3.1 Ratio of Two Elements During Binary Mixing.....	114
11.3.2 Mixing Hyperbolae in Ratio–Ratio Plots	114
11.4 Assimilation and Fractional Crystallization (AFC).....	117
11.5 Composite Models.....	119
11.5.1 Crystallization with Incomplete Crystal Separation (Batch Crystallization + Binary Mixing)	120
11.5.2 Fluxed Melting (Binary Mixing + Batch Melting)	121
References.....	123
12 Reverse (Dilute) Trace-Element Models	125
12.1 Reverse Fractional Crystallization (Using Rayleigh’s Law)	125
12.2 Reverse Batch Partial Melting.....	127
12.3 Reverse Mixing	128
References.....	128
13 Trace Elements as Essential Structural Constituents of Accessory Minerals: the Solubility Concept	129
13.1 Solubility Formulae for Common Accessory Minerals.....	129
13.1.1 Zircon, $ZrSiO_4$	129
13.1.2 Monazite, $(LREE)PO_4$	131
13.1.3 Apatite, $Ca_5(PO_4)_3(F,Cl,OH)$	134
13.2 Evolution Through Saturation	136
References.....	139
14 Forward Modelling in R	141
References.....	152
15 Reverse Modelling in R	153

Part IV Radiogenic Isotopes

16 Direct Models	159
16.1 Binary Mixing	159
16.1.1 Single Isotopic Ratio	159
16.1.2 Pair of Isotopic Ratios	161
16.2 AFC Formulation for Isotopes.....	163
References.....	166
17 Reverse Models	167
17.1 Binary Mixing	167
17.2 AFC.....	167
References.....	168
18 Forward Modelling in R	169
18.1 Binary Mixing	169
18.2 AFC.....	173
19 Reverse Modelling in R	175
Reference.....	177

Part V Practical Modelling

20 Choosing an Appropriate Model	181
20.1 Evidence for Crystallization	181
20.1.1 Final Solidification During Emplacement	181
20.1.2 Fractional Crystallization at Depth.....	182
20.2 Evidence For Melting	183
20.2.1 Crustal Anatexis	183
20.2.2 Melting of the Mantle.....	184
20.3 Magma Mixing and Assimilation	185
20.3.1 Mixing and Mingling of Magmas.....	185
20.3.2 Assimilation.....	186
References.....	187
21 Semi-Quantitative Geochemical Approach	191
21.1 Assessing Trace-Element Compatibility	191
21.2 Order of (In)Compatibility	192
21.3 Process Identification	195
21.3.1 Mixing vs. Crystallization/Melting.....	195
21.3.2 Crystallization vs. Melting in a Log-Log Diagram.....	195
21.3.3 Crystallization vs. Melting Using Incompatible Elements ...	198
21.4 Mixing Test	199
21.5 Identifying Fractionating Minerals Using Log-Log Plots.....	202
References.....	203
22 Constraining a Model	205
22.1 Choosing an Appropriate Strategy.....	205

22.2	Constraining a Fractionation or Melting Model	206
22.2.1	The Differentiated Liquid(s)/Melt: C_L	206
22.2.2	The Primitive Liquid/Source: C_0	206
22.2.3	Composition of the Solid Phases (Cumulate/Restite).....	208
22.2.4	Partition Coefficients.....	211
22.3	Dealing with Accessory Minerals.....	212
22.3.1	Assessing the Role of Accessory Minerals.....	212
22.3.2	Modelling with Accessories	214
22.4	Constraining the End-Members of a Mixing Model.....	221
	References.....	222
23	Numerical Tips and Tricks	225
23.1	The Size of the Geochemical Space	225
23.2	Reducing the System	227
23.3	Colinearity	227
23.4	Breaking Minerals into End Members	228
23.5	Coupling Majors and Traces	228
23.6	This Space Left Blank for Your Own Tricks	229
	References.....	229
24	Common Sense in Action.	231
24.1	Physical Constraints	231
24.1.1	Thermodynamic Constraints	231
24.1.2	Mechanical (Rheological) Constraints	232
24.2	Scale and Speed of Processes—Approach to Equilibrium.....	234
24.3	Is Your Model Worth Your Efforts?	235
24.3.1	How Well Can We Discriminate Between Models?	236
24.3.2	Dangerous Projections.....	237
24.3.3	K_D vs. C_0 —What Should You Improve First?	238
24.4	Back to the Field!.....	239
	References.....	240
 Part VI Worked Examples		
25	Differentiation of a Calc-Alkaline Series: Example of the Atacazo-Ninahuilca volcanoes, Ecuador.	245
25.1	Geological Setting	245
25.2	Data Exploration and Implications	246
25.2.1	Isotopic Data	246
25.2.2	Major Elements	247
25.2.3	Trace Elements.....	248
25.3	Geochemical Modelling	250
25.3.1	First Step: Atacazo	252
25.3.2	Second Step: Ninahuilca	256
25.4	Summary	258
	References.....	260

26 Progressive Melting of a Metasedimentary Sequence: the Saint-Malo Migmatitic Complex, France	261
26.1 Geological Setting	261
26.2 Major and Trace Elements.....	262
26.3 Geochemical Modelling	264
26.3.1 Mode Evolution During melting	265
26.3.2 Major and Trace Elements.....	268
26.3.3 Zircon	271
References.....	275

Appendix A R Syntax in a Nutshell

1 Direct Mode	277
1.1 Basic Operations.....	277
1.1.1 Starting and Terminating the R Session	277
1.1.2 Seeking Help and Documentation	278
1.2 Fundamental Objects of the R Language.....	279
1.2.1 Commands.....	279
1.2.2 Handling Objects in Memory	281
1.2.3 Attributes to Objects.....	282
1.3 Numeric Vectors.....	282
1.3.1 Assignment.....	282
1.3.2 Vector Arithmetic.....	282
1.3.3 Names.....	283
1.3.4 Generating Regular Sequences	283
1.3.5 Functions to Manipulate Numeric Vectors.....	284
1.4 Character Vectors	284
1.5 Logical Vectors	285
1.5.1 Logical Operators	285
1.5.2 Missing Values (NA, NaN).....	286
1.6 Arrays, Matrices, Data Frames	286
1.6.1 Matrix/Data Frame Operations	287
1.7 Indexing/Subsetting of Vectors, Arrays and Data Frames.....	288
1.7.1 Vectors	289
1.7.2 Matrices/Data Frames.....	289
1.8 Lists	290
1.9 Coercion of Individual Object Types	291
1.10 Factors.....	292
1.10.1 Basic Usage of Factors	292
1.10.2 Conversion of Numeric Vectors to Factors	292
1.10.3 Frequency Tables	293
1.10.4 Using Factors to Handle Complex Datasets	293
1.11 Data Input/Output, Files	293
1.11.1 Reading Data	293
1.11.2 Sample Data Sets.....	295
1.11.3 Saving Data	295

- 2 Graphics**..... 295
 - 2.1 Obtaining and Annotating Binary Plots..... 295
 - 2.2 Additional High-Level Plotting Functions 302
 - 2.3 Creating Custom Layouts and Axes 305
 - 2.4 Exporting Graphs from R and Graphical Devices 308
 - 2.5 Interaction with Plots..... 308
- 3 Programming in R**..... 309
 - 3.1 Input and Output..... 309
 - 3.2 Conditional Execution 310
 - 3.3 Loops..... 310
 - 3.4 User-Defined Functions..... 311
 - 3.4.1 Arguments to Functions..... 311
 - 3.4.2 Assignments in Functions 312
 - 3.5 An Alternative to Loops—*sapply* 313
 - References..... 313

Appendix B Introduction to *GCDkit*

- 1 First Steps with *GCDkit***..... 315
 - 1.1 Installation..... 315
 - 1.2 *GCDkit* Overview: The User Interface 316
 - 1.3 Working with Data 318
 - 1.3.1 Data Format..... 318
 - 1.3.2 Loading Data 319
 - 1.3.3 Merging Data 321
 - 1.3.4 Choosing Data..... 322
 - 1.3.5 Grouping..... 322
 - 1.4 Plotting..... 323
 - 1.4.1 Plot Settings 326
 - 1.4.2 Single Plot Editing 327
 - 1.4.3 Plates and Plate Editing..... 328
 - 1.4.4 Spiderplots..... 328
 - 1.4.5 Classification and Geotectonic Diagrams 329
 - 1.5 Calculations..... 329
 - 1.6 Exporting from *GCDkit* 331
- 2 Under the Bonnet: *GCDkit* Internals**..... 332
 - 2.1 R language and *GCDkit* 332
 - 2.2 Data Variables 333
 - 2.3 System Variables..... 333
 - 2.4 Tailoring *GCDkit* to Suit your Needs..... 334
 - 2.5 Plugins..... 334
 - References..... 336

Appendix C Solving Systems of Linear Algebraic Equations in R

1.1 Linear Algebraic Equation Systems (Single Solution)..... 337
1.2 Overdetermined Systems (Unconstrained Least-Square Method)..... 338
1.3 Constrained Least-Square Method..... 339
References..... 340
Index 341

Chapter 1

Introduction

Very soon after the birth of igneous geochemistry, geologists like Alfred Harker (Harker 1909) recognized the existence of igneous rock “series”, i.e. rock suites sharing common geochemical features and having progressively changing compositions. Such variation was, and still frequently is, ascribed to evolution by fractional crystallization at depth, in a putative magma chamber. Research over the following century, however, has demonstrated that the chemistry of magmatic suites may in fact be shaped by many contrasting petrogenetic processes. Geochemistry, especially in combination with petrology, represents a powerful tool for deciphering and parameterizing of such processes.

1.1 Causes of Whole-Rock Chemical Variation in Igneous Suites

Human beings—and geologists in particular—have always been fascinated by magmas. Due to the well-known increase of temperature with depth, it was believed for a long time that there is a planetary-scale reservoir of molten rocks beneath the crust (e.g., Kircher 1664; Moro 1740; Cordier 1827). This archaic concept has long been abandoned as seismic data demonstrated that, apart from the outer core, the interior of the Earth is solid (Oldham 1906; Gutenberg 1914; Jeffreys 1926, among others). Suddenly a more complex picture has arisen—that of vigorous deep interactions between solid and liquid materials, including at least two successive petrogenetic processes: melting and crystallization. Of course, these mechanisms are inaccessible to direct observation, which is why their investigation has been mainly indirect, based on petrological and geochemical methods.

In the beginning of the 20th century, two distinct and complementary approaches to the problem emerged. The first one, based on experiments, was developed by Bowen (1912, 1928) who demonstrated the existence of mineral reaction series in magmatic systems. Indeed, during the crystallization of magma, minerals do not grow simultaneously but, as the magma cools, the individual mineral phases appear in a succession determined by their crystallization temperature. This concept showed crystallization as a dynamic process with a certain temporal

development. Thus, the evolution is not linear, but it can take different directions in response to the changes in physico-chemical parameters and, in turn, of mineral chemistry of crystallizing assemblages.

It was about the same time that a second approach, exemplified by Harker (1909) was developed based on interpretation of whole-rock compositions. This author came up with the concept of a variation diagram, plotting oxides of major elements against an “index of differentiation”. Harker’s suggestion to use SiO_2 as a differentiation index was ground-breaking at the time and marked the dawn of modern geochemistry. He showed that when the bulk composition of rocks belonging to the same petrographic province, or even a single volcanic (or plutonic) complex, are plotted in such variation diagrams, they define more or less continuous evolutionary trends (Fig. 1.1). Harker proposed to interpret these trends in terms of magmatic differentiation, directly correlated to the nature of the crystallizing mineral phases.

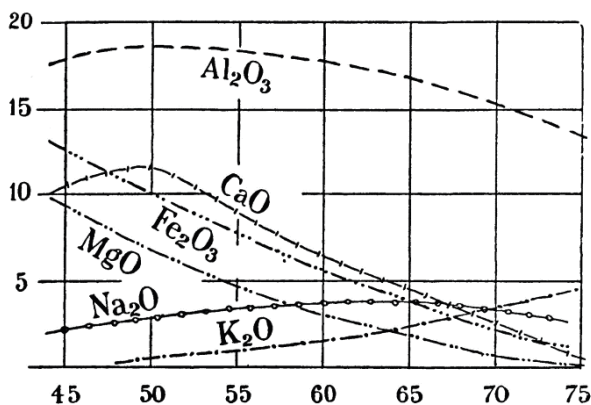


Fig. 1.1 An example of early depiction of differentiation trends in binary plots of silica vs. major-element oxides, for the volcanic rocks from Lassen Peak (California) (Harker 1909). These later became known as the Harker plots.

Even though both these approaches have been an important step forward, they have for long remained essentially descriptive, or qualitative at best. The first attempts on quantifying and modeling the behaviour of trace elements in magmas date back to the late 1960’s (Gast 1968; Shaw 1970). Similarly, even if the chemical fractionation laws had been long known for gases (Rayleigh 1896), it was only at this same period that they were invoked to model the fractionation of crystallizing magmatic liquids (Neumann et al. 1954; Greenland 1970; Albarède and Bottinga 1972). Also the analysis of mineral chemistry was revolutionized by the appearance of the first commercially available electron microprobes (Castaing 1951). Lastly, the prestigious lunar program in the 1960’s required precise and accurate chemical, and then isotopic, analyses of small samples, leading to innovations (Johnson et al. 2013).

A further boost to geochemical modelling came with the advancement of radiogenic isotope methods (originally Thermal-Ionization Mass Spectrometry, TIMS, and from late 1990's also Inductively Coupled Mass Spectrometry, ICP-MS). In 1970's analytical techniques became available revolutionising whole-rock trace-element determinations, providing precise and reproducible data needed for petrogenetic modelling (e.g., X-Ray Fluorescence Spectrometry, XRF; Instrumental Neutron Activation Analysis, INAA) later joined by Inductively Coupled Plasma Optical Emission Spectrometry, ICP-OES and, in particular, ICP-MS (Potts 1987; Sylvester 2001). Obviously related was the development of the theoretical principles, including new geochemical projections (see Rollinson 1993 and references therein) or innovative approaches to numerical description and modelling of petrogenetic processes (summarized, above all, in excellent monographs of Albarède 1995 and Shaw 2006).

This revolution in whole-rock geochemistry has been joined, especially in the last twenty years, by novel and cost-effective methods for *in situ* determinations of mineral composition, most importantly Secondary Ion Mass Spectrometry (SIMS) and Laser-Ablation Inductively Coupled Plasma Mass Spectrometry (LA ICP-MS). This advancement is ongoing, and seems to be accelerating nowadays.

1.2 Conventional Software for Igneous Geochemistry

With the modern analytical techniques has inevitably arrived a flood of precise geochemical data on major- and trace elements, as well as a seemingly endless number of isotope systems. This technical progress goes hand in hand with the increasing accessibility of data over the Internet, in the form of online publications, their supplementary datasets, or web-based databases such as EarthChem (www.earthchem.org) or GeoRoc (georoc.mpch-mainz.gwdg.de/georoc).

Quick and efficient handling of such large datasets represents a true challenge in modern geochemistry. This is routinely achieved by personal computers, also enabling the calculation of rather complicated thermodynamic and petrogenetic models in the comfort of one's own office.

1.2.1 Spreadsheets

The most accessible and generally available are the spreadsheets. They belong to basic software preloaded on many computers, thus requiring no extra costs. Even though relatively easy to use, they are not very suitable for geochemical calculations. Dedicated geochemical tools, mostly designed for Microsoft Excel aided by VBA macros, are rather scarce, and their functionality rudimentary (Sidder 1994; Su et al. 2003; Zhou and Li 2006; Wang et al. 2008) even though some more sophisticated tools for petrogenetic modelling are also available (Ersoy 2013; Keskin 2013). Moreover, spreadsheets endure low efficiency for repeated tasks as well as limited protection of the primary data; for more complicated calculations the

worksheet becomes too complex and prone to errors. The graphical output is poor and requires much tweaking to become truly of publication quality. In our view, spreadsheets are useful only for organization of the data (although databases are superior for the task) and production of tables for final publication.

1.2.2 Dedicated Programs (PC Compatibles)¹

A number of dedicated software tools have been written in a variety of programming languages that PC users could employ. Some of them were designed for DOS or 16-bit versions of Windows and thus became obsolete, such as MinCalc (Melin and Kunst 1992), NewPet (Clarke et al. 1994), MinPet (Richard 1995), or Norman (Janoušek 2001). Others are more recent and still being continuously developed, most notably IgPet (Carr 2014; www.rockware.com), PetroGraph (Petrelli et al. 2005), accounts.unipg.it/~maurip/SOFTWARE.htm) and WinRock (Kanen 2004, www.geologynet.com/winrock.htm).

Unfortunately, it is often difficult to figure out exactly which algorithms have been employed by a given program. The documentation is never detailed enough and it is not a common practice to make the source code available. Even if it is, any modifications or additions to the original program could be tedious, or impossible for legal reasons, or merely because the user may not be a skilled programmer. Moreover, many of the programs require complex formatting of the input data, and/or fail to produce high-quality graphical output. Of concern to many colleagues also is that some of the applications are rather costly and/or have a peculiar user interface.

1.3 A Revolution? The R Language

Clearly the best approach to many problems outlined above would be to write our own software. But we suggest that it would not be wise to develop it from scratch; much better is to employ a comprehensive computing environment such as Mathematica or Matlab, with a built-in computational, graphical and input/output functionality. However, also these packages are commercial, hindering the distribution of any product to potential users, especially in economically challenged countries.

1.3.1 What is R?

Fortunately, with the appearance of the R language at the turn of millennium, we now have a powerful, yet simple and free, open-source toolbox, ideal for development of geochemical packages. Put in simple terms, R is an environment for efficient data processing, their visualization and statistical analysis as well as a

¹ Apart from thermodynamic software, dealt with in one of the Next step boxes in Chap. 22.

high-level functional/object-oriented programming language. It was developed originally by Ihaka and Gentleman (1996) from the University of Auckland. Subsequently an open group of experts formed the *R Development Core Team* who continue to oversee the development of the project (www.r-project.org). Version 1.00 was released in 2000; the current one at the time of writing this book is 3.1.2 (Pumpkin Helmet).

The syntax of R (see Appendix A) is based on, and largely compatible with, its successful predecessor, the S language. The latter was developed in Bell Laboratories in 1975, and followed by *The New S Language* in late 1980's (Becker et al. 1988). The commercial version, S-PLUS, is currently being distributed by TIBCO Software (www.tibco.com).

The chief advantage of R is—apart from a somewhat more efficient implementation—that it is freely available, with all the source code, for all the main platforms (MS Windows, Unix/Linux and Mac OS). The R language includes arithmetic and database functions (plus data import in many formats, also via SQL and ODBC), functions for matrix manipulation/arithmetic and a large number of statistical tools.

The graphic output is publication-quality, including mathematical symbols. It can be exported into a number of data formats (PostScript, WMF, PDF, TIFF, PNG...), for incorporation into DTP programs and word processors or for further editing in graphical packages such Corel Draw or Adobe Illustrator.

R allows interactive as well as batch use (as a true programming language). For the latter, it enables writing user-defined functions involving conditions or loops. R is easily extensible with user-contributed packages. Apart from this, an overwhelming majority of programs designed originally for S/S-PLUS work—directly or after cosmetic changes—in R. Most of the R system is written in R; for computationally intensive tasks, C, C++, and FORTRAN code can be linked and called at run time.

1.3.2 Geochemical Data Toolkit (*GCDkit*)

The Geochemical Data Toolkit (*GCDkit*) (Janoušek et al. 2006, 2011) is a free-ware Windows package for interpretation and graphical presentation of whole-rock geochemical data from igneous rocks. It not only provides a graphical user interface (GUI) to (a fraction) of relevant functions built into R, but also introduces brand new specialized geochemical tools. These include recalculations (simple geochemical indexes, norms, interpretation of the Sr–Nd isotopic data...) and graphs (e.g., binary and ternary plots, spiderplots, as well as templates for classification and geotectonic diagrams). It is designed so that no programming skills are needed for ordinary use. At the same time, the possibility of typing in R/*GCDkit* commands is preserved. From R, *GCDkit* inherits modularity, expandability and lucidity. An introduction to its basic functionality is given in Appendix B, and examples of use are in the forthcoming text.

References

- Albarède F (1995) Introduction to geochemical modeling. Cambridge University Press, Cambridge
- Albarède F, Bottinga Y (1972) Kinetic disequilibrium in trace element partitioning between phenocrysts and host lava. *Geochim Cosmochim Acta* 36:141–156
- Becker RA, Chambers JM, Wilks AR (1988) The new S language. Chapman & Hall, London
- Bowen NL (1912) The order of crystallization in igneous rocks. *J Geol* 20:457–468
- Bowen NL (1928) The evolution of the igneous rocks. Princeton University Press, Princeton
- Carr M (2014) IgPet, a graphics and modeling program for igneous petrology. Terra Softa, Somerset, New Jersey, U.S.A.
- Castaing R (1951) Application des sondes électroniques à une méthode d'analyse ponctuelle chimique et cristallographique. Publication ONERA, vol 55. University of Paris, Paris (PhD Thesis)
- Clarke D, Mengel F, Coish RA, Kosinowski MHF (1994) NewPet for DOS, version 94.01.07. Department of Earth Sciences, Memorial University of Newfoundland, Canada
- Cordier PLA (1827) Essai sur la température de l'intérieur de la Terre. Mémoires de l'Académie des sciences de l'Institut de France 7:473–556
- Ersoy Y (2013) PETROMODELER (Petrological Modeler): a Microsoft® Excel® spreadsheet program for modelling melting, mixing, crystallization and assimilation processes in magmatic systems. *Turkish J Earth Sci* 22:115–125
- Gast PW (1968) Trace element fractionation and the origin of tholeiitic and alkaline magma types. *Geochim Cosmochim Acta* 32:1057–1086
- Greenland LP (1970) An equation of trace element distribution during magmatic crystallization. *Amer Miner* 55:455–465
- Gutenberg B (1914) Über Erdbebenwellen VIIA. Beobachtungen an Registrierungen von Fernbeben in Göttingen und Folgerungen über die Konstitution des Erdkörpers. *Nachr d Kön Ges d Wiss Göttingen, math-phys Kl* 125–176
- Harker A (1909) The natural history of igneous rocks. Methuen & Co., London
- Ihaka R, Gentleman R (1996) R: a language for data analysis and graphics. *J Comp Graph Stat* 5:299–344
- Janoušek V (2001) Norman, a QuickBasic programme for petrochemical re-calculation of whole-rock major-element analyses on IBM PC. *J Czech Geol Soc* 46:9–13
- Janoušek V, Farrow CM, Erban V (2006) Interpretation of whole-rock geochemical data in igneous geochemistry: introducing Geochemical Data Toolkit (GCDkit). *J Petrol* 47:1255–1259
- Janoušek V, Farrow CM, Erban V, Trubač J (2011) Brand new Geochemical Data Toolkit (GCDkit 3.0)—is it worth upgrading and browsing documentation? (Yes!). *Geol výzk Mor Slez* 18:26–30
- Jeffreys H (1926) The rigidity of the Earth's central core. *Monthly Notices of the Royal Astronomical Society, Geophysical Supplement* 1:371–383
- Johnson CM, McLennan SM, McSween HY, Summons RE (2013) Smaller, better, more: five decades of advances in geochemistry. In: Bickford ME (ed) *The web of geological sciences: advances, impacts, and interactions*. Geological Society of America Special Papers, vol 500, pp 259–302
- Kanen (2004) WinRock (a manual). MinServ, ISBN 0 9756723 8 X
- Keskin M (2013) AFC-Modeler: a Microsoft® Excel® workbook program for modelling assimilation combined with fractional crystallization (AFC) process in magmatic systems by using equations of DePaolo (1981). *Turkish J Earth Sci* 22:304–319
- Kircher A (1664) *Mundus subterraneus*, Tomus 1–2. Apud Joannem Janssonium & Elyseum Weyerstraten, Amsterdam
- Melín M, Kunst M (1992) MINCALC Development Kit 2.1. Geological Institute of the Czech Academy of Sciences, Prague

- Moro AL (1740) De crostacei e degli altri marini corpi che si trovano su' monti. Appresso Stefano Monti, Venezia
- Neumann H, Mead J, Vitaliano CJ (1954) Trace element variation during fractional crystallization as calculated from the distribution law. *Geochim Cosmochim Acta* 6:90–99
- Oldham RD (1906) The constitution of the interior of the Earth, as revealed by earthquakes. *Q J Geol Soc Lond* 62:456–475
- Petrelli M, Poli G, Perugini D, Peccerillo A (2005) PetroGraph: a new software to visualize, model, and present geochemical data in igneous petrology. *Geochem Geophys Geosyst* 6: Q07011
- Potts PJ (1987) A Handbook of silicate rock analysis. Blackie & Son Ltd., Glasgow and London
- Rayleigh L (1896) Theoretical considerations respecting the separation of gases by diffusion and similar processes. *Philosophical Magazine Series 5* 42:493–498
- Richard LR (1995) MinPet: mineralogical and petrological data processing system, version 2.02. MinPet Geological Software, Québec, Canada
- Rollinson HR (1993) Using geochemical data: evaluation, presentation, interpretation. Longman, London
- Shaw DM (1970) Trace element fractionation during anatexis. *Geochim Cosmochim Acta* 34:237–243
- Shaw DM (2006) Trace elements in magmas. A theoretical treatment. Cambridge University Press, Cambridge
- Sidder GB (1994) Petro.calc.plot, Microsoft Excel macros to aid petrologic interpretation. *Comput and Geosci* 20:1041–1061
- Su YJ, Langmuir CH, Asimow PD (2003) PetroPlot: A plotting and data management tool set for Microsoft Excel. *Geochem Geophys Geosyst* 4:1030, doi:10.1029/2002GC000323
- Sylvester P (ed) (2001) Laser ablation-ICPMS in the Earth sciences: principles and applications. Mineralogical Association of Canada Short Course Series, vol 29
- Wang X, Ma W, Gao S, Ke L (2008) GCDPlot: An extensible Microsoft Excel VBA program for geochemical discrimination diagrams. *Comput and Geosci* 34:1964–1969
- Zhou J, Li X (2006) GeoPlot: an Excel VBA program for geochemical data plotting. *Comput and Geosci* 32:554–560

Part I R/GCDkit at Work

In this section we will demonstrate practical use of the R language to solve common problems in igneous geochemistry. The text usually starts with a brief discussion of the geological background, followed by a R code (see Appendix A for an overview of R syntax) and its equivalent (or more elegant ☺) solution in *GCDkit* (for introduction to the system or for reference, see Appendix B).

Chapter 2

Data Manipulation and Simple Calculations

2.1 Loading and Manipulating Data

When starting a new session in R, with or without *GCDkit*, the first task is to import data. In plain R, tabular data, common in igneous geochemistry, can be loaded most conveniently by the `read.table` command. The other possibility is to access one of the built-in datasets using the `data` command. In *GCDkit* the analyses are usually read by the `loadData` function, or copied from any Windows application (such as a spreadsheet) via the clipboard.

Seldom are all the values available for all the samples. There are two types of missing data: concentrations below the detection limit and those not determined. If statistical evaluation is desired, especially by multivariate methods, information that elemental concentration is lower than a certain threshold fundamentally differs from the situation when it is completely unknown and can attain any value. One of the available strategies to deal with the first case (Rock 1988; van den Bogaard and Tolosana-Delgado 2013) is to replace the data below the detection limit by its half (Reimann et al. 2008). Clearly, thus estimated values should not represent a high proportion of the given variable. Regarding the not analyzed data, the R language has facilities to handle appropriately any completely missing values (denoted NA), e.g. during plotting or mean calculations.

Once data are loaded, the most common tasks include display, subsetting (modest database functionality) and simple arithmetics. Below we are going to practice such skills on vectors and data frames, the most common data types.



Exercise 2.1: Subsetting a numeric vector, vector operations

GCDkit contains several built-in datasets, normally needed just for correct system functioning. One of these is atomic weights, stored in the named vector `mw`. We will use it to show some simple vector operations.

- Display the whole vector. What is the atomic weight of Rb?
- What is the average value of the whole vector?
- Which atoms have the atomic weight higher than 170?
- Display the names of six lightest and six heaviest elements in the dataset.



```

a) GCDkit-> mw
      Ag      Al      As      Au      B      Ba
107.86820  26.98154  74.92160  196.96650  10.81100  137.33000
      Be      Bi      Br      C      Ca      Cd
  9.01218  208.98040  79.90400  12.01100  40.07800  112.41000 ...

GCDkit-> mw["Rb"]
      Rb
85.4678

b) GCDkit-> mean(mw)
[1] 107.9206

c) GCDkit-> names(mw) [mw>170]
[1] "Au" "Bi" "Hf" "Hg" "Ir" "Lu" "Np" "Os" "Pb" "Pt" "Pu"
[12] "Re" "Ta" "Th" "Tl" "U" "W" "Yb"

d) GCDkit-> sort(mw) [1:6]
      H      Li      Be      B      C      N
  1.00797  6.94100  9.01218  10.81100  12.01100  14.00670
GCDkit-> rev(sort(mw)) [1:6]
      Pu      U      Np      Th      Bi      Pb
244.0640  238.0290  237.0482  232.0381  208.9804  207.2000

```



Exercise 2.2: Loading files, matrix/data frame manipulations

The file *sazava.data* contains selected major- and trace-element analyses from the ~354 Ma old Sázava suite of the Central Bohemian Plutonic Complex (CBPC; Bohemian Massif, Czech Republic) (Janoušek et al. 2000, 2004).

- Read analyses stored in the tab-delimited data file into a data frame `WR`.
- Find out the names of available variables (= column names).
- What is the MgO content of sample Sa-1?
- Show all available numeric data for samples Po-1 and Po-4.
- Calculate the total of the column "Na₂O".
- Display names of three samples with the lowest and the highest SiO₂ contents.
- Calculate averages of all variables.
- Display a table with three columns: SiO₂, MgO and Na₂O/K₂O.



`sazava.data`



```
a) > sazava <- read.table("sazava.data", sep="\t")
```



```
GCDkit-> loadData("sazava.data") # Alternative in GCDkit1
GCDkit-> sazava <- cbind(labels,WR)

b) > colnames(sazava)
[1] "Intrusion" "Locality" "Petrology" "Outcrop"
[5] "Symbol" "Colour" "SiO2" "TiO2"
[9] "Al2O3" "FeO" "Fe2O3" "MnO"...
```

```
c) > sazava["Sa-1", "MgO"]
[1] 3.21
```

```
d) > sazava <- sazava[, -(1:6)] # Stripping 1st six columns
> sazava[c("Po-1", "Po-4"), ]
      SiO2 TiO2 Al2O3 FeO Fe2O3 MnO MgO CaO Na2O K2O
Po-1 62.95 0.28 20.02 1.65 0.67 0.05 0.55 6.61 3.91 1.99
Po-4 71.09 0.30 15.09 2.12 0.38 0.06 0.52 3.75 3.68 1.87 ...
```

```
e) > sum(sazava[, "Na2O"])
[1] 39.13
```

```
f) > silica <- sazava[, "SiO2"]
> names(silica) <- rownames(sazava)
> names(sort(silica)) [1:5]
[1] "Gbs-2" "Gbs-1" "Sa-4" "Gbs-20" "SaD-1"
> names(rev(sort(silica))) [1:5]
[1] "Po-5" "Po-4" "Po-3" "Po-1" "Sa-1"
```

```
g) > apply(sazava, 2, mean, na.rm=TRUE)
      SiO2      TiO2      Al2O3      FeO
57.95285714 0.63928571 16.94285714 4.73071429
      Fe2O3      MnO      MgO      CaO
1.74642857 0.13785714 3.57000000 8.16000000 ...
```

```
h) > x <- cbind(sazava[, "SiO2"], sazava[, "MgO"],
+             sazava[, "Na2O"]/sazava[, "K2O"])
> colnames(x) <- c("SiO2", "MgO", "Na2O/K2O")
> rownames(x) <- rownames(sazava)
> x
      SiO2 MgO Na2O/K2O
Sa-1 59.98 3.21 1.008000
Sa-2 55.17 3.67 1.976471 ...
```

2.2 Linking Whole-Rock Chemistry with Mineral Stoichiometry

After loading, a common task is to recast the bulk geochemical analyses into several indexes, related to the mineralogy of the rocks. This is often followed by

¹ Caution, two variables will be created in this case. WR will contain only the numeric values, all textual information will be transferred into data frame labels. See Appendix B for details.

normative recalculations. The aim is to better understand the modal chemistry, classification and, together with statistical methods, the distribution of elements within the dataset. R, as a statistical language, is well suited to such a task. Furthermore, user-defined functions serve to add new features tailored to our needs.

2.2.1 Basic Indexes

The calculations in R can be best demonstrated on an example of simple geochemical indexes. Arguably the most used, and quite powerful, are the recalculations of Fe as total ferrous or ferric oxides, and two types of Mg numbers²:

$$FeOt = FeO + 0.89981 \times Fe_2O_3 [wt. \%] \quad (2.1)$$

$$mg\# = 100 \frac{MgO}{FeO + MgO} [mol. \%] \quad (2.2)$$

$$Mg\# = 100 \frac{MgO}{FeOt + MgO} [mol. \%] \quad (2.3)$$

Many major-element based diagrams are constructed using some conversion of wt. % oxides into cation numbers; this allows easy comparison with mineral formulae. For instance, the popular alumina saturation index, A/CNK (Shand 1943) (sometimes also abbreviated as ASI) mimics the stoichiometry of feldspars:

$$A/CNK = \frac{Al_2O_3}{CaO + Na_2O + K_2O} [mol. \%] \quad (2.4)$$

A similar index, distinguishing peralkaline rocks (with excess alkalis), is:

$$A/NK = \frac{Al_2O_3}{Na_2O + K_2O} [mol. \%] \quad (2.5)$$

If $A/CNK > 1$, there is excess Al over the amount needed to form feldspars. Such rocks are termed peraluminous, while those with $A/CNK < 1$ and $A/NK > 1$ are metaluminous and those with $A/CNK \sim 1$ subaluminous (Shand 1943). The A/CNK value has a direct link to modal mineralogy—presence of Ca- and/or alkali-rich phases such as amphiboles and pyroxenes indicates an Al deficit and the host rock is metaluminous. Biotite is weakly peraluminous and thus its occurrence points to weakly peraluminous nature of the rock (Miller 1985). Strongly peraluminous granitoids (*sensu* Miller 1985) contain additional more peraluminous phases like muscovite, or even alumosilicates (kyanite, sillimanite or andalusite), cordierite, garnet, tourmaline, topaz or corundum (Clarke 1981). However, the

² The Fe numbers (Frost et al. 2001; Frost and Frost 2008) are defined analogously.

definition of the ASI does differ between authors—sometimes the Ca is corrected for apatite³, or even the definition is misleading, not reflecting the feldspars stoichiometry at all (Frost et al. 2001)⁴.



Exercise 2.3: Calculating simple indexes

On the Sázava dataset we can demonstrate how to define a function calculating a geochemical index. In this way the system can be enriched, quickly and efficiently.

a) Given the molecular weights below, design a function to calculate *mg* number.

FeO	MgO	Al ₂ O ₃	CaO	Na ₂ O	K ₂ O
71.85	40.31	101.96	56.08	61.98	94.20

b) Write a function returning Shand's indexes (A/CNK and A/NK).

c) Calculate all these values for the Sázava dataset.

d) Recast the major-element oxides on 100% volatile-free basis.



sazava.data



```
> sazava <- read.table("sazava.data", sep="\t")
> MW <- c(71.85, 40.31, 101.96, 56.08, 61.98, 94.20)
> oxides <- c("FeO", "MgO", "Al2O3", "CaO", "Na2O", "K2O")
> names(MW) <- oxides
> # Transpose as the division of a matrix by a vector
> # proceeds along columns, not rows.
> mol <- t(sazava[, oxides])/MW[oxides]

a) > mgno <- function() {
>   mg <- 100*mol["MgO", ]/(mol["FeO", ]+mol["MgO", ])
>   return(mg)
> }

b) > ank <- function() {
>   ANK <- mol["Al2O3", ]/(mol["Na2O", ]+mol["K2O", ])
>   return(ANK)
> }
> acnk <- function() {
>   ACNK <- mol["Al2O3", ]/(mol["Na2O", ]+mol["K2O", ]+
+     mol["CaO", ])
>   return(ACNK)
> }

c) > # Calculate the indexes
> x <- cbind(mgno(), acnk(), ank())
> colnames(x) <- c("mg.no", "A/CNK", "A/NK")
```

³ NB that *GCDkit* does not perform this correction.

⁴ See *GCDkit* help to the function `Frost`.

```
> x
      mg.no      A/CNK      A/NK
Sa-1  51.16987  0.8355806  2.396569
Sa-2  55.42955  0.7619109  2.307463
Sa-3  51.92059  0.8079150  2.562820 ...

d) > major <- c("SiO2", "TiO2", "Al2O3", "Fe2O3", "FeO", "MnO",
+              "MgO", "CaO", "Na2O", "K2O", "P2O5")
> sums <- apply(sazava[,major], 1, sum)
> anh <- sazava[,major]/sums*100
> anh
      SiO2      TiO2      Al2O3      Fe2O3      FeO
Sa-1  60.30565  0.6334205  16.50915  1.3573296  5.489644
Sa-2  56.25000  0.7238989  17.33279  2.7120718  5.362969
Sa-3  56.03133  0.7628153  17.89056  2.1663954  5.909276 ...
```



Calculation of molecular weights in *GCDkit* utilises the function `molecularWeight`. It returns also the number of cations and oxygens per formula and thus the result needs to be subset, e.g. as follows:

```
GCDkit-> molecularWeight("Al2O3")[1]
      MW
101.9613
```



Simple geochemical indexes in *GCDkit*

Upon loading new data, several useful petrological indexes are calculated automatically, including `FeOt`, `mg#` and `Mg#`, as well as `A/CNK` and `A/NK` values that are then available, e.g. for plotting. Moreover, a matrix `WRanh` contains the major-element oxides recast to 100% anhydrous basis.

Therefore, the exercise a–c has a simple *GCDkit* solution:

```
GCDkit-> loadData("sazava.data")
GCDkit-> WR[,c("mg#", "A/CNK", "A/NK")]
GCDkit-> WRanh
```

2.2.2 Cationic Parameters

Niggli (1948) stressed the importance of simple cationic values for petrogenetic interpretation of igneous rocks. Several of the Niggli's cationic values, *si*, *al*, *fm*, *c*, *alk*, *k*, *mg*, *ti*, *p*, *c/fm*, and *qz* are still in use. The concept was further elaborated in multicationic parameters of the French authors, based on millications:

$$milli_{\alpha} = n_{\alpha} \times \frac{C_{\alpha}}{MW_{\alpha}} \times 1000 \quad (2.6)$$

where MW_{α} is molecular weight and n_{α} number of atoms in the oxide formula (e.g., the later is 1 for CaO , 2 for Na_2O , and again 2 for Al_2O_3). Note that even if the original

analyses (wt. % oxides) did sum up to 100, there is no reason for the total millifications to attain a specific value. For some applications (e.g. zircon saturation, Sect. 13.1.1) it is required to normalize this total to 1.

For classification purposes, De La Roche et al. (1980) used a projection of two parameters, $R_1 = 4Si - 11(Na + K) - 2(Fe + Ti)$ and $R_2 = 6Ca + 2Mg + Al$, thus incorporating all major-element oxides. Besides that, the R_1 - R_2 plot has petrogenetic and geotectonic implications (Batchelor and Bowden 1985).

In the complex classification system of Debon and Le Fort (1983, 1988), arguably the most useful parameters are $A = Al - (K + Na + 2Ca)$ (reflecting peraluminosity), $B = Fe + Mg + Ti$ (maficity), $P = K - (Na + Ca)$ (proportion of K-feldspar among feldspars) and $Q = Si/3 - (K + Na + 2Ca/3)$ (quartz content).



Millications and related classification schemes

Upon loading a new data into *GCDkit*, the analyses are all recalculated to millications and stored in a data matrix `milli`. There are also functions calculating millications-based indexes, as well as generating some of the related plots (De La Roche et al. 1980; Debon and Le Fort 1983, 1988; Batchelor and Bowden 1985; Villaseca et al. 1998). See help for `LaRocheCalc`, `LaRoche`, `DebonCalc`, `Debon`, `Batchelor` and `Villaseca` to find out more.

2.2.3 Normative Calculations and Classification of Igneous Rocks

The norms, even though introduced early in the history of igneous petrology, are not obsolete. For instance, the CIPW norm (designed by Cross et al. 1902) remains important part of the TAS classification of volcanic rocks, where it serves for distinguishing some rock types (Le Bas et al. 1986; Le Maitre 2002). The calculation involves a hierarchical list of rules that tend to be often ambiguous and giving, to a varied extent, different results (Hutchison 1974, 1975; Verma et al. 2002, 2003). Another shortcoming of the CIPW norm is that it does not include hydrous minerals and therefore yields phases often not matching modal mineralogy in the studied igneous rocks, especially acidic ones.



Calculating norms in *GCDkit*

Most of the *GCDkit*'s normative recalculation schemes have been adopted from its predecessor, NORMAN (Janoušek 2001). Available are modules for the CIPW norm, including the modification with Bt and Hbl (Hutchison 1974, 1975), Catanorm (Hutchison 1974 and references therein), and Improved Granite Mesonorm (Mielke and Winkler 1979). The curious reader can type `CIPW` (without brackets!) at the *GCDkit* prompt, and look at the code of the function. See help for `CIPW`, `CIPWhb`, `Catanorm` and `Mesonorm` for details.



Dealing with results of *GCDkit* calculations

The most recent values calculated are always stored in the variable `results`. The results (i.e., the namesake variable) can be copied to the clipboard, appended to the data (to the data matrix `WR`) or saved into a variety of formats from a menu that appears after right-clicking the *R-Console* window.

2.3 Statistics

Early in the interpretation of a newly acquired geochemical dataset it is handy to examine descriptive statistics for selected elements or oxides. R contains a plethora of statistical tools, either built in, or provided as additional modules (packages). At this stage, however, simple functions such as `mean`, `median`, `sd` (standard deviation) and `summary` (a statistical overview) suffice. Revealing are also simple graphical tools such as boxplots (box-and-whiskers plots; function `boxplot`) and histograms (`hist`). Scatter matrices (`pairs`) serve to spot potentially significant correlations. See Appendix B for syntax and further details; the specific problem of dealing with a more complex data set containing several groups of data (using factors) is dedicated to Section 2.4.



Statistics in *GCDkit*

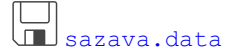
The command line interface of the standard R environment on the one hand allows much control for experienced users but on the other tends to discourage many scientists, accustomed to menu-driven software. *GCDkit* builds on the diverse functionality of the R language by providing a graphical user interface (GUI) to at least some of the most commonly used statistical functions, including simple descriptive statistics, histograms, boxplots, strip plots, correlation diagrams as well as more sophisticated methods of multivariate statistics (such as hierarchical clustering and principal components analysis). This interface is accessible from the menu *Calculations/Statistics*. Nevertheless the *R-Console* is still available for standard commands.

The more sophisticated tools are beyond the scope of the current text and the interested reader is referred to R/S documentation or special publications (e.g., Chambers and Hastie 1992; Venables and Ripley 1999; Maindonald and Braun 2003; Reimann et al. 2008; van den Bogaard and Tolosana-Delgado 2013).



Exercise 2.4: Simple statistics

- Compute means for all columns (variables) in the file `sazava.data`.
- Display boxplot for strontium, and find out all the main statistical parameters characterizing its distribution (the range, median, number of observations and not determined cases...).
- Plot all the possible combinations of binary diagrams (a scatterplot matrix) for the following oxides: SiO_2 , MgO , CaO , Na_2O , K_2O , and P_2O_5 .



```

> sazava <- read.table("sazava.data", sep="\t")
> sazava <- sazava[,-(1:6)]
# or sazava[,7:ncol(x)] to get solely the numeric data

a) > result <- apply(sazava,2,mean,na.rm=TRUE)
> round(result,2)
      SiO2      TiO2      Al2O3      FeO      Fe2O3      MnO
  57.95    0.64    16.94    4.73    1.75    0.14 ...

b) > boxplot(sazava[, "Sr"], xlab="Sr", ylab="ppm")
> summary(sazava[, "Sr"])
  Min. 1st Qu.  Median    Mean 3rd Qu.    Max.   NA's
  278.0  392.5   430.0   443.0  537.5   599.0    2.0

c) > oxides <- c("SiO2", "MgO", "CaO", "Na2O", "K2O", "P2O5")
> pairs(sazava[, oxides])
  
```

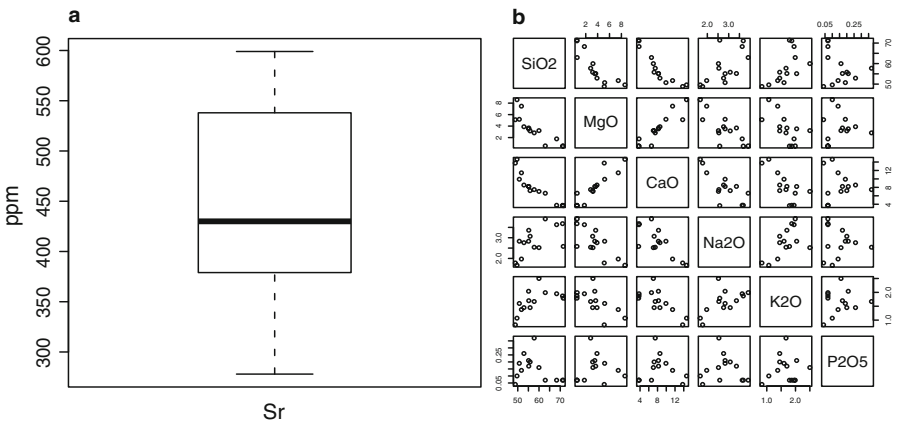


Fig. 2.1 **a** Boxplot of Sr distribution in the Sázava dataset (Exercise 2.4). **b** Scatterplot matrix for selected major-element oxides, plotted using the function `pairs`.

2.4 Classification and Grouping—Using Factors

Imagine that the studied plutonic complex consists of several igneous suites. Then whole-rock analysis for each sample can be accompanied by an indication as to which suite it belongs. A factor collecting this classification information enables, for instance, calculating an average *A/CNK* value for each of the suites separately. We should first demonstrate the definition of factors and then use them for increasingly difficult statistical and classification tasks.

2.4.1 Statistical Examination of Complex Data Sets

Statistical examination of complex geochemical data sets including, for instance, analyses for several intrusions, is tedious. Fortunately factors in R, in connection with the function `tapply`, offer a very flexible and elegant solution.



Exercise 2.5: Using factors to deal with complex datasets I

- a) For the Sázava dataset define a factor `intrusion` based on the specification given in the column ‘Intrusion’ that splits the suite into three groups: `basic` (quartz diorites to Amp gabbros of numerous smaller bodies), `Sazava` (Sázava intrusion proper: mainly Amp–Bt tonalites to quartz diorites) and `Pozary` (Požáry trondhjemite).
- b) Display all possible values (levels) of this factor.
- c) Using the factor `intrusion`, calculate the mean SiO_2 contents for each of the rock groups in the Sázava dataset.
- d) Analogously, calculate the mean concentrations of Ba.



`sazava.data`



```
> sazava <- read.table("sazava.data", sep="\t")

a) > intrusion <- factor(sazava[, "Intrusion"])
> intrusion
 [1] Sazava Sazava Sazava Sazava Sazava basic  basic  basic
 [9] basic  basic  Pozary Pozary Pozary Pozary
Levels: basic Pozary Sazava

b) > levels(intrusion)
 [1] "basic" "Pozary" "Sazava"

c) > tapply(sazava[, "SiO2"], intrusion, mean)
  basic Pozary Sazava
51.778 68.440 55.738

d) > tapply(sazava[, "Ba"], intrusion, mean)
  basic Pozary Sazava
  NA 1291.25  NA
```

In the last command, two of three groups gave NA because there are some missing values present:

```
> tapply(sazava[, "Ba"], intrusion, is.na)
$basic
 [1] FALSE FALSE  TRUE FALSE FALSE
$Pozary
 [1] FALSE FALSE FALSE FALSE
```



```
$Sazava
[1] FALSE FALSE TRUE FALSE FALSE
```

If the missing values are to be ignored and the mean for the remaining analyses calculated, we can pass the parameter `na.rm=TRUE` to the function `mean`:

```
> tapply(sazava[, "Ba"], intrusion, mean, na.rm=TRUE)
  basic Pozary Sazava
676.25 1291.25  682.25
```

The R language provides additional, arguably even more powerful tools. For instance, `aggregate` applies a given function to each of the variables (i.e., columns) of a numeric matrix or data frame \times respecting grouping (defined by a factor or list of factors). Analogous is the function `by`, which splits a data frame into several smaller ones based on a factor (or list of factors).



Exercise 2.6: Using factors to deal with complex datasets II

- Utilizing the function `summary`, calculate basic statistical parameters for SiO_2 distribution in each of the rock groups of the Sázava suite (factor `intrusion`).
- What are the means for selected trace elements (Ba, Rb, Sr and Zr) in individual intrusions?
- Using the function `by`, print basic statistical summaries for major-element oxides in each of the rock groups.



`sazava.data`



```
> sazava <- read.table("sazava.data", sep="\t")
> intrusion <- factor(sazava[, "Intrusion"])
```

```
a) > tapply(sazava[, "SiO2"], intrusion, summary)
$basic
  Min. 1st Qu.  Median    Mean 3rd Qu.    Max.
 48.84  49.63   51.72   51.78   52.90   55.80
$Pozary
  Min. 1st Qu.  Median    Mean 3rd Qu.    Max.
 62.95  66.96   69.69   68.44   71.17   71.42
$Sazava
  Min. 1st Qu.  Median    Mean 3rd Qu.    Max.
 50.72  55.09   55.17   55.74   57.73   59.98
```

```
b) > trace <- c("Rb", "Sr", "Ba", "Zr")
> aggregate(sazava[, trace], list(Rock=intrusion), mean,
+          na.rm=TRUE)
  Rock  Rb    Sr    Ba    Zr
1 basic 34.5 346.25 676.25 65.75
2 Pozary 59.5 460.75 1291.25 157.25
3 Sazava 60.5 522.00  682.25  61.00
```

```
c) > by(sazava[,7:17],list(Rock=intrusion),summary)
Rock: basic
      SiO2           TiO2           Al2O3
Min.   :48.84   Min.   :0.340   Min.   :13.34
1st Qu.:49.63   1st Qu.:0.670   1st Qu.:14.17 ... etc.
```



Groups in *GCDkit*

GCDkit allows each of the samples to be assigned to a group and these groups are subsequently utilised by statistical and plotting functions. Groups can be defined on the basis of a single label, a value of a numerical variable, position in classification diagram (e.g., TAS) or cluster analysis. In command line mode or a batch file it is simplest to use the *GCDkit* function `groupsByLabel`. The information regarding current grouping is stored in a vector `groups`; default grouping after loading a new data file or selecting a subset is on plotting symbol.

```
# GCDkit solution
GCDkit-> loadData("sazava.data")
GCDkit-> groupsByLabel("Intrusion")
      Sa-1      Sa-2      Sa-3      Sa-4      Sa-7      SaD-1
"Sazava" "Sazava" "Sazava" "Sazava" "Sazava"  "basic"...
Assigned groups:
  basic Pozary Sazava
    5      4      5
```



Statistics in complex datasets—the *GCDkit* way

Two functions provide basic statistical parameters for complex datasets with several groups, such as igneous suites (and optional plotting of histograms and/or boxplots): `summarySingleByGroup` (for a single variable) and `summaryByGroup` (several elements/oxides). If only the range of certain variable(s) is desired, use the function `summaryRangesByGroup`.

```
# Continuing from the previous example.. (output is omitted)
GCDkit-> summarySingleByGroup("SiO2")

GCDkit-> trace <- c("Rb","Sr","Ba","Zr")
GCDkit-> summaryByGroup(trace)
GCDkit-> summaryRangesByGroup(trace)

GCDkit-> summaryByGroup(major)
```

2.4.2 Conversion of Numeric Vectors to Factors

The function `cut` splits a numeric vector `x` into given number of intervals and codes its individual items according to the rank they fall into. So this function can be used for simple classification purposes.



Exercise 2.7: Classification using factors

- Classify samples in the Sázava set according to SiO₂ contents (wt. %) in four groups, U (< 45), B (45–52), I (52–63) and A (> 63).



sazava.data



```
> sazava <- read.table("sazava.data", sep="\t")
> silica <- cut(sazava[, "SiO2"], breaks=c(0, 45, 52, 63, 100),
+   labels=c("U", "B", "I", "A"))
> silica
[1] I I I B I I B B B I I A A A
Levels: U B I A
```

Note that the levels that do not occur in the data at all (here the ultrabasic rocks, U) are not dropped. If we want to know the classification of individual samples, we convert the factor `silica` to a character vector:

```
> acidity <- as.vector(silica)
> names(acidity) <- rownames(sazava)
> acidity
Sa-1   Sa-2   Sa-3   Sa-4   Sa-7   SaD-1   Gbs-1   Gbs-20
  "I"    "I"    "I"    "B"    "I"    "I"    "B"    "B"
Gbs-2  Gbs-3  Po-1   Po-3   Po-4   Po-5
  "B"    "I"    "I"    "A"    "A"    "A"
```



Grouping according to a single numeric variable

Similar task, i.e. classification of samples into several groups according to values of a numeric variable, is done by *GCDkit* function `cutMy`.

```
# GCDkit solution
GCDkit-> loadData("sazava.data")
GCDkit-> cutMy("SiO2", c(0, 45, 52, 63, 100), c("U", "B", "I", "A"))
      SiO2 Interval
Sa-1   59.98      I
Sa-2   55.17      I
Sa-3   55.09      I
Sa-4   50.72      B
Sa-7   57.73      I ...
```

2.4.3 Frequency (Contingency) Tables

A nifty application of factors enables the creation of frequency tables.



Exercise 2.8: Frequency tables

Continuing from the previous exercise, we demonstrate making frequency tables.

- a) Using the factor `intrusion`, count the number of analyses obtained from each of the rock groups in the Sázava dataset.
- b) Analogously, count the number of ultrabasic, basic, intermediate and acid rocks (factor `silica` from the previous exercise).
- c) Set up a frequency table showing the dependence of `silica` on the rock type.



[sazava.data](#)



```
> intrusion <- factor(sazava[, "Intrusion"])
```

```
a) > table(intrusion)
```

```
intrusion
  basic Pozary Sazava
      5      4      5
```

```
b) > table(silica)
```

```
silica
  U B I A
  0 4 7 3
```

```
c) > table(intrusion, silica)
```

```
          silica
intrusion U B I A
  basic   0 3 2 0
  Pozary  0 0 1 3
  Sazava  0 1 4 0
```

References

- Batchelor RA, Bowden P (1985) Petrogenetic interpretation of granitoid rock series using multicationic parameters. *Chem Geol* 48:43–55
- Chambers JM, Hastie TJ (1992) *Statistical models in S*. Chapman & Hall, London
- Clarke DB (1981) The mineralogy of peraluminous granites; a review. *Canad Mineral* 19:3–17
- Cross W, Iddings JP, Pirsson LV, Washington HS (1902) A quantitative chemico-mineralogical classification and nomenclature of igneous rocks. *J Geol* 10:555–690
- De La Roche H, Leterrier J, Grandclaude P, Marchal M (1980) A classification of volcanic and plutonic rocks using R_1R_2 -diagram and major element analyses—its relationships with current nomenclature. *Chem Geol* 29:183–210
- Debon F, Le Fort P (1983) A chemical-mineralogical classification of common plutonic rocks and associations. *Trans Roy Soc Edinb, Earth Sci* 73:135–149
- Debon F, Le Fort P (1988) A cationic classification of common plutonic rocks and their magmatic associations: principles, method, applications. *Bull Minéral* 111:493–510
- Frost BR, Frost CD (2008) A geochemical classification for feldspathic igneous rocks. *J Petrol* 49:1955–1969
- Frost BR, Barnes CG, Collins WJ, Arculus RJ, Ellis DJ, Frost CD (2001) A geochemical classification for granitic rocks. *J Petrol* 42:2033–2048

- Hutchison CS (1974) Laboratory handbook of petrographic techniques. John Wiley & Sons, New York
- Hutchison CS (1975) The norm, its variations, their calculation and relationships. *Schweiz mineral petrogr Mitt* 55:243–256
- Janoušek V (2001) Norman, a QuickBasic programme for petrochemical re-calculation of whole-rock major-element analyses on IBM PC. *J Czech Geol Soc* 46:9–13
- Janoušek V, Bowes DR, Rogers G, Farrow CM, Jelfinek E (2000) Modelling diverse processes in the petrogenesis of a composite batholith: the Central Bohemian Pluton, Central European Hercynides. *J Petrol* 41:511–543
- Janoušek V, Braithwaite CJR, Bowes DR, Gerdes A (2004) Magma-mixing in the genesis of Hercynian calc-alkaline granitoids: an integrated petrographic and geochemical study of the Sázava intrusion, Central Bohemian Pluton, Czech Republic. *Lithos* 78:67–99
- Le Bas MJ, Le Maitre RW, Streckeisen A, Zanettin B (1986) A chemical classification of volcanic rocks based on the total alkali-silica diagram. *J Petrol* 27:745–750
- Le Maitre RW (2002) *Igneous rocks: a classification and glossary of terms: recommendations of the International Union of Geological Sciences, Subcommission on the Systematics of Igneous Rocks*. Cambridge University Press, Cambridge
- Maindonald J, Braun J (2003) *Data analysis and graphics using R*. Cambridge University Press, Cambridge
- Mielke P, Winkler HGF (1979) Eine bessere Berechnung der Mesonorm für granitische Gesteine. *Neu Jb Mineral, Mh* 471–480
- Miller CF (1985) Are strongly peraluminous magmas derived from pelitic sources? *J Geol* 93:673–689
- Niggli P (1948) *Gesteine und Minerallagerstätten*. Birkhäuser, Basel
- Reimann C, Filzmoser P, Garrett R, Dutter R (2008) *Statistical data analysis explained: applied environmental statistics with R*. John Wiley & Sons, Chichester
- Rock NMS (1988) *Numerical geology. A source guide, glossary and selective bibliography to geological uses of computers and statistics*. Lecture Notes in Earth Sciences, vol 18. Springer, Berlin
- Shand SJ (1943) *Eruptive rocks. Their genesis, composition, classification, and their relation to ore-deposits with a chapter on meteorite*. John Wiley & Sons, New York
- van den Bogaard P, Tolosana-Delgado R (2013) *Analyzing compositional data with R*. Springer, Berlin
- Venables WN, Ripley BD (1999) *Modern applied statistics with S-Plus*. Springer, Berlin
- Verma SP, Torres-Alvarado IS, Sotelo-Rodriguez ZT (2002) SINCLAS: standard igneous norm and volcanic rock classification system. *Comput and Geosci* 28:711–715
- Verma SP, Torres-Alvarado IS, Velasco-Tapia F (2003) A revised CIPW norm. *Schweiz mineral petrogr Mitt* 83:197–216
- Villaseca C, Barbero L, Herreros V (1998) A re-examination of the typology of peraluminous granite types in intracontinental orogenic belts. *Trans Roy Soc Edinb, Earth Sci* 89:113–119

Chapter 3

Classical Plots

In this chapter, R recipes are presented to produce the most common graphs used in igneous geochemistry, such as binary plots (simple and multiple, e.g. Harker plots), ternary plots, spiderplots, classification and geotectonic diagrams. Especially for the latter two types, the text does not intend to be exhaustive. A comprehensive review can be found in Rollinson (1993) and in documentation/help to the *GCDkit* package (especially the file `diagrams.pdf`).

3.1 Binary Plots

The most common graph used in igneous geochemistry is a binary plot of two variables, linear or logarithmic. Often, as x axis serves some fractionation index, i.e. a chemical species mimicking the progressive development of the igneous suite studied (e.g., SiO_2 for felsic, and MgO or mg# for mafic rock associations).

3.1.1 Plotting Simple Binary Plots

We shall demonstrate here the use of the basic plotting and annotation capabilities of R. Appendix A contains all the necessary details, including the explanation of function `expression`, as well as of `abline` and `curve` that can be used for adding simple trends to the graphs.



Exercise 3.1: Simple binary plots

In this exercise we focus on graphical analysis of the Sázava dataset.

- Build a binary plot SiO_2 –CaO. Choose suitable ranges for the axes, label them and annotate data points by sample names. Assign the plotting symbols according to individual rock types (utilizing the pre-defined column “`Symbol`”).
- Plot a line $\text{SiO}_2/\text{CaO} = 10$ passing through origin $[0, 0]$.
- Plot a diagram $\log \text{Zr}$ – $\log \text{Ba}$ and fit the data points, using the least-square linear regression, by a straight line.



```

> sazava <- read.table("sazava.data",sep="\t")
> windows(width=10,height=5) # Empty window of correct size
> par(mfrow=c(1,2)) # Split screen for 2 graphs
> par(mar=c(4,4,1,1)) # Outer margins for all graphs

a) > plot(sazava[, "SiO2"],sazava[, "CaO"],cex=1.2,
+ xlab=expression(SiO[2]),ylab="CaO",
+ pch=sazava[, "Symbol"], xlim=c(49,75),ylim=c(0,15))
> text(sazava[, "SiO2"],sazava[, "CaO"],rownames(sazava),
+ pos=4,cex=0.7)

b) > abline(0,0.1)

c) > plot(sazava[, "Zr"],sazava[, "Ba"],xlab="Zr",ylab="Ba",
+ pch=15,cex=1.5,log="xy")
> lq <- lm(log10(sazava[, "Ba"])~log10(sazava[, "Zr"]))
> # lq is an arbitrary variable name
> # note the logarithms of the base 10 in the formula
> lq
Call:
lm(formula = log10(sazava[, "Ba"]) ~ log10(sazava[, "Zr"]))
Coefficients:
      (Intercept)  log10(sazava[, "Zr"])
          1.1994              0.8847
> abline(lq,lty=2,lwd=2,col="darkgreen")
    
```

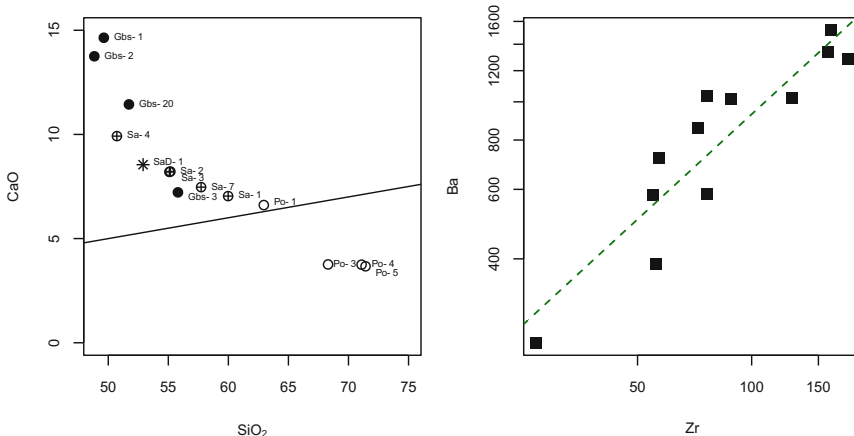


Fig. 3.1 Binary plots from the Sázava dataset (Exercise 3.1). On the right is displayed the linear regression computed using the function `lm` and plotted by the function `abline`.

```

We shall provide the GCDkit solution as well:
GCDkit-> loadData("sazava.data")
GCDkit-> binary("SiO2", "CaO", cex=1.2)
GCDkit-> abline(0,0.1)
    
```



Plot editing from the command prompt

Owing to the fact that most of the single plots in *GCDkit* are in fact *Figaro* templates (see Appendix B), they can be post-processed, i.e. many of their properties altered using functions from the menu *Plot editing*. They can also be modified directly from a command line or batch file. Moreover, function `figUser` enables setting several graphical parameters at once (that are to be separated by semicolons)¹, including those for which no separate “`figSomething`” commands are available (see `?par` for their meaning). In addition, `figIdentify` can be used to (interactively) label the datapoints on the active graph. Do not forget to click on “Stop” when you are done.

For a list of further available functions and more detailed explanation, see help pages to `figEdit`, `figColours`, `figScale`, `figZoom` and `figUser`.

On our Zr–Ba graph we can demonstrate post-processing of a single *GCDkit* plot:

```
GCDkit-> binary("Zr", "Ba", log="xy", pch=15, cex=1.5,
+             col="black", fit=TRUE)
GCDkit-> figMain("Demonstration") # Add main title
GCDkit-> figXlab("Zirconium (ppm)") # Modify x axis label
GCDkit-> figCol("darkred")        # Colour of symbols
GCDkit-> figCex(2)                 # Size of symbols
GCDkit-> figCexLab(0.8)            # Scaling of axes labels
GCDkit-> figCexMain(1.5)          # Size of main title
GCDkit-> figXlim(c(10,300))       # Limits of the x axis
GCDkit-> figUser("pch="+\"")      # Plotting symbol
GCDkit-> figUser("main=\"My plot\"; las=2; bg=\"khaki\";
+             font.main=4; cex.main=2; col.main=\"blue\"")
GCDkit-> figBw() # Set everything to black and white
```



Annotating plots in *GCDkit*

GCDkit provides a function `annotate` “guessing” the correct formatting of axis labels or of other text strings. It is called silently by many plotting functions in the system; see, for instance:

```
GCDkit-> binary("K2O/Na2O", "Al2O3")
```



Plotting results of numeric calculations

So far we have plotted only numeric data stored internally by the *GCDkit* variable `WR`. In fact, it is also rather simple to plot the results of calculations (such as the output of a normative scheme). This involves three steps: calculation, appending the results to the data (using function `addResults`) and plotting as usual.

¹ NB that the argument to `figUser` is a single text string. Thus any quotation marks therein have to be preceded by an escape character, i.e. the backslash.

Here is an example of a CIPW-normative Ab–Q–Or ternary plot:

```
GCDkit-> loadData("sazava.data")
GCDkit-> results <- CIPW(WR)
GCDkit-> addResults()
GCDkit-> ternary("Ab", "Q", "Or")
```

3.1.2 Constant Sum Effect (Closure)

Numerous workers have argued that much of correlation observed in binary plots involving silica is spurious, due to the constant sum effect (e.g., Chayes 1960; Skala 1979; Rock 1988; Rollinson 1992, 1993). This effect arises from the fact that major elements sum up to 100 % and thus, if one oxide increases in abundance, all others must decrease. Therefore, everything must be anti-correlated with silica. In any binary diagram (especially using SiO_2 which is the most abundant component), this results in formation of a “Forbidden zone”, into which no analyses could plot (Harker 1909) (Fig. 3.2a).

One solution to this problem has been proposed by Bonin (1986) who introduced the SiO_2 vs. oxide^* plots (Fig. 3.2b), where oxide^* represents the proportion of the relevant oxide in the non-silica portion of the rock (in wt. %):

$$\text{oxide}^* = 100 \times \frac{\text{oxide}}{(100 - \text{SiO}_2)} \quad (3.1)$$

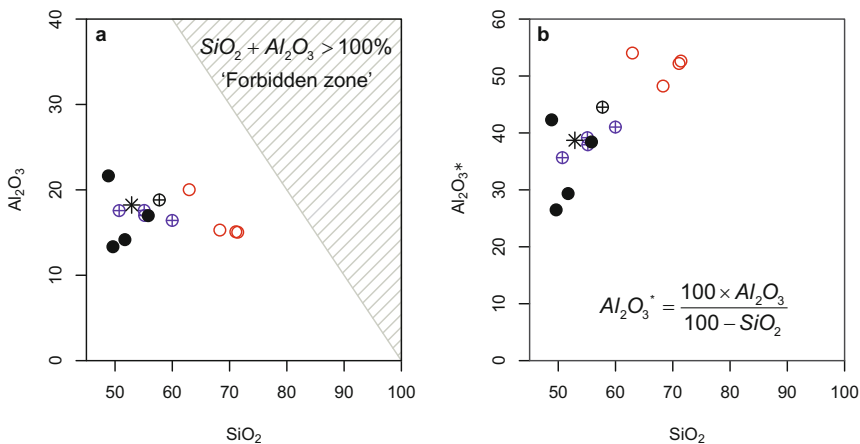


Fig. 3.2 Derivation of an oxide^* diagram for the Sázava dataset. **a** Alumina plotted in wt. %. Note the “Forbidden zone”, approached by the trend as differentiation progresses, meaning that Al_2O_3 becomes an increasingly important part of the “non-silica” portion of the rock. This is underlined by the sharp increase in Al_2O_3^* (**b**).

Another possibility is to measure the distance between the analyses and a reference trend at the same SiO_2 contents. Liégeois et al. (1998) invoked *sliding normalization* against a reference series fitted by a second-order polynomial. Moyen et al. (2009) defined a parameter Δ , a *distance* from a reference line in the Harker plot. Another classic numerical remedy is *log-ratio transformations* (Aitchison 1986). See Reimann et al. (2008) with van den Bogaard and Tolosana-Delgado (2013) for details and van den Boogaart and Tolosana-Delgado (2008) for R implementation.

3.2 Harker Plots and Other Basic Multiple Plots

One of the most useful, most commonly employed and at the same time most questioned graphs in igneous geochemistry are the Harker plots, i.e. binary plots of silica versus major-element oxides.



Exercise 3.2: Harker plots

- Using a loop and function `par(mfrow)`, write a short program that would plot six binary plots of SiO_2 vs. major-element oxides of your choice.



sazava.data



```
> sazava <- read.table("sazava.data",sep="\t")
> windows(width=8,height=6)
> par(mfrow=c(2,3)) # Split screen for 6 graphs
> ee <- c("Al2O3", "MgO", "CaO", "Na2O", "K2O", "P2O5")
> for(f in ee) {
>   plot(sazava[, "SiO2"], sazava[, f], xlab="SiO2", ylab=f,
+       pch=sazava[, "Symbol"], cex=1.5)
> }
```

We can prepare a more sophisticated version of this program, using annotations provided by `expression` in conjunction with the function `parse`. The code would then be:

```
> windows(width=8,height=6)
> par(mfrow=c(2,3))
> lab <- c("Al[2]*O[3]", "MgO", "CaO", "Na[2]*O", "K[2]*O",
+         "P[2]*O[5]")
> for(f in 1:length(ee)) {
>   plot(sazava[, "SiO2"], sazava[, ee[f]],
+       xlab=expression(SiO[2]),
+       ylab=parse(text=as.expression(lab[f])),
+       pch=sazava[, "Symbol"], cex=1.5)
> }
```

And a *GCDkit* solution is:

```
GCDkit-> loadData("sazava.data")
GCDkit-> multiple("SiO2", "Al2O3, MgO, CaO, Na2O, K2O, P2O5")
```

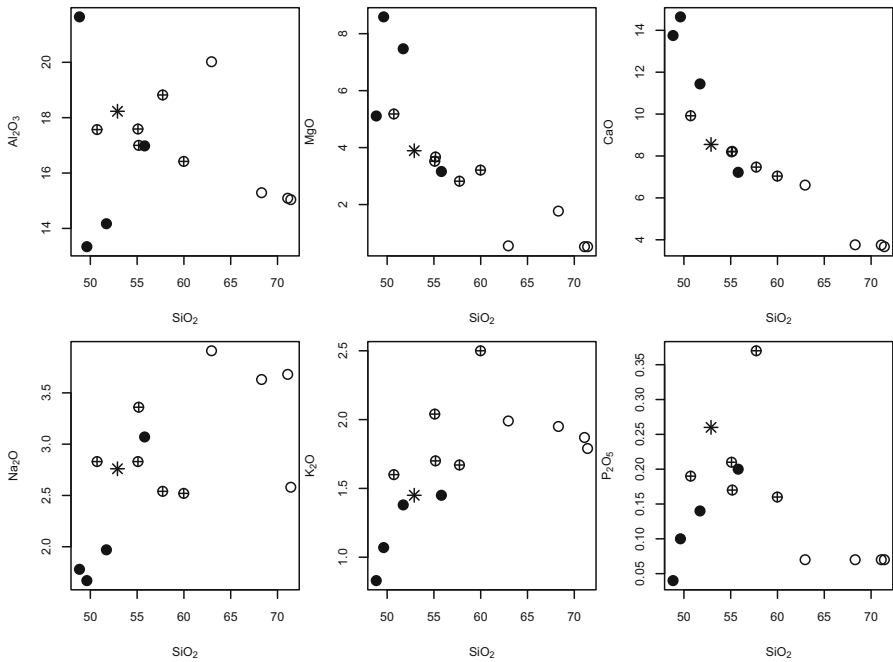


Fig. 3.3 Selected Harker plots from the Sázava dataset (Exercise 3.2).

3.3 Ternary Plots

Ternary plots rank among important and widely used geochemical tools. Setting the sides of the triangle to equating a unity, its vertices (bottom-left, top, and bottom-right) have $[x, y]$ coordinates of $A[0, 0]$, $B[0.5, \sqrt{3}/2]$ and $C[1, 0]$. The ternary coordinates $[a, b, c]$ of a data point X can be transformed to binary ones $[x, y]$ (Fig. 3.4) as follows:

$$x = 1 - a - \frac{b}{2} \quad \text{and} \quad y = \frac{\sqrt{3}}{2} b. \quad (3.2)$$

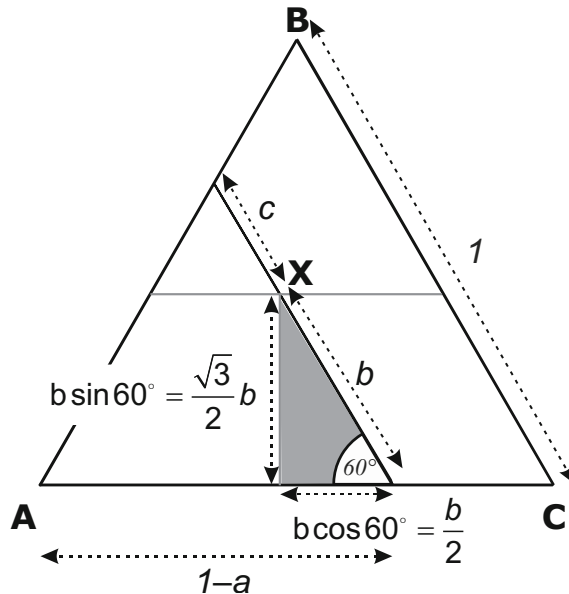


Fig. 3.4 Ternary diagram—plotting ternary $[a, b, c]$ data points in binary $[x, y]$ coordinates.

We can now use standard R functions for binary plot; the trick is that (binary) axes are not shown and triangle outline is drawn using `lines`.



Exercise 3.3: Ternary plots

- a) Design a function plotting ternary diagrams.
- b) Display a Ba–Rb–Sr ternary plot for the Sázava suite.



```
a) > tri <- function(alab,blab,clab) {
>   sums <- apply(sazava[,c(alab,blab,clab)],1,sum)
>   a <- sazava[,alab]/sums
>   b <- sazava[,blab]/sums
>   plot(1-a-b/2,sqrt(3)*b/2,xlab="",ylab="",xlim=c(0,1),
+       ylim=c(0,1),axes=FALSE,asp=1)
>   # axes=FALSE: no plotting of axes; asp: aspect ratio
>   x1 <- c(0,1,.5,0)
>   y1 <- c(0,0,sqrt(3)/2,0)
>   lines(x1,y1)
>   text(-0.05,0,alab)
>   text(1.05,0,clab)
>   text(0.5,sqrt(3)/2+0.05,blab)
> }
```

```
b) > sazava <- read.table("sazava.data", sep="\t")
> tri("Ba", "Rb", "Sr")
```

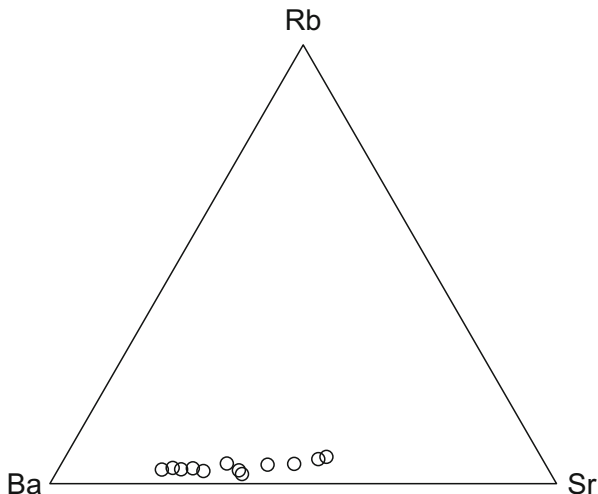


Fig. 3.5 Ternary diagram Ba–Rb–Sr for analyses of the Sázava suite (Exercise 3.3).

```
GCDkit-> loadData("sazava.data")
GCDkit-> ternary("Ba", "Rb", "Sr", pch=1)
```

3.4 Classification Plots in *GCDkit*

Classification diagrams play an important role in the life of igneous geochemists. The traditional way of their programming would be to define each of the fields as a set of Boolean conditions. This is tedious, and for some diagrams with irregular boundaries nearly impossible. Moreover, such a code is prone to errors.

Fortunately *GCDkit* comes with a revolutionary solution to this problem. The *Figaro* templates defined for classification plots consist of sets of closed polygons. Then the general classification algorithm² looks for the name of the polygon into which the rock analysis falls according to x–y coordinates, returning its name.

Of course, the templates could not only be binary, but also ternary graphs. They are drawn by the function `plotDiagram` that can be invoked with several parameters, the most important being the first two—the name of the template and a logical value controlling whether a sample selection dialogue is to be invoked (see `?plotDiagram`):

```
GCDkit-> loadData("sazava.data")
GCDkit-> plotDiagram("LarochePlut", FALSE)
```

² Function `classify` with essentially a GIS-like capability, based on the package `sp` written by Edzer Pebesma, Roger Bivand and others.

Classification on the basis of the current diagram can be requested from menu *Plot editing*|*Classify* or, if the template name is specified as an argument, by the function `classify`:

```
GCDkit-> classify("LarochePlut")
Samples classified by: R1 - R2 (De la Roche et al. 1980)
      diorite          gabbro  gabbro-norite
           4              1          1
gabbrodiorite  granodiorite ultramafic rock
           3              2          1
      unclassified
           2
      LarochePlut
Sa-1  "diorite"
Sa-2  "gabbrodiorite"
Sa-3  "gabbrodiorite" ... etc.
```

A vector of resulting rock names is stored in a variable `results`. The analyses falling outside the defined polygons are labelled as 'unclassified'.



Needless to say that the classification diagrams are often misused—and it is a responsibility of each user to become familiar with the original work and use the given scheme as appropriate.

3.5 Geotectonic Diagrams

Deciphering the tectonic setting of ancient igneous suites is of great scientific and practical interest. One of the key tools, geotectonic diagrams, gained popularity with improving analytical facilities in 1970–1980's (e.g., Pearce and Cann 1973; Pearce and Norry 1979; Wood 1980; Shervais 1982; Mullen 1983; Pearce et al. 1984; Meschede 1986 – see Rollinson 1993 for review). Originally the diagrams were largely empirical and the discrimination boundaries fitted by eye, but rigorous statistical treatment including (linear or quadratic) discriminant analysis has become increasingly popular (Vermeesch 2006).

Geotectonic diagrams tend to work because rocks from similar tectonic settings are likely to have formed by the same combination of sources and processes. The problem is that several prior assumptions have to be made (often silently):

- the studied suite had a geotectonic position that can be compared with some of simple settings predicted by the global tectonics paradigm (thus the diagrams are not usable for Archaean rocks or suites from complex settings),
- its geochemical signature has not been significantly modified by processes such as fractional crystallization, crystal accumulation or magma mixing,
- elemental mobility during alteration/weathering can be neglected,
- analytical determinations are precise enough, often at sub-ppm level.

After the initial adoration, geotectonic diagrams became evil for many colleagues, while others proposed schemes in which the geochemical rationale vanished to be replaced by abstract, and rather mechanical, statistical treatment (Verma and Rivera-Gómez 2013; Verma et al. 2013 and references therein).

In our view, some classic diagrams are useful, especially if the original definition and scope are strictly adhered to. Fruitful seems the concept of spiderplot-based geochemical proxies (elemental ratios), advocated by J. Pearce. These may constrain, for instance, the depth of melting, the degree of mantle enrichment, or of contamination by subduction-related fluids/melts. For example of application to back-arcs and ophiolites, see Pearce and Stern (2006) and Pearce (2008, 2014).

Selected, presumably little mobile elements from basic lavas are the most valuable, as the parental magmas come from a primary source (mantle) and do not originate by recycling of crustal material (Pearce 1996a). On the other hand, acid igneous rocks—especially collisional granitoids—are often generated from several times recycled crustal materials and may inherit the signature of the older source(s) (Arculus 1987; Förster et al. 1997). Any danger of misinterpretation can be minimized if the geology, petrology, age and whole geochemical signature are all taken into account (Barbarin 1990; Bonin 1990; Pearce 1996b; Clemens 2012).



GCDkit comes with many geotectonic diagrams (see `diagrams.pdf` in the help system for their overview). Please note that these templates are somewhat restricted in use, e.g. they cannot be employed for classification.

3.6 Spiderplots

Geochemists often like to express the compositional differences between the studied sample and given geochemical reservoir in the form of so-called spiderplots (also known as spiderdiagrams/spidergrams or (better) multi-element diagrams). Spiderplots allow representing much of the sample's composition on a single graph. Technically these are logarithmic plots of elemental concentrations (allowing comparison of concentrations that differ by several orders of magnitude) in the sample divided (normalized) by those in the selected standard. The order of the elements along the axis is critical as it can by itself generate artificial anomalies (Dupré et al. 1994). Normally, the elements are arranged in a logical sequence according to their geochemical behaviour (often based on bulk distribution coefficients, with the more incompatible ones on the left) (Hofmann 1988) (see also Sect. 21.2).

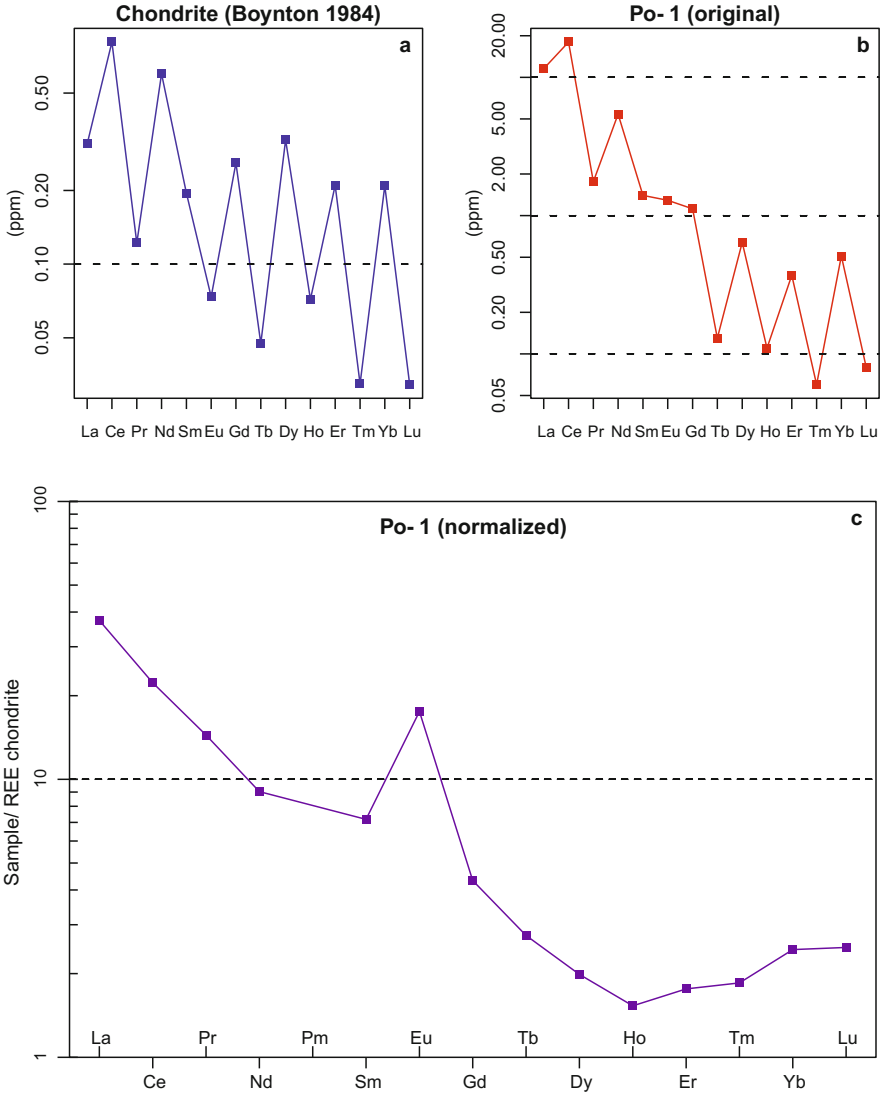


Fig. 3.6 a–b All Solar System material shows a zigzag pattern of elemental abundances (here, REE). This so-called Oddo-Harkins effect reflects the processes during nucleosynthesis and the overall stability of elements in the Universe. Here are shown the un-normalized patterns (ppm) for average chondrite meteorites (Boynton 1984) and the Požáry trondhjemite Po-1 from the Sázava dataset. **c** Normalization to a common reference (chondrites in this case) compensates for this effect and allows focusing on differences between individual terrestrial rocks.

The added value of spiderplots consists in elimination of the Oddo-Harkins effect: in the Solar System, the abundances of even-numbered elements are greater than those of neighbouring odd-numbered ones. Moreover, abundances generally decrease with increasing atomic number. Non-normalized data thus show zigzag, slightly sloped patterns (Fig. 3.6a–b). Normalized patterns (spiderplots) smooth out such differences (Fig. 3.6c).

There are many normalization schemes currently in use, differing by elements considered, their order and values. Arguably the most common schemes are:

- Chondrites (or “Bulk Silicate Earth”). An all-purpose normalization. Commonly found in two versions, REE only or extended (including LILE and HFSE).
- Primitive Mantle (conceptually, before the extraction of continental crust) (Sun and McDonough 1989; McDonough and Sun 1995).
- Normal Mid-Ocean Ridge Basalts (NMORB). Obviously useful for basalts, and specifically for those of ocean-floor or subduction settings (Sun and McDonough 1989; Pearce 2014).
- Ocean-Island Basalts (for intraplate settings).
- Averages of various crustal reservoirs, such as Continental Crust, Upper Crust or Lower Crust (Taylor and McLennan 1985, 1995).
- Ocean Ridge Granites (ORG)—used in studying granites (Pearce et al. 1984).

The other possibility is to normalize by the most primitive sample of your suite (a nice way to show the progressive differentiation or elemental mobility during alteration!). Moreover, there are specialized normalizing schemes for some elemental groups, such as Platinum Group Elements (PGE) (see Rollinson 1993 and references therein for a review of the commonly used schemes).

For plotting the spiderplots in R, the trick consists in using `plot` with `axes = FALSE` argument, then drawing the custom axes by the separate `axis` command.



Exercise 3.4: Spiderplots

The arguably most commonly used spiderplots are chondrite-normalized REE plots (e.g., Table 3.1).

Table 3.1 REE contents in C1 chondrites (Boynnton 1984)

La	Ce	Pr	Nd	Sm	Eu	Gd
0.31	0.808	0.122	0.6	0.195	0.0735	0.259
Tb	Dy	Ho	Er	Tm	Yb	Lu
0.0474	0.322	0.0718	0.21	0.0324	0.209	0.0322



[boynnton.data](#)
[sazava.data](#)

- a) Write a function that would normalize REE concentrations in the sample by chondritic contents (stored in a comma-delimited file `boynton.data`).
- b) Calculate the normalized REE concentrations for analyses of the Sázava suite and display—using the functions `plot`, `axis`, `points` and `lines`—spiderplots for two Požáry trondhjemites, Po-1 and Po-4.



```
a) > x <- read.table("boynton.data", sep=",")
> chondrite <- as.numeric(x) # conversion to numeric vector
> names(chondrite) <- names(x)

> norm <- function(x, chon){ # normalizing function
>   z <- t(x[,names(chon)])/chon
>   return(z)
> }

b) > sazava <- read.table("sazava.data", sep="\t")
> y <- norm(sazava, chondrite) # normalized values
> plot(y[, "Po-1"], type="o", log="y", axes=FALSE, xlab="",
+   ylab="REE/chondrite", ylim=c(0.1, 100), col="darkgreen")
> axis(1, 1:length(chondrite), labels=names(chondrite),
+   cex.axis=0.75)
> axis(2, cex.axis=0.75)
> points(y[, "Po-4"], col="blue")
> lines(y[, "Po-4"], col="blue")
> abline(h=(10^(-1:3)), lty="dashed") # grid
> box() # bounding box
```

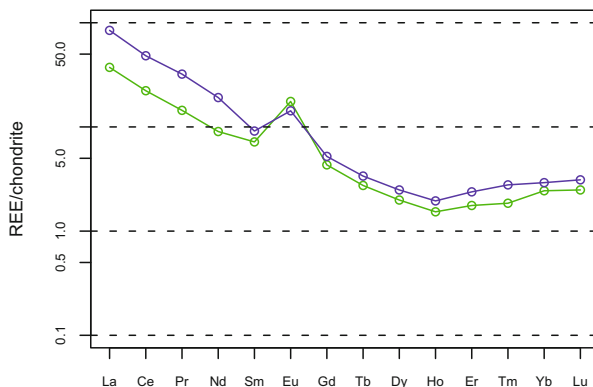


Fig. 3.7 Chondrite-normalized REE patterns for two Požáry trondhjemites (Exercise 3.4).



Plotting spiderplots in *GCDkit*

The preceding exercise can be reproduced easily, using the mother-of-all spiderplot functions in *GCDkit*, `spider`. To see normalization schemes available in *GCDkit*, type `?selectNorm`. Specialized spiderplots are dealt with in Chap. 4.2. You can try some of the examples below (see `?spider` for more, including a complete list of arguments and different ways to define the norm to use).

```
GCDkit-> loadData("sazava.data")
GCDkit-> spider(WR[c("Po-1", "Po-4"), ], "Boynton", 1, 500,
+             pch=1:2, col=1:2, legend=TRUE)
GCDkit-> spider(WR, "Boynton", field=TRUE, fill.col=TRUE,
+             shaded.col="khaki", 0.1, 1000)
GCDkit-> spider(WR, "Boynton", 0.1, 1000, pch=labels$Symbol,
+             col=labels$Colour)
GCDkit-> spider(WR, "Boynton", field=TRUE, density=0.02,
+             angle=45, col="gray", fill.col=FALSE, add=TRUE)
```

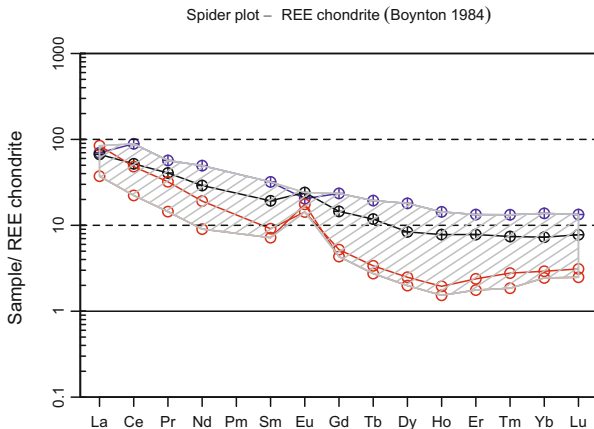


Fig. 3.8 Example of a chondrite-normalized REE spiderplot as produced by *GCDkit*.

3.7 Multiple Plots by Groups

GCDkit employs the concept of plates for collections of two or more (originally) stand-alone plots in a single plotting window. Typical examples are Harker plots, or diagrams using the same template plotted for individual data groups. To menu *Plots|Multiple plots by groups* is attached the function `figMulti` that displays a grid of plots, one for each of the groups in the current dataset, based on the most recently plotted single diagram template. These may be binary or ternary plots—including the complex templates of classification or geotectonic plots—or even spiderplots.

```
GCDkit-> loadData("sazava.data")
GCDkit-> groupsByLabel("Intrusion")
GCDkit-> plotDiagram("LarochePlut", FALSE)
GCDkit-> figRemove() # Less cluttered, no field labels
GCDkit-> figMulti(nrow=1, ncol=3)
# Three plots in a single row
```

Properties of the whole plate or all its diagrams can be changed simultaneously, using the `plate...()` functions. For instance:

```
GCDkit-> plateCex(2)      # symbols size, the whole plate
GCDkit-> plateCexMain(2)  # main title
GCDkit-> plateCexLab(1.8) # axis labels size
GCDkit-> plateBW()       # set plate to black and white
```

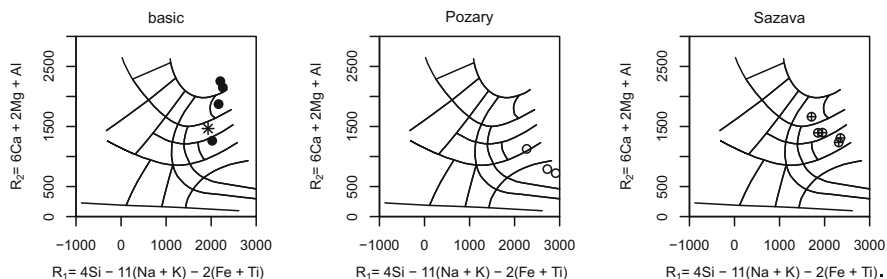


Fig. 3.9 Multiple plot for individual rock groups in the Sázava dataset. It is based on the *GCDkit* template for multicaticonic classification of De La Roche et al. (1980) with textual labels of fields intentionally omitted.

In order to retrieve a single diagram from a plate, use the function `plateExtract(diagram, which=NULL, ...)`, that draws the graph specified by a sequence number (`which`) from the plate diagram. For example:

```
GCDkit-> plateExtract("PearceGranite", 2)
# Second plot of Pearce et al. (1984)
```

References

- Aitchison J (1986) The statistical analysis of compositional data. Methuen, New York
- Arculus RJ (1987) The significance of source versus process in the tectonic controls of magma genesis. *J Volcanol Geotherm Res* 32:1–12
- Barbarin B (1990) Granitoids: main petrogenetic classifications in relation to origin and tectonic setting. *Geol J* 25:227–238
- Bonin B (1986) Ring complexes and anorogenic magmatism. Elsevier, Amsterdam
- Bonin B (1990) From orogenic to anorogenic settings: evolution of granitoid suites after a major orogenesis. *Geol J* 25:261–270
- Boynton WV (1984) Cosmochemistry of the rare earth elements: meteorite studies. In: Henderson P (ed) *Rare Earth Element Geochemistry*. Elsevier, Amsterdam, pp 63–114
- Chayes F (1960) On correlation between variables of constant sum. *J Geophys Res* 65:4185–4193
- Clemens JD (2012) Granitic magmatism, from source to emplacement: a personal view. *Applied Earth Science (Trans Inst Min Metall B)* 121:107–136
- De La Roche H, Leterrier J, Grandclaude P, Marchal M (1980) A classification of volcanic and plutonic rocks using R1R2–diagram and major element analyses—its relationships with current nomenclature. *Chem Geol* 29:183–210
- Dupré B, Schiano P, Polve M, Joron JL (1994) Variability; a new parameter which emphasizes the limits of extended rare earth diagrams. *Bull Soc Géol France* 165:3–13

- Förster H-J, Tischendorf G, Trumbull RB (1997) An evaluation of the Rb vs. (Y + Nb) discrimination diagram to infer tectonic setting of silicic igneous rocks. *Lithos* 40:261–293
- Harker A (1909) *The natural history of igneous rocks*. Methuen & Co., London
- Hofmann AW (1988) Chemical differentiation of the Earth: the relationship between mantle, continental crust, and oceanic crust. *Earth Planet Sci Lett* 90:297–314
- Liégeois J-P, Navez J, Hertogen J, Black R (1998) Contrasting origin of post-collisional high-K calc-alkaline and shoshonitic versus alkaline and peralkaline granitoids. *Lithos* 45:1–28
- McDonough WF, Sun S (1995) The composition of the Earth. *Chem Geol* 120:223–253
- Meschede M (1986) A method of discriminating between different types of mid-ocean ridge basalts and continental tholeiites with the Nb–Zr–Y diagram. *Chem Geol* 56:207–218
- Moyen JF, Champion D, Smithies RH (2009) The geochemistry of Archaean plagioclase-rich granites as a marker of source enrichment and depth of melting. *Earth Environ Sci Trans R Soc Edinb* 100:35–50
- Mullen ED (1983) MnO/TiO₂/P₂O₅: a minor element discriminant for basaltic rocks of oceanic environments and its implications for petrogenesis. *Earth Planet Sci Lett* 62:53–62
- Pearce JA (1996a) A user's guide to basalt discrimination diagrams. In: Wyman DA (ed) *Trace element geochemistry of volcanic rocks: applications for massive sulphide exploration*. Geological Association of Canada, Short Course Notes, vol 12, pp 79–113
- Pearce JA (1996b) Sources and settings of granitic rocks. *Episodes* 19:120–125
- Pearce JA (2008) Geochemical fingerprinting of oceanic basalts with applications to ophiolite classification and the search for Archean oceanic crust. *Lithos* 100:14–48
- Pearce JA (2014) Immobile element fingerprinting of ophiolites. *Elements* 10:101–108
- Pearce JA, Cann JR (1973) Tectonic setting of basic volcanic rocks determined using trace element analyses. *Earth Planet Sci Lett* 19:290–300
- Pearce JA, Norry MJ (1979) Petrogenetic implications of Ti, Zr, Y, and Nb variations in volcanic rocks. *Contrib Mineral Petrol* 69:33–47
- Pearce JA, Stern RJ (2006) Origin of back-arc basin magmas: trace element and isotope perspectives. In: Christie DM, Fisher CR, Lee S-M, Givens S (eds) *Back-arc spreading systems: geological, biological, chemical, and physical interactions*. Geophysical Monograph Series, vol 166. American Geophysical Union, pp 63–86
- Pearce JA, Harris NBW, Tindle AG (1984) Trace element discrimination diagrams for the tectonic interpretation of granitic rocks. *J Petrol* 25:956–983
- Reimann C, Filzmoser P, Garrett R, Dutter R (2008) *Statistical data analysis explained: applied environmental statistics with R*. John Wiley & Sons, Chichester
- Rock NMS (1988) *Numerical geology. A source guide, glossary and selective bibliography to geological uses of computers and statistics*. Lecture Notes in Earth Sciences, vol 18. Springer, Berlin
- Rollinson HR (1992) Another look at the constant sum problem in geochemistry. *Mineral Mag* 56:469–475
- Rollinson HR (1993) *Using geochemical data: evaluation, presentation, interpretation*. Longman, London
- Shervais JW (1982) Ti–V plots and the petrogenesis of modern and ophiolitic lavas. *Earth Planet Sci Lett* 59:101–118
- Skala W (1979) Some effects of the constant-sum problem in geochemistry. *Chem Geol* 27:1–9
- Sun SS, McDonough WF (1989) Chemical and isotopic systematics of oceanic basalts: implications for mantle composition and processes. In: Saunders AD, Norry M (eds) *Magmatism in the ocean basins*. Geological Society of London Special Publications, vol 42, pp 313–345
- Taylor SR, McLennan SM (1985) *The continental crust: its composition and evolution*. Blackwell, Oxford
- Taylor SR, McLennan SM (1995) The geochemical evolution of the continental crust. *Rev Geophys* 33:241–265
- van den Boogaart KG, Tolosana-Delgado R (2008) “compositions”: a unified R package to analyze compositional data. *Comput and Geosci* 34:320–338

- van den Bogaard P, Tolosana-Delgado R (2013) *Analyzing compositional data with R*. Springer, Berlin
- Verma SP, Rivera-Gómez MA (2013) New computer program TecD for tectonomagmatic discrimination from discriminant function diagrams for basic and ultrabasic magmas and its application to ancient rocks. *J Iber Geol* 39:167–179
- Verma SP, Pandarinath K, Verma SK, Agrawal S (2013) Fifteen new discriminant-function-based multi-dimensional robust diagrams for acid rocks and their application to Precambrian rocks. *Lithos* 168–169:113–123
- Vermeesch P (2006) Tectonic discrimination diagrams revisited. *Geochem Geophys Geosyst* 7:Q06017
- Wood DA (1980) The application of a Th–Hf–Ta diagram to problems of tectonomagmatic classification and to establishing the nature of crustal contamination of basaltic lavas of the British Tertiary volcanic province. *Earth Planet Sci Lett* 50:11–30

Chapter 4

Specialized Plots

This chapter presents several other types of geochemical plots that are implemented in *GCDkit*. It does not aim at being systematic and comprehensive; instead it focusses on arguably the most useful or interesting among them that could be suitable for common applications in igneous geochemistry.

4.1 Log–log Binary Plots

Plotting a binary plot in logarithmic coordinates enables examining both the elemental concentrations and their ratios. In this projection the fan of lines passing through the origin corresponding to analyses of constant ratio in a standard binary plot (Fig. 4.1a) is transformed into a series of parallel lines of identical slope in logarithmic coordinates (Fig. 4.1b). In R, log–log diagrams are plotted using the function `plot`, specifying `log = "xy"`.

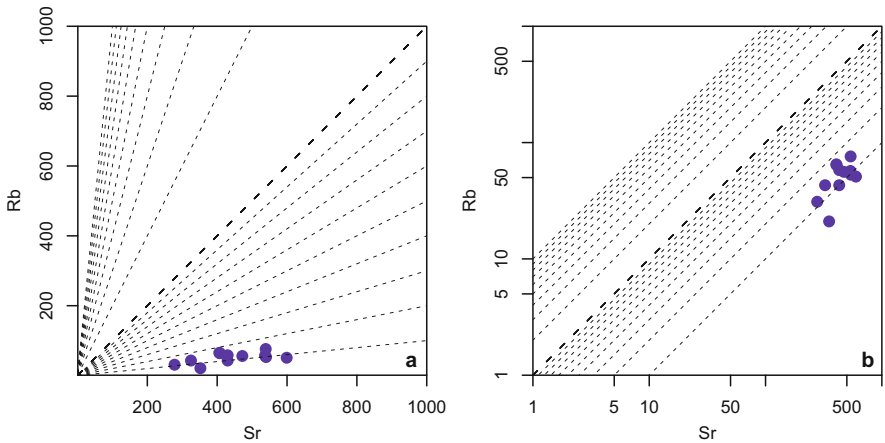


Fig. 4.1 Using log–log diagrams to depict values and ratios. **a** A linear scale diagram. Dashed lines (going through the origin) correspond to $Rb/Sr = 0.1, 0.2, \dots, 0.9, 1, 2, 3, \dots$ to 10. **b** The same diagram on a log–log scale.

4.2 Specialized Spiderplots

Apart from the standard spiderplots with patterns for individual samples or (semi-transparent) shaded/hatched fields for several of them, *GCDkit* produces also some specialized types of this graph. For instance, the colours of individual patterns can be coded according to an independent conditioning variable, such as SiO_2 or MgO (function `spider.contour`, Fig. 4.2a). Or a set of spiderplots, for each group one, can be obtained using the function `figMulti`, such as:

```
GCDkit-> loadData("sazava.data")
GCDkit-> groupsByLabel("Intrusion")
GCDkit-> spider(WR, "Boynton", 1, 100, pch=labels$Symbol,
+             col=labels$Colour, cex=2)
GCDkit-> figMulti(nrow=1, ncol=3, plot.symb=TRUE)
```

Here, the shaded field indicates the overall variation in the whole dataset.

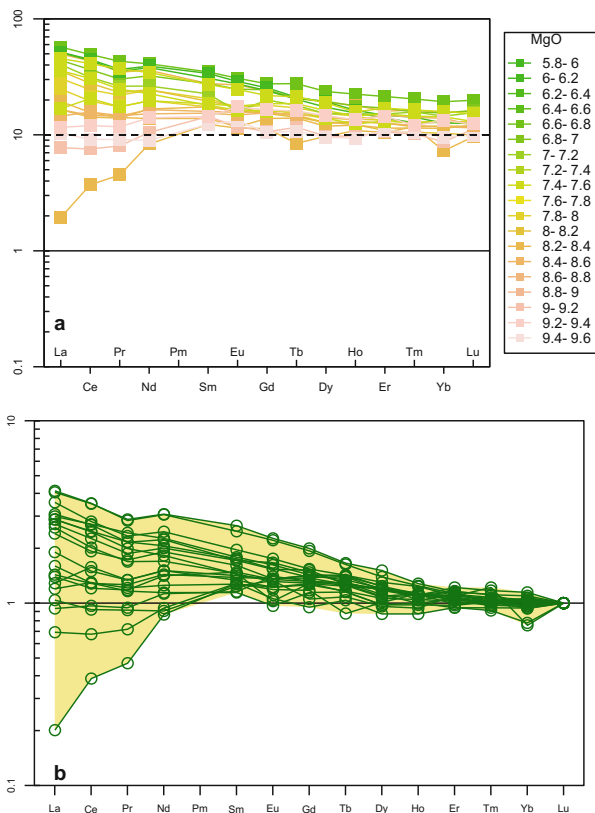


Fig. 4.2 Chondrite-normalized (Boynton 1984) REE patterns for dolerites from the Devonian Vrbno Group, Silesia (Czech Republic) (Janoušek et al. 2014) colour-coded by MgO contents (a) and double-normalized (Sect. 4.2.1) (setting $\text{Lu}_N = 1$) (b).

4.2.1 Double-Normalized Spiderplots

The double-normalized spiderplots strip effects of fractional crystallization from a source-related variation produced by partial melting (Thompson et al. 1983; Pearce et al. 2005; Pearce and Stern 2006). As a first step, trace-element data are normalized by the given reservoir, as for a common spiderplot. Then these normalized concentrations are re-adjusted so that the normalized content of the selected element in each analysis equals to a desired value (typically unity) (Fig. 4.2b). Double-normalized spiderplots are plotted by the function `spider2norm`.

4.2.2 Spider Boxplots, Spider Box and Percentile Plots

With increasing number of samples plotted, spiderplots soon become cluttered, obstructing any significant geochemical patterns present. This led Janoušek et al. (2004) to design a diagram useful for comparison of multielement patterns of large data sets, especially if containing large proportion of missing data. In these ‘*spider boxplots*’, no individual patterns are drawn. Instead, the statistical distribution of each element is portrayed by a boxplot, and thus the minima, maxima, quartiles, median and outliers are immediately seen.

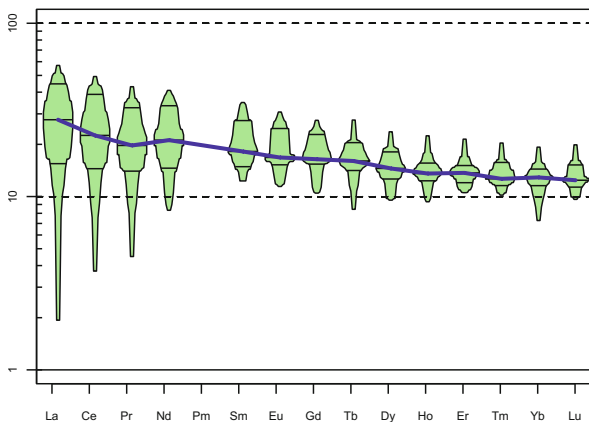


Fig. 4.3 Chondrite-normalized (Boynton 1984) spider box and percentile plot for REE in Vrbno Group dolerites (see the previous figure) generated by the function `spiderBoxplot`.

By analogy, in ‘*spider box and percentile plots*’, the statistical distributions of normalized elements are plotted in the form of a box and percentile plot (Esty and Banfield 2003) (Fig. 4.3). Here, the ‘boxes’ contain the information of a percentile plot (i.e. their widths reflect precise distribution of the data). However, there is no loss of information due to grouping, as all data are shown. Both subtypes are generated by the function `spiderBoxplot`.

4.3 Contour Plots

Frequency distribution of large datasets in diagrams can be portrayed by contours, produced by functions `addContours` (Fig. 4.4a) and `filledContourFig` (Fig. 4.4b)—i.e., interfaces to standard R functions, `contour` and `filled.contour`.

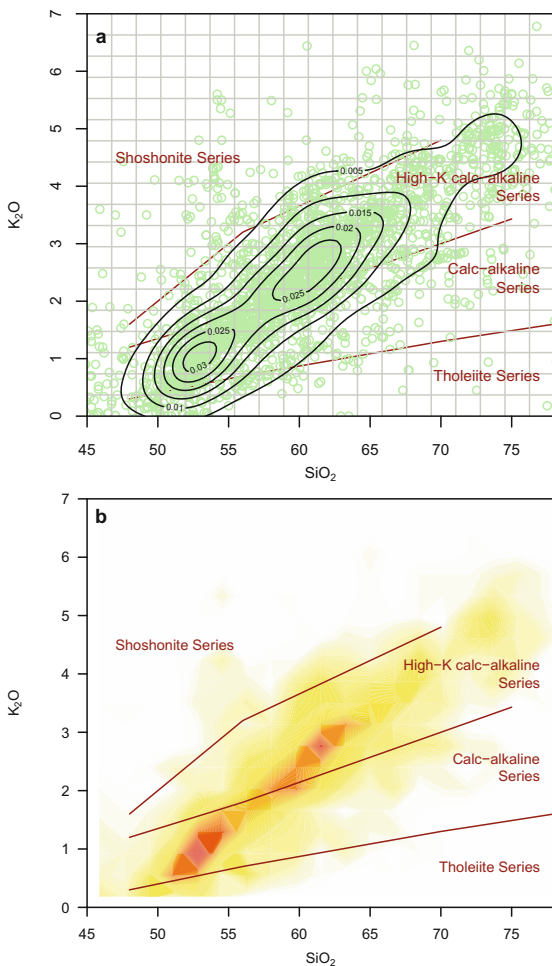


Fig. 4.4 **a** SiO₂-K₂O plot (Peccerillo and Taylor 1976) of over 3,800 analyses of Andean igneous rocks from the GeoRoc database (georoc.mpch-mainz.gwdg.de/georoc). Superimposed are contours showing the values of the probability density function. **b** Filled contours, based on counting over the 20×20 grid shown in the above panel.

4.4 Anomaly Plots

Most igneous geochemists treat whole-rock geochemical data essentially in the same way, looking for general patterns and most typical values. On the other hand, economic geologists and exploration companies search for anomalies that can be potentially of economic interest.

Keeping these needs in mind, we have implemented into *GCDkit* an anomaly plot, based on work by Reimann et al. (2002). The function `peterplot` draws a conventional binary diagram in which the type and size of the plotting symbols are assigned according to the distribution of a third, conditioning variable (for instance our element of interest). Its distribution is shown as boxplot (Fig. 4.5). The values between the 25th and the 75th percentiles obtain a small dot, the higher ones are denoted by ‘+’ and lower ones by ‘•’. If the given value is an outlier, it is shown as either ‘+’ or ‘o’ and the plotting size is doubled.

Optionally, the plotting symbols and their sizes can be set permanently, for use in other diagrams throughout the *GCDkit* system. Then it is possible to see, for instance, where the samples rich in gold plot in the TAS diagram.

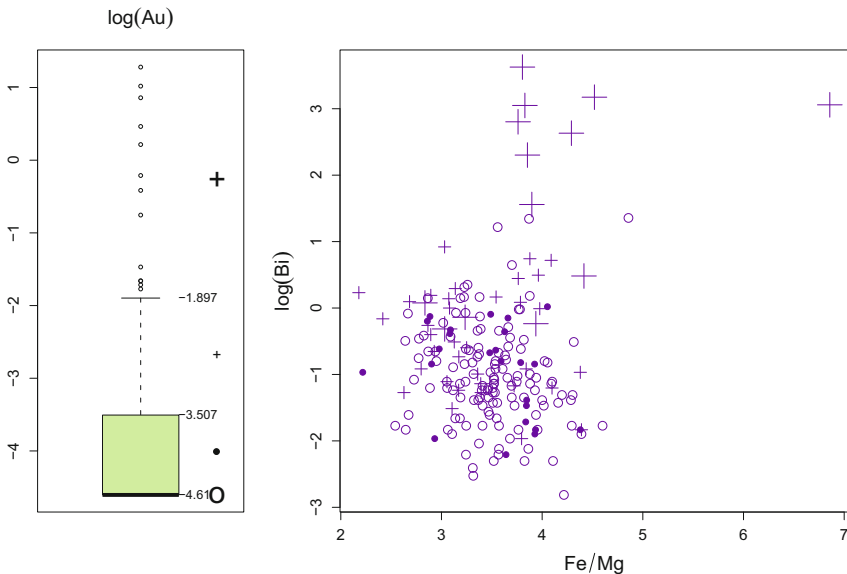


Fig. 4.5 Anomaly plot for the sandstone analyses from the drill core CYDD0020, Coyote Au deposit, Granites–Tanami Orogen (Western Australia) (Bagas et al. 2009). The Au distribution is skewed and ranging over several orders of magnitude (therefore the logarithmic scale). The concentration of gold into rocks with Fe/Mg of 4–5 is apparent, as is its correlation with Bi.

4.5 Stripplots and Strip Boxplots

Stripplot shows 1D scatter plots for each of the groups, with some artificial noise (jitter) added in the x axis direction to make the individual points better visible. Stripplots are a good alternative to boxplots when sample sizes are small. For this reason, they are implemented mainly in GCDkit's isotope (SrNd.r) plugin (see *GCDkit* box, Sect. 5.5).

'*Strip boxplot*' (Fig. 4.6) is a newly designed diagram that is based on stripplots. Each of the stripplots portraying the distribution of the selected variable in individual groups is underlain by a boxplot. Thus, the median, quartiles and range are immediately apparent. Optionally, the data points can be replaced by variously sized and coloured circles, depicting distribution of a second variable.

Plotting of this type of diagrams is done by the function `stripBoxplot`.

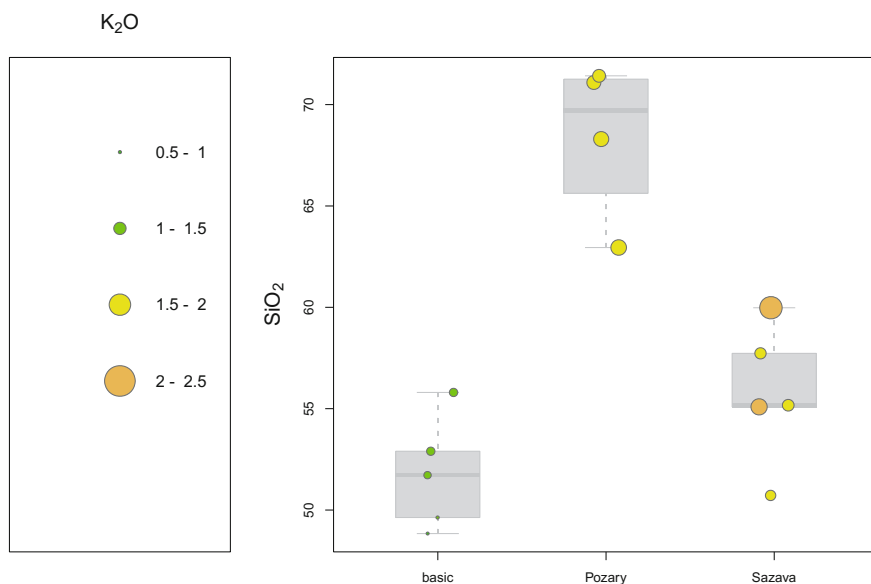


Fig. 4.6 Strip boxplot showing distribution of SiO_2 and K_2O in individual rock groups of the Sázava suite, Central Bohemian Plutonic Complex. The figure was plotted using the command `stripBoxplot(yaxis="SiO2", zaxis="K2O", pal="terrain.colors")`.

References

- Bagas L, Anderson JAC, Bierlein FP (2009) Palaeoproterozoic evolution of the Killi Killi Formation and orogenic gold mineralization in the Granites-Tanami Orogen, Western Australia. *Ore Geol Rev* 35:47–67
- Boynnton WV (1984) Cosmochemistry of the rare earth elements: meteorite studies. In: Henderson P (ed) *Rare Earth Element Geochemistry*. Elsevier, Amsterdam, pp 63–114
- Esty WW, Banfield JD (2003) The box-percentile plot. *J Stat Softw* 8:1–14
- Janoušek V, Finger F, Roberts MP, Frýda J, Pin C, Dolejš D (2004) Deciphering the petrogenesis of deeply buried granites: whole-rock geochemical constraints on the origin of largely undepleted felsic granulites from the Moldanubian Zone of the Bohemian Massif. *Trans Roy Soc Edinb, Earth Sci* 95:141–159
- Janoušek V, Aichler J, Hanžl P, Gerdes A, Erban V, Pecina V, Žáček V, Pudilová M, Hrdličková K, Mixa P, Žáčková E (2014) Constraining genesis and geotectonic setting of metavolcanic complexes: a multidisciplinary study of the Devonian Vrbno Group (Hrubý Jeseník Mts., Czech Republic). *Int J Earth Sci* 103:455–483
- Pearce JA, Stern RJ (2006) Origin of back-arc basin magmas: trace element and isotope perspectives. In: Christie DM, Fisher CR, Lee S-M, Givens S (eds) *Back-arc spreading systems: geological, biological, chemical, and physical interactions*. Geophysical Monograph Series, vol 166. American Geophysical Union, pp 63–86
- Pearce JA, Stern RJ, Bloomer SH, Fryer P (2005) Geochemical mapping of the Mariana arc-basin system: implications for the nature and distribution of subduction components. *Geochem Geophys Geosyst* 6:Q07006
- Peccerillo A, Taylor SR (1976) Geochemistry of Eocene calc-alkaline volcanic rocks from the Kastamonu area, Northern Turkey. *Contrib Mineral Petrol* 58:63–81
- Reimann C, Filzmoser P, Garrett RG (2002) Factor analysis applied to regional geochemical data: problems and possibilities. *Appl Geochem* 17:185–206
- Thompson RN, Morrison MA, Dickin AP, Hendry GL (1983) Continental flood basalts... Arachnids rule OK? In: Hawkesworth CJ, Norry MJ (eds) *Continental basalts and mantle Xenoliths*. Shiva, Nantwich, pp 158–185

Chapter 5

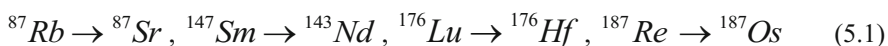
Radiogenic Isotopes

In contrast to the light stable isotopes (e.g., O, H, Li, C), the utility of the relatively heavy radiogenic isotopes (e.g., Sr, Nd, Pb, Hf) consists in the fact that they should not be fractionated by equilibrium, closed-system processes (so named, as no components external to the magmatic system are involved) such as partial melting, fractional crystallization or crystal accumulation. In these cases the radiogenic isotopes enable us to fingerprint the magma sources. Alternatively, these ratios may be used to prove the operation of open-system processes, for instance magma mixing or crustal assimilation. Subsequently, compositions and proportions of end-members involved can often be constrained.

The aim of this chapter is to explain basic numerical approaches in interpreting radiogenic isotope data in igneous geochemistry, with a particular emphasis on Sr–Nd–Hf–Os isotopes. The text is concerned with calculation of initial ratios, ages, ϵ and γ values, single- and two-stage model ages and fitting of isochrons. Theoretical background is explained only briefly as detailed accounts are readily available in several textbooks (Geyh and Schleicher 1990; Faure and Mensing 2004; Dickin 2005; Allègre 2008 to name just a few).

5.1 Recalculation of Elemental to Isotopic Ratios

Many of the parent–daughter dating methods are based on similar principles. The parent (radioactive) isotope (e.g., ^{87}Rb , ^{147}Sm or ^{176}Lu) decays to the daughter (radiogenic) isotope (e.g., ^{87}Sr , ^{143}Nd or ^{176}Hf):



As the mass spectrometer is only capable of measuring isotopic ratios, the content of daughter isotope is expressed as a ratio to a stable, non-radiogenic isotope, whose natural abundance does not change with time (for simplicity termed here I ; e.g., $^{87}\text{Sr}/^{86}\text{Sr}$, $^{143}\text{Nd}/^{144}\text{Nd}$ or $^{176}\text{Hf}/^{177}\text{Hf}$). Age calculation also requires the amount of the parental isotope to be expressed as a ratio to the same non-radiogenic stable isotope of the daughter element (R ; e.g., $^{87}\text{Rb}/^{86}\text{Sr}$, $^{147}\text{Sm}/^{144}\text{Nd}$ or $^{176}\text{Lu}/^{177}\text{Hf}$). Whereas the I ratios are measured directly with the mass spectrometry,

ter (TIMS or ICP-MS), R ratios must be calculated from elemental concentrations obtained by isotope dilution, ICP-MS, XRF or other analytical methods.

The concept behind the derivation of the conversion formulae is illustrated here using the Rb–Sr system. Combining the relation between atomic weight and molar abundance we obtain (Faure 1986):

$$\frac{{}^{87}\text{Rb}}{{}^{86}\text{Sr}} = \left(\frac{C_{\text{Rb}} \times Ab_{{}^{87}\text{Rb}}}{AW_{\text{Rb}}} \right) \left(\frac{AW_{\text{Sr}}}{C_{\text{Sr}} \times Ab_{{}^{86}\text{Sr}}} \right) \quad (5.2)$$

where C_{Sr} , C_{Rb} are concentrations (ppm), Ab = isotopic abundances, AW = atomic weights. The problem is that both AW_{Sr} and $Ab_{{}^{87}\text{Rb}}$ are a function of the isotopic composition of the sample, and thus depend on its ${}^{87}\text{Sr}/{}^{86}\text{Sr}$ ratio. If the atomic weight is expressed as a sum of weights of individual isotopes multiplied by their abundances, the right-hand side of Eq. (5.2) can be rewritten as:

$$\frac{C_{\text{Rb}}}{C_{\text{Sr}}} \times \left(\sum_{\psi} \left(\frac{{}^{\psi}\text{Sr}}{{}^{86}\text{Sr}} \times AW_{\psi\text{Sr}} \right) + \frac{{}^{87}\text{Sr}}{{}^{86}\text{Sr}} \times AW_{{}^{87}\text{Sr}} \right) \times \frac{\frac{{}^{87}\text{Rb}}{{}^{85}\text{Rb}}}{\sum_{\zeta} \left(\frac{{}^{\zeta}\text{Rb}}{{}^{85}\text{Rb}} \times AW_{\zeta\text{Rb}} \right)} \quad (5.3)$$

where the sums refer to all non-radiogenic isotopes of Sr ($\psi = 84, 86, 88$) and all isotopes of Rb ($\zeta = 85, 87$), respectively. All Sr ratios are expressed relative to ${}^{86}\text{Sr}$; both Rb ratios relative to ${}^{85}\text{Rb}$. The ${}^{87}\text{Sr}/{}^{86}\text{Sr}$ values (i.e. D), C_{Rb} and C_{Sr} are to be determined; the rest are constants that can be obtained from literature (e.g., Audi et al. 2003; Berglund and Wieser 2011 and references therein). The third term may be substituted by simpler, yet less precise ratio $Ab_{{}^{87}\text{Rb}}/AW_{\text{Rb}}$. The literature data vary slightly; based on those from Faure (1986), we obtain:

$$\frac{{}^{87}\text{Rb}}{{}^{86}\text{Sr}} = \left(\frac{C_{\text{Rb}}}{C_{\text{Sr}}} \right) \left[2.6939 + 0.2832 \frac{{}^{87}\text{Sr}}{{}^{86}\text{Sr}} \right] \quad (5.4)$$

Similarly, for the ${}^{147}\text{Sm}/{}^{144}\text{Nd}$ isotopic ratio can be derived:

$$\frac{{}^{147}\text{Sm}}{{}^{144}\text{Nd}} = \left(\frac{C_{\text{Sm}}}{C_{\text{Nd}}} \right) \left[0.53151 + 0.14252 \frac{{}^{143}\text{Nd}}{{}^{144}\text{Nd}} \right] \quad (5.5)$$

using Nd stable isotopic ratios from Wasserburg et al. (1981), renormalized to ${}^{146}\text{Nd}/{}^{144}\text{Nd} = 0.7219$. For whole-rock samples, especially if the fractionation between Sm and Nd is small and thus the variability of the ${}^{143}\text{Nd}/{}^{144}\text{Nd}$ can be neglected (relatively to the precision of concentrations), the term in square brackets in Eq. (5.5) collapses to 0.6047.

For the Lu–Hf system, the relevant equation is:

$$\frac{{}^{176}\text{Lu}}{{}^{177}\text{Hf}} = \left(\frac{C_{\text{Lu}}}{C_{\text{Hf}}} \right) \left[0.13517 + 0.02613 \frac{{}^{176}\text{Hf}}{{}^{177}\text{Hf}} \right] \quad (5.6)$$

If the ${}^{176}\text{Hf}/{}^{177}\text{Hf}$ ratio is close to that of CHUR (‘normal’ whole-rock samples), the expression in square brackets collapses to 0.142 (Faure and Mensing 2004).

Lastly, ${}^{187}\text{Re}/{}^{188}\text{Os}$ can be calculated as follows, provided that the ${}^{186}\text{Os}$ is not influenced by the decay of ${}^{190}\text{Pt}$:

$$\frac{{}^{187}\text{Re}}{{}^{188}\text{Os}} = \left(\frac{C_{\text{Re}}}{C_{\text{Os}}} \right) \left[4.7393 + 0.6285 \frac{{}^{187}\text{Os}}{{}^{188}\text{Os}} \right] \quad (5.7)$$

5.2 Calculation of Initial Ratios or Ages

Using our notation, an equation between I , R and age t (in years) can be written as:

$$I = R(e^{\lambda t} - 1) \quad (5.8)$$

Where λ is the relevant decay constant (see Ickert 2013 for discussion):

$$\lambda_{87\text{Rb}} = 1.42 \times 10^{-11} \text{y}^{-1} \text{ (Steiger and Jäger 1977) (old but still widely used value)}$$

$$\lambda_{87\text{Rb}} = 1.3968 \times 10^{-11} \text{y}^{-1} \text{ (Rotenberg et al. 2012) (new determination)}$$

$$\lambda_{147\text{Sm}} = 6.54 \times 10^{-12} \text{y}^{-1} \text{ (Lugmair and Marti 1978)}$$

$$\lambda_{176\text{Lu}} = 1.867 \times 10^{-11} \text{y}^{-1} \text{ (Söderlund et al. 2004)}$$

$$\lambda_{187\text{Re}} = 1.6668 \times 10^{-11} \text{y}^{-1} \text{ (Selby et al. 2007)}$$

Equation (5.8) assumes that initially, t years ago, there was no daughter isotope present. This can be (nearly) justified for some minerals, forming so-called (parent-) rich systems (Allègre 2008). As an example may serve a Li-mica that is Rb rich and whose Sr will soon become dominated by the radiogenic component. However, generally there is always some common Sr, Nd or Hf present. Assuming that its composition (initial ratio) is I_i , Eq. (5.8) changes into:

$$I = I_i + R(e^{\lambda t} - 1) \quad (5.9)$$

If the age is known, the isotopic ratios can be easily ‘age-corrected’ (i.e. initial ratios back-calculated) and used in petrogenetic considerations.

On the other hand, knowing the initial ratio, e.g. by analysis of a (parent-) poor system (e.g., Sr in apatite that contains little Rb and thus its ${}^{87}\text{Sr}/{}^{86}\text{Sr}$ is nearly con-

stant, close to the initial composition), Eq. (5.9) can be developed into a formula giving the age:

$$t = \frac{1}{\lambda} \ln \left(\frac{I - I_i}{R} + 1 \right) \quad (5.10)$$



Exercise 5.1: Initial ratios and ages

The Sr–Nd isotopic study of the Central Bohemian Plutonic Complex (CBPC) (Janoušek et al. 1995) has proven a diversity of sources and processes involved in genesis of individual intrusions and suites. The file contains an excerpt from the data for several granitoid types and two country rocks.



[cbpizo.data](#)

Table 5.1 Selected Sr–Nd isotopic data for the Central Bohemian Plutonic Complex

ID	Rock type	Rb (ppm)	Sr (ppm)	$^{87}\text{Sr}/^{86}\text{Sr}$	Sm (ppm)	Nd (ppm)	$^{143}\text{Nd}/^{144}\text{Nd}$
Sa-1	Sázava	76	555.8	0.70700	4.57	24.2	0.512476
Koz-2	Kozárovce	164.1	486.9	0.71258	5.91	31.7	0.512210
Bl-2	Blatná	185	439.1	0.71434	6.85	43.8	0.512101
Se-9	Sedlčany	308.1	307.8	0.72620	8.17	40.2	0.512080
Ri-1	Říčany	310.7	374.1	0.72154	4.06	24.1	0.512053
CR-1	shale	110	80.4	0.72596	3.3	17.3	0.512061
CR-5	paragneiss	160	86.4	0.74670	9.4	50.6	0.511880

- Import the data file into a matrix `izo`, calculate the $^{87}\text{Rb}/^{86}\text{Sr}$ and $^{147}\text{Sm}/^{144}\text{Nd}$ ratios and attach them to the matrix as the last data columns.
- Design functions yielding Sr and Nd initial ratios; back-calculate these at 350 and 300 Ma ago; can you program a single function with an argument identifying the isotopic system (Sr or Nd)?
- Calculate the age of the sample Koz-2 assuming that its initial ratio is 0.705.



```
> izo <- read.table("cbpizo.data", sep="\t", check.names=F)
> colnames(izo)[c(3,6)] <- c("87Sr/86Sr", "143Nd/144Nd")
> sr <- izo[,1]/izo[,2]*(2.6939+0.2832*izo[,3])
> nd <- izo[,4]/izo[,5]*(0.53151+0.14252*izo[,6])
> izo <- cbind(izo,sr,nd)
> colnames(izo)[7:8] <- c("87Rb/86Sr", "147Sm/144Nd")
> print(izo[,7:8])
```

```

87Rb/86Sr 147Sm/144Nd
Sa-1 0.3957418 0.11416466
Koz-2 0.9759392 0.11270205
Bl-2 1.2202168 0.09453854
Se-9 2.9023859 0.12285315
Ri-1 2.4070655 0.10183487
CR-1 3.9669665 0.11530714
CR-5 5.3803064 0.11229157

> initial <- function(data,system="Sr",age){
> # data = matrix to be recalculated
> # system = "Sr" or "Nd", age = age in Ma
> lambda <- c(1.42*10^-11,6.54*10^-12)
> names(lambda) <- c("Sr","Nd")
> R <- cbind(data[, "147Sm/144Nd"],data[, "87Rb/86Sr"])
> colnames(R) <- c("Nd","Sr")
> I <- cbind(data[, "143Nd/144Nd"],data[, "87Sr/86Sr"])
> colnames(I) <- c("Nd","Sr")
> X <- I[,system]-R[,system]*(exp(lambda[system]*
> age*10^6)-1)
> return(X)
> }
> izo <- cbind(izo,initial(izo,"Sr",350),
> initial(izo,"Sr",300),initial(izo,"Nd",350),
> initial(izo,"Nd",300))
> colnames(izo)[9:12] <- c("87Sr/86Sr.350","87Sr/86Sr.300",
> "143Nd/144Nd.350","143Nd/144Nd.300")
> print(izo[,9:12])
      87Sr/86Sr.350 87Sr/86Sr.300 143Nd/144Nd.350
Sa-1      0.7050283      0.7053105      0.5122144
Koz-2      0.7077175      0.7084136      0.5119517
Bl-2      0.7082604      0.7091308      0.5118844 ...

> age <- 1/1.42e-11*log((izo["Koz-2","87Sr/86Sr"]-0.705)/
> izo["Koz-2","87Rb/86Sr"]+1)
> print(age/1e6)
[1] 544.85

```

5.3 Epsilon, Delta and Gamma Values

The initial Nd isotopic ratios usually do not differ much among individual whole-rock samples. This is due to a relatively long half-life of Sm and a very limited fractionation between Sm and Nd caused by their similar ionic radii, identical charge and thus also geochemical behaviour.

The isotopic evolution of Nd in the Earth is described in terms of the so-called Chondritic Uniform Reservoir (CHUR: DePaolo 1988). This model mantle is defined to have Sm/Nd and initial $^{143}\text{Nd}/^{144}\text{Nd}$ ratios equal to those of chondritic meteorites (Jacobsen and Wasserburg 1980). The CHUR is widely used for comparison of initial isotopic compositions of studied rocks with that of undifferentiated mantle at the time of their generation. This is done through the ϵ_{Nd} notation:

$$\varepsilon_{Nd}^i = \left(\frac{\left(\frac{{}^{143}Nd}{{}^{144}Nd} \right)_i^{SA}}{\left(\frac{{}^{143}Nd}{{}^{144}Nd} \right)_{CHUR}^i} - 1 \right) \times 10^4 \quad (5.11)$$

Where: t = intrusion age, indexes i decipher initial isotopic ratios [Eq.(5.9)], SA = sample. The present-day composition of the CHUR is ${}^{147}Sm/{}^{144}Nd_{CHUR} = 0.1967$ and ${}^{143}Nd/{}^{144}Nd_{CHUR} = 0.512638$ (Jacobsen and Wasserburg 1980) or ${}^{147}Sm/{}^{144}Nd_{CHUR} = 0.1960$ and ${}^{143}Nd/{}^{144}Nd_{CHUR} = 0.512630$ (Bouvier et al. 2008). For an overview of alternatives, as well as of error propagation, see Ickert (2013).

This notation makes it much easier to compare the initial Nd isotope ratios of samples of different ages. In earlier days, it also removed the effects of the different fractionation corrections employed during analysis in individual laboratories (Faure 1986). Note that all Nd isotopic data and formulae presented in this text are based on normalization to ${}^{146}Nd/{}^{144}Nd = 0.7219$, a common practice nowadays.

As Nd is more incompatible than Sm, partial melting of a mantle peridotite would produce melts with Sm/Nd ratios lower than the source. On the other hand, the residue would be enriched in Sm and yield a higher Sm/Nd ratio (Fig. 5.1a). Thus old crustal rocks formed originally by CHUR-like mantle melting should have present-day ${}^{143}Nd/{}^{144}Nd$ lower than CHUR ($\varepsilon_{Nd} < 0$) and mantle domains with long-term depletion will, over time, develop higher ${}^{143}Nd/{}^{144}Nd$ ($\varepsilon_{Nd} > 0$).

Comparable geochemical behaviour is shown also by the Hf isotopes, for which we can define ε_{Hf} values by analogy to Eq. (5.11). The present-day composition of the CHUR is ${}^{176}Lu/{}^{177}Hf_{CHUR} = 0.0336$ and ${}^{176}Hf/{}^{177}Hf_{CHUR} = 0.282785$ (Bouvier et al. 2008). Again, for an overview of alternatives, see Ickert (2013).

On the other hand, the Rb–Sr system behaves in an opposite way. Rubidium is more incompatible than Sr in the course of mantle melting and thus the crust is characterized by high Rb/Sr producing, over the time, high ${}^{87}Sr/{}^{86}Sr$ ratios. The ε values, even though seldom used for the Sr isotopes, would be strongly positive.

The geochemical-reservoir normalized compositions can be also expressed as γ values¹, as is customary for the Re–Os system:

$$\gamma_{Os}^i = \left(\frac{\left(\frac{{}^{187}Os}{{}^{188}Os} \right)_i^{SA}}{\left(\frac{{}^{187}Os}{{}^{188}Os} \right)_{Mantle}^i} - 1 \right) \times 10^2 \quad (5.12)$$

¹ The δ notation, used for stable isotopes, is analogous (just multiply by 10^3 rather than 10^2).

In fact, this forms a logic system, whereby 10^n is expressed by $(n+1)^{th}$ letter in the Greek alphabet.

The present-day mantle values are $^{187}\text{Re}/^{188}\text{Os} = 0.422$ and $^{187}\text{Os}/^{188}\text{Os} = 0.1283$ (Walker et al. 2002).

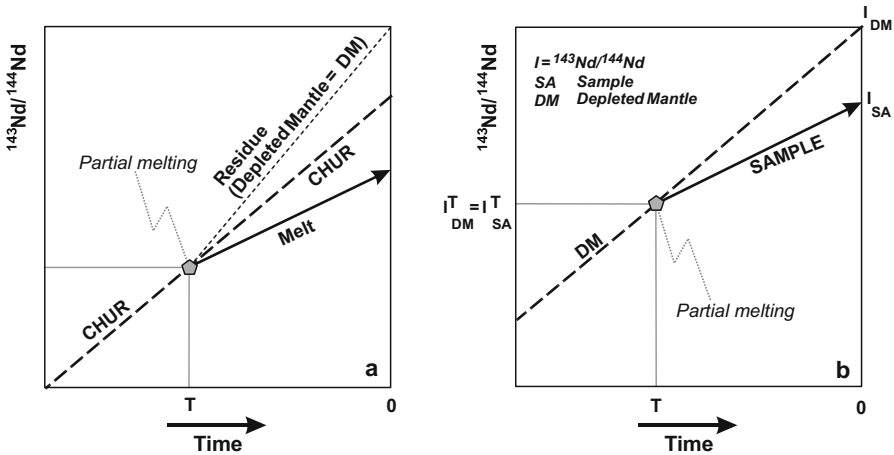


Fig. 5.1 **a** Isotopic evolution of Nd in a Chondritic Uniform Reservoir (CHUR), igneous rock formed by its partial melting and the residual solid—Depleted Mantle (after Faure 1986); **b** Theoretical concept of a single-stage Nd model age as an intersection between the mantle evolution line (here Depleted Mantle) and that for the given sample.



Exercise 5.2: Epsilon Nd values

- Write a function returning the initial ϵ_{Nd} values.
- Calculate these for the CBPC granitoids from the previous exercise at 350 Ma.
- Plot a binary diagram of initial $^{87}\text{Sr}/^{86}\text{Sr}$ isotopic ratios versus initial ϵ_{Nd} values.



```
> epsilon <- function(data,age){
>   RCHUR <- 0.1967; ICHUR <- 0.512638 # J & Wasserburg
>   CHUR <- ICHUR-RCHUR*(exp(6.54e-12*age*10^6)-1)
>   X <- (initial(data,"Nd",age)/CHUR-1)*10^4
>   names(X) <- rownames(data)
>   return(X)
> }

> round(epsilon(izo,350),2)
Sa-1 Koz-2 Bl-2 Se-9 Ri-1 CR-1 CR-5
0.53 -4.60 -5.91 -7.59 -7.18 -7.62 -11.02

> plot(initial(izo,age=350),epsilon(izo,350),
>       xlab=expression(" ^{87}Sr/" ^{86}Sr[i]),
>       ylab=expression(epsilon[Nd]^i),pch=11,cex=1.5,
>       cex.lab=1.5,cex.axis=1.5)
```

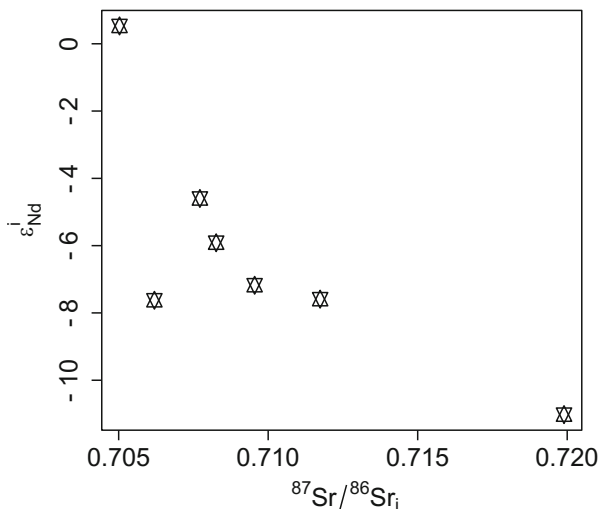


Fig. 5.2 Diagram $^{87}\text{Sr}/^{86}\text{Sr}$ – ϵ_{Nd} for granitoids of the CBPC (age-corrected to 350 Ma).

5.4 Model Ages

The model ages represent an apparent age of extraction from a model geochemical reservoir. These include, for instance, intercepts with various mantle evolution models. The principle will be explained here for neodymium but the same approach can be adopted for some other systems (notably Lu–Hf).

The relative immobility of LREE in course of the weathering and low-grade metamorphism enables calculation of time in the past when the given sample had the Nd isotopic composition identical to its presumed model source reservoir (most often CHUR or Depleted Mantle, DM – DePaolo 1988). Important prerequisites for such an interpretation are: 1) the sample was generated from the source that can be approximated by the given model reservoir, 2) this happened in a single or, at most, two steps, 3) there was a significant change in the Sm/Nd ratio during the melting and 4) the sample remained a closed system throughout its history (Arndt and Goldstein 1987). Following McCulloch and Wasserburg (1978), the Nd model ages have been often interpreted as ‘crust-formation ages’ for the given crustal segment. These may be significant especially if obtained from clay-rich (meta-) sedimentary rocks, averaging large source regions of the crust (Michard et al. 1985).

5.4.1 Single-Stage Nd Model Ages

Single-stage Nd model age can be derived by setting (Fig. 5.1b):

$$I_{SA}^T = I_{DM}^T \quad (5.13)$$

where SA denotes the sample and DM the appropriate model reservoir (here Depleted Mantle). The equation:

$$I_{SA} - R_{SA} \left(e^{\lambda T} - 1 \right) = I_{DM} - R_{DM} \left(e^{\lambda T} - 1 \right) \quad (5.14)$$

is solved for T (the model age) using the present-day Nd isotopic compositions of the sample and the model reservoir:

$$T = \frac{1}{\lambda} \ln \left(\frac{I_{SA} - I_{DM}}{R_{SA} - R_{DM}} + 1 \right) \quad (5.15)$$

The present-day composition of the Depleted Mantle is $^{147}\text{Sm}/^{144}\text{Nd} = 0.222$ and $^{143}\text{Nd}/^{144}\text{Nd} = 0.513114$ (Michard et al. 1985). For an overview of alternatives, and error propagation in model age calculations, see Ickert (2013).



Exercise 5.3: Single-stage Nd model ages

- Design a function yielding single-stage Depleted Mantle Nd model ages.
- Calculate these for the granitoids of the CBPC. Use the data from the previous exercises or load them from the file.



[cbpizo2.data](#)



```
> # Needed only when the data are to be newly loaded:
> izo <- read.table("cbpizo2.data", sep="\t", check.names=F)

> DMAGE <- function(data) {
>   IDM <- 0.513114
>   RDM <- 0.222
>   lambda <- 6.54e-12
>   R <- data[, "147Sm/144Nd"]
>   I <- data[, "143Nd/144Nd"]
>   X <- 1/lambda*log((I-IDM)/(R-RDM)+1)/10^9
>   names(X) <- rownames(data)
>   return(X)
> }

> round(DMAGE(izo), 2)
Sa-1 Koz-2 Bl-2 Se-9 Ri-1 CR-1 CR-5
0.90 1.26 1.21 1.59 1.34 1.50 1.71
```

5.4.2 Two-Stage Nd Model Ages

In interpreting sources of crustally-derived rocks, such as granites, the single-stage Nd model ages are clearly inappropriate. For this purpose the two-stage model has

been designed (Liew and Hofmann 1988) which compensates for effects of possible second Sm/Nd fractionation (first having occurred at mantle melting) in course of the intracrustal partial melting. In the following formulae, the indexes *DM*, *CC*, *SA* denote Depleted Mantle, average continental crust and the sample, respectively. *T* = two-stage Nd model age, *t* = crystallization age of the sample, 0 refers to the present day (Fig. 5.3):

$$T = \frac{1}{\lambda} \ln \left(\frac{I_{SA}^0 - (e^{\lambda t} - 1)(R_{SA}^0 - R_{CC}^0) - I_{DM}^0}{(R_{CC}^0 - R_{DM}^0)} + 1 \right) \quad (5.16)$$

$$\left(\frac{^{143}\text{Nd}}{^{144}\text{Nd}} \right)_{DM}^0 = 0.513151, \quad \left(\frac{^{147}\text{Sm}}{^{144}\text{Nd}} \right)_{DM}^0 = 0.219, \quad \left(\frac{^{147}\text{Sm}}{^{144}\text{Nd}} \right)_{CC}^0 = 0.12$$

(Liew and Hofmann 1988)

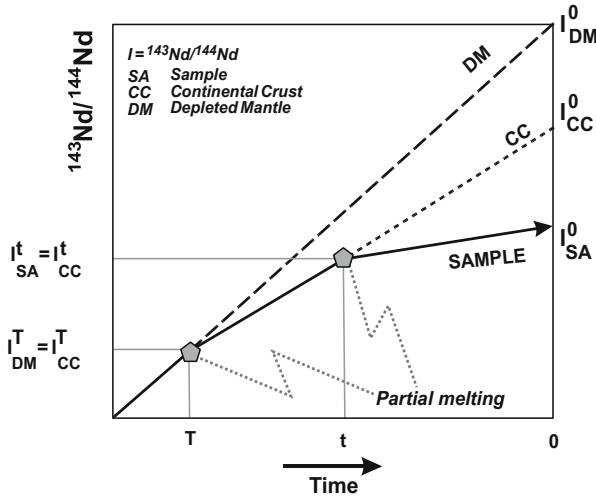


Fig. 5.3 Theoretical concept of a two-stage Nd model age. An intermediate reservoir with Sm/Nd ratio of typical continental crustal rocks (*CC*) is assumed.



Exercise 5.4: Two-stage Nd model ages

- Design a function returning two-stage Depleted Mantle Nd model ages.
- Calculate these for the granitoids of the CBPC. Use the data from the previous exercises or load them from the file (in that case see beginning of Exercise 5.3).



cbpizo2.data



```

> DMLHAGE <- function(data, age) {
>   R <- data[, "147Sm/144Nd"]
>   I <- data[, "143Nd/144Nd"]
>   IDM <- 0.513151
>   RDM <- 0.219
>   RCC <- 0.12
>   lambda <- 6.54e-12
>   A <- I - (exp(lambda*age*1e6) - 1) * (R - RCC) - IDM
>   B <- RCC - RDM
>   X <- 1/lambda*log(A/B+1)/10^9
>   names(X) <- rownames(data)
>   return(X)
> }
> round(DMLHAGE(izo, 350), 2)
  Sa-1 Koz-2 Bl-2 Se-9 Ri-1 CR-1 CR-5
  1.02  1.42  1.52  1.66  1.62  1.66  1.92

```

5.5 Isochron Ages

An elegant remedy to the problem of unknown initial ratio in the geochronological calculations is to use a cogenetic suite of whole-rock or mineral samples. In fact, Eq. (5.9) corresponds to a straight line in the isochron diagrams R vs I , e.g., $^{87}\text{Rb}/^{86}\text{Sr}$ vs $^{87}\text{Sr}/^{86}\text{Sr}$:

$$y = a + bx \quad (5.17)$$

where a is an intercept (initial isotopic ratio), and b the slope of the isochron:

$$b = tg\alpha = (e^{\lambda t} - 1) \quad (5.18)$$

giving a formula for the isochron age:

$$t = \frac{1}{\lambda} \ln(b + 1) \quad (5.19)$$

The isochrons are usually fitted using dedicated software, most frequently Isoplot (Ludwig 2003). The algorithm utilizes weighted linear regression (York 1969). This means that it takes into account the errors in both coordinates at each individual data point (Provost 1990; Kullerud 1991 and references therein).



Exercise 5.5: Isochrons

The file `acari.data` contains Rb-Sr isotopic data for granite Serra do Acari (Brazil) (Provost 1990 and references therein). On this example, we will demonstrate the use of simple (i.e. not weighted) linear regression in fitting isochrons.

Table 5.2 Rb–Sr isotopic data for the Serra do Acari granite

Sample	$^{87}\text{Rb}/^{86}\text{Sr}$	1σ	$^{87}\text{Sr}/^{86}\text{Sr}$	1σ
AT-R-173	5.743	0.062	0.858993	0.000034
AT-R-167	22.290	0.280	1.290200	0.000050
AT-R-157	42.170	0.530	1.760370	0.000069
AT-R-165	61.230	0.980	2.248950	0.000140
AT-R-158	99.000	1.800	3.182530	0.000170
AT-R-169	232.000	3.300	6.548880	0.000470

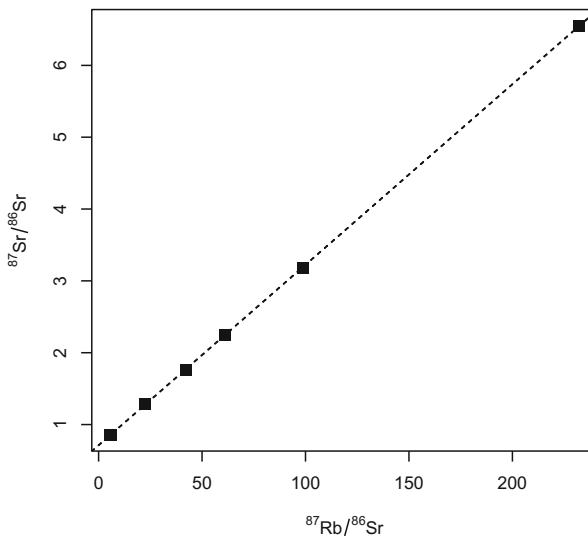


acari.data

- Read the data file and plot an isochron diagram $^{87}\text{Rb}/^{86}\text{Sr}$ – $^{87}\text{Sr}/^{86}\text{Sr}$
- Fit the data by a straight line, calculate age and initial Sr ratio for the granite



```
> acari <- read.table("acari.data", sep="\t")
> colnames(acari) <- c("87Rb/86Sr", "er.x", "87Sr/86Sr", "er.y")
> plot(acari[,1], acari[,3],
>       xlab=expression("87Rb/86Sr"),
>       ylab=expression("87Sr/86Sr"), pch=15, cex=1.5)
```

**Fig. 5.4** Rb–Sr isochron for granite Serra do Acari (Exercise 5.5).

```
> izoch <- lm(acari[,3]~acari[,1])
> print(izoch)
Call:
lm(formula = acari[, 3] ~ acari[, 1])
Coefficients:
(Intercept)  acari[, 1]
 0.71171      0.02513
```

```
> abline(izoch, lty="dashed")
> age <- 1/1.42e-11*log(izoch$coeff[2]+1)
> print(age/1e6)
1747.657
```



The Sr–Nd plugin in GCDkit

GCDkit comes with a plugin `SrNd.r`, which takes care of the recalculation and plotting of Sr–Nd isotopic data. It is loaded automatically, whenever columns named “ $^{87}\text{Sr}/^{86}\text{Sr}$ ” and/or “ $^{143}\text{Nd}/^{144}\text{Nd}$ ” are encountered in your datafile. The data can, optionally, contain also a column named “Age”, specifying an age (or ages) in Ma to which the isotopic data should be recalculated. Otherwise, the user is prompted to enter this value when the dataset is loaded. If columns labelled “ $^{87}\text{Rb}/^{86}\text{Sr}$ ” or “ $^{147}\text{Sm}/^{144}\text{Nd}$ ” are absent, these are calculated based upon concentrations of Rb, Sr, Sm and Nd, as well as Sr and Nd isotopic composition using Eq. (5.4) and (5.5).

The plugin calculates initial $^{87}\text{Sr}/^{86}\text{Sr}$ and/or $^{143}\text{Nd}/^{144}\text{Nd}$ ratios, as well as epsilon Nd values and several types of Nd model ages. All recalculated isotopic data are stored in numeric matrix `init`. Moreover, the plugin can draw binary plots involving isotope data, or their combination with any other whole-rock geochemical parameters, boxplots and stripplots of isotope-related values, together with Sr and Nd growth diagrams and crude isochrons. See `?srnd` for details.

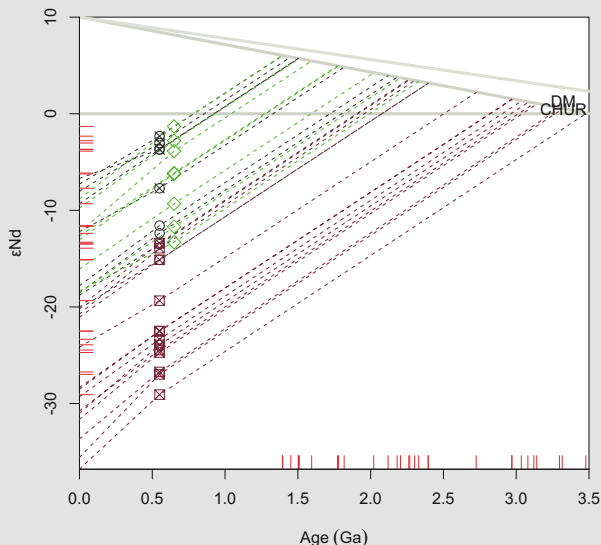


Fig. 5.5 An example of a two-stage Nd growth diagram as plotted by *GCDkit*. Shown is the development of metasedimentary and metaigneous rocks from the Coastal Terrane and Congo Craton (Kaoko Belt, Namibia). See fig. 8 in Konopásek et al. (2014) for data sources. The extra tick marks on the ordinate indicate the initial ϵ_{Nd} values of the samples, on the abscissa the two-stage Depleted Mantle Nd model ages (Liew and Hofmann 1988).

References

- Allègre CJ (2008) *Isotope geology*. Cambridge University Press, Cambridge
 Arndt NT, Goldstein SL (1987) Use and abuse of crust-formation ages. *Geology* 15:893–895

- Audi G, Wapstra AH, Thibault C (2003) The Ame2003 atomic mass evaluation: (II). Tables, graphs and references. *Nucl Phys A* 729:337–676
- Berglund M, Wieser M E (2011) Isotopic compositions of the elements 2009 (IUPAC Technical Report). *Pure App Chem* 83:397–410
- Bouvier A, Vervoort JD, Patchett PJ (2008) The Lu–Hf and Sm–Nd isotopic composition of CHUR: constraints from unequilibrated chondrites and implications for the bulk composition of terrestrial planets. *Earth Planet Sci Lett* 273:48–57
- DePaolo DJ (1988) Neodymium isotope geochemistry. Springer, Berlin
- Dickin AP (2005) Radiogenic isotope geology. Cambridge University Press, Cambridge
- Faure G (1986) Principles of isotope geology. John Wiley & Sons, Chichester
- Faure G, Mensing TM (2004) Isotopes: principles and applications. Wiley, New Jersey
- Geyh MA, Schleicher H (1990) Absolute age determination. Springer, Berlin
- Ickert RB (2013) Algorithms for estimating uncertainties in initial radiogenic isotope ratios and model ages. *Chem Geol* 340:131–138
- Jacobsen SB, Wasserburg GJ (1980) Sm–Nd isotopic evolution of chondrites. *Earth Planet Sci Lett* 50:139–155
- Janoušek V, Rogers G, Bowes DR (1995) Sr–Nd isotopic constraints on the petrogenesis of the Central Bohemian Pluton, Czech Republic. *Geol Rundsch* 84:520–534
- Konopásek J, Košler J, Sláma J, Janoušek V (2014) Timing and sources of pre-collisional Neoproterozoic sedimentation along the SW margin of the Congo Craton (Kaoko Belt, NW Namibia). *Gondwana Res* 26:386–401
- Kullerød L (1991) On the calculation of isochrons. *Chem Geol (Isot Geosci Sect)* 87:115–124
- Liew TC, Hofmann AW (1988) Precambrian crustal components, plutonic associations, plate environment of the Hercynian Fold Belt of Central Europe: indications from a Nd and Sr isotopic study. *Contrib Mineral Petrol* 98:129–138
- Ludwig KR (2003) Isoplot/Ex version 3.00. A geochronological toolkit for Microsoft Excel, User's Manual. Berkeley Geochronology Center Special Publications, vol 4, pp 1–70
- Lugmair GW, Marti K (1978) Lunar initial $^{143}\text{Nd}/^{144}\text{Nd}$: differential evolution line of the lunar crust and mantle. *Earth Planet Sci Lett* 39:349–357
- McCulloch MT, Wasserburg GJ (1978) Sm–Nd and Rb–Sr chronology of the continental crust formation. *Science* 200:1003–1011
- Michard A, Gurriet P, Soudant M, Albarède F (1985) Nd isotopes in French Phanerozoic shales: external vs. internal aspects of crustal evolution. *Geochim Cosmochim Acta* 49:601–610
- Provost A (1990) An improved diagram for isochron data. *Chem Geol (Isot Geosci Sect)* 80:85–99
- Rotenberg E, Davis DW, Amelin Y, Ghosh S, Bergquist BA (2012) Determination of the decay-constant of ^{87}Rb by laboratory accumulation of ^{87}Sr . *Geochim Cosmochim Acta* 85:41–57
- Selby D, Creaser RA, Stein HJ, Markey RJ, Hannah JL (2007) Assessment of the ^{187}Re decay constant by cross calibration of Re–Os molybdenite and U–Pb zircon chronometers in magmatic ore systems. *Geochim Cosmochim Acta* 71:1999–2013
- Söderlund U, Patchett PJ, Vervoort JD, Isachsen CE (2004) The ^{176}Lu decay constant determined by Lu–Hf and U–Pb isotope systematics of Precambrian mafic intrusions. *Earth Planet Sci Lett* 219:311–324
- Steiger RH, Jäger E (1977) Subcommittee on Geochronology; convention on the use of decay constants in geo- and cosmochronology. *Earth Planet Sci Lett* 36:359–362
- Walker RJ, Horan MF, Morgan JW, Becker H, Grossman JN, Rubin AE (2002) Comparative ^{187}Re – ^{187}Os systematics of chondrites: implications regarding early solar system processes. *Geochim Cosmochim Acta* 66:4187–4201
- Wasserburg GJ, Jacobsen SB, DePaolo DJ, McCulloch MT, Wen T (1981) Precise determination of Sm/Nd ratios, Sm and Nd isotopic abundances in standard solutions. *Geochim Cosmochim Acta* 45:2311–2324
- York D (1969) Least-squares fitting of a straight line with correlated errors. *Earth Planet Sci Lett* 5:320–324

Part II Modelling Major Elements

In igneous geochemistry it is customary to discriminate between major ($> \text{ca. } 1 \text{ wt. } \%$) and trace ($< \text{ca. } 0.1 \text{ wt. } \%$) elements, with minor elements falling in between. However, no exact cut-off values have been codified separating these three groups. In the current book, we distinguish majors (occurring in large concentrations and combining to the main rock-forming minerals), dilute traces (that substitute only in very low concentrations in crystal lattice of other phases) and essential structural components (with low whole-rock contents but crystallizing own accessory minerals as soon as saturation is reached—see Part III). The main reason for such a division is that the approach to modelling of igneous processes does differ fundamentally among these three elemental groups.

This definition can lead to slightly unexpected results, whereby elements such as K would be regarded as traces in mafic/ultramafic systems, whereas Cr in ultramafic rocks or Zr or even REE in high-silica alkali magmas are major elements. Although somewhat unusual, this approach actually allows for a better description of the relevant systems.

Chapter 6

Direct Models

The key assumption in geochemical modelling is that the process studied is closed in a thermodynamic sense, i.e. the system exchanges heat but no matter with its surroundings. Although this is often disputable (for instance, a fractionating reservoir out of which magmas are successively tapped, defining a continuous differentiation series, is *not* a closed system!), it is nevertheless a very useful assumption, in that it allows a mass-balance approach.

Traditionally, models for crystallization, melting and mixing are treated in different ways. It will be shown at the end of this chapter, however, that they are all different expressions of the same underlying mass-balance relation. For the sake of clarity, crystallization is described in some detail while melting will be presented much more concisely.

6.1 Mass Balance During Crystallization

Fractional crystallization consists in removal, from an initial (primitive) liquid, of one or several mineral phases that form a solid cumulate. While cumulate is extracted, the composition of the remaining liquid evolves, giving rise to a differentiated liquid (Fig. 6.1).

As the cumulate forms, the amount of liquid remaining in the system decreases, starting at 1 (pure liquid) and decreasing to 0 (pure solid).

The amount of liquid remaining is defined as:

$$F = \frac{W_L}{W_0} \quad (6.1)$$

Since the system is closed, $W_S + W_L = W_0$, and so:

$$1 - F = \frac{W_S}{W_0} = F_C \quad (6.2)$$

sometimes referred to as the degree of crystallization.

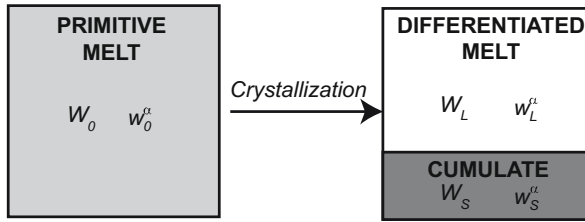


Fig.6.1 Definition of variables used in the mass-balance equation for crystallization in a closed system. The subscripts 0 , L and S are used for the primitive melt, the differentiated melt and the cumulate, respectively. W , with the relevant suffix (W_0 , W_S , etc.) denotes the total weight of one portion of the system, while w^α (with relevant suffix) stands for the amount of one component (element α) in a portion of the system.

In a closed system, the total mass w^α of any given element (α) is the same before and after crystallization. So, for each element:

$$w_0^\alpha = w_L^\alpha + w_S^\alpha \quad (6.3)$$

At this stage, it is convenient to use concentrations $C^\alpha = w^\alpha/W$ for each part of the system rather than absolute masses. Therefore:

$$C_0^\alpha W_0 = C_L^\alpha W_L + C_S^\alpha W_S \quad (6.4)$$

Since $F = W_L/W_0$ and $W_S/W_0 = 1 - F$, Eq. (6.4) becomes:

$$C_0^\alpha W_0 = F W_0 C_L^\alpha + (1 - F) W_0 C_S^\alpha \quad (6.5)$$

Equation (6.5) is commonly simplified, and written omitting the α suffix, as the wellknown mass-balance equation:

$$C_0 = F C_L + (1 - F) C_S \quad (6.6)$$

6.1.1 Graphical Solutions

In an n -dimensional space, Eq. (6.6) implies that the points representing C_S , C_0 and C_L are aligned (Fig. 6.2). This is known as the “lever rule” by analogy with a lever balancing two masses on either side of a fulcrum. The weight on the left-hand side is proportional to the length of the right-hand side arm, and conversely.

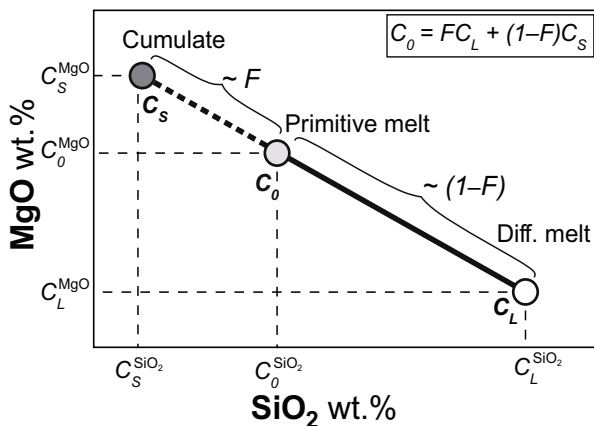


Fig. 6.2 The “lever rule” in a binary diagram (here, SiO₂ vs. MgO) is the expression of the mass-balance equation. The points representing C_S , C_0 and C_L are linearly aligned; the distance between C_0 and C_S is proportional to F and the distance between C_0 and C_L to $(1 - F)$.

6.1.2 Cumulate Composition

In the simplest case, the cumulate is made of a single mineral, and therefore its composition is equal to the mineral’s (Fig. 6.3a). This is however not a very realistic situation. In the more plausible case of a two-mineral (A and B) cumulate, its composition falls on a line connecting them (Fig. 6.3b). If the mass fraction of the mineral A in the cumulate is m_A , the cumulate chemistry can be expressed as:

$$C_S = m_A c_A + m_B c_B = m_A c_A + (1 - m_A) c_B \tag{6.7}$$

Equation (6.7) can be generalized to a cumulate containing any number of minerals:

$$C_S^\alpha = \sum_{i=1}^n (m_i c_i^\alpha) \tag{6.8}$$

where m_i is the mass fraction of mineral i in the cumulate ($0 < m_i < 1$, all summing up to 1, i.e. $\sum_{i=1}^n m_i = 1$) and c_i^α the concentration of element α in mineral i .

This is actually a mixing equation, as we will see in Sect. 6.5. In a binary plot, the cumulate composition falls in the polygon defined by individual minerals (Fig. 6.3c).

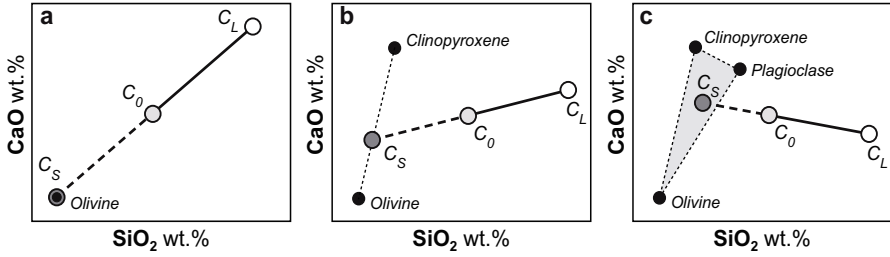


Fig. 6.3 Examples showing the relationships between a cumulate formed of one to three minerals (C_S), the primitive (C_0) and the differentiated (C_L) liquids.

6.1.3 Analytical Formulation

The mass-balance equation can be expressed in a matrix form. This will be required further on for the reverse model, and does also allow easier programming (see Chap. 9).

For each element α , one mass-balance equation [(6.6)] can be written. Taking into account all major elements ($\alpha = 1$ to p), a system with p equations is obtained:

$$\left\{ \begin{array}{l} C_0^{SiO_2} = FC_L^{SiO_2} + (1-F)C_S^{SiO_2} \\ C_0^{TiO_2} = FC_L^{TiO_2} + (1-F)C_S^{TiO_2} \\ \dots \\ C_0^{P_2O_5} = FC_L^{P_2O_5} + (1-F)C_S^{P_2O_5} \end{array} \right. \quad (6.9)$$

Likewise, assuming a cumulate made of n minerals (plagioclase, orthopyroxene...), Eq. (6.8) is expressed as:

$$\left\{ \begin{array}{l} C_S^{SiO_2} = \sum_{i=1}^n (m_i c_i^{SiO_2}) = m_{Pl} c_{Pl}^{SiO_2} + m_{Opx} c_{Opx}^{SiO_2} + \dots + m_n c_n^{SiO_2} \\ C_S^{TiO_2} = \sum_{i=1}^n (m_i c_i^{TiO_2}) = m_{Pl} c_{Pl}^{TiO_2} + m_{Opx} c_{Opx}^{TiO_2} + \dots + m_n c_n^{TiO_2} \\ \dots \\ C_S^{P_2O_5} = \sum_{i=1}^n (m_i c_i^{P_2O_5}) = m_{Pl} c_{Pl}^{P_2O_5} + m_{Opx} c_{Opx}^{P_2O_5} + \dots + m_n c_n^{P_2O_5} \end{array} \right. \quad (6.10)$$

At this stage, it is convenient to express compositions as vectors (with coordinates defined in the compositional space):

$$\overline{\mathbf{C}}_S = \begin{pmatrix} C_S^{SiO_2} \\ C_S^{TiO_2} \\ \vdots \\ C_S^{P_2O_5} \end{pmatrix} \quad (6.11)$$

and make similar formulations for $\overline{\mathbf{C}}_0$ and $\overline{\mathbf{C}}_L$.

The compositions of all individual cumulate minerals can, in the same way, be recast as a matrix with p elements in rows and n minerals in columns:

$$\overline{\overline{\mathbf{C}}}_C = \begin{pmatrix} c_{Pl}^{SiO_2} & c_{Oppx}^{SiO_2} & \dots & c_n^{SiO_2} \\ c_{Pl}^{TiO_2} & c_{Oppx}^{TiO_2} & \dots & c_n^{TiO_2} \\ \vdots & \vdots & \ddots & \vdots \\ c_{Pl}^{P_2O_5} & c_{Oppx}^{P_2O_5} & \dots & c_n^{P_2O_5} \end{pmatrix} \quad (6.12)$$

Further defining a vector $\overline{\mathbf{m}}$ with n mineral mass fractions:

$$\overline{\mathbf{m}} = \begin{pmatrix} m_{Pl} \\ m_{Oppx} \\ \vdots \\ m_n \end{pmatrix} \quad (6.13)$$

Eq. (6.10) can be recast in a more compact (and computer-friendly) form:

$$\overline{\mathbf{C}}_S = \overline{\overline{\mathbf{C}}}_C \times \overline{\mathbf{m}} \quad (6.14)$$

6.1.4 Generating a Magmatic Series Through Crystallization

The previous treatment assumes a single-step process, i.e. one during which the whole cumulate is formed and separated from the melt at once, without any change in cumulate composition or its mineral proportions. In reality, crystallization is progressive and the chemistry of the cumulate would evolve. Then a continuous process has to be modelled as a series of discrete steps. During each step, the cumulate composition can be assumed to be constant, and the *differentiated* liquid of each step becomes the *initial* liquid of the next one.

Constant Cumulate Composition

If the cumulate chemistry remains constant, the compositions of all successive differentiated liquids plot along the same, straight line linking them to the cumulate (C_S) and C_0 (Fig. 6.4). Although the process is actually stepwise (with minerals fractionating out of the “new” liquid at each stage), lever rule analysis shows that this is similar to keeping the same C_0 and decreasing the value of F .

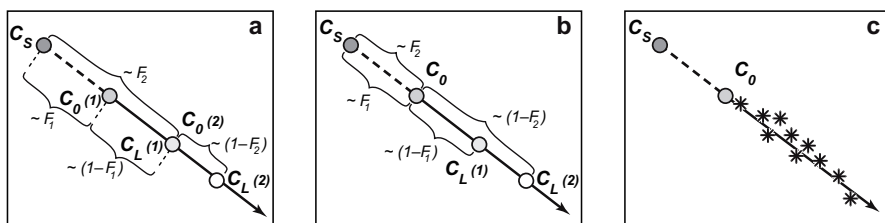


Fig. 6.4 A liquid line of descent governed by a cumulate of constant composition. (a) and (b) show two different, but numerically equivalent explanations. In (a), the differentiated liquid of step $(t-1)$ becomes the primitive liquid of step (t) ; this is the situation closest to the reality. In (b), the same process can be described as a succession of evolved liquids formed from the same primitive melt, but with decreasing F values. Panel (c) shows the resulting pattern, with samples corresponding to a *series* of differentiated liquids plotting along a straight line extending from the cumulate, and the primitive liquid.

The line that relates the series of liquids generated from the same parental magma (C_0) by extraction of a mono- or poly-mineral cumulate with a constant composition, is called a *liquid line of descent*. Mass balance implies that the cumulate composition, C_s , falls on the same line (on the side opposite to the liquids).

Changing Cumulate Composition

However, a cumulate with a constant composition is rare in natural systems. Rather, the cumulate composition often evolves in course of differentiation, producing more complex trends. For instance, for two discrete cumulate compositions (Fig. 6.5a), the resulting line of descent is inflexed, with each segment pointing towards one specific cumulate. In the case of gradual cumulate evolution, the trend is a curve that can be regarded as being made of a succession of infinitely small linear segments (Fig. 6.5b). At any point, the cumulate plots on the tangent of the curved liquid line of descent. The hump that appears on the trend does not necessarily imply that some phase appeared or disappeared in the cumulate, and may just represent a progressive change in cumulate modal composition.

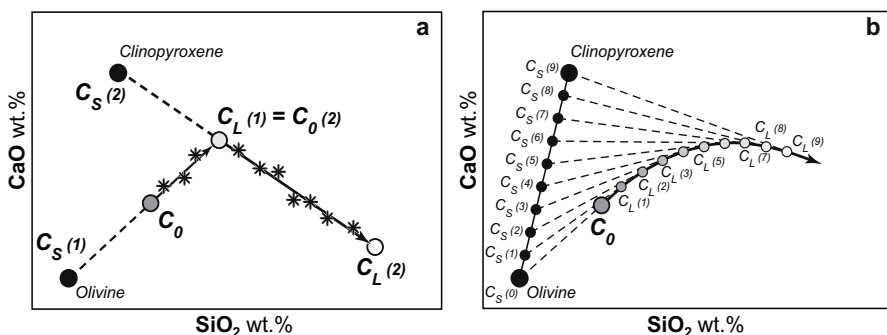


Fig. 6.5 The liquid lines of descent controlled by a cumulate of evolving composition: in two distinct steps (a) and progressively (b), the latter depicted as a series of successive small steps.

Incomplete Liquid/Solid Separation

Especially in felsic systems, where the settling of crystals is extremely slow due to the high viscosity of the magma, the separation of the cumulate and residual liquids may often be incomplete. The resulting geochemical trend can be described as a combination of two simple processes:

- Fractional crystallization, forming a cumulate and a differentiated melt, and
- Mixing between the cumulate and the differentiated melt.

This mixing is, of course, superposed on the fractionation trend. The final result is fairly similar to the simpler case of pure fractionation, except that the compositions of some rocks now fall on the cumulate–initial liquid join (Fig. 6.6).

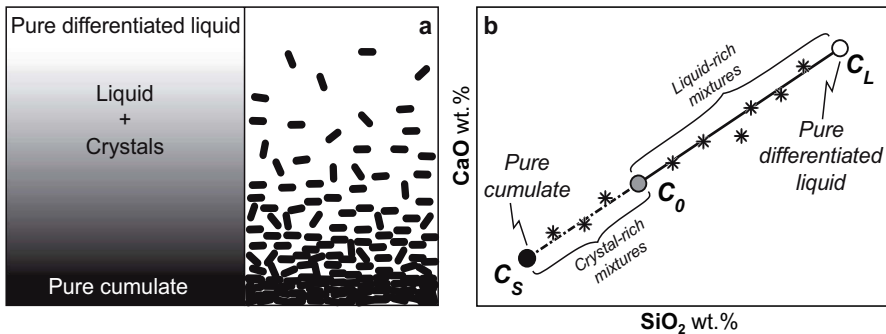


Fig. 6.6 Geochemical patterns generated by crystallization, complicated by partial cumulate extraction. **a** Conceptual sketch of this situation. **b** Since mixing is superposed on the liquid line of descent, the magma compositions can plot on the cumulate side of the line of descent.

6.2 Partial Melting

In terms of mass-balance modelling of major elements, melting resembles crystallization. The primitive liquid is now replaced by the source (the solid rock that is melting), the cumulate by the residual solid (restite) and the differentiated liquid by the newly-formed melt. The main difference is that *F* increases during the process (melt is now progressively formed, and not consumed).

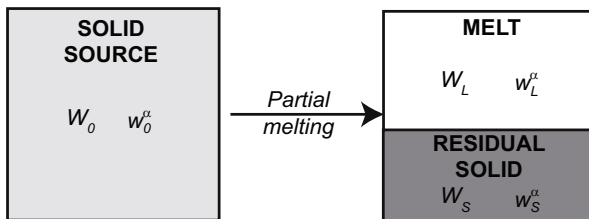


Fig. 6.7 Definition of variables used to write the mass-balance equation during partial melting in a closed system. Cf. Fig 6.1.

Similarly to fractional crystallization, partial melting does also split a homogeneous solid source into a melt and a solid residue. Consequently partial melting can be described by the same mass-balance equation as fractional crystallization:

$$C_0 = FC_L + (1 - F)C_S \quad (6.15)$$

Although this equation is written identically to Eq. (6.6), it is worth noting that here C_0 refers to the solid source (as opposed to the primitive liquid) and C_S to the restite (rather than the cumulate).

As previously [see Eq. (6.8)], the restite composition can be expressed as:

$$C_S^\alpha = \sum_{i=1}^n (m_i c_i^\alpha) \quad (6.16)$$

Or, in matrix form similar to Eq. (6.14):

$$\overline{C}_S = \overline{C}_R \times \overline{m} \quad (6.17)$$

Practically, a few differences can be noted:

- Partial melting only seldom generates well-defined liquid lines of descent, so common for crystallization,
- Peritectic minerals (Sect. 6.3) occur often during melting and their role can hardly be neglected (especially in the genesis of felsic magmas by crustal anatexis),
- Portions of the restite (either peritectic minerals, or minerals unaffected by the melting reaction) are commonly entrained into the partial melts. Incomplete liquid/cumulate separation is less common (or less clearly observed) during crystallization,
- Consequently, melting with a restite of changing composition (“progressive melting”), although a common phenomenon, is hard to constrain based solely on the interpretation of the major-element data from a magmatic series (see, however, Worked example 2, Part VI).

6.3 Peritectic Reactions

A peritectic reaction occurs when a new mineral phase is consumed (or formed) together with the melt. For instance the reaction $\text{Opx} = \text{Melt} + \text{Ol}$ is important during melting of mantle peridotites or pyroxenites. A reaction $\text{Bt} + \text{Pl} + \text{Qz} + \text{Sil} = \text{Melt} + \text{Grt}$ (Clemens and Vielzeuf 1987) is probably one of the main ones involved in crustal melting and granite generation. Peritectic reactions do also take place during crystallization; e.g., the reaction $\text{Melt} + \text{Ol} = \text{Opx}$ can occur during the differentiation of basaltic liquids.

Slight modifications to the simple mass-balance equation for *melting* (6.15) allow writing a new relation taking into account peritectic minerals (Fig. 6.8a):

$$C_0 = FC_L + QC_Q + (1 - F - Q)C_S \tag{6.18}$$

with Q and C_Q referring to the amount, and the composition, of the peritectic phase, respectively.

This formulation amounts to splitting the solid (the “restite”) into its peritectic, and non-peritectic portions, i.e. one assumes that some of the restite minerals were unaffected by the melting. Of course, this is oversimplified; melting tends to be a multivariant, continuous reaction during which the mineral compositions change. Thus it is not necessarily possible or meaningful to make this distinction, and the classical equation may be more appropriate.

In the case of *crystallization*, different formulations may be written, depending on the definition of the system considered. Assuming that it includes the initial melt (C_0), and the eventually consumed minerals (C_Q), the mass balance gives (Fig. 6.8b):

$$(1 - Q)C_0 + QC_Q = FC_L + (1 - F)C_S \tag{6.19}$$

In this case, $(1 - F)$ does not reflect the degree of crystallization anymore. Liquid was present in certain amount $(1 - Q)$ before the fractionation event described. The proportion of melt consumed (i.e., the degree of crystallization) is therefore:

$$1 - \frac{F}{(1 - Q)} \tag{6.20}$$

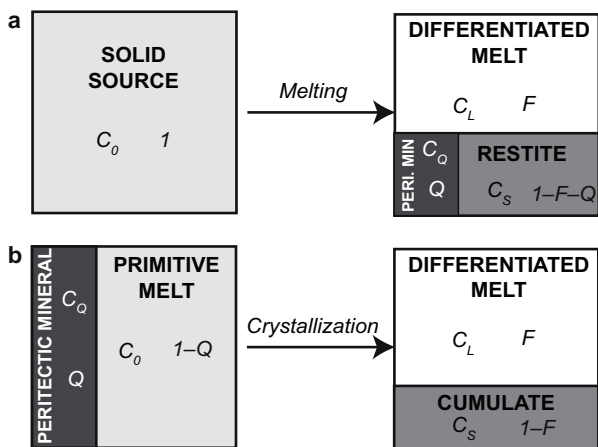


Fig. 6.8 Definition of variables used to write the mass-balance equations including peritectic phases during closed-system melting (a) or crystallization (b). For explanation, see text.

This illustrates that mass balance, in a general form, is expressed as:

$$\sum_i^{n_{START}} (m_{START} c_{START}) = \sum_i^{n_{END}} (m_{END} c_{END}) \quad (6.21)$$

with the mass fractions of each initial, and final phases summing up to 1:

$$\sum_i^{n_{START}} m_{START} = \sum_i^{n_{END}} m_{END} = 1 \quad (6.22)$$

Clearly, all the mass-balance equations written so far were special cases of this general formulation.

6.4 Mixing

Mixing is also governed by mass-balance relationships. The composition of a mixture M between two end-members, 1 and 2, is:

$$C_M = f_1 C_1 + (1 - f_1) C_2 \quad (6.23)$$

where f_1 is the weight proportion of end-member 1 in the mixture. The graphical representation is also familiar (Fig. 6.9a).

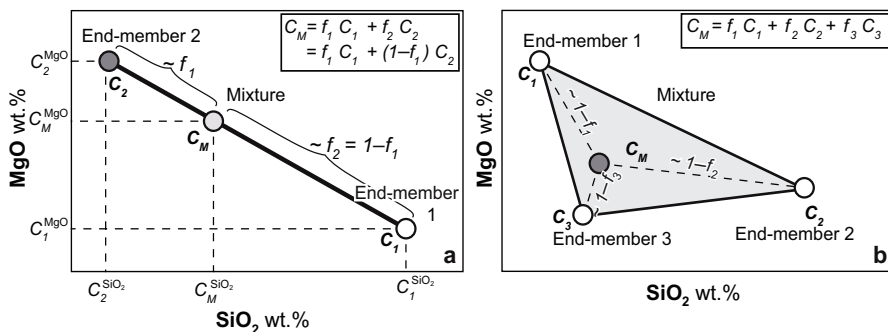


Fig. 6.9 Graphical expression of mass balance during mixing. **a** Mixing between two end-members, 1 and 2, in a binary diagram involving concentrations of arbitrary two elements (or oxides), here SiO_2 and MgO . Note that the pattern is indistinguishable from the one generated by crystallization (or melting), cf. Fig. 6.2. **b** Mixing between three end-members, 1 to 3. The products of the mixing plot in the grey triangle (a polygon, if more end-members are involved).

If m components ($m \geq 2$) are involved (e.g., Fig. 6.9b), the equation becomes:

$$C_M = \sum_{k=1}^m (f_k C_k) \quad (6.24)$$

where C_k is the concentration in component k that enters the mixing in proportion f_k ($0 < f_k < 1$; $\sum_{k=1}^m f_k = 1$).

This is nothing else than a weighted average of individual components, and the binary mixing Eq. (6.23) is its special case. In a binary diagram, the components of the mixing define a polygon (Fig. 6.9b), and the mixture is located therein (specifically at the center of mass, assuming the weight of each apex is f_k). In three-dimensional diagrams, the mixing region is a polyhedron with m apices (and in a p -dimension diagram, a hyper-volume with m apices).

As discussed in Sect. 6.1.3, this equation can also be written in a matrix form, with the concentration of the mixture expressed as a vector \overline{C}_M of p (elements) length and the mass fractions of each end-member forming a vector \overline{f} of m (end members) length. Moreover, the compositions of the end-members are recast as a matrix \overline{C}_E of p (elements) rows and m (end members) columns. Equation (6.24) becomes, in matrix form:

$$\overline{C}_M = \overline{C}_E \times \overline{f} \quad (6.25)$$

6.5 Crystallization and Partial Melting—Are These Just Special Cases of Mixing?

By now it should be clear that the mass-balance formulations used for crystallization, melting and mixing are effectively the same. Indeed, generating a differentiated melt C_L from a parental melt C_0 , with a cumulate made of n minerals is equivalent to mixing the cumulate minerals with the differentiated liquid in order to recover the composition of the parental liquid. In this case, if F is the melt fraction, and m the mineral proportions in the cumulate, the proportions in the mixing are F for the melt and $(1 - F) \times m_i$ for each mineral i . The mass-balance equation can be expressed as:

$$C_0^\alpha = FC_L^\alpha + (1 - F) \sum_{i=1}^n (m_i c_i^\alpha) \quad (6.26)$$

which we can recast in a matrix form:

$$\overline{C}_0 = \overline{C} \times \overline{f}' \quad (6.27)$$

with:

$$\vec{f}' = \begin{pmatrix} (1-F)m_{Pl} \\ (1-F)m_{Opx} \\ \vdots \\ (1-F)m_n \\ F \end{pmatrix} \quad (6.28)$$

and:

$$\vec{C} = \begin{pmatrix} c_{Pl}^{SiO_2} & c_{Opx}^{SiO_2} & \dots & c_n^{SiO_2} & c_L^{SiO_2} \\ c_{Pl}^{TiO_2} & c_{Opx}^{TiO_2} & \dots & c_n^{TiO_2} & c_L^{TiO_2} \\ \vdots & \vdots & \ddots & \vdots & \vdots \\ c_{Pl}^{P_2O_5} & c_{Opx}^{P_2O_5} & \dots & c_n^{P_2O_5} & c_L^{P_2O_5} \end{pmatrix} \quad (6.29)$$

Again, this approach will prove to be very useful when solving reverse problems (Chap. 7).

Reference

Clemens JC, Vielzeuf D (1987) Constraints on melting and magma production in the crust. *Earth Planet Sci Lett* 86:287–306

Chapter 7

Reverse Models

Although direct approach can be used to predict the compositions generated by a certain well-defined process, and compare them with observations, the real geological problems are seldom soluble in this way. Geochemists more generally face a reverse problem in which only the differentiated liquid compositions are observed¹ (e.g., as a series of lavas from a volcano or igneous province), while the other parameters such as the composition of the primitive melt, or the nature of the cumulate controlling the liquid line of descent, are not known.

7.1 An Under-Determined Problem

In the case of fractional crystallization, examining Eq. (6.27) reveals that the following parameters remain to be determined (assuming the composition C_L^α of the differentiated lava is known from sampled rocks):

- composition C_0^α of the primitive magma (for the p elements considered),
- composition C_s^α of the cumulate, itself a function of:
 - compositions C_i^α of all n cumulate minerals i ,
 - mineral mass fractions m_i in the cumulate,
- degree of fractionation ($I-F$).

In a system with p elements and n possible cumulate minerals, there is therefore a total of $p \times n$ (cumulate mineral compositions) + p (primitive liquid) + $n + 1$ (mineral proportions and F) – 1 (because all the m_i sum up to 1) variables. On the other hand, the matrix equation (6.27) represents a system of only p equations. It is therefore clear that some of the variables must be constrained using realistic geological assumptions, whereas others can be calculated from these hypotheses (Sect. 22.1).

¹ The following discussion is written for crystallization but the same logic can be applied to melting. Mixing is slightly different and thus it is addressed separately in Sect. 7.3.

7.2 Least-Square Solution to Crystallization/Melting Problems

As will be discussed in Part V, a common situation is that it has been possible to identify a plausible primitive magma C_0 and to decide, or guesstimate, the composition of the cumulate minerals c_i .

This requires solving system (6.27) for $\overline{f'}$. Only in a rare, but fortunate case when $n = p$ (\overline{C} is a square matrix), the system has a unique solution.

In fact, one is typically dealing with $p = 8$ to 10 major elements and $n \leq 6$ minerals². The system (6.27) is now *over-determined*, as it has more equations (p) than unknowns (n), and has no exact solution (\overline{C} is not a square matrix and thus cannot be inverted). It is nevertheless possible to find an approximate one that best fits all constraints (Appendix C). Solving this system means that an estimate of the vector $\overline{f'}$ should be chosen so that the computed and real elements of the vector \overline{C}_0 differ from each other as little as possible.

$$\overline{C}_0^* = \overline{C} \times \overline{f}'^* \quad (7.1)$$

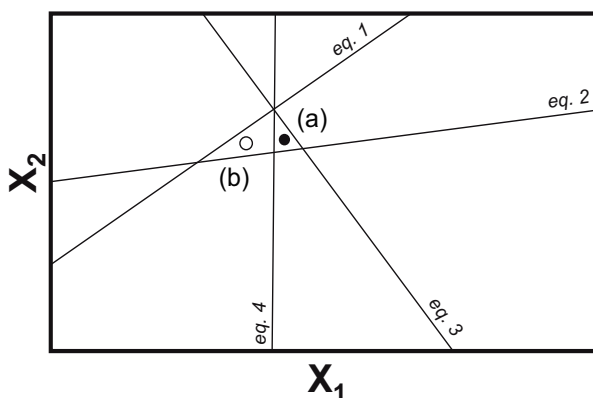


Fig. 7.1 Two unknowns and four equations: the system is overdetermined and has no exact solution. However (a) is an approximated one. It is the best least-square solution (it minimizes the distance to all four equations). Even though (b) is not the mathematical “best” solution, it is only marginally worse and may be geologically more realistic.

² It is very unlikely that $n > p$ (in which case the system would be under-determined, and have an infinity of solutions). Whereas this could happen from a numerical or geochemical point of view, the phase rule actually precludes such a situation. Crystallization is a multivariant process (at least the temperature and the composition of the melt phase do change!), so if the variance $v \geq 2$, the phase rule $v = p$ (number of chemical components) + 2 - n (number of phases) implies that it is impossible to have $n > p$.

This is commonly solved by the least-square approximation:

$$\overline{f}^{r*} = (\overline{C}^T \times \overline{C})^{-1} \times \overline{C}^T \times \overline{C}_0 \quad (7.2)$$

The sum of squares of residuals R^2 is a useful quantifier for the goodness of fit:

$$R^2 = \left| \overline{C}_0^* - \overline{C}_0 \right|^2 \quad (7.3)$$

For further details on the least-square method and its implementation in R, see Appendix C, Albarède (1995) and Janoušek and Moyen (2014).

7.3 Least-Square Solution to Mixing Problems

In a mixing problem, geological constraints are different. Typically, the possible end-members are known or at least can be assumed. The questions that can be answered by modelling are:

- Can the observed ‘hybrid’ composition be explained as a mixture of the assumed end-members?
- If so, what is the proportion of each of them?

This amounts to solving Eq. (6.25) for \overline{f} .

A general solution for mixing of an arbitrary number of components³ can be again obtained by least-square method (Appendix C):

$$\overline{f}^{r*} = (\overline{C}_E^T \times \overline{C}_E)^{-1} \times \overline{C}_E^T \times \overline{C}_M \quad (7.4)$$

As previously, R^2 gives an estimate of the quality of the model, i.e. whether the composition observed can really be explained in terms of mixing.

A special case of such reverse mixing is that of the modal recalculations. Knowing the mineral compositions, it is possible to recast them into the composition of any given rock. This approach is used routinely in experimental petrology to obtain the likely mode (in wt. %) from run-product analyses.

References

- Albarède F (1995) Introduction to geochemical modeling. Cambridge Univ Press, Cambridge
- Fourcade S, Allègre CJ (1981) Trace-elements behavior in granite genesis—a case-study the calc-alkaline plutonic association from the Querigut Complex (Pyrenées, France). *Contrib Mineral Petrol* 76:177–195
- Janoušek V, Moyen J-F (2014) Mass balance modelling of magmatic processes in GCDkit. In: Kumar S, Singh RN (eds) *Modelling of magmatic and allied processes*. The Society of Earth Scientists Series, vol 83. Springer, Berlin, pp 225–238

³ In the case of a binary mixing, the problem can be simplified and a graphical method known as the “mixing test” (Fourcade and Allègre 1981) applied (Sect. 21.4).

Chapter 8

Forward Modelling in R



Exercise 8.1: Fractional crystallization

Table 8.1 gives major-element compositions of a Mauna Kea picrite (Matzen et al. 2011) and of an ideal olivine (F_{O90}).

Table 8.1

wt. %	basalt	olivine
SiO ₂	45.15	40.87
TiO ₂	1.4	0.00
Al ₂ O ₃	7.51	0.00
FeO	11.97	9.77
MgO	25.34	49.35
CaO	6.68	0.00
Na ₂ O	1.18	0.00



MaunaKea.data

Assuming that the chemistry of picrite corresponds to that of the parental melt, calculate the compositions of fractionated magma after 5, 10, 20 and 35% crystallization of the ideal olivine.



From the mass-balance equation (6.6), one can derive for the fractionated magma composition (C_L) for each element (j):

$$C_L^j = \frac{C_0^j - c_{Ol}^j F_c}{(1 - F_c)} \quad (8.1)$$

Where: C_L = the unknown chemistry of the differentiated melt, C_0 = parental picritic magma composition, Ol = olivine, F_C = degree of fractional crystallization. This equation is the core of the following code:

```
> x <- read.table("MaunaKea.data", sep="\t")
> c0 <- x[,1] # composition of parental magma
> ol <- x[,2] # olivine composition
> fc <- c(0.05,0.1,0.2,0.35) # degrees of fractionation
> # Cycle for each of the degrees of fractionation (variable ee)
> for (ee in fc){
>   y <- (c0-ol*ee)/(1-ee) # fractionated magma [Eq.(8.1)]
>   x <- cbind(x,y)
> }
> colnames(x) <- c("C0", "Ol", fc)
> print(round(x, 2))
      C0   Ol  0.05  0.1  0.2  0.35
SiO2  45.15 40.87 45.38 45.63 46.22 47.45
TiO2   1.40  0.00  1.47  1.56  1.75  2.15
Al2O3  7.51  0.00  7.91  8.34  9.39 11.55
FeO   11.97  9.77 12.09 12.21 12.52 13.15
MgO   25.34 49.35 24.08 22.67 19.34 12.41
CaO    6.68  0.00  7.03  7.42  8.35 10.28
Na2O   1.18  0.00  1.24  1.31  1.47  1.82
```



Exercise 8.2: Fractional crystallization

Table 8.2 contains analyses of Sázava tonalite (Janoušek et al. 2004) and some of its rock-forming minerals (Janoušek et al. 2000):

Table 8.2

wt. %	Tonalite	Pl	Bt	Amp
SiO ₂	55.09	53.41	35.32	45.35
TiO ₂	0.75	0	2.11	1.39
Al ₂ O ₃	17.59	29.48	15.31	9.47
FeO _t	7.73	0.09	23.56	18.57
MgO	3.52	0	9.05	9.82
CaO	8.2	11.27	0.01	11.92
Na ₂ O	2.83	5.05	0.1	1.08
K ₂ O	2.04	0.12	9.81	1.02



sazava_fc.data

- Calculate the composition of residual melt after 20% fractional crystallization of a cumulate consisting of 50 % Pl, 30 % Bt and 20 % Amp.

- What is the composition of the cumulate?



Again, a slight modification of the mass-balance equation gives:

$$C_L^j = \frac{C_0^j - C_S^j F_c}{(1 - F_c)} \tag{8.2}$$

```
> x <- read.table("sazava_fc.data", sep="\t")
> x <- as.matrix(x) # dataframe needs to be transformed to
# a matrix for matrix multiplication
> c0 <- x[,1] # composition of parental magma
> mins <- x[, -1] # composition of fractionating phases
> m <- c(0.5, 0.3, 0.2) # mineral proportions in cumulate
> fc <- 0.2 # degree of fractionation
> ccum <- mins%*%m # cumulate composition [Eq. (6.8)]
> cl <- (c0 - ccum*fc) / (1 - fc) # and of residual liquid [Eq. (8.2)]
> x <- cbind(x, ccum, cl)
> colnames(x) <- c("tonalite", colnames(mins), "cumulate", "dif.magma")
> print(round(x, 2))
      tonalite  Pl  Bt  Amp  cumulate  dif.magma
SiO2  55.09 53.41 35.32 45.35  46.37  57.27
TiO2   0.75 0.00  2.11  1.39   0.91   0.71
Al2O3  17.59 29.48 15.31  9.47  21.23  16.68
FeO  7.73  0.09 23.56 18.57  10.83   6.96
MgO  3.52  0.00  9.05  9.82   4.68   3.23
CaO  8.20 11.27  0.01 11.92   8.02   8.24
Na2O  2.83  5.05  0.10  1.08   2.77   2.84
K2O  2.04  0.12  9.81  1.02   3.21   1.75
```



Exercise 8.3: Fractional crystallization

Fractionation of komatiitic magma can be modelled as a three-stage process, with successive cumulates forming. Table 8.3 gives the SiO₂ and CaO contents in the primitive komatiitic liquid, olivine and clinopyroxene.

Table 8.3

wt. %	SiO ₂	CaO
Primitive liquid	48.14	5.99
Ol	40.6	0
Cpx	51.2	20.73

The three successive fractionation stages are:

- (1) 40% fractionation of pure olivine,
- (2) 15% fractionation of 60% olivine + 40% clinopyroxene,

(3) 20% fractionation of pure clinopyroxene.

- Calculate the final composition of the magma.
- What is the total degree of fractionation?
- Plot a SiO_2 – CaO diagram showing the evolution of the magma.



```

> c0 <- c(48.14,5.99)           # primitive magma
> names(c0) <- c("SiO2","CaO")
> ol <- c(40.6,0)              # olivine
> cpx <- c(51.2,20.73)         # clinopyroxene

> # First stage
> fc1 <- 0.4                    # degree of fractionation
> cl1 <- (c0-ol*fc1)/(1-fc1)    # composition of the residual liquid

> # Second stage
> fc2 <- 0.15                   # degree of fractionation
> m.ol <- 0.6                   # proportion of olivine
> m.cpx <- 0.4                  # proportion of clinopyroxene
> cs <- m.ol*ol+m.cpx*cpx       # cumulate composition
> cl2 <- (cl1-cs*fc2)/(1-fc2)   # composition of the residual liquid

> # Third stage
> fc3 <- 0.2                    # degree of fractionation
> cl3 <- (cl2-cpx*fc3)/(1-fc3)  # composition of the residual liquid

> # Results
> res <- cbind(c0,cl1,cl2,cl3)
> print(round(res,3))           # print the results, rounded off
      c0    cl1    cl2    cl3
SiO2 48.14 53.167 54.636 55.495
CaO   5.99  9.983 10.282  7.670

> # Degree of fractionation
> step1 <- fc1
> step2 <- (1-step1)*fc2
> step3 <- (1-step1-step2)*fc3
> cat("Total degree of fractionation is",step1+step2+step3,"\n")
Total degree of fractionation is 0.592

> # Plot
> plot(c0[1],c0[2],xlab=expression(SiO[2]),ylab="CaO",xlim=c(45,60),
+      ylim=c(4,11),pch=16,cex=2)
> arrows(c0[1],c0[2],cl1[1],cl1[2],col="darkred",lwd=1.5)
> arrows(cl1[1],cl1[2],cl2[1],cl2[2],col="darkblue",lwd=1.5)
> arrows(cl2[1],cl2[2],cl3[1],cl3[2],col="darkgreen",lwd=1.5)

```

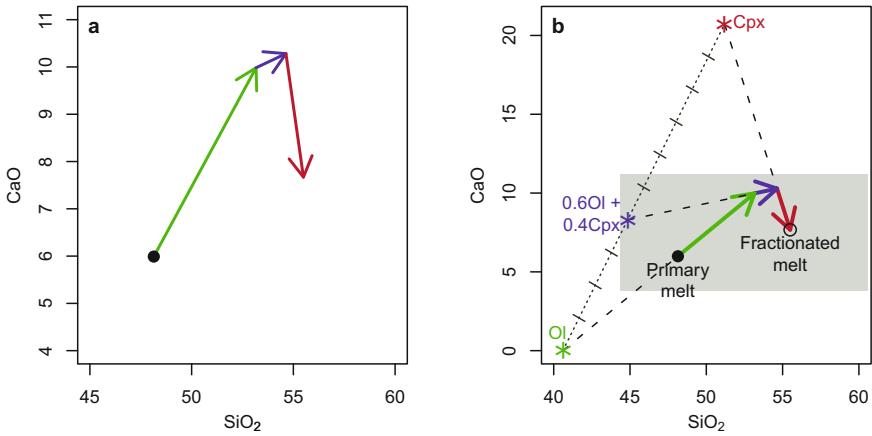


Fig. 8.1 Sequential fractionation of Ol, Ol + Cpx mixture, and Cpx (Exercise 8.3). Output of the code (a) and conceptual model (b). In (b) are also shown the three cumulates, and a gray box denoting the field of view of figure (a).



Exercise 8.4: Partial melting

Consider the case of fertile mantle peridotite melting at a mid-oceanic ridge, forming basalt. The contents of selected elements in the source mantle and the basalt are as follows (Caron et al. 1992):

Table 8.4

wt. %	Al ₂ O ₃	TiO ₂
Basalt	15	0.7
Fertile peridotite (lherzolite)	4	0.17
Depleted peridotite (harzburgite)	1	0.4

- Plot the compositions in a Al₂O₃ – TiO₂ diagram.
- Using the lever rule, determine the composition of the solid component (restite) after 10 % melting of the fertile mantle.
- Graphically indicate the maximum melt amount possible.
- How much melt can be formed if the source is a depleted peridotite?



Mass balance in this case follows from Eq. (6.15):

$$C_S^j = \frac{C_0^j - FC_L^j}{(1 - F)} \tag{8.3}$$


```
> # Build matrix with two columns of the input data, fill along rows
> qq <- matrix(c(15,0.7,4,0.17,1,0.4),ncol=2,byrow=TRUE)
> colnames(qq) <- c("Al2O3","TiO2")
> rownames(qq) <- c("basalt","fertile","depleted")
> # Plot the diagram
> plot(qq[, "Al2O3"],qq[, "TiO2"],xlim=c(0,16),ylim=c(0,1),
+      xlab=expression(Al[2]*O[3]),ylab=expression(TiO[2]),
+      xaxs="i",yaxs="i") # no extra space at axes
> text(qq[,1],qq[,2]+0.03,rownames(qq),adj=c(0.5,0))
> ff <- 0.1 # degree of melting
> residue <- (qq["fertile",]-ff*qq["basalt",])/(1-ff) # [Eq. (8.3)]
> points(residue[1],residue[2],pch=8,col="red")
> print(residue,3)
Al2O3 TiO2
2.778 0.111

> # Define the melting trend by slope and intercept
> b <- (qq["basalt",2]-qq["fertile",2])/(qq["basalt",1]-
+ qq["fertile",1]) # slope of the melting trend
> a <- qq["basalt",2]-b*qq["basalt",1]
> abline(a,b,lty="dashed") # plot a straight line
```

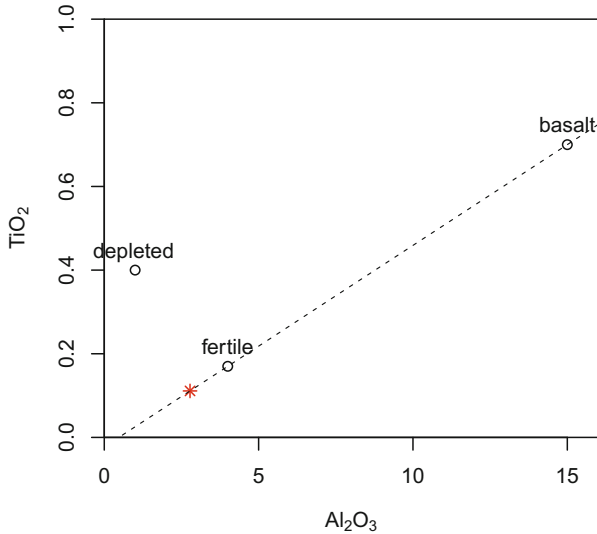


Fig. 8.2 Mass balance of fertile mantle peridotite partial meting (Exercise 8.4). The asterisk indicates the residue after 10 % melting.



Exercise 8.5: Generalized mixing

Table 8.5 contains compositions of three ideal rock-forming minerals making up a model olivine gabbro:

Table 8.5

	wt. % SiO ₂	Al ₂ O ₃	FeOt	MgO	CaO	Na ₂ O
Pl	50.54	31.70	0.00	0.00	14.36	3.40
Ol	39.19	0.00	18.75	42.06	0.00	0.00
Di	55.49	0.00	0.00	18.61	25.90	0.00



[gabbro_modal.data](#)

- Calculate whole-rock geochemical composition of gabbro that contains 50 % Pl, 30 % Ol and 20 % Di.



This is a simple calculation leading to a matrix multiplication of a vector with mineral proportions by a matrix of mineral compositions read from the datafile.

```
> mins <- read.table("gabbro_modal.data", sep="\t")
> mins <- as.matrix(mins) # Needed prior to matrix multiplication
> print(mins)
      SiO2 Al2O3  FeOt  MgO  CaO Na2O
Pl 50.54  31.7  0.00  0.00 14.36  3.4
Ol 39.19   0.0 18.75 42.06  0.00  0.0
Di 55.49   0.0  0.00 18.61 25.90  0.0
> m <- c(0.5,0.3,0.2)
> print(m%*%mins)
      SiO2 Al2O3  FeOt  MgO  CaO Na2O
[1,] 48.125 15.85  5.625 16.34 12.36  1.7
```



Precisely the same task is performed by the *GCDkit* function `WRComp`.

```
GCDkit-> print(WRComp(mins,m))
      SiO2 Al2O3  FeOt  MgO  CaO  Na2O
48.125 15.850  5.625 16.340 12.360  1.700
```

References

- Caron J-M, Gauthier A, Schaaf A, Ulysse J, Wozniak J (1992) *Comprendre et enseigner la Planète Terre*. Ophrys, Paris
- Janoušek V, Bowes DR, Rogers G, Farrow CM, Jelínek E (2000) Modelling diverse processes in the petrogenesis of a composite batholith: the Central Bohemian Pluton, Central European Hercynides. *J Petrol* 41:511–543
- Janoušek V, Braithwaite CJR, Bowes DR, Gerdes A (2004) Magma-mixing in the genesis of Hercynian calc-alkaline granitoids: an integrated petrographic and geochemical study of the Sázava intrusion, Central Bohemian Pluton, Czech Republic. *Lithos* 78:67–99
- Matzen AK, Baker MB, Beckett JR, Stolper EM (2011) Fe–Mg partitioning between olivine and high-magnesian melts and the nature of Hawaiian parental liquids. *J Petrol* 52:1243–1263

Chapter 9

Reverse Modelling in R



Exercise 9.1: Fractional crystallization (reversed Ex. 8.2)

Table 9.1

	wt. % tonalite	dif. magma	Pl	Bt	Amp
SiO ₂	55.09	57.270	53.41	35.32	45.35
TiO ₂	0.75	0.710	0	2.11	1.39
Al ₂ O ₃	17.59	16.681	29.48	15.31	9.47
FeOt	7.73	6.956	0.09	23.56	18.57
MgO	3.52	3.230	0	9.05	9.82
CaO	8.2	8.245	11.27	0.01	11.92
Na ₂ O	2.83	2.845	5.05	0.1	1.08
K ₂ O	2.04	1.748	0.12	9.81	1.02



sazava_fc2.data

- Given the compositions of the parental magma (tonalite), differentiated melt and crystallizing minerals (Table 9.1), estimate (by the least-square method) the degree of fractional crystallization and mineral proportions in the cumulate.



The least-square solution is in R provided by the function `lsfit`, while setting `intercept = FALSE`, so that the model passes through the origin (see Appendix A).

```
> x <- read.table("sazava_fc2.data", sep="\t")
> x <- data.matrix(x)
> cc <- x[,-1]      # matrix, 1st column contains dif. magma,
>                  # the remaining the mineral compositions
> C0 <- x[,1]      # parental magma composition
> ee <- lsfit(cc,C0,intercept=FALSE)
>                  # least-square solution
```

```

> fc <- 1-ee$coeff[1] # degree of fractional crystallization
> f <- ee$coeff[-1]  # if these are normalized to sum up to 1
> m <- f/sum(f)      # we get the mineral proportions
> cat(round(100*fc,3),"% fc ", "\n")
19.996 % fc
> print(m*100,4)
   Pl   Bt   Amp
50.00 30.01 19.99
> cat("\nRsquared: ", sum(ee$residuals^2), "\n")
Rsquared:  0.0000001728938

```



Exercise 9.2: Partial melting

Granitic melt is extracted from a metasediment. The melt and sediment composition, as well as possible restitic minerals, are given in Table 9.2.

Table 9.2

wt. %	Paragneiss	Melt	Bt	Pl	Qtz	Sil
SiO ₂	65.87	73.18	37.03	63.39	100.00	62.07
Al ₂ O ₃	16.29	15.17	15.37	22.97	0	36.45
Fe ₂ O ₃	5.59	0.61	25.50	0.00	0	1.48
MgO	2.01	0.47	8.90	0.00	0	0
CaO	1.84	1.80	0	4.13	0	0
Na ₂ O	3.92	3.30	0.10	9.23	0	0
K ₂ O	3.66	4.99	9.89	0.27	0	0
TiO ₂	0.82	0.49	3.21	0.00	0	0



[paragneiss_melting.data](#)

- What is the degree of melting and modal composition of the restite?



In this exercise we will once more use the least-square method. In this case we will try to recombine the melt and various minerals in the residue to reproduce the (unmelted) source composition.

```

> x <- read.table("paragneiss_melting.data", sep="\t")
> x <- as.matrix(x)      # convert for matrix multiplication
> c0 <- x[,1]           # paragneiss composition
> cc <- x[,-1]          # melt and residual minerals matrix
> ee <- lsfit(cc, c0, intercept=FALSE)
> ff <- ee$coeff[1]     # degree of partial melting
> z <- ee$coeff[-1]     # if these are normalized to sum up to 1

```

```
> m <- z/sum(z)           # we get the mineral proportions
> cat(round(100*ff,3),"% partial melting of:","\n")
30.015 % partial melting of:
> print(m*100,4)
      Bt      Pl      Qtz      Sil
30.007 45.015 19.991  4.988
```



Exercise 9.3: "Normative" calculations

Let's consider further the previous exercise.



[paragneiss_melting.data](#)

- Given the compositions of the paragneiss, the residual minerals and of the melt, what is the chemical and modal composition of the restite after 40% melting?



Here we are going to combine direct and reverse approaches. First we calculate the bulk composition of the residue using mass-balance equation (analogous to Exercise 8.4), and then we recast it to individual minerals using the least-square algorithm ("normative calculation").

```
> x <- read.table("paragneiss_melting.data",sep="\t")
> x <- as.matrix(x)           # convert for matrix multiplication
> c0 <- x[,1]                 # paragneiss composition
> c1 <- x[,2]                 # melt chemistry
> mins <- x[,-c(1,2)]         # mineral compositions
> ff <- 0.40                  # degree of partial melting
> res <- (c0-ff*c1)/(1-ff)    # mass balance for residue [Eq. (8.3)]
> print(round(res,2))
  SiO2 Al2O3 Fe2O3 MgO CaO Na2O K2O TiO2
61.00 17.04  8.91 3.04 1.87 4.33 2.77 1.04

> ee <- lsfit(mins,res,intercept=FALSE) # least-square fit gives
> m <- ee$coeff                # mineral proportions in the residue
> print(round(m,2))
      Bt      Pl      Qtz      Sil
0.34 0.46 0.17 0.04
```



Exercise 9.4: “Normative” calculations (reversed Ex. 8.5)

Table 9.3

wt. % gabbro	Pl	OI	Di	
SiO ₂	48.125	50.54	39.19	55.49
Al ₂ O ₃	15.85	31.7	0	0
FeO	5.625	0	18.75	0
MgO	16.34	0	42.06	18.61
CaO	12.36	14.36	0	25.9
Na ₂ O	1.7	3.4	0	0



[gabbro_modal2.data](#)

- Given the analyses of a gabbro and its mineral constituents (Table 9.3), estimate the wt. % of individual minerals using the least-square method.



This is analogous to the second part of the previous exercise.

```
> x <- read.table("gabbro_modal2.data", sep="\t")
> x <- as.matrix(x) # convert data frame to numeric matrix
> rock <- x[,1]     # whole-rock composition of the gabbro
> mins <- x[,-1]   # mineral compositions
> m <- lsfit(mins, rock, intercept=FALSE)$coeff
> print(round(m*100), 2)
      Pl      OI      Di
      50      30      20
```



Such “normative” calculations by standard (unconstrained) least-squares and more sophisticated constrained least-square algorithms (Appendix C) are obtained in *GCDkit* from menu *Calculations|Norms...|Mode*. Unconstrained “modal” contents of minerals, both raw and recast to 100 %, are calculated by the function `Mode`; constrained solution is available via the function `ModeC`. Further details can be found on the relevant help page, see `?Mode`.

```
GCDkit-> Mode(rock,t(mins)) # transpose, oxides should be in columns
```

```
#####
#           Unconstrained LQ           #
#####
Estimated mineral proportions (%):
  Pl  Ol  Di Sum
  50  30  20 100

Rsquared:  0
           Pl      Ol      Di estimated difference
SiO2  48.125 50.54 39.19 55.49      48.125      0
Al2O3 15.850 31.70  0.00  0.00      15.850      0
FeOt   5.625  0.00 18.75  0.00      5.625      0
MgO   16.340  0.00 42.06 18.61      16.340      0
CaO   12.360 14.36  0.00 25.90      12.360      0
Na2O   1.700  3.40  0.00  0.00      1.700      0

GCDkit-> ModeC(rock,t(mins))# same, but constrained least-squares
#####
# Constrained LQ (Albaredo 1995) #
#####
Estimated mineral proportions (%):
  Pl  Ol  Di Sum
  50  30  20 100

Rsquared:  0
           Pl      Ol      Di estimated difference
SiO2  48.125 50.54 39.19 55.49      48.125      0
Al2O3 15.850 31.70  0.00  0.00      15.850      0
FeOt   5.625  0.00 18.75  0.00      5.625      0
MgO   16.340  0.00 42.06 18.61      16.340      0
CaO   12.360 14.36  0.00 25.90      12.360      0
Na2O   1.700  3.40  0.00  0.00      1.700      0
```

In this particular case, both calculations give the same results.

Part III Modelling Trace Elements

Equilibrium (the underlying assumption to most petrological and geochemical modelling) is attained when the activities of all components in the geological system become equal (Spear 1994). In magma, such equilibrium should govern the partitioning of an element between the crystal and surrounding liquid. However, the relationships between activities and concentrations are not straightforward, as it is difficult, if not impossible, to express them in a rigorous form for all elements and minerals present in the system. Hence, geochemical modelling relies on several simplifying assumptions.

For major elements, the mineral chemistry is generally nearly constant during melting or crystallization. Thus the easiest approach is to ignore the activities altogether, and measure, or assume, the mineral chemistries. Note, however, that even in this case activities and equilibria can be calculated (Holland and Powell 1998).

Trace elements¹ pose a different challenge. With a few exceptions (Kelsey and Powell 2011), no activity–composition models are available. Also, the trace-element contents in minerals are highly variable, and usually poorly constrained. It is, therefore, generally not possible to use the same mass-balance approach as for major elements.

In the case of trace elements that occur in small amounts in the crystal lattice (so are sufficiently ‘dilute’), the activity should be proportional to their concentration (Henry 1803). The coefficient of proportionality depends on the nature of the mineral but *not* on the concentration of the element. Consequently, activities can be again ignored and replaced by the simpler concept of element partitioning between different phases (in igneous petrology, a liquid and crystal(s)). Whereas the major-element modelling relies on the *absolute concentrations* in the solid phase, the key parameter for the trace elements is the *ratio* of their concentrations in the solid phases and the liquid (Chap. 10).

¹ In this text the term “trace element” implies low whole-rock content. However, such an element can still be the main component of an accessory mineral, as is the case for Zr in zircon (ZrSiO₄).

This approach, however, fails when dealing with trace-element-rich phases. Some elements, termed essential structural constituents (ESC) (Hanson and Langmuir 1978), form a substantial part of the crystal lattice of certain accessory minerals. These are e.g., Zr in zircon, P in apatite or P, Th and LREE in monazite. Henry's Law is not applicable anymore and the strategy based on partition coefficients is inappropriate. Furthermore, activity–composition relationships are not perfectly, or not at all, established. The best approach is therefore largely empirical, based on experiments and on the notion of the mineral solubility in a silicate melt (Chap. 13).

References

- Hanson GN, Langmuir CH (1978) Modelling of major elements in mantle–melt systems using trace element approaches. *Geochim Cosmochim Acta* 42:725–741
- Henry W (1803) Experiments on the quantity of gases absorbed by water, at different temperatures, and under different pressures. *Phil Trans R Soc London* 93:29–274
- Holland TJB, Powell R (1998) An internally consistent thermodynamic dataset for phases of petrological interest. *J Metamorph Geol* 16:309–343
- Kelsey DE, Powell R (2011) Progress in linking accessory mineral growth and breakdown to major mineral evolution in metamorphic rocks: a thermodynamic approach in the Na_2O – CaO – K_2O – FeO – MgO – Al_2O_3 – SiO_2 – H_2O – TiO_2 – ZrO_2 system. *J Metamorph Geol* 29:151–166
- Spear FS (1994) *Metamorphic phase equilibria and pressure–temperature–time paths*. Mineralogical Society of America Monographs. Mineralogical Society of America, Washington

Chapter 10

Dilute Trace Elements: Partition Coefficients

10.1 Crystal Networks and Substitutions

Minerals can be regarded as piles of O atoms, leaving gaps (“sites”) for cations in between. Depending on the size of the site and the global charge balance in the crystal, different ions can fit in. For instance in silicates, tetrahedral sites are smaller than octahedral ones. Therefore a tetrahedral site can accept Si^{4+} or Al^{3+} but not Ca^{2+} or Mg^{2+} that, in turn, can fit in an octahedral site. In addition, the electric charge of ions must be such that the charge balance of the mineral is preserved. It is thus possible to replace (“substitute”) an ion by another one with the same or similar physical properties (size and charge). The better the match, the easier/more extensive the substitution could be. This means that elements can be more or less *compatible* with the crystal lattice.

10.2 Partition Coefficients

In igneous petrology, the compatibility of an element in a crystal lattice is expressed relative to the melt. This property is defined as a *partition coefficient* of element α between a mineral and the liquid¹:

$$K_{D\alpha}^{min/L} = \frac{c_{min}^{\alpha}}{C_L^{\alpha}} \quad (10.1)$$

that is often written, in short, as K_D . If $K_D > 1$, $c_{min} > C_L$ and the element is said to be *compatible* (it concentrates into the mineral rather than in the liquid). Otherwise, i.e. when $C_L > c_{min}$, the element is *incompatible* (remaining in the liquid).

¹ Various geochemistry texts use different symbols for the partition coefficients, defined here, and the bulk distribution coefficients of the Sect. 10.4. We employ K_D for partition coefficients (single mineral) and D for the bulk distribution coefficients (several minerals combined).

Note that the concept of compatibility/incompatibility is not absolute, but depends on the element, the mineral and the liquid composition². Consider, for instance, Yb in basaltic systems (Fig. 10.1), which is incompatible in most main rock-forming minerals but strongly compatible in garnet ($K_D > 5$). The same Yb, in a felsic system, becomes compatible in hornblende as well (and in clinopyroxene to a lesser degree).

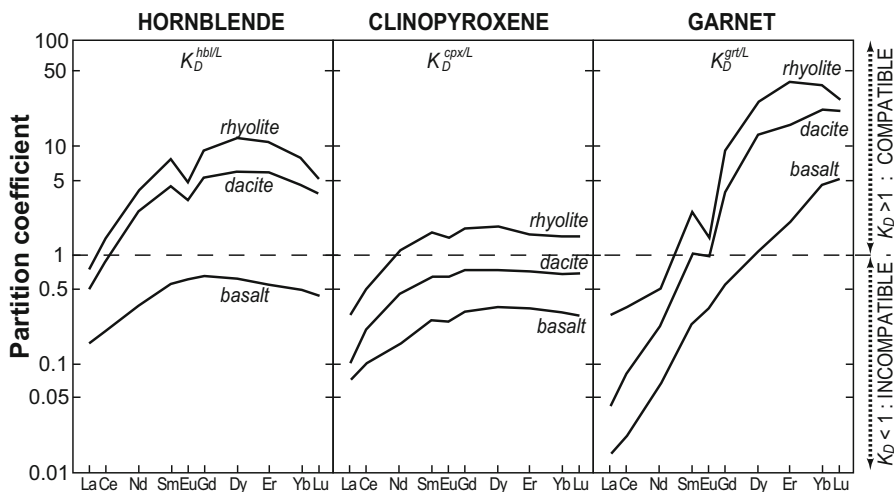


Fig. 10.1 Graphical representation of REE partition coefficients in selected rock-forming minerals in equilibrium with liquids of different compositions (Arth 1976; Hanson 1980). Although this figure resembles classical spidergrams, the values shown are not normalized concentrations, but partition coefficients. Note that while the partition coefficients for individual phases may change by an order of magnitude as a function of melt composition, the overall shapes of these curves tend to be preserved.

10.3 Controls on the Values of Partition Coefficients

Partition coefficients for a given mineral/element couple do also vary as a function of other system parameters. They are, first of all, very sensitive to the degree of polymerization, and thus to the composition, of the melt (Fig. 10.1). For instance, Bédard (2005) demonstrated that the K_D for Cr in olivine can vary by as much as 2–3 orders of magnitude when the melt's MgO content changes from 2 to 20 wt. %. The presence of volatiles (especially H_2O) in the melt also strongly influences the value of K_D .

² In fact, a partition coefficient can be determined both for major and trace elements, but Henry's Law does not apply for elements whose concentration in the crystals is too high.

The K_D values are equally sensitive to temperature (Fig. 10.2a). However, both temperature and melt compositions are normally tightly correlated. There is also a certain influence of pressure, albeit usually minor.

Finally, the redox state of the system influences the K_D values. This behaviour is well documented for Eu in plagioclase (Fig. 10.2b), but this is the case for all elements that commonly occur in several oxidation states (Ce, V, U...).

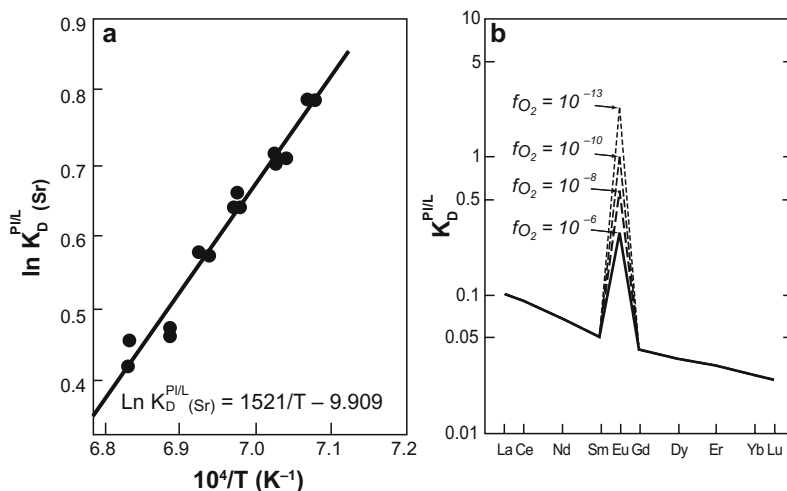


Fig. 10.2 Controls on partition coefficients. **a** A $10^4/T$ vs. $\ln K_D^{P/L}$ graph for Sr in plagioclase (Sun et al. 1974) showing that the partition coefficient is strongly dependent on temperature. **b** K_D for REE in plagioclase, as a function of oxygen fugacity (Drake and Weill 1975). The decrease in oxygen fugacity (reducing environment) results in an increase of the $K_{D(\text{Eu})}$ value. Regardless of f_{O_2} , the K_D value for Eu in plagioclase is much higher than for any other REE, which is commonly the cause of negative Eu anomalies in many magmatic rocks.

On the other hand, Henry's Law implies that the K_D value does not depend on the concentration of the (dilute) trace element in the system (or in its subcomponents). The maximum concentration below which this approximation remains valid is not rigorously defined, though. All the models described in Chapters 11–12 implicitly assume that K_D is independent of concentration.

10.4 Bulk Distribution Coefficients

When the cumulate or the residue contains several mineral phases, the situation becomes more complex. Each mineral equilibrates with the liquid according to its own K_D . Thus, the concentrations in each phase are affected not only by the total content of this element in the system, but also by the nature and the relative abundance of the other fractionating minerals. Imagine a system where a magmatic liquid equilibrates with two minerals (in comparable abundances), one with

high K_D , and another with low K_D . The high- K_D phase would extract from the liquid almost all the element—leaving even less available for the low- K_D one.

This leads to the concept of a “bulk distribution coefficient”, D , that accounts for the behaviour of the solid phases as a whole. It can be expressed as the ratio of the concentration in the bulk solid (C_S) and in the liquid (C_L):

$$D_\alpha^{S/L} = \frac{C_S^\alpha}{C_L^\alpha} \quad (10.2)$$

Contrarily to C_L that is a single phase, C_S refers to the bulk solid, which is typically made of several minerals. Consequently, the trace-element content in the cumulate (or residue) can be expressed as a mixture of n mineral phases. Therefore, the mass-balance reads:

$$C_S^\alpha = \sum_{i=1}^n m_i c_i^\alpha \quad (10.3)$$

Combination of previous equations yields:

$$D_\alpha^{S/L} = \sum_{i=1}^n m_i K_{D\alpha}^{i/L} \quad (10.4)$$

In this way, D is expressed as a function of the partition coefficients for individual minerals. In petrogenetic modelling, D is a key parameter, exerting strong influence on trace-element behaviour.

References

- Arth JG (1976) Behavior of trace elements during magmatic processes: a summary of theoretical models and their applications. *J Res US Geol Surv* 4:41–47
- Bédard J (2005) Partitioning coefficients between olivine and silicate melts. *Lithos* 83:394–419
- Drake MJ, Weill DF (1975) Partition of Sr, Ba, Ca, Y, Eu²⁺, Eu³⁺ and other REE between plagioclase feldspar and magmatic liquid: an experimental study. *Geochim Cosmochim Acta* 39:689–712
- Hanson GN (1980) Rare earth elements in petrogenetic studies of igneous systems. *Ann Rev Earth Planet Sci* 8:371–406
- Sun C-O, Williams RJ, Sun S-S (1974) Distribution coefficients of Eu and Sr for plagioclase–liquid and clinopyroxene–liquid equilibria in oceanic ridge basalt: an experimental study. *Geochim Cosmochim Acta* 38:1415–1433

Chapter 11

Direct (Dilute) Trace-Element Models

Trace-element modelling of crystallization or melting involves a balance between solid phases and melt assessed by the partitioning concept. Most geochemists use different equations for melting (*batch* melting) and crystallization (*fractional* crystallization). We will show, however, that this choice of models—warranted as it may be—is not the only option available. Deciding between batch and fractional processes can be critical in choosing a correct modelling strategy.

In *batch (closed-system) processes*, the direction of evolution (melting or fractionation) is irrelevant, and the numerical expression identical, since they are both governed exclusively by the mass balance between the solid and the liquid. On the other hand, the formulation is distinct for *fractional melting* and *crystallization*, as these represent essentially open systems.

The logic for *mixing* modelling is rather different. Partitioning between liquid and solid phases is not a factor anymore. Mixing is, normally, treated in the same way for the whole range of elements although it will be shown that certain approaches—seldom used for majors—may be more useful for trace elements.



Equilibrium, batch, fractional—a matter of terminology

In the geochemical literature, several terms are deeply ingrained. *Melting* is described as “*batch*” or “*fractional*”, whereas *crystallization* is “*equilibrium*” (rarely) or “*fractional*” (more commonly, to the point that sometimes “fractionation” is used as a synonym for “crystallization”).

The term “equilibrium” is somewhat misleading—as fractional processes also involve equilibrium between the melt and crystals, albeit an infinitesimal one (see Part V, Sect. 24.2). In addition, “batch” melting and “equilibrium” crystallization refer to very similar processes, i.e. those without separation of the liquid from the solid before their completion.

We therefore decided to use “*batch*” and “*fractional*” qualifiers for both melting and crystallization—which in this book results in the absence of the term “*equilibrium crystallization*” and its replacement by the (so far) uncommon expression “*batch crystallization*”.

11.1 Crystallization

11.1.1 Batch Crystallization

During batch crystallization, newly crystallizing phases remain in the system (the crystals are not removed from the melt) until the process is complete. Such a situation resembles that of experimental capsules (closed system). The liquid–solid relations can be described in terms of the mass balance:

$$C_0 = FC_L + (1 - F)C_S \quad (11.1)$$

and C_S can be deduced from Eq. (10.2):

$$C_S = DC_L \quad (11.2)$$

thus giving:

$$C_L = \frac{C_0}{D + F(1 - D)} \quad (11.3)$$

Although known as the “batch melting” equation (Gast 1968; Shaw 1970), it does also apply to batch crystallization.

11.1.2 Fractional Crystallization

In this scenario, the crystals are immediately removed from the system as they form. Therefore, the equilibrium defined by Eq. (10.2) exists only for infinitesimal crystal (or melt) amounts. The differential expression linking the liquid composition with its amount, F , is:

$$(D - 1) \frac{dF}{F} = \frac{dC_L}{C_L} \quad (11.4)$$

In order to get a general expression, Eq. (11.4) must be integrated over the whole range of relevant F values. As demonstrated e.g. in Albarède (1995) or Zou (2007), for constant D this leads to the equation:

$$\frac{C_L}{C_0} = F^{(D-1)} \quad (11.5)$$

known as Rayleigh’s fractionation law, initially established for gas fractionation (Rayleigh 1896). For strongly incompatible elements ($D \sim 0$), it changes to:

$$\frac{C_L}{C_0} \rightarrow \frac{1}{F} \quad (11.6)$$

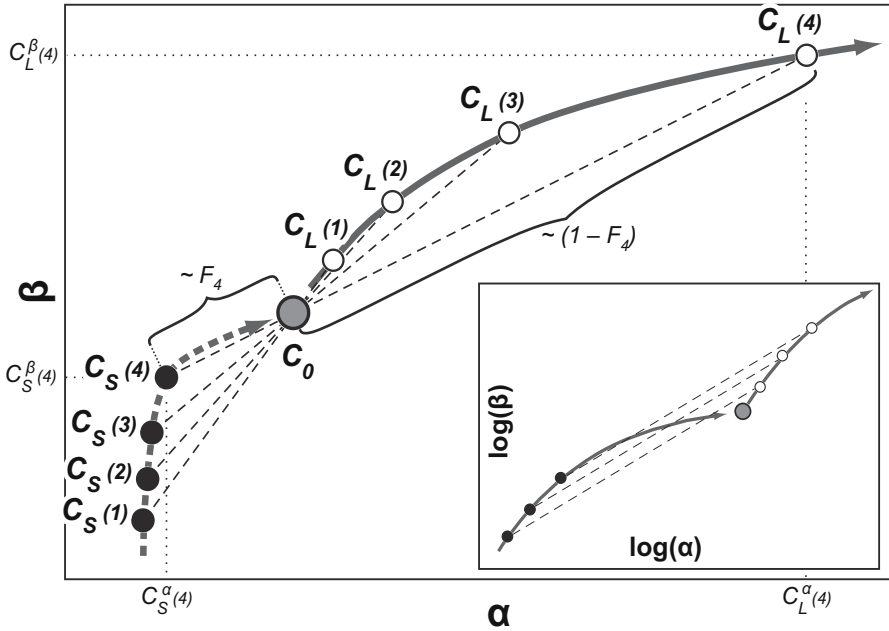


Fig. 11.1 A graphical representation of the mass-balance during batch crystallization ($D_\alpha = 0.05$, $D_\beta = 0.7$). At every stage of the process (1–4), the mass-balance holds: C_S , C_0 and C_L are linearly aligned (dashed lines). The F progressively decreases: C_S approaches C_0 (reaching it, when the whole system is solid) whereas C_L starts at C_0 and moves away from it. The trajectories of both C_S and C_L are curved. The distribution coefficient, D , has no simple graphical expression here. However, in the logarithmic coordinates (inset), both the horizontal, and the vertical distances between C_L and C_S (and therefore the slope of the dashed connecting line) remain constant at all stages. On the other hand, the mass-balance constraint has no simple graphical expression in log coordinates, as Eq. (11.1) implies no particular relationships between $\log(C_0)$, $\log(C_S)$ and $\log(C_L)$. Batch melting would result in the same pattern, except that C_L would move towards, and C_S away from, C_0 with increasing F values.

The C_L above then represents the maximum value that can be attained by Rayleigh-type fractionation at a given F .

Two equations (11.5) can be combined for a ratio of two elements, α and β :

$$\left(\frac{C^\alpha}{C^\beta} \right)_L = \left(\frac{C^\alpha}{C^\beta} \right)_0 F^{(D_\alpha - D_\beta)} \tag{11.7}$$

Clearly, the ratio of two elements with the same D ($D_\alpha \sim D_\beta$) remains nearly constant in course of crystallization, still mimicking that of the parental melt.

When it forms, the cumulate is in (local) equilibrium with the melt. From Eq. (10.2) we derive its instantaneous composition ($C_{S.inst}$):

$$\frac{C_{S.inst}}{C_0} = DC_L = DF^{(D-1)} \tag{11.8}$$

Each cumulate fragment is immediately removed but still may be accumulated elsewhere (e.g., at the bottom or walls of the magma chamber). Therefore, it may be more sensible to calculate the bulk (or aggregated) composition of the cumulate (i.e., the time-integrated composition of all instantaneous cumulates). From the mass-balance relation as well as the liquid composition [Eq. (11.5)] we obtain:

$$\frac{C_{S.bulk}}{C_0} = \frac{1 - F^D}{1 - F} \tag{11.9}$$

that, for strongly compatible elements ($D \gg 1$), changes into:

$$\frac{C_{S.bulk}}{C_0} = \frac{1}{1 - F} \tag{11.10}$$

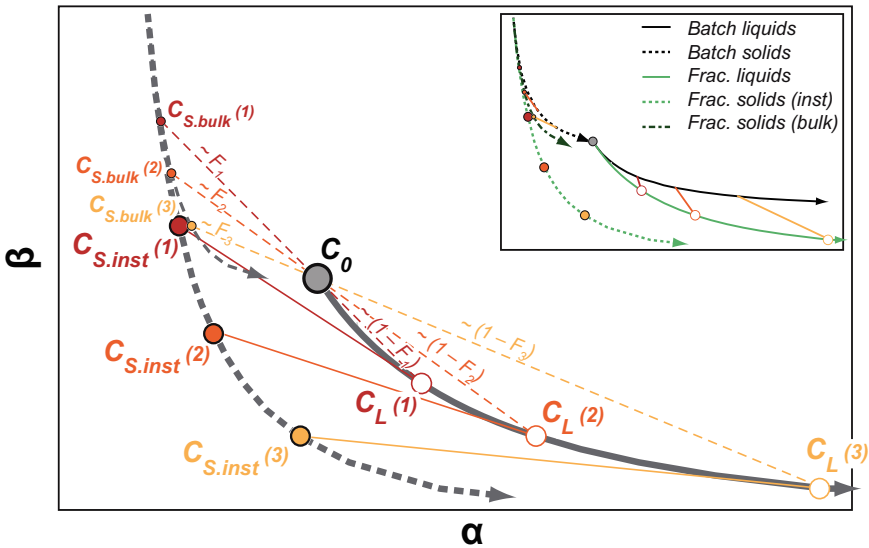


Fig. 11.2 A graphical representation of the fractional crystallization of an incompatible (α ; $D_\alpha = 0.3$) and a compatible (β ; $D_\beta = 2$) elements. Mass-balance applies to the whole system, i.e. the bulk solid and the liquid. On the other hand, there is no mass-balance link between the instantaneous solid, and the liquid (i.e., the composition C_0 does not plot on the tie-line between $C_{S.inst}$ and C_L). Inset compares the liquid evolution during the fractional and batch crystallization (the same coordinates). The former produces more “extreme” compositions, richer in incompatible elements (α) but poorer in compatible ones (β). As in Fig. 11.1, the partitioning has no simple graphical meaning in linear coordinates (but would generate tie-lines of constant slope and length between liquid and instantaneous solid in log coordinates).

11.1.3 Comparing Different Models

Liquids

Unlike batch crystallization, fractional crystallization is a very efficient way of quickly removing compatible elements from the melt (Fig. 11.3). For incompatible elements, however, the difference between fractional and batch processes is small, except at very low F (i.e. extreme crystallization). In both cases, there is an upper limit on the concentration that can be reached by crystallization [Eq. (11.6)]: for $D = 0$, both Rayleigh's and Shaw's equations collapse to $C_L/C_0 = 1/F$. This creates a 'Forbidden domain' that no liquid can enter in the F vs. C_L/C_0 diagram (Fig. 11.3). Very low values of D generate curves that are very close to the border of this domain, to the point of being practically undistinguishable.

Solids

It is important to distinguish between *batch* solids, on the one hand, and *bulk* and *instantaneous* solids generated by Rayleigh-type processes, on the other. At $F = 0$, batch and bulk solids (but *not* Rayleigh instantaneous solids) converge towards $C_S/C_0 = 1$ since the system is fully solidified. There is also a 'Forbidden domain', for very high values of D , defined by Eq. (11.10). Instantaneous solids, however, do not follow mass-balance constraints; the corresponding curves may enter the 'Forbidden domain', and do not converge to $C_L/C_0 = 1$. Again, for incompatible elements, the differences are minute. On the other hand, Rayleigh instantaneous solids are quickly impoverished in compatible elements (as they are in equilibrium with strongly depleted liquids), compared to bulk and batch solids.

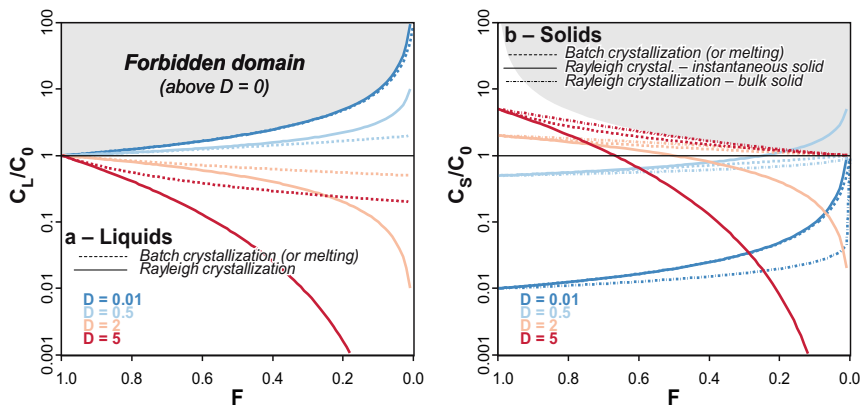


Fig. 11.3 Comparison between batch and fractional crystallization models as a function of F . Colours correspond to different D values, and line stroke to the individual models. Note that the horizontal scale is reverted, as the liquid fraction F decreases with progressive crystallization. The 'Forbidden domain' corresponds to the grey areas.

11.2 Melting

11.2.1 Batch Melting

Batch melting can be described by the same equation as the batch crystallization [Eq. (11.3)]:

$$C_L = \frac{C_0}{D + F(1 - D)} \quad (11.11)$$



In the batch melting equation, D corresponds to the bulk distribution coefficient of the solid residue *after* melting (so *not* of the original source). Expressions using the mode of the original source are given in Sect. 11.2.4.

11.2.2 Fractional Melting

When the melt is progressively extracted, the system behaves symmetrically to the fractional crystallization. In this case, the phase leaving is the melt, and that staying behind the solid residue. Similarly to the Rayleigh-type fractional crystallization [Eq. (11.5)], integrating the instantaneous mass-balance equation gives:

$$\frac{C_S}{C_0} = (1 - F)^{\left(\frac{1}{D} - 1\right)} \quad (11.12)$$

Note the symmetry of this formulation with Eq. (11.5), if substituting F by $1 - F$ and D by $1/D$. Both equations refer to the composition of the non-extracted phase, i.e. C_L for fractional crystallization, but C_S for fractional melting.

As, at any moment, the instantaneous liquid equilibrates with the solid, the combination of equations (10.2) and (11.12) gives the composition of a single melt increment at a given melt fraction F :

$$\frac{C_{L,inst}}{C_0} = \frac{1}{D} (1 - F)^{\left(\frac{1}{D} - 1\right)} \quad (11.13)$$

This equation describes the evolution of each (infinitesimally small) drop of melt as it forms, just before it is extracted from the source. Actually, each successive melt increment is likely to be collected, mixed with the previously formed melt, and re-homogenized, but not necessarily at the melting site. The mass-balance relation holds between the source, the aggregated liquid and the solid, allowing derivation of the equation for *fractional melting with accumulation* (also known as *aggregated melting*). Again, note that the form of this equation resembles Eq. (11.9):

$$\frac{C_{L.bulk}}{C_0} = \frac{1 - (1 - F)^{1/D}}{F} \tag{11.14}$$

11.2.3 Comparing Different Models

Fractional melting behaves analogously to fractional crystallization, in that it quickly removes incompatible elements from the source. Therefore, the residue is more efficiently depleted in incompatible elements compared to batch processes. On the other hand, the evolution of compatible elements does not differ much during batch and fractional melting, except for high F values (Fig. 11.4).

The evolution of melts formed by fractional melting is somewhat counter-intuitive. The fast depletion of the source in incompatible elements does not mean that the melts become extremely rich in these. Rather, the composition of instantaneous melts changes dramatically as melting progresses, their incompatible-element contents decreasing fast. Furthermore, when instantaneous melts are aggregated, the chemistry of the resulting liquid is not significantly different from that of “batch” melts. Simply any difference created by the fractional nature of the process is smoothed out by the subsequent homogenization.

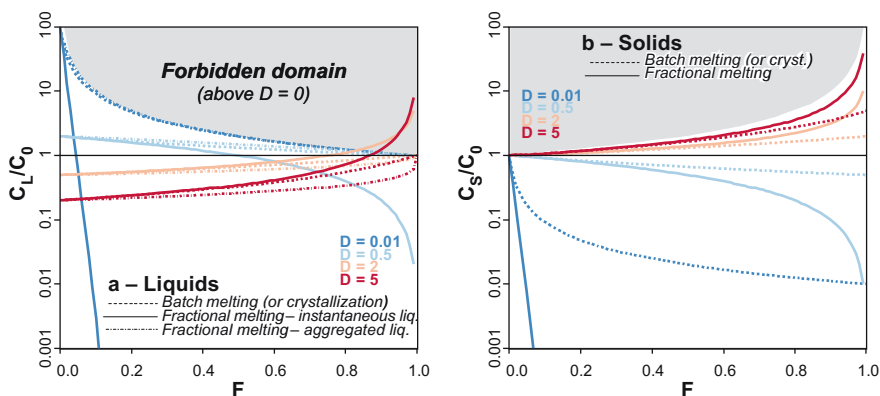


Fig. 11.4 Comparison of batch and fractional melting. These diagrams are analogous to Fig. 11.3, except that the melt fraction F increases with progressive melting. The melts (a) converge towards $C_L/C_0 = 1$ for $F = 1$, with a notable exception of the instantaneous melt of fractional melting, which is not tied by mass-balance constraints, and can also enter the ‘Forbidden domain’. The evolution of complementary solids (residues) is shown in (b).

11.2.4 Alternative Formulations of the Melting Equations

In most (if not all) cases, the modal composition of the residue would differ from that of the unmelted source. This is because melting occurs through melting reactions with a given stoichiometry, and it is extremely unlikely that the rock has

exactly the same mineral proportions. In order to account for this situation, some authors invoked the concept of “non-modal” melting. They proposed using two different bulk distribution coefficients, one for the original (unmelted) source (D_0) and another (D_P) for the mineral assemblage entering the melt:

$$D_{0\alpha} = \sum_{i=1}^n m_{0i} K_{D\alpha}^{i/L} \quad (11.15)$$

$$D_{P\alpha} = \sum_{i=1}^n p_i K_{D\alpha}^{i/L} \quad (11.16)$$

where m_0 are the mineral proportions in the (unmelted) source, and p the contributions of each mineral phase to the melt (Fig. 11.5).

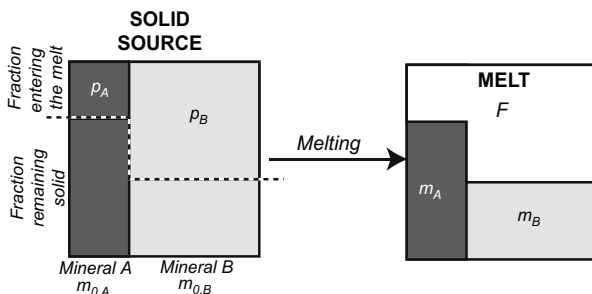


Fig. 11.5 Definition of the various mineral proportions used in the alternative melting formulations in the case of two minerals A and B . m_0 corresponds to the mode of the solid source before melting. Only a fraction of the original minerals contributes to the melt, with mineral proportions p , that are distinct from m_0 (except in the rare case of modal melting). On the right, m correspond to the proportions of minerals present in the restite after melting; $m_{0i} = Fp_i + (1 - F)m_i$.

Each set of mineral proportions (m , m_0 , p) sums to 1:

$$\sum_{i=1}^n m_{0i} = \sum_{i=1}^n m_i = \sum_{i=1}^n p_i = 1 \quad (11.17)$$

This allows recasting the *batch melting* Eq. (11.11) as:

$$C_L = \frac{C_0}{D_0 + F(1 - D_P)} \quad (11.18)$$

For modal melting (i.e. the unlikely case when the minerals melt in the same proportions as they are present in the source), $m_0 = p = m$ and thus $D_P = D_0$:

$$C_L = \frac{C_0}{D_0 + F(1 - D_0)} \quad (11.19)$$

i.e., it reduces back to the common batch melting equation.



The original definition of the batch melting equation [Eq. (11.11)] may be superior in that it takes into account modal proportions *after* melting. Thus it can be applied universally, for modal as well as non-modal melting. On the other hand, it requires knowledge (or assumptions) of the modal composition of the restite that may or may not be easier to obtain than the initial modal composition of the source prior to melting.

Analogous notation can be used to describe *fractional melting*:

$$C_{L.inst} = \frac{C_0}{D_0} \left(1 - \frac{D_p F}{D_0} \right)^{\left(\frac{1}{D_p} - 1 \right)} \quad (11.20)$$

and *fractional melting with accumulation*:

$$C_{L.bulk} = \frac{C_0}{F} \left(1 - \left(1 - \frac{D_p F}{D_0} \right)^{\frac{1}{D_0}} \right) \quad (11.21)$$

Whether these formulations are more useful than the ones using the D based on the solid residue depends on the specific problem.



In all the models proposed above, D is taken as a constant throughout the fractionation/melting history. This is actually highly unlikely, because, in natural systems, (1) the proportions of the crystallizing phases may change, abruptly or gradually, during fractionation (e.g., amphibole replaces pyroxene during the fractional crystallization of a calc-alkaline magma) as may the stoichiometry of the melting reactions, and (2) the K_D values depend on the composition of the liquid, as well as P–T conditions. This issue can be tackled by two methods:

Analytical approach

Equation (11.5) can be adapted to the case of variable D . For instance, when D is a linear function of F , $D = a + bF$, it becomes (Greenland 1970):

$$\frac{dC_L}{C_L} = (a + bF - 1) \frac{dF}{F} \quad (11.22)$$

which integrates to:

$$C_L = C_0 e^{[(a-1)\ln F + b(F-1)]} \quad (11.23)$$

Note that if $b = 0$, D is constant and the equation collapses to Rayleigh's law. It is possible to derive analogous, or even more complex equations (Zou 2007), by putting other constraints on the evolution of D during fractionation (or by writing similar equations for melting). However, one is limited to cases when it is possible to express D evolution using a (reasonably simple) mathematical function¹.

Numerical approach

A more empirical approach consists in breaking down the melting (or crystallization) process into several successive steps, during each of which D can be assumed to be constant. For each stage t , $C_0(t)$ is taken as being the end-product of the previous one ($C_L(t-1)$); thus D is calculated using the modal composition of the cumulate/residue stable during the specific step. This modal composition can be constrained by petrology, experimental data or otherwise [Worked Example 2].

11.3 Mixing

The mixing equation for individual (major or trace) elements relies on a simple mass balance, and consequently, it does not invoke any partitioning at all. Therefore, Eq. 6.24 established for the major-elements is also applicable for traces, and the graphical representation remains the same (cf. Fig. 6.9):

$$C_M = \sum_{k=1}^m (f_k C_k) \quad (11.24)$$

11.3.1 Ratio of Two Elements During Binary Mixing

When two components (1 and 2) mix in proportions f such that $f_1 + f_2 = 1$, the relation between two elements (α and β) in the mixture can be established as follows:

$$R_M = \frac{C_M^\alpha}{C_M^\beta} = \frac{f_1 C_1^\alpha + (1 - f_1) C_2^\alpha}{f_1 C_1^\beta + (1 - f_1) C_2^\beta} \quad (11.25)$$

11.3.2 Mixing Hyperbolae in Ratio–Ratio Plots

The treatment of binary mixing in a ratio–ratio plot of four trace elements² (a , b , u and v) (Fig. 11.6) stems from Vollmer (1976) and Langmuir et al. (1978) with

¹ Specifically, one that can be integrated symbolically. Of course, it is always possible to integrate any differential equation using numerical methods such as finite differences implemented in R, for instance in the package `RootSolve`.

² Ratios between two major elements, or a major and a trace element, would behave in the same way but are seldom used.

step-by-step derivation of the formulae shown in Zou (2007). Based on Eq. (11.25), we can write for each of the ratios:

$$x_m = \left(\frac{v}{b}\right)_m = \frac{v_1 f_1 + v_2 (1 - f_1)}{b_1 f_1 + b_2 (1 - f_1)}, \quad y_m = \left(\frac{u}{a}\right)_m = \frac{u_1 f_1 + u_2 (1 - f_1)}{a_1 f_1 + a_2 (1 - f_1)} \quad (11.26)$$

As $v = bx$, and $u = ay$, the coordinates are:

$$x_m = \frac{b_1 x_1 f_1 + b_2 x_2 (1 - f_1)}{b_1 f_1 + b_2 (1 - f_1)}, \quad y_m = \frac{a_1 y_1 f_1 + a_2 y_2 (1 - f_1)}{a_1 f_1 + a_2 (1 - f_1)} \quad (11.27)$$

Both Eq. (11.27) can be merged, eliminating f_1 :

$$\frac{b_2 (x_2 - x_m)}{(b_1 - b_2) x_m - b_1 x_1 + b_2 x_2} = \frac{a_2 (y_2 - y_m)}{(a_1 - a_2) y_m - a_1 y_1 + a_2 y_2} \quad (11.28)$$

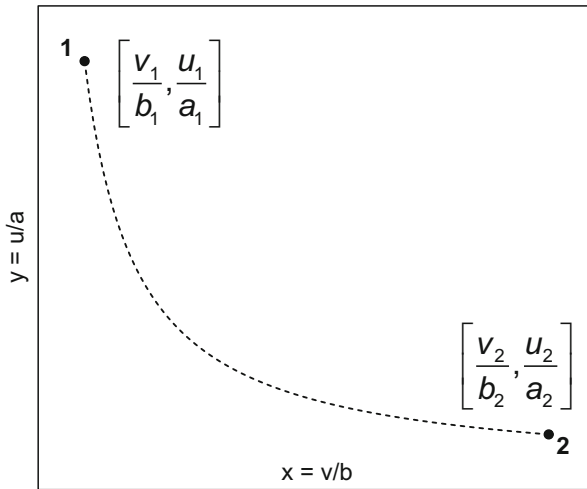


Fig. 11.6 Schematic drawing of a mixing hyperbola in the $x = v/b$ vs. $y = u/a$ coordinates.

which can be rearranged as:

$$Ax_m + Bx_m y_m + Cy_m + D = 0 \quad (11.29)$$

and thus:

$$y_m = -\frac{(Ax_m + D)}{(Bx_m + C)} \quad (11.30)$$

In a x - y plot, this equation defines a hyperbola whose curvature is controlled by B (and becomes a straight line if $B = 0$).

The coefficients A , B , C , D for the general mixing hyperbola [Eq. (11.29)] are presented in Table 11.1 for two independent trace-element ratios v/b and u/a . This table also shows some special cases encountered in igneous geochemistry (such as ratio–ratio plots with a common denominator or element–ratio plots) (see also Langmuir et al. 1978; Zou 2007).

Table 11.1 Various cases of the general mixing hyperbola equation [Eq. (11.29)]

Binary plot type	x	y	Further constraints	Coefficients (using the ratios)	Coefficients	Becomes a straight line ($B=0$) when:
ratio–ratio (general)	v/b	u/a	–	$A = a_2 b_1 y_2 - a_1 b_2 y_1$ $B = a_1 b_2 - a_2 b_1$ $C = a_2 b_1 x_1 - a_1 b_2 x_2$ $D = a_1 b_2 x_2 y_1 - a_2 b_1 x_1 y_2$	$A = b_1 u_2 - b_2 u_1$ $B = a_1 b_2 - a_2 b_1$ $C = a_2 v_1 - a_1 v_2$ $D = u_1 v_2 - u_2 v_1$	$\frac{a_1}{a_2} = \frac{b_1}{b_2}$
ratio–ratio (common denominator)	v/a	u/a	$a = b$	$A = a_1 a_2 (y_2 - y_1)$ $B = 0$ $C = a_1 a_2 (x_1 - x_2)$ $D = a_1 a_2 (x_2 y_1 - x_1 y_2)$	$A = a_1 u_2 - a_2 u_1$ $B = 0$ $C = a_2 v_1 - a_1 v_2$ $D = v_2 u_1 - v_1 u_2$	Always
element–ratio	v	u/a	$b = 1$	$A = a_2 y_2 - a_1 y_1$ $B = a_1 - a_2$ $C = a_2 x_1 - a_1 x_2$ $D = a_1 x_2 y_1 - a_2 x_1 y_2$	$A = u_2 - u_1$ $B = a_1 - a_2$ $C = a_2 v_1 - a_1 v_2$ $D = v_2 u_1 - v_1 u_2$	$a_1 = a_2$
element–ratio (same element on both axes)	a	u/a	$b = 1, v = a$	$A = a_2 y_2 - a_1 y_1$ $B = a_1 - a_2$ $C = 0$ $D = a_1 a_2 (y_1 - y_2)$	$A = u_2 - u_1$ $B = a_1 - a_2$ $C = 0$ $D = a_2 u_1 - a_1 u_2$	$a_1 = a_2$
two elements	v	u	$a = b = 1$	$A = y_2 - y_1$ $B = 0$ $C = x_1 - x_2$ $D = x_2 y_1 - x_1 y_2$	$A = u_2 - u_1$ $B = 0$ $C = v_1 - v_2$ $D = v_2 u_1 - v_1 u_2$	Always

11.4 Assimilation and Fractional Crystallization (AFC)

The AFC model describes the compositional evolution of a magma that undergoes simultaneous assimilation and fractionation. This is, for instance, the case of a mantle-derived magma contaminated by the continental crust through which it ascends. The model assumes that the extra heat needed for assimilation (which is an endothermic process) is provided by the latent heat of crystallization. Already O’Hara (1977) developed equations describing trace-element (and isotope) behaviour during open-system fractionation in a periodically recharged magma chamber with assimilation. The forward AFC model was elaborated by Allègre and Minster (1978), Taylor (1980) and De Paolo (1981).

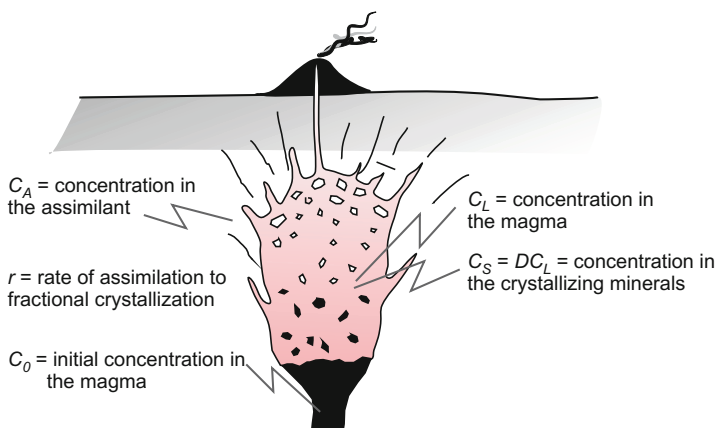


Fig. 11.7 Schematic representation of the AFC process for trace elements (after De Paolo 1981).

The instantaneous mass balance of the process (Fig. 11.7) is:

$$dW_L + dW_C + dW_A = 0 \tag{11.31}$$

with W_L , W_C and W_A referring to the amounts of the given element in the melt, crystallized phases and assimilated material, respectively. The evolution of the magma chemistry is then controlled by interplay of two key parameters: D , the bulk distribution coefficient and r , rate of assimilation to fractional crystallization (i.e., the mass ratio of material assimilated to that crystallized) (De Paolo 1981):

$$r = \frac{\dot{W}_A}{\dot{W}_C} \tag{11.32}$$

Defining the fraction of the liquid remaining, F :

$$F = \frac{W_0 - W_C + W_A}{W_0}, \tag{11.33}$$

using the definition of D , rearranging the Eq. (11.31) and integrating eventually leads to a somewhat complex formulation (De Paolo 1981; Zou 2007):

$$\frac{C_L}{C_0} = F^{-z} + \frac{r}{z(r-1)} \frac{C_A}{C_0} (1 - F^{-z}), \text{ where } z = \frac{r + D - 1}{r - 1} \quad (11.34)$$

Or,

$$\frac{C_L}{C_0} = F^{\frac{D}{1-r}} + \frac{r}{(r + D - 1)} \frac{C_A}{C_0} \left(1 - F^{\frac{D}{1-r}} \right) \quad (11.35)$$

The formulation for isotopes is treated separately in Sect. 16.2.

It is worth noting that Eq. (11.35) encompasses, as boundary conditions, both Rayleigh-type fractional crystallization ($r \rightarrow 0$ or $C_A/C_0 = 0$) and binary mixing ($r \rightarrow \infty$ and $D = 0$).

When D is small, the magma enrichment is more important than during the simple fractional crystallization (Fig. 11.8).

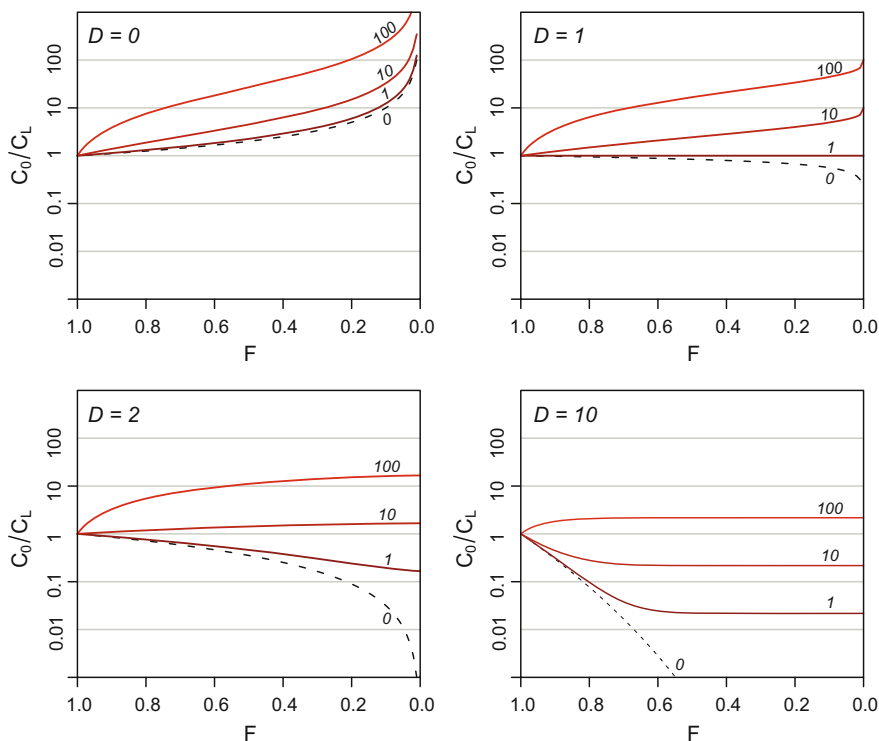


Fig. 11.8 Effects of AFC upon concentration of an element in the melt for various values of bulk distribution coefficient (D). The curves were calculated assuming $r = 2$ and are labelled by the ratios C_A/C_0 ; $C_A/C_0 = 0$ corresponds to pure fractional crystallization.

For strongly incompatible elements ($D \sim 0$), and as F approaches zero, the Eq. (11.35) changes into (De Paolo 1981):

$$\frac{C_L}{C_0} \approx \frac{1}{F} \left(1 - \frac{C_A}{C_0} \frac{r}{(r-1)} \right) \quad (11.36)$$

On the other hand, for strongly compatible elements ($D \gg 1$) we obtain (if $r < 1$):

$$C_L \approx \frac{rC_A}{r + D - 1} \quad (11.37)$$

The critical value of r representing a divide between fractionation- and assimilation-controlled AFC (i.e. $C_L/C_0 = 1$) can be calculated as (Albarède 1995):

$$r_c = \frac{1 - D}{1 - \frac{C_A}{C_0}} \quad (11.38)$$



Direct AFC models can be calculated and plotted by Petrograph (Petrelli et al. 2005) or special spreadsheets (Ersoy and Helvacı 2010; Keskin 2013).



It is worth noting that the original AFC formulation (De Paolo 1981, 1985) deals only with masses and chemical species (elements and isotopes) but does not take into account thermodynamic parameters. In natural systems, thermodynamic constraints put a limit especially on the r value. Indeed, crystallization is an exothermic process, while assimilation is endothermic. Consequently, the rate of assimilation to fractional crystallization (r) is governed by the thermal state of the assimilant (Reiners et al. 1995) and is unlikely to exceed 1 (Sect. 24.1.1).

The problem has been tackled by more comprehensive models of Energy-Constrained Assimilation–Fractional Crystallization (EC-AFC) (Spera and Bohrsen 2001) or its subsequent modifications with magma recharge and eruption (EC-E'RA χ FC) (Spera and Bohrsen 2004). They are implemented in a stand-alone program (Bohrsen and Spera 2007). However, these approaches require tightly constrained input parameters as well as a well-known magma plumbing system (Fowler et al. 2004).

11.5 Composite Models

By combining the basic laws described above (mass balance and trace-element partitioning), it is possible to derive a range of composite models.

Fairly complex equations can be found in the literature, describing a range of situations (open/closed system, fractionation/batch, crystallization and contamination, etc.). However, in the light of all uncertainties associated with geochemical data (analytical errors, sampling bias, alteration...) and their modelling (partition

coefficients...), it is unclear how much our knowledge is improved by using these complex formulations. Typically, a more sophisticated model requires more data and thus the uncertainty of the results would rapidly increase. Still, several examples are given here, as an illustration of how simple equations can be combined.

11.5.1 Crystallization with Incomplete Crystal Separation (Batch Crystallization + Binary Mixing)³

This scenario has been already discussed for majors, Sect. 6.1.4. Similar equations can be derived for trace elements by coupling batch crystallization (the crystals are *not* separated from the residual melt!) and mixing equations. For major elements, both equations are expressed in terms of mass balance, and therefore identical, which in binary diagrams results in overlapping straight lines.

However, this does not hold for trace elements (Fig. 11.9). In a binary diagram, the liquid and cumulate compositions plot along curves, while mixing results in straight lines. So, contrary to major elements, both trends are not superposed. The mixtures between crystals and liquid plot in an area delimited by the fractionation curves and the mixing lines, resulting in an irregular array centred on C_0 . The composition of the mixture, C_M , is given by the mass balance:

$$C_M = f_L C_L + (1 - f_L) C_S \quad (11.39)$$

Combining this equation with that for the batch crystallization (11.3) gives:

$$C_M = f_L \frac{C_0}{D + F(1 - D)} + (1 - f_L) D \frac{C_0}{D + F(1 - D)} \quad (11.40)$$

that may be reorganized as:

$$C_M = \frac{D + f_L(1 - D)}{D + F(1 - D)} C_0 \quad (11.41)$$

Apart from bulk distribution coefficients, this equation depends on two parameters (f_L and F). Therefore it generates a butterfly-shaped array of compositions (Fig.11.9).

³ Note that restite unmixing would be treated in the same way.

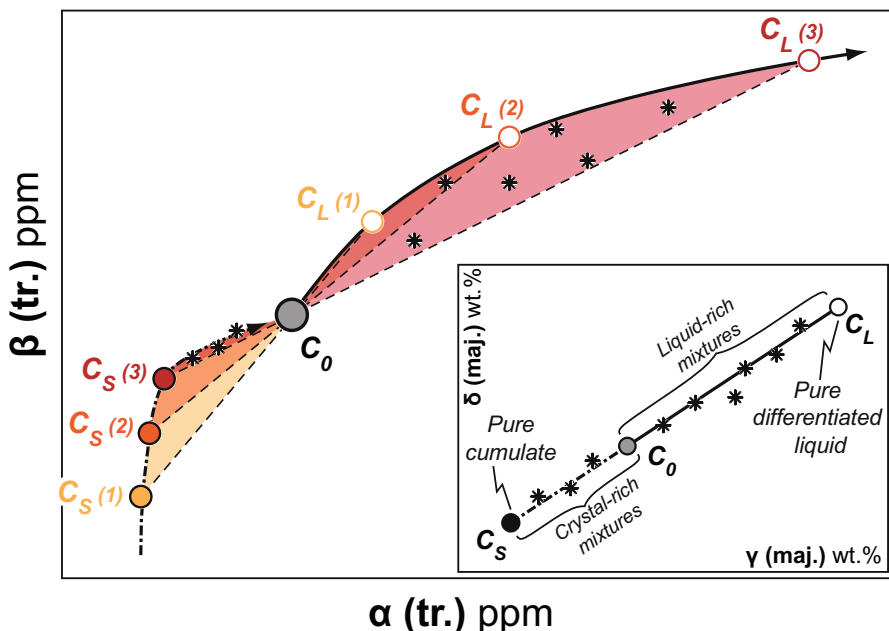


Fig. 11.9 Trace-element effects of crystallization with incomplete crystal separation, compared with the same figure for major elements (inset, and Fig. 6.6). α and β are trace elements, γ and δ majors. During differentiation, the liquid and the cumulate evolve along the thick black curves. At any given stage, mixing between the liquid C_L and the solid C_S defines a dashed straight line (passing also through C_0). The compositions of the mixtures at different stages therefore evolve in the coloured domains. This highlights the difference in modelling strategies: major elements are treated assuming a cumulate with constant composition, whereas for traces, the constant parameter is the ratio of concentrations (D).

11.5.2 Fluxed Melting (Binary Mixing + Batch Melting)

This example illustrates how a rather simple combination of two basic laws is able to describe the scenario of fusion induced by an influx of fluid (or melt). One may treat this case as a combination of mixing (between the source and the fluid/melt) with batch melting (of the metasomatized source).

Using subscripts a ($0 \leq a \leq 1$) for the contaminant and 0 for the pristine source, the compositions of the metasomatized source (C_{ms}) and melt C_L are:

$$C_{ms} = aC_a + (1 - a)C_0 \tag{11.42}$$

$$C_L = \frac{C_{ms}}{D + F(1 - D)} = \frac{aC_a + (1 - a)C_0}{D + F(1 - D)} \tag{11.43}$$

In this scenario, F/a represents the melt balance (gain/loss) during the interactions, and is a key parameter controlling the final liquid composition (Fig. 11.10).

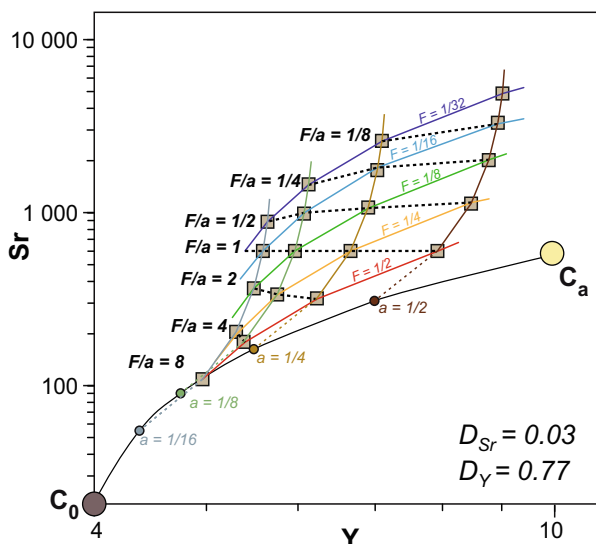


Fig. 11.10 Fluxed melting applied to the mantle contaminated by a felsitic adakitic melt (Moyen 2009), in a $\log(Y)$ vs. $\log(\text{Sr})$ diagram. The mixing between the pristine mantle and the contaminant yields the curve between C_0 and C_a . Various points along this line (for different values of a) represent the “source” (metasomatized mantle in this case, C_{ms}), that subsequently undergoes batch melting (the sub-vertical curves rising from the mixing line). The resulting compositions are plotted for various values of F . As F increases during melting, the melt composition moves towards the relevant C_{ms} value.



Often, combined trace-element models do not have to be developed from scratch. There is considerable literature addressing the philosophy and mathematics underlying these. Most notably, two monographs deal with trace elements in magmas (Shaw 2006) and quantitative igneous geochemistry in general (Zou 2007). Moreover, Albarède (1976) and Langmuir (1989) provided fundamental works on the effects of imperfect crystal–liquid separation during fractional crystallization (including trapped intercumulus melt). Open-system melting processes were reviewed by Shaw (2000). Lastly, there is a series of papers by M. J. O’Hara and co-workers dealing, for instance, with problems of crystal–liquid separation during fractional crystallization/melting (O’Hara 1993, 1995) or even defining complex models including development of periodically replenished, periodically tapped, continuously fractionated magma chambers (O’Hara 1977; O’Hara and Matthews 1981).

References

- Albarède F (1976) Some trace element relationships among liquid and solid phases in the course of the fractional crystallization of magmas. *Geochim Cosmochim Acta* 40:667–673
- Albarède F (1995) Introduction to geochemical modeling. Cambridge Univ Press, Cambridge
- Allègre CJ, Minster JF (1978) Quantitative models of trace-element behavior in magmatic processes. *Earth Planet Sci Lett* 38:1–25
- Bohrson WA, Spera FJ (2007) Energy-Constrained Recharge, Assimilation, and Fractional Crystallization (EC-RA χ FC): a Visual Basic computer code for calculating trace element and isotope variations of open-system magmatic systems. *Geochim Geophys Geosyst* 8:Q11003
- De Paolo DJ (1981) Trace element and isotopic effects of combined wallrock assimilation and fractional crystallization. *Earth Planet Sci Lett* 53:189–202
- De Paolo DJ (1985) Isotopic studies of processes in mafic magma chambers: I. The Kiglapait Intrusion, Labrador. *J Petrol* 26:925–951
- Ersoy Y, Helvacı C (2010) FC–AFC–FCA and mixing modeler: a Microsoft[®] Excel[®] spreadsheet program for modeling geochemical differentiation of magma by crystal fractionation, crustal assimilation and mixing. *Comput Geosci* 36:383–390
- Fowler SJ, Bohrson WA, Spera FJ (2004) Magmatic evolution of the Skye Igneous Centre, Western Scotland: modelling of assimilation, recharge and fractional crystallization. *J Petrol* 45:2481–2505
- Gast PW (1968) Trace element fractionation and the origin of tholeiitic and alkaline magma type. *Geochim Cosmochim Acta* 32:1057–1086
- Greenland LP (1970) An equation of trace element distribution during magmatic crystallization. *Amer Miner* 55:455–465
- Keskin M (2013) AFC-Modeler: a Microsoft[®] Excel[®] workbook program for modelling assimilation combined with fractional crystallization (AFC) process in magmatic systems by using equations of DePaolo (1981). *Turkish J Earth Sci* 22:304–319
- Langmuir CH (1989) Geochemical consequences of in situ crystallization. *Nature* 340:199–205
- Langmuir CH, Vocke RD, Hanson GN (1978) A general mixing equation with application to Icelandic basalts. *Earth Planet Sci Lett* 37:380–392
- Moyen J-F (2009) High Sr/Y and La/Yb ratios: the meaning of the “adakitic signature”. *Lithos* 112:556–574.
- O’Hara MJ (1977) Geochemical evolution during fractional crystallisation of a periodically refilled magma chamber. *Nature* 266:503–507
- O’Hara MJ (1993) Trace element geochemical effects of imperfect crystal–liquid separation. In: Prichard HM, Alabaster T, Harris NBW, Neary CR (eds) *Magmatic processes and plate tectonics*. Geological Society of London Special Publications, vol 76, pp 39–59
- O’Hara MJ (1995) Imperfect melt separation, finite increment size and source region flow during fractional melting and the generation of reversed or subdued discrimination of incompatible trace elements. *Chem Geol* 121:27–50
- O’Hara MJ, Matthews RE (1981) Geochemical evolution in an advancing, periodically replenished, periodically tapped, continuously fractionated magma chamber. *J Geol Soc London* 138:237–277
- Petrelli M, Poli G, Perugini D, Peccerillo A (2005) PetroGraph: a new software to visualize, model, and present geochemical data in igneous petrology. *Geochim Geophys Geosyst* 6:Q07011
- Rayleigh JWS (1896) Theoretical considerations respecting the separation of gases by diffusion and similar processes. *Phil Mag* 42:77–107
- Reiners PW, Nelson BK, Ghiorso MS (1995) Assimilation of felsic crust by basaltic magma: thermal limits and extents of crustal contamination of mantle-derived magmas. *Geology* 23:563–566
- Shaw DM (1970) Trace element fractionation during anatexis. *Geochim Cosmochim Acta* 34:237–243

- Shaw DM (2000) Continuous (dynamic) melting theory revisited. *Canad Mineral* 38:1041–1063
- Shaw DM (2006) Trace elements in magmas: a theoretical treatment. Cambridge University Press, Cambridge
- Spera FJ, Bohron WA (2001) Energy constrained open-system magmatic processes I: general model and Energy-Constrained Assimilation and Fractional Crystallization (EC-AFC) formulation. *J Petrol* 42:999–1018
- Spera FJ, Bohron WA (2004) Open-system magma chamber evolution: an Energy-Constrained geochemical model incorporating the effects of concurrent Eruption, Recharge, variable Assimilation and Fractional Crystallization (EC-E'RA χ FC). *J Petrol* 45:2459–2480
- Taylor HP (1980) The effects of assimilation of country rocks on $^{18}\text{O}/^{16}\text{O}$ and $^{87}\text{Sr}/^{86}\text{Sr}$ systematics in igneous rocks. *Earth Planet Sci Lett* 47:243–254
- Vollmer R (1976) Rb–Sr and U–Th–Pb systematics of alkaline rocks: the alkaline rocks from Italy. *Geochim Cosmochim Acta* 40:283–295
- Zou H (2007) Quantitative geochemistry. Imperial College Press, London

Chapter 12

Reverse (Dilute) Trace-Element Models

In theory, it is possible to apply reverse modelling to trace elements, using a least-square technique very similar to that presented for major elements (Chap. 7). Practically however, this is seldom done, as most geochemists prefer forward models, with cumulus mineral proportions constrained by major elements. Still, for the sake of completeness, the reverse modelling approach is discussed here.

12.1 Reverse Fractional Crystallization (Using Rayleigh's Law)

When C_L and C_0 have been identified, and values of partition coefficients estimated, it is possible to determine proportions (m_i) of each mineral ($i = 1$ to n) in the cumulate as well as the degree of fractional crystallization ($1-F$). The key is to linearize Rayleigh's Eq. (11.5) for each of the elements ($j = 1$ to p) (Albarède 1995):

$$\ln\left(\frac{C_L}{C_0}\right)_j = (D_j - 1) \ln F = \sum_{i=1}^n \left(\left(K_{D_j}^{i/L} - 1 \right) m_i \right) \ln F \quad (12.1)$$

Similar to major elements (Sect. 7.2), this equation can be written in a matrix form. Defining the unknown as a vector of length n :

$$\vec{M} = \begin{pmatrix} m_1 \ln F \\ m_2 \ln F \\ \vdots \\ m_n \ln F \end{pmatrix} \quad (12.2)$$

the matrix \vec{D} of partition coefficients (less one) as:

$$\overline{\overline{\mathbf{D}}} = \begin{pmatrix} K_{D_1}^{1/L} - 1 & \dots & K_{D_1}^{n/L} - 1 \\ \vdots & \ddots & \vdots \\ K_{D_p}^{1/L} - 1 & \dots & K_{D_p}^{n/L} - 1 \end{pmatrix} \quad (12.3)$$

(n columns for minerals, p rows for elements) and the composition vector [left hand side of the Eq. (12.1)] as:

$$\overrightarrow{\mathbf{C}}_v = \begin{pmatrix} \ln \left(\frac{C_L^1}{C_0^1} \right) \\ \vdots \\ \ln \left(\frac{C_L^p}{C_0^p} \right) \end{pmatrix} \quad (12.4)$$

Eq. (12.1) can be recast in matrix form as:

$$\overrightarrow{\mathbf{C}}_v = \overline{\overline{\mathbf{D}}} \times \overline{\mathbf{M}} \quad (12.5)$$

The Eq. (12.5) can be solved for $\overline{\mathbf{M}}$ by the least-square method (Appendix C).

Since $\sum_{i=1}^n m_i = 1$, the sum of all its components is:

$$\sum \overline{\mathbf{M}} = \sum_{i=1}^n m_i \ln F = \ln F \quad (12.6)$$

The fraction of melt remaining, F , can be retrieved from $\overline{\mathbf{M}}$:

$$F = e^{\sum \overline{\mathbf{M}}} \quad (12.7)$$

and the m_i values are obtained by [Eq. (12.2)]:

$$\begin{pmatrix} m_1 \\ m_2 \\ \vdots \\ m_n \end{pmatrix} = \frac{\overrightarrow{\mathbf{M}}}{\ln F} \quad (12.8)$$

12.2 Reverse Batch Partial Melting

The approach used above for fractional crystallization is feasible because we could establish a linear form of the Rayleigh's law. This is not possible with the batch melting equation. However, reverse modelling of batch melting can be performed when distribution coefficients for some elements can be estimated. For instance, during mantle peridotite melting, several elements are likely to be strongly incompatible and thus their D close to zero. If $D \rightarrow 0$, Eq. (11.11) changes to:

$$\frac{C_L}{C_0} = \frac{1}{F} \quad (12.9)$$

As soon as the F value is determined, the batch melting equation [Eq. (11.11)] can be modified for each of the p elements:

$$\left(\frac{C_0}{C_L} \right)_j - F = D_j (1-F) = \sum_{i=1}^n \left(K_{D_j}^{i/L} m_i \right) (1-F) \quad (12.10)$$

Since F is now known, the equation can be recast in matrix form. Defining the unknowns as a vector of length n (for n minerals):

$$\vec{M} = \begin{pmatrix} m_1 (1-F) \\ m_2 (1-F) \\ \vdots \\ m_n (1-F) \end{pmatrix} \quad (12.11)$$

the matrix $\overline{\overline{D}}$ of partition coefficients as:

$$\overline{\overline{D}} = \begin{pmatrix} K_{D_1}^{1/L} - 1 & \dots & K_{D_1}^{n/L} - 1 \\ \vdots & \ddots & \vdots \\ K_{D_p}^{1/L} - 1 & \dots & K_{D_p}^{n/L} - 1 \end{pmatrix} \quad (12.12)$$

(n columns for minerals, p rows for elements) and the composition vector [left hand side of the Eq. (12.10)] of length p :

$$\vec{C}_v = \begin{pmatrix} \left(\begin{array}{c} C_0^l \\ C_L^l \end{array} \right) - F \\ \vdots \\ \left(\begin{array}{c} C_0^p \\ C_L^p \end{array} \right) - F \end{pmatrix} \quad (12.13)$$

The Eq. (12.10) can be recast in matrix form as:

$$\vec{C}_v = \overline{\overline{D}} \times \overline{M} \quad (12.14)$$

and solved for \overline{M} by the least-square method.

The m_i values can be retrieved by:

$$\begin{pmatrix} m_1 \\ m_2 \\ \vdots \\ m_n \end{pmatrix} = \frac{\overline{M}}{(1-F)} \quad (12.15)$$



Note that numerical methods can be used to solve any system, even when it cannot be linearized. In R these algorithms are implemented by several functions, such as `optim` or `fsolve` (the latter of package `pracma`).

12.3 Reverse Mixing

The reverse modelling of binary mixing, i.e. essentially fitting mixing curves (which are commonly hyperbolae, Table 11.1) to real trace-element analyses, is best done by the least-square method. However, the approach is essentially the same, and arguably much more usable, in interpreting the isotope data. For this reason, the theoretical treatment of this problem is left to Part IV.

Reference

Albarède F (1995) Introduction to geochemical modeling. Cambridge Univ Press, Cambridge

Chapter 13

Trace Elements as Essential Structural Constituents of Accessory Minerals: the Solubility Concept

Accessory minerals such as zircon, monazite or apatite have annoying properties in terms of geochemical modelling. Some elements that appear only as traces in a rock can be stoichiometric components of such minerals. As a consequence, their activity–composition relationships do not obey Henry’s Law, i.e. K_D values are not independent of the concentration anymore. Neither can be such cases treated using a mass-balance approach (applied for ‘proper’ major elements) as the whole-rock abundance is low and we lack information on exact distribution of the given essential structural constituents (ESC) among all phases in the system.

The preferred modelling approach is based on the solubility of a relevant accessory phase into the melt. Let’s take zircon and fractional crystallization as an example. This mineral crystallizes when the Zr concentration in the melt exceeds a certain threshold, called saturation level, which mainly depends on the melt temperature and composition. When the melt is saturated, any excess Zr is incorporated in newly formed zircon crystals. Knowing the zircon stoichiometry, it is possible to use the saturation level to constrain the amount of zircon in the cumulate. Thus the effect of this accessory mineral on the whole trace-element budget can be modelled.

13.1 Solubility Formulae for Common Accessory Minerals

13.1.1 Zircon, $ZrSiO_4$

The zircon solubility in felsic silicate melts has attracted special attention because of the importance of this mineral in geochronology:

(1) Based on experimental calibration, the Zr saturation level has been expressed as (Watson and Harrison 1983):

$$\ln\left(\frac{c_{Zrn}^{Zr}}{(C_L^{Zr})_{sat}}\right) = (-3.80 - (0.85(M - 1))) + \frac{12900}{T} \quad (13.1)$$

where T is temperature in K, $c_{zircon}^{Zr} = 497644$ ppm (49.7 wt. %) is the stoichiometric amount of Zr in an ideal (substitution-free) zircon, and M is a whole-rock chemical parameter based on cation fractions¹:

$$M = \frac{Na + K + 2Ca}{Al \times Si} \quad (13.2)$$

Equation (13.1) was determined for a normal peraluminous granite having $M \approx 1.3$, and applies in the range $0.9 < M < 1.7$ (Fig. 13.1).

Reversing Eq. (13.1), the zircon saturation temperature can be expressed as:

$$T = \frac{12900}{\ln\left(\frac{497644}{(C_L^{Zr})_{sat}}\right) + 3.80 + 0.85(M - 1)} \quad (13.3)$$

(2) A revised formulation based on the linear regression of the same experimental data has been proposed by Kelsey et al. (2008):

$$\ln\left(\frac{c_{Zrn}^{Zr}}{(C_L^{Zr})_{sat}}\right) = \frac{11574}{T} - 0.679 FM - 1.7965 \quad (13.4)$$

Where FM is defined, again using cation fractions, as:

$$FM = \frac{Na + K + 2(Ca + Fe + Mg)}{Al \times Si} \quad (13.5)$$

¹ These are cation *fractions*, i.e. the sum of all major cations, including those not involved in this equation (Fe, Mg...) must equal 1. Consequently, these values differ from e.g. millications [Sect. 2.2.2] that are not normalized. Practically, this means that M cannot be calculated without knowing the composition of the magmatic liquid for all major elements.

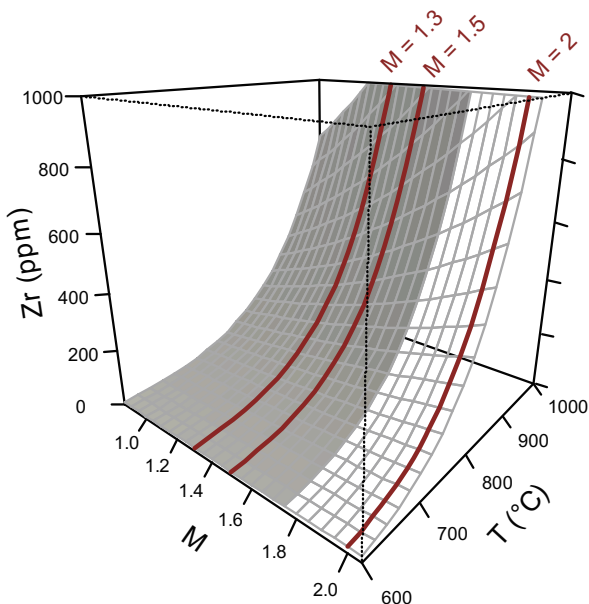


Fig. 13.1 Graphical representation of zircon saturation equation [Eq. (13.1), Watson and Harrison (1983)]. The Zr saturation value is plotted as a function of the temperature (in °C) and the parameter M . The dark red lines show the saturation levels for M values of a typical andesite (2), dacite (1.5) and rhyolite (1.3), or their plutonic equivalents. Saturation levels depend slightly on M values, and strongly on T (Exercise 14.5). During crystallization, both parameters decrease, resulting in a drastic drop of the Zr saturation level. For high M (> 1.7), the surface has been extrapolated (white region), as it is out of scope of the original calibration.

13.1.2 Monazite, $(LREE)PO_4$

Monazite is a more complex mineral, which can incorporate all LREE (La, Ce, Pr, Nd, Sm), as well as Gd and possibly Th. Two main approaches have been used, either modelling the solubility of this accessory (taken as a whole), or looking at the partitioning between melt and monazite for individual LREE (s.l.).

Monazite saturation

Several models for monazite saturation have been proposed, considering different elements and parameters:

(1) Montel (1993) established an equation for LREE (including Gd) saturation in melts in equilibrium with monazite:

$$\left(\sum A_L^{LREE}\right)_{sat} = e^{9.50 + 2.34D^{Montel} + 0.3879\sqrt{H_2O} - \frac{13318}{T}} \quad (13.6)$$

where H_2O is expressed in wt. % and T in K. In this equation, $(\sum A_L^{LREE})$ is the sum of the atomic amounts of LREE from La to Gd (excluding Eu):

$$\left(\sum A_L^{LREE}\right)_{sat} = \sum_{j=La}^{Gd} \frac{C_L^{REE_j}}{AW_j} \quad (13.7)$$

with AW_j being the atomic weight of REE j and $C_L^{REE_j}$ the concentration in ppm. D^{Montel} is defined as (in cation fractions):

$$D^{Montel} = \frac{(Na + K + Li + 2Ca)}{Al} \times \frac{1}{(Al + Si)} \quad (13.8)$$

The monazite saturation temperature can be derived from Eq. (13.6) as:

$$T = \frac{13318}{9.5 + 2.34D^{Montel} + 0.3879\sqrt{H_2O} - \ln\left(\sum A_L^{LREE}\right)_{sat}} \quad (13.9)$$

(2) Monazite is however a solid solution that can include Th and U besides LREE. Hence, Eq. (13.6) must be multiplied by $X_{\Sigma REEPO_4}^{Mnz}$, which is the molar proportion of the REE-bearing monazite:

$$\left(\sum A_L^{LREE}\right)_{sat}^{Corr} = X_{\Sigma REEPO_4}^{Mnz} \left(\sum A_L^{LREE}\right)_{sat} \quad (13.10)$$

If unknown, a typical value of $X_{\Sigma REEPO_4}^{Mnz}$ is 0.83 (Montel 1993).

This set of equations must not be used for Ca-rich magmas, where allanite is likely to be the main LREE-bearing mineral. In addition, the Fe and Mg contents of the magma should be low. For granitic compositions, typical D^{Montel} values range from 0.9 to 1.1.

(3) Kelsey et al. (2008) established a different formula, resembling their Eq. (13.4) used for zircon:

$$\ln\left(\frac{C_{Mnz}^{\Sigma LREE}}{(C_L^{\Sigma LREE})_{sat}}\right) = \frac{-310}{T} - 1.324 FM + 7.5852 \quad (13.11)$$

The stoichiometric amount of LREE in monazite, $(LREE)PO_4$, C_{Mnz}^{LREE} , is 566,794 ppm and FM is defined by Eq. (13.5). Unlike in Eq. (13.6), the REE are expressed here in ppm (i.e. weight units).

(4) A new calibration accounts for the effects of pressure (Stepanov et al. 2012):

$$\ln(C_{melt}^{\Sigma LREE}) = 16.16 + 0.23\sqrt{H_2O} - \frac{11494}{T} - 19.4\frac{P}{T} + \ln X_{\Sigma REEPO_4}^{Mnz} \quad (13.12)$$

where only the concentrations (in ppm) of the light REE (La to Sm) are considered, H_2O is in wt. %, T temperature in K and P pressure in kbar.

Partitioning of various LREE in monazite

Monazite/melt partitioning of each REE (and Th)² can be, for each element, expressed as (Montel 1993, 1996):

$$A_L^{REE_j} = X_{\Sigma REEPO_4}^{Mnz} \times e^{\frac{W_j}{RT}} \times e^{9.50+2.34D^{Montel}+0.3879\sqrt{H_2O}-\frac{13318}{T}} \quad (13.13)$$

where $A_L^{REE_j}$ represents the atomic amount of element REE_j in the melt, i.e.:

$$A_L^{REE_j} = \frac{C_L^{REE_j}}{AW_j} \quad (13.14)$$

and $X_{\Sigma REEPO_4}^{Mnz}$ is the proportion of the REE-bearing end-member in the monazite.

W_j/R is a constant depending on the element (W_j = molar energy in $J.mol^{-1}$, R = universal gas constant, $8.31 J/mol^{-1}K^{-1}$):

Element	Th	La	Ce	Pr	Nd	Sm	Gd
W_j/R	-520	-260	-116	31	177	460	750

Note that Eq. (13.11) is not equivalent to Eq. (13.6), and both models predict (slightly) different total REE in the melt (Fig. 13.2):

$$\left(\Sigma A_L^{LREE}\right)_{sat} \neq \sum_{j=La}^{Gd} A_L^{REE_j} \quad (13.15)$$

² Thorium is not a REE, but Montel (1996) proposed to treat it in the same way.

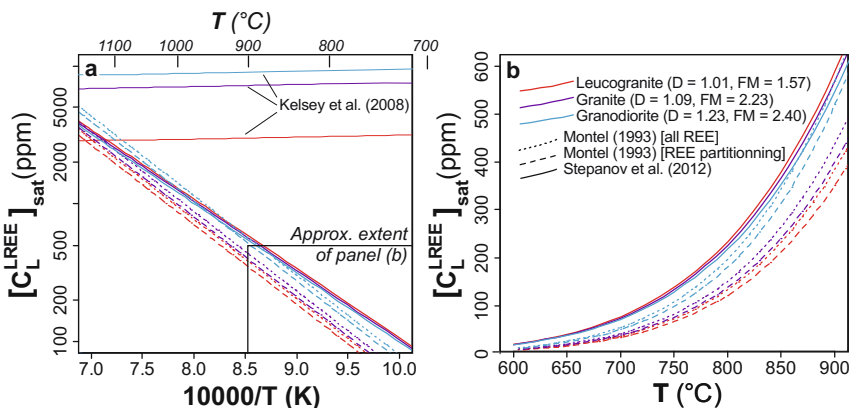


Fig. 13.2 Comparison of different monazite solubility equations. In order to make comparison possible, the “total LREE” of Montel’s Eq. (13.6) has been converted to weight units (ppm), assuming that the relative proportions of REE are the same as calculated by Eq. (13.11). Stepanov et al.’s Eq. (13.12) (at 5 kbar) is based only on five LREE (La to Sm), but the concentrations of Gd are generally sufficiently low to make little difference. The distinct sets of curves correspond to an average leucogranite ($FM = 1.57$, $D^{Montel} = 1.01$), a S-type biotite granite ($FM = 2.23$, $D^{Montel} = 1.09$) and a granodiorite ($FM = 2.40$, $D^{Montel} = 1.23$, probably out of the application field of the models because of its significant Ca contents). As pointed out by Stepanov et al. (2012), Kelsey’s equation predicts very high saturation values, which would imply that monazite should be nearly always dissolved in melts. However, Kelsey et al.’s formulation has a stronger dependency on the melt composition that offsets this effect to a point. The remaining models give mutually comparable results, their variation not exceeding 10–20 %.

13.1.3 Apatite, $Ca_5(PO_4)_3(F,Cl,OH)$

Based on experimental work, Harrison and Watson (1984) proposed an equation for apatite solubility in metaluminous melts ($A/CNK < 1$):

$$\ln \left(\frac{c_{Ap}^{P_2O_5}}{(c_L^{P_2O_5})_{sat.HW}} \right) = \frac{8400 + 26400 \left(\frac{c_L^{SiO_2}}{100} - 0.5 \right)}{T} - \left(3.1 + 12.4 \left(\frac{c_L^{SiO_2}}{100} - 0.5 \right) \right) \quad (13.16)$$

where $c_L^{SiO_2}$ and $c_L^{P_2O_5}$ are wt. % in the melt, T is temperature in K and $c_{Ap}^{P_2O_5}$ is the stoichiometric P_2O_5 content in pure apatite (42 wt. %). This equation applies to melts with 45–75 wt. % SiO_2 , 0–10 wt. % H_2O at a range of crustal pressures.

The apatite saturation temperature can be expressed from Eq. (13.16) as:

$$T = \frac{8400 + 26400 \left(\frac{C_L^{SiO_2}}{100} - 0.5 \right)}{\ln \left(\frac{42}{\left(C_L^{P_2O_5} \right)_{sat.HW}} \right) + 3.1 + 12.4 \left(\frac{C_L^{SiO_2}}{100} - 0.5 \right)} \quad (13.17)$$

However, peraluminous melts ($A/CNK > 1$) are able to dissolve much more apatite than predicted by Harrison and Watson's (1984) equation. This is due to the formation of aluminium–phosphate complexes in peraluminous aluminosilicate melts, in which P^{5+} is bonded with Al^{3+} to form $AlPO_4$ species (Mysen et al. 1999 and references therein). Three strategies were proposed to tackle the effect of enhanced solubility in peraluminous melts (Fig. 13.3):

(1) Bea et al. (1992)—based on experiments of Holtz and Johannes (1991), they proposed correcting the saturation values $\left(C_L^{P_2O_5} \right)_{sat.HW}$ of Harrison and Watson (1984) as follows:

$$\left(C_L^{P_2O_5} \right)_{sat} = \left(C_L^{P_2O_5} \right)_{sat.HW} \times e^{\frac{6429(A/CNK-1)}{T-273.15}} \quad (13.18)$$

(2) Pichavant et al. (1992)—experimental correction, at 750–1000 °C, 2–5 kbar:

$$\left(C_L^{P_2O_5} \right)_{sat} = \left(C_L^{P_2O_5} \right)_{sat.HW} + (A/CNK - 1) e^{\frac{-5900}{T} - 3.22 \times \frac{C_L^{SiO_2}}{100} + 9.31} \quad (13.19)$$

(3) Wolf and London (1994)—experimental, at 750 °C and 200 MPa only:

$$\left(C_L^{P_2O_5} \right)_{sat} = -3.4 + 3.1 \times A/CNK \quad (13.20)$$



Saturnin and solubility models in GCDkit

GCDkit comes with a plugin *Saturation.r* containing a set of functions to calculate the zircon, monazite, and apatite saturation levels/temperatures.

This plugin is based on a previous standalone R script *Saturnin*, documented in Janoušek (2006).

The *GCDkit* functions performing the saturation calculations are named `zrSaturation`, `mzSaturation` and `apSaturation`. See the respective help pages for references and further details.

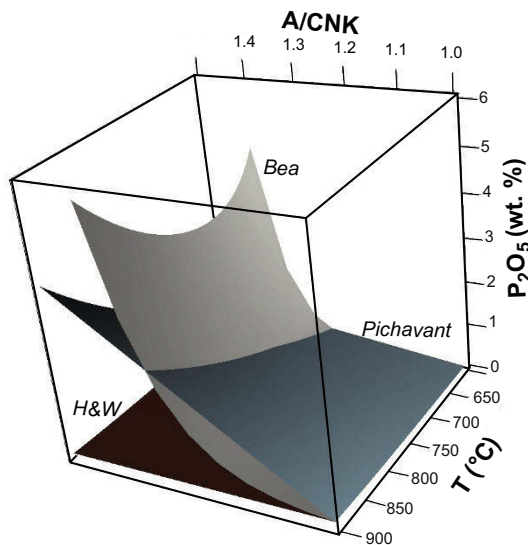


Fig. 13.3 Comparison of different apatite solubility equations in peraluminous melts ($A/CNK > 1$) as a function of temperature and A/CNK . Grey, after Bea et al. (1992); blue, Pichavant et al. (1992). Dark brown (H&W): original (very low) solubility after Harrison and Watson (1984).



The solubility equations for other accessory minerals are not so well established. This is unfortunate as, in calc-alkaline magmas, allanite ($(LREE, Ca, Y)_2(Al, Fe^{+3})_3(SiO_4)_3(OH)$) (Klimm et al. 2008) or, in peraluminous melts, xenotime ($(Y, HREE)PO_4$) (Tropper et al. 2013) have a significant effect on REE behaviour.

Titanite ($CaTiSiO_5$) stability may also be approached in terms of solubility (although recent progress in activity–composition laws rather allows to treat it in terms of thermodynamic equilibria: White et al. 2000). Moreover, there are also some data on solubility of rutile (TiO_2) (Ryerson and Watson 1987; Hayden and Watson 2007; Kularatne and Audétat 2014), and even rarer phases, such as columbite ($Fe^{2+}Nb_2O_6$) (Fiege et al. 2011).

13.2 Evolution Through Saturation

The saturation value of the given ESC controlled by accessory minerals is strongly dependent on composition and temperature. For instance, mafic/hot magmas can dissolve large amounts of Zr, much more than any of them typically contains. Magmas at such conditions are undersaturated (with respect to zircon) and Zr will behave as a typical incompatible element, following common fractionation (or melting) paths. In contrast, felsic, cooler magmas can dissolve less Zr: their Zr contents are typically buffered by solubility.

The resulting evolution is thus complex. Considering a fairly basic magma series that evolves by *fractional crystallization*, the concentration of the given ESC in the magma would initially increase, until it reaches the saturation level. From this saturation point, the ESC concentration would drop, following the saturation curve. The resulting inflexed pattern resembles the broken-line evolution described for major elements (in Sect. 6.1.4). Indeed, it also corresponds to a change in cumulate modal composition—onset of the relevant accessory phase crystallization. In Fig. 13.4, the saturation is reached at ca. 900 °C, for $M \approx 1.7$. From this point on, zircon crystallizes and Zr concentration decreases. For a saturated rock series, it is possible to read a value of T for each sample: here T evolves from 900 °C at $M = 1.7$ to about 700 °C at $M = 1.2$.

The position of the saturation point depends on several parameters. During *crystallization*, these are C_0 , D (at the undersaturated stage) and the shape of the saturation curve (a function of T and the magma composition). At higher C_0 and/or lower D , saturation is reached sooner (Fig. 13.5). It is worth noting that many acid igneous suites are saturated throughout their whole history, thus lacking the undersaturated segment completely. Thus the evolutionary path during fractionation is predetermined by the nature of the source and conditions of partial melting.

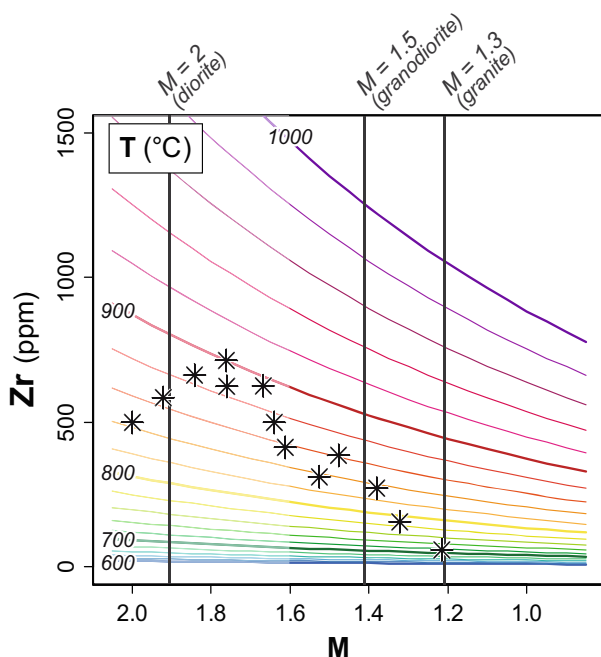


Fig. 13.4 Comparing Zr saturation levels with Zr contents in a hypothetical magmatic series (asterisks). The coloured isotherms are a graphical representation of Watson and Harrison's (1983) zircon solubility equation [Eq. (13.1)]. This corresponds to a projection of Fig. 13.1 on the M –Zr plane, with the horizontal scale reversed, so that differentiation proceeds to the right.

Watson and Harrison (1984) presented two *partial melting* scenarios related to the concentration of the ESC in the source (C_0) compared to the saturation level (C_{sat}) (e.g., Fig. 13.6 for Zr). If $C_0 > C_{sat}$, the melt is saturated throughout the melting event and its ESC content buffered at a constant level, independent of the degree of melting. In such a scenario, typical of low-T crustal anatexis, undissolved zircon cores (inheritance) are likely to be preserved (Miller et al. 2003). The ESC content of the residue rises in course of progressive melting. On the other hand, when $C_0 < C_{sat}$, the melt remains saturated in ESC only until the source is exhausted. From this point on, melt batches would be progressively depleted in the ESC. Zircon is not stable in such an undersaturated melt and any grain that comes in contact with it would eventually dissolve.

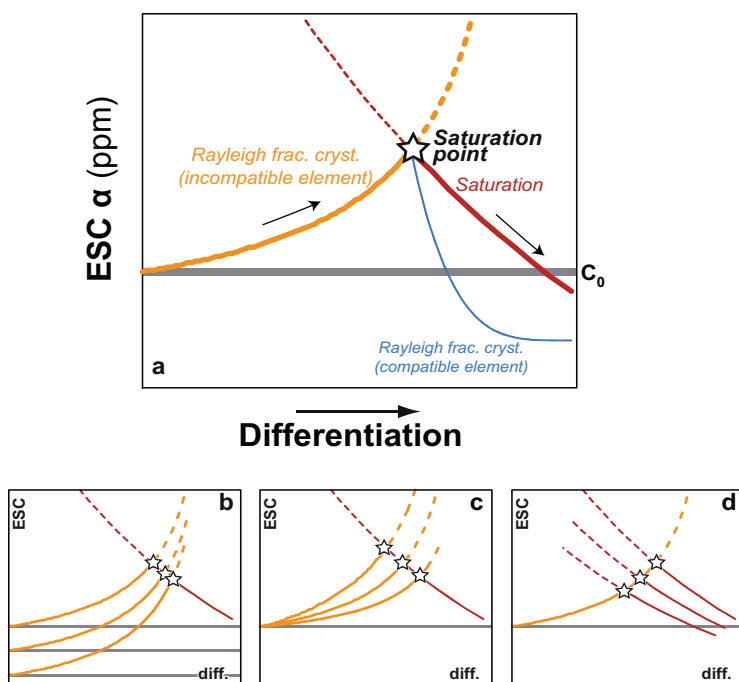


Fig. 13.5 a Behaviour of an ESC-type trace element in a magma evolving by fractional crystallization (Montel 1996). Below are shown panels demonstrating effects of C_0 (b), D (c) and the cooling path (T) of the magma (d) on the position of the saturation point.

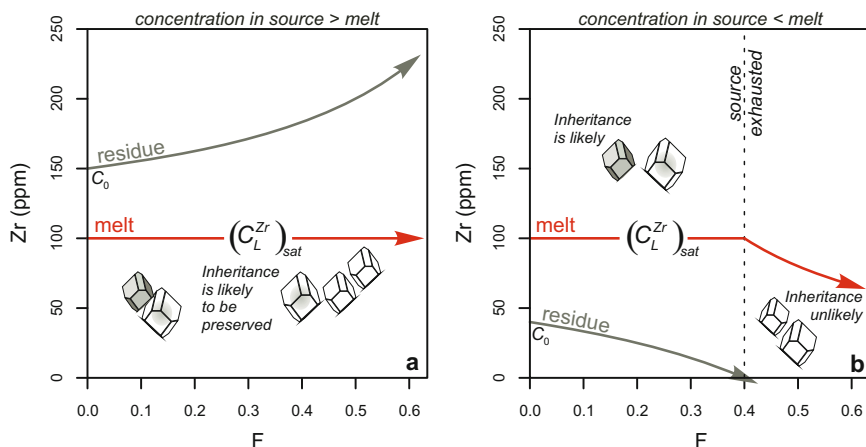


Fig. 13.6 Binary plot of F vs. Zr (ppm), showing the compositional evolution of the melt (red arrow) as well as of the corresponding residue (grey arrow), during partial melting. In the first case (a) the concentration of the ESC in the source is higher and in the second (b) lower than the saturation threshold (= concentration in the melt). After Watson and Harrison (1984).

References

- Bea F, Fershtater G, Corretgé L (1992) The geochemistry of phosphorus in granite rocks and the effect of aluminium. *Lithos* 29:43–56
- Fiege A, Kirchner C, Holtz F, Linnen RL, Dziony W (2011) Influence of fluorine on the solubility of manganotantalite ($MnTa_2O_6$) and manganocolumbite ($MnNb_2O_6$) in granitic melts—an experimental study. *Lithos* 122:165–174
- Harrison TM, Watson EB (1984) The behavior of apatite during crustal anatexis: equilibrium and kinetic considerations. *Geochim Cosmochim Acta* 48:1467–1477
- Hayden LA, Watson EB (2007) Rutile saturation in hydrous siliceous melts and its bearing on Ti-thermometry of quartz and zircon. *Earth Planet Sci Lett* 258: 561–568
- Holtz F, Johannes W (1991) Genesis of peraluminous granites I. Experimental investigation of melt compositions at 3 and 5 kbar and various H_2O activities. *J Petrol* 32:935–958
- Janoušek V (2006) Saturnin, R language script for application of accessory-mineral saturation models in igneous geochemistry. *Geol Carpath* 57:131–142
- Kelsey DE, Clark C, Hand M (2008) Thermobarometric modelling of zircon and monazite growth in melt-bearing systems: examples using model metapelitic and metapsammitic granulites. *J Metamorph Geol* 26:199–212
- Klimm K, Blundy JD, Green TH (2008) Trace element partitioning and accessory phase saturation during H_2O -saturated melting of basalt with implications for subduction zone chemical fluxes. *J Petrol* 49:523–553
- Kularatne K, Audétat A (2014) Rutile solubility in hydrous rhyolite melts at 750–900 °C and 2 kbar, with application to titanium-in-quartz (TitaniQ) thermobarometry. *Geochim Cosmochim Acta* 125:196–209
- Miller CF, McDowell SM, Mapes RW (2003) Hot and cold granites? Implications of zircon saturation temperatures and preservation of inheritance. *Geology* 31:529–532
- Montel J-M (1993) A model for monazite/melt equilibrium and application to the generation of granitic magmas. *Chem Geol* 110:127–146

- Montel J-M (1996) Géochimie de la fusion de la croûte continentale. Mémoire d'habilitation à diriger des recherches (= habilitation thesis), Université Blaise-Pascal, Clermont-Ferrand
- Mysen BO, Holtz F, Pichavant M, Beny JM, Montel J-M (1999) The effect of temperature and bulk composition on the solution mechanism of phosphorus in peraluminous haplogranitic magma. *Amer Miner* 84:1336–1345
- Pichavant M, Montel J-M, Richard LR (1992) Apatite solubility in peraluminous liquids—experimental data and an extension of the Harrison–Watson model. *Geochim Cosmochim Acta* 56:3855–3861
- Ryerson FJ, Watson EB (1987) Rutile saturation in magmas; implications for Ti–Nb–Ta depletion in island-arc basalts. *Earth Planet Sci Lett* 86: 225–239
- Stepanov AS, Hermann J, Rubatto D, Rapp RP (2012) Experimental study of monazite/melt partitioning with implications for the REE, Th and U geochemistry of crustal rocks. *Chem Geol* 300:200–220
- Tropper P, Manning C, Harlov D (2013) Experimental determination of CePO_4 and YPO_4 solubilities in H_2O – NaF at 800° C and 1 GPa: implications for rare earth element transport in high-grade metamorphic fluids. *Geofluids* 13:372–380
- Watson EB, Harrison TM (1983) Zircon saturation revisited: temperature and composition effects in a variety of crustal magmas types. *Earth Planet Sci Lett* 64:295–304
- Watson EB, Harrison TM (1984) Accessory minerals and the geochemical evolution of crustal magmatic systems: a summary and prospectus of experimental approaches. *Phys Earth Planet Inter* 35:19–30
- White RW, Powell R, Holland TJB, Worley B (2000) The effect of TiO_2 and Fe_2O_3 on metapelitic assemblages at greenschist and amphibolite facies conditions: mineral equilibria calculations in the system K_2O – FeO – MgO – Al_2O_3 – SiO_2 – H_2O – TiO_2 – Fe_2O_3 . *J Metamorph Geol* 18:497–511
- Wolf MB, London D (1994) Apatite dissolution into peraluminous haplogranitic melts: an experimental study of solubilities and mechanisms. *Geochim Cosmochim Acta* 58:4127–4145

Chapter 14

Forward Modelling in R



Exercise 14.1: Equilibrium/fractional crystallization

- Plot a graph illustrating the evolution of normalized trace-element concentrations $\log(C_L/C_0)$ as a function of the melt fraction F , for both batch [Eq. (11.3)] and fractional [Eq. (11.5)] crystallization processes. Computation should be done for different values of the bulk distribution coefficient ($D = 0.01, 0.1, 0.5, 2, 5$).



```
> # Create an empty plot (type="n"), with the correct range
> plot(1, type="n", xlim=c(0, 1), ylim=c(0.001, 100), log="y",
+      xlab="F", ylab=expression(C[L]/C[0]))
> dd <- c(0.01, 0.1, 0.5, 2, 5) # Bulk distribution coefficients
> for (i in 1:length(dd)){
>   # Calculate and plot the fractional crystallization model
>   curve(x^(dd[i]-1), from=0, to=1, lty="solid", lwd=2, col=i,
+        add=TRUE)
>   # Calculate and plot the batch crystallization model
>   curve(1/(x+dd[i]*(1-x)), from=0, to=1, lty="dashed", col=i,
+        add=TRUE)
> }
> # Add a horizontal grid and legend
> abline(h=10^(-3:2), col="gray")
> legend("topright", pch=16, col=1:length(dd), legend=dd, title="D",
+       bg="white")
```

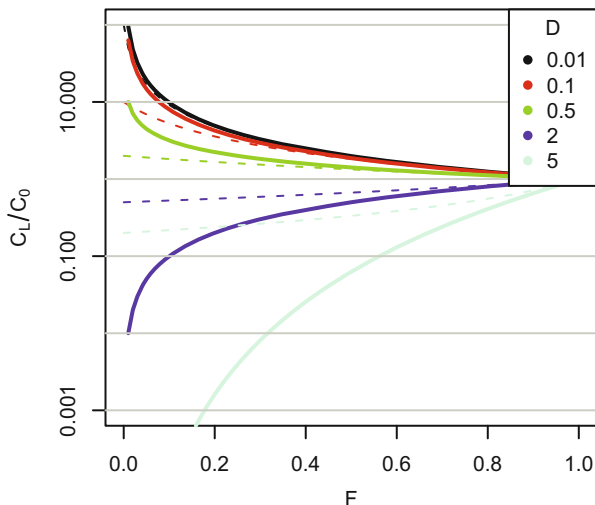


Fig. 14.1 Curves showing the evolution of the residual liquid composition during fractional (solid) and batch (dashed) crystallization for various values of bulk distribution coefficient D (Exercise 14.1). Compare with Fig. 11.3.



Exercise 14.2: Fractional crystallization

Table 14.1 shows the REE concentrations in a tonalitic magma (ppm), as well as the partition coefficients for crystallizing mineral phases.

Table 14.1

	Concentration		Partition coefficients		
	Source H34	Pl	Amp	Ilm	All
La	32.04	0.4	0.74	0.005	960
Ce	61.9	0.27	1.52	0.006	940
Nd	25.75	0.21	4.26	0.0075	750
Sm	3.97	0.13	7.77	0.01	620
Eu	0.966	2.15	5.14	0.007	56
Gd	2.3	0.097	10	0.017	440
Dy	1.16	0.064	13	0.028	200
Er	0.46	0.055	12	0.035	100
Yb	0.37	0.049	8.4	0.075	54
Lu	0.057	0.046	6	0.1	41

A differentiated magma is generated by 30 % fractional crystallization of a parental magma (H34); the cumulate consists of plagioclase, hornblende and ilmenite.

- Calculate the differentiated magma composition for a cumulate made up of 49 % plagioclase, 49 % hornblende, and 2 % ilmenite.
- Same question if the cumulate is 48.5 % plagioclase, 48.5 % hornblende, 2 % ilmenite and 1 % allanite.
- By means of the *GCDkit* function *spider*, plot chondrite-normalized REE patterns¹ (using normalization values after Boynton 1984).



```
> x <- read.table("ttg.data", sep="\t")
> x <- as.matrix(x) # transform dataframe to matrix
> c0 <- x[,1] # parental magma composition
> kd <- x[,-1] # table of partition coefficients
> fc <- 0.3 # degree of fractionation
> ff <- 1-fc # fraction of the melt left
> m1 <- c(0.49,0.49,0.02,0) # mineral props in cumulate (1)
> dd1 <- kd%*%m1 # bulk distrib. coeff. [Eq.(10.4)]
> names(m1) <- colnames(dd1)
> c11 <- c0*ff^(dd1-1) # melt composition
> cs1 <- dd1*c11 # instantaneous solid
> csavg1 <- c0*(1-ff^dd1)/(1-ff) # average solid
> m2 <- c(0.485,0.485,0.02,0.01) # mineral props in cumulate (2)
> dd2 <- kd%*%m2 # bulk distrib. coeff. [Eq. (10.4)]
> names(m2) <- colnames(dd2)
> c12 <- c0*ff^(dd2-1) # melt composition
> cs2 <- dd2*c12 # instantaneous solid
> csavg2 <- c0*(1-ff^dd2)/(1-ff) # average solid
> result <- cbind(c0,dd1,dd2,cs1,csavg1,c11,cs2,csavg2,c12)
> colnames(result) <- c("C0","D1","D2","CS1","CSavg1","CL1","CS2",
+ "CSavg2","CL2")
> print(round(result,2))
```

	C0	D1	D2	CS1	CSavg1	CL1	CS2	cSavg2	CL2
La	32.04	0.56	10.15	20.95	19.30	37.50	12.43	103.94	1.22
Ce	61.90	0.88	10.27	56.73	55.43	64.67	23.31	201.04	2.27
Nd	25.75	2.19	9.67	36.89	46.54	16.84	11.31	83.10	1.17
Sm	3.97	3.87	10.03	5.52	9.91	1.43	1.59	12.86	0.16
Eu	0.97	3.57	4.10	1.38	2.32	0.39	1.31	2.47	0.32
Gd	2.30	4.95	9.30	2.78	6.35	0.56	1.11	7.39	0.12
Dy	1.16	6.40	8.34	1.08	3.47	0.17	0.71	3.67	0.08...

¹ For a pure R method to plot spider diagrams, see Exercise 3.4

```
GCDkit-> data <- t(result[,c("C0", "CL1", "CL2")])
GCDkit-> spider(data, "Boynton", 0.1, 1000, pch=c(15, 1, 16), col=c("black",
+ "red", "blue"))
```



In the example we have just set up the minimum and maximum of the y axis, and assigned plotting symbols with colours. For explanation of further options, see `?spider`.

Spider plot – REE chondrite (Boynton 1984)

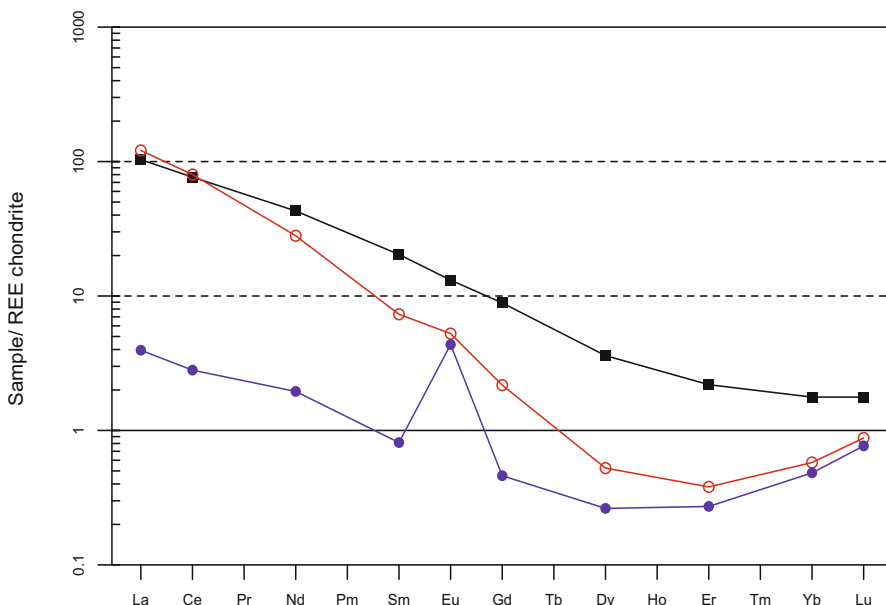


Fig. 14.2 Chondrite-normalized REE patterns, illustrating the differentiation of a parental tonalitic magma (black squares) in case of allanite-free (red circles) and allanite-bearing (blue circles) cumulates (Exercise 14.2).



Exercise 14.3: Partial melting

Two types of mantle, primitive (PRIMA) and depleted (DM), undergo partial melting at two different pressures: 5 and 15 kbar, i.e. in the spinel and garnet stability fields. The Table 14.2 contains the average compositions of the two mantle sources, as well as K_D values for their main mineral constituents. The following table (Table 14.3) shows the modal compositions of the two peridotite types after melt extraction.

Table 14.2

	La	Ce	Nd	Sm	Eu	Gd	Er	Yb	Lu
DM	0.08	0.54	0.74	0.3	0.12	0.43	0.38	0.39	0.06
PRIMA	0.62	1.64	1.23	0.38	0.15	0.53	0.43	0.44	0.07
Ol	0.007	0.006	0.006	0.007	0.007	0.013	0.026	0.049	0.045
Opx	0.03	0.02	0.03	0.05	0.05	0.15	0.23	0.34	0.42
Cpx	0.056	0.092	0.23	0.445	0.474	0.582	0.583	0.542	0.506
Spl	2	1.9	1.8	1.6	1.7	1.55	1.5	1.4	1.3
Grt	0.001	0.007	0.026	0.102	0.7	1.94	4.4	6.167	6.95



 mantle_melting.data

Table 14.3

kbar	Ol	Opx	Cpx	Spl	Grt
5	0.6716	0.1640	0.0853	0.0791	0.0000
15	0.6079	0.2388	0.1037	0.0000	0.0496

 mantle_melting_modal.data

- Given the mineral proportions in spinel and garnet lherzolite residues, calculate the *D* values at both pressures.
- For each of the selected *F* values (0.01, 0.02, 0.05, 0.1 and 0.2), calculate the REE compositions of the melt in the four cases (two peridotite types, PRIMA and DM, at two pressures).
- Plot the corresponding REE patterns.



```
> x <- read.table("mantle_melting.data", sep="\t")
> x <- as.matrix(x); REE <- colnames(x)
> prima <- x["PRIMA",] # PRIMA composition
> dm <- x["DM",] # DM composition
> kd <- x[c(-1,-2),] # table of partition coefficients
> m <- read.table("mantle_melting_modal.data", sep="\t")
> m <- as.matrix(m) # table of mineral props after melting
> dd <- m%*%kd # bulk distrib. coeff. [Eq.(10.4)]
> print(round(dd,3))

      La      Ce      Nd      Sm      Eu      Gd      Er      Yb      Lu
5  0.173 0.165 0.171 0.177 0.188 0.206 0.224 0.246 0.245
15 0.017 0.018 0.036 0.067 0.100 0.200 0.349 0.473 0.525
```

```

> ff <- c(0.01,0.02,0.05,0.1,0.2) # degrees of melting
> # function calculating batch melt composition [Eq. (11.11)]
> batch <- function(c0,ff,dd){
>   out <- sapply(ff,function(i){
>     z <- c0/(dd+i*(1-dd))
>     return(z)
>   })
>   out <- t(out)
>   rownames(out) <- ff
>   return(out)
> }
> # Shallow melting, calculation
> shallow1 <- batch(prima,ff,dd["5",]) # PRIMA
> print(shallow1,3)
      La   Ce   Nd   Sm   Eu   Gd   Er   Yb   Lu
0.01 3.43 9.44 6.86 2.05 0.766 2.48 1.86 1.74 0.277 ...
> shallow2 <- batch(dm,ff,dd["5",]) # DM
> print(shallow2,3)
      La   Ce   Nd   Sm   Eu   Gd   Er   Yb   Lu
0.01 0.442 3.11 4.13 1.616 0.612 2.01 1.64 1.540 0.237 ...
> # Shallow melting, plotting - PRIMA is blue, DM green
GCDkit-> mantle1 <- rbind(prima,dm) # Two mantle sources
GCDkit-> col0 <- c("darkblue","darkgreen")
GCDkit-> spider(mantle1,"Boynton",0.1,100,pch=16,cex=1.5,lwd=1.5,
+             col=col0,main="Shallow melting (5 kbar)")

```



GCDkit contains a useful auxiliary function `selectPalette`. It takes two parameters, one being the number of the colours to be extracted, the second a palette name. Legal names of palettes are: "grays", "reds", "blues", "greens", "cyans", "violets", "yellows", "rainbow", "topo.colors", "heat.colors", "terrain.colors", "cm.colors" and "jet.colors".

```

GCDkit-> col1 <- selectPalette(nrow(shallow1),"blues")
GCDkit-> col2 <- selectPalette(nrow(shallow2),"greens")
GCDkit-> shallow <- rbind(shallow1,shallow2)
GCDkit-> col <- c(col1,col2)
GCDkit-> spider(shallow,"Boynton",pch="",col=col,add=TRUE)
GCDkit-> legend("bottomright",legend=rep(ff,2),pch=15,col=col,
+             bg="white",ncol=2,title="PRIMA/DM")

```

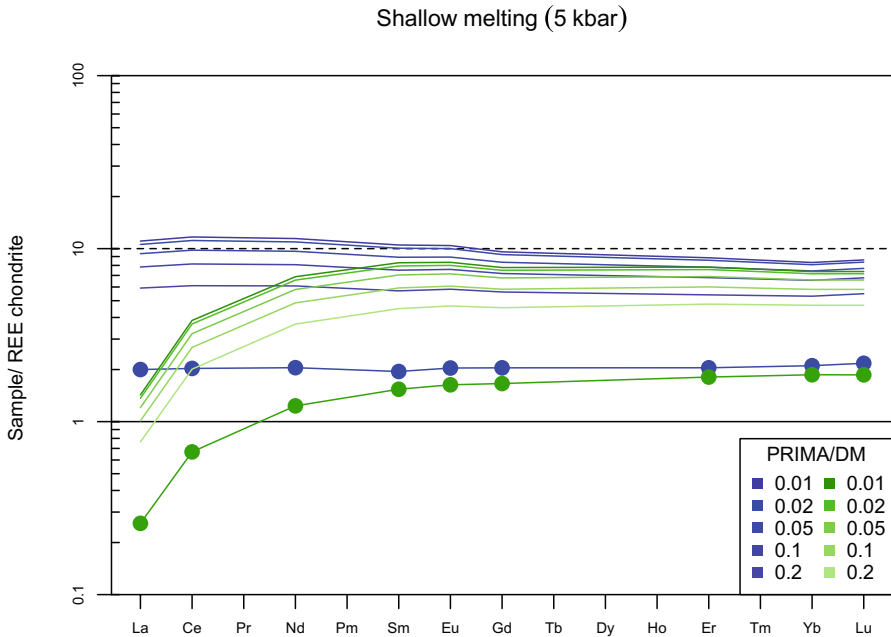



Fig. 14.3 Chondrite-normalized REE patterns for various degrees of a shallow (spinel stability field) batch melting of Primitive Mantle (PRIMA, blue circles) and Depleted Mantle (DM, green circles) (Exercise 14.3). Note how these patterns resemble E-MORB and N-MORB, respectively.

```
> # Deep melting, calculation
> deep1<-batch(prima,ff,dd["15",]) # PRIMA
> print(deep1,3)
      La      Ce      Nd      Sm      Eu      Gd      Er      Yb      Lu
0.01 22.88 58.32 26.99 4.96 1.376 2.55 1.208 0.920 0.132 ...

> deep2<-batch(dm,ff,dd["15",]) # DM
> print(deep2,3)
      La      Ce      Nd      Sm      Eu      Gd      Er      Yb      Lu
0.01 2.952 19.20 16.24 3.91 1.101 2.06 1.068 0.815 0.1133 ...

> # Deep melting, plotting - PRIMA is blue, DM green
GCDkit-> mantle2 <- rbind(prima,dm) # Two mantle sources
GCDkit-> col <- c("darkblue","darkgreen")
GCDkit-> spider(mantle2,"Boynton",0.1,100,pch=16,cex=1.5,lwd=1.5,
+             col=col,main="Deep melting (15 kbar)")
GCDkit-> col1 <- selectPalette(nrow(deep1),"blues")
GCDkit-> col2 <- selectPalette(nrow(deep2),"greens")
GCDkit-> deep <- rbind(deep1,deep2)
GCDkit-> col <- c(col1,col2)
GCDkit-> spider(deep,"Boynton",pch="",col=col,add=TRUE)
```

```
GCDkit-> legend("bottomright", legend=rep(ff,2), pch=15, col=col,
+           bg="white", ncol=2, title="PRIMA/DM")
```

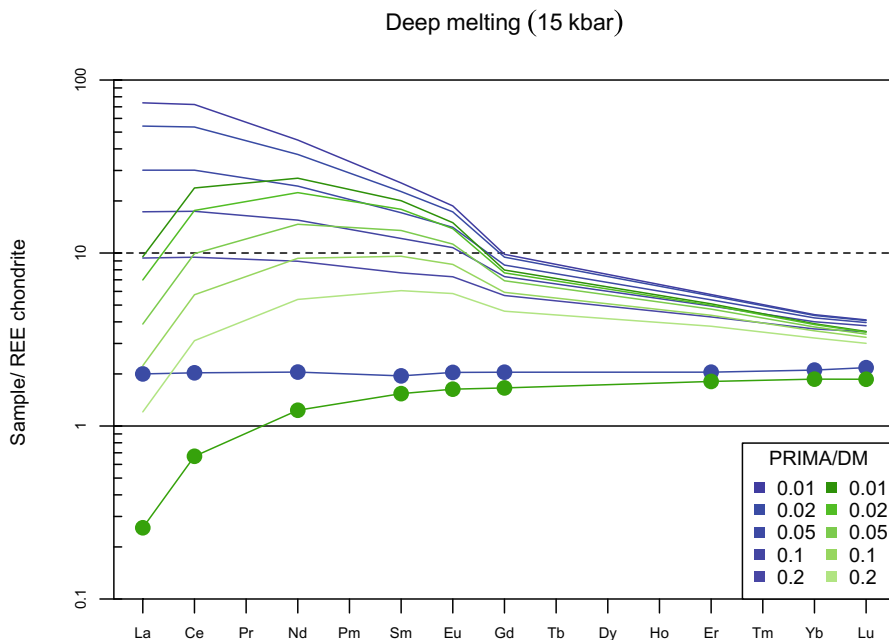


Fig. 14.4 Chondrite-normalized REE patterns for various degrees of a deep (garnet stability field) batch melting of Primitive Mantle (PRIMA, blue circles) and Depleted Mantle (DM, green circles). Magmas resembling OIB are generated from the PRIMA source, but the DM/deep melts resemble no common type of basalts (Exercise 14.3).



Exercise 14.4: Binary mixing

Table 14.4 contains selected trace-element contents in an average Mid-Ocean Ridge Basalt (NMORB, Sun and McDonough 1989) and an Upper Continental Crust (UCC, Taylor and McLennan 1995).

Table 14.4

	Rb	Zr	Nb
NMORB	0.56	74	2.33
UCC	112	190	25

- Draw a mixing hyperbola between the two end members in a Rb vs. Zr/Nb plot.



```

> elems <- c("Rb","Zr","Nb")
> ucc <- c(112,190,25); names(ucc) <- elems
> morb <- c(0.56,74,2.33); names(morb) <- elems
> plot(1,1,xlim=c(0,120),ylim=c(0,35),xlab="Rb (ppm)",ylab="Zr/Nb",
+      type="n") # Only axes are set up
> # Parameters of the mixing hyperbola (Table 11.1)
> AA <- ucc["Zr"]-morb["Zr"]
> BB <- morb["Nb"]-ucc["Nb"]
> CC <- ucc["Nb"]*morb["Rb"]-morb["Nb"]*ucc["Rb"]
> DD <- ucc["Rb"]*morb["Zr"]-morb["Rb"]*ucc["Zr"]
> curve((-AA*x-DD)/(BB*x+CC),from=morb["Rb"],to=ucc["Rb"],add=TRUE,
+       col="darkred") # Eq. (11.29)
> points(morb["Rb"],morb["Zr"]/morb["Nb"],pch=19)
> text(morb["Rb"],morb["Zr"]/morb["Nb"],pos=3,"MORB")
> points(ucc["Rb"],ucc["Zr"]/ucc["Nb"],pch=19)
> text(ucc["Rb"],ucc["Zr"]/ucc["Nb"],pos=3,"UCC")
> x <- seq(morb["Rb"],ucc["Rb"],length=11)
> y <- (-AA*x-DD)/(BB*x+CC) # Eq. (11.30)
> points(x,y,pch=1)

```

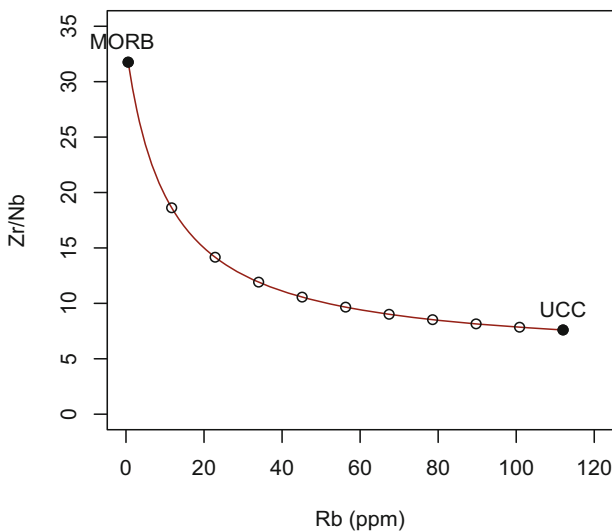


Fig. 14.5 Binary plot Rb vs. Zr/Nb showing effects of a basalt contamination by an average upper continental crust (Exercise 14.4). Note that this is largely a mathematical exercise, as high degrees of crustal contamination are precluded by thermal constraints (endothermic process triggering crystallization—see AFC, Sect. 11.4, 24.1.1).



Exercise 14.5: Saturation models for accessory minerals

The file contains major-element and Zr contents in Boggy Plain Suite of the Lachlan Fold Belt (New South Wales, Australia) from Ph.D. thesis of D. Wyborn (1983) imported from the OzChem compilation by Geoscience Australia, <http://www.ga.gov.au> (Budd et al. 2000).

 [boggy_plain.data](#)

Based on the Watson and Harrison's (1983) zircon saturation model, in *GCDkit*:

- Plot a binary graph of temperature (°C) vs. Zr saturation levels (ppm) contoured for variable values of the M parameter [Eq. (13.1)].
- Plot a binary graph of M vs. Zr (ppm) for the Boggy Plain Suite with superimposed isotherms of zircon saturation temperatures in °C [Eq. (13.3)].
- Examine how zircon saturation temperatures depend on the whole-rock SiO₂.



In order to be able to use the *Saturation* plugin (see *GCDkit* Box in Sect. 13.2), we have to load data into *GCDkit*, either from the menu, or using the function `loadData`. Note that it closes all graphical windows already open.

```
GCDkit-> loadData("boggy_plain.data")
GCDkit-> windows(width=10,height=6) # Open an empty window
GCDkit-> par(mfrow=c(1,2))          # Split it into two

GCDkit-> # Plot 1
GCDkit-> # Create an empty plot (type="n") with an appropriate range
GCDkit-> plot(1,1,xlim=c(650,950),ylim=c(0,650),xlab=
+           expression(T*degree*C),ylab="Zr (ppm)",type="n")
GCDkit-> M <- seq(0.9,2.0,by=0.1)   # Setup the M values
GCDkit-> col <- selectPalette(length(M),"blues") # The colours
GCDkit-> for (i in 1:length(M)){
GCDkit->   curve(497644/exp(-3.8-0.85*(M[i]-1)+12900/(x+273.15)),
+             lty="solid",lwd=2,col=col[i],add=TRUE)
GCDkit-> }
GCDkit-> # Legend colour-coded for individual M values
GCDkit-> legend("bottomright",text.col=col,legend=M,title="M",
+             bg="white",ncol=2)

GCDkit-> # Plot 2
GCDkit-> # Call plugin with arbitrary T, we do not use Zr sat values
GCDkit-> sat.data <- zrSaturation(T=800)
GCDkit-> # Create a plot with Boggy Plain data of appropriate range
```

```
GCDkit-> plot(sat.data[, "M"], WR[, "Zr"], xlim=c(0.9, 2.5),
+           ylim=c(0, 250), xlab="M", ylab="Zr (ppm)", pch=19)
GCDkit-> tt <- seq(650, 950, by=50) # Setup the temperatures
GCDkit-> col <- selectPalette(length(tt), "reds") # The colours
GCDkit-> for (i in 1:length(tt)){
GCDkit->   curve(497644/exp(-3.8-0.85*(x-1)+12900/(tt[i]+273.15))),
+           lty="solid", lwd=2, col=col[i], add=TRUE)
GCDkit->   # Prepare textual labels
GCDkit->   lab <- eval(substitute(expression(x*degree*C),
+           list(x=tt[i])))
GCDkit->   M <- 0.9
GCDkit->   text(M, 497644/exp(-3.8-0.85*(M-1)+12900/
+           (tt[i]+273.15))-5, lab, adj=0, col=col[i])
GCDkit-> }
```

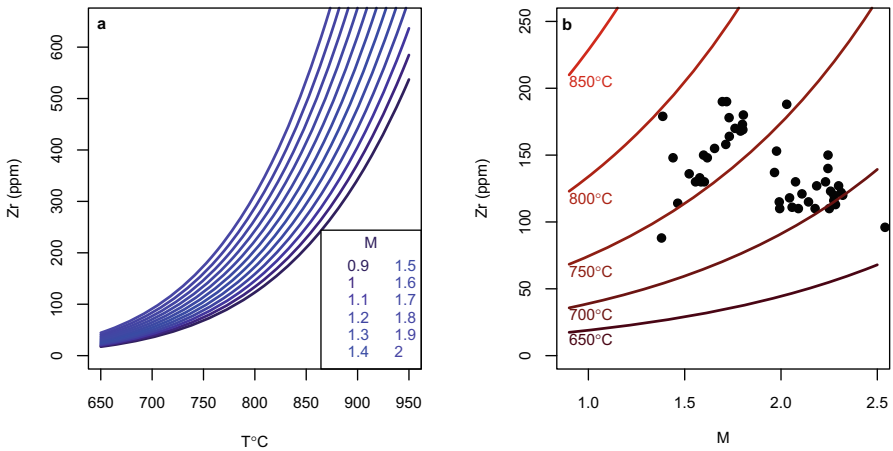


Fig. 14.6 Zircon saturation calculations (Watson and Harrison 1983) for Boggy Plain Suite, Australia (Wyborn 1983). **a** Binary plot of temperature (°C) vs. the Zr saturation level. **b** Binary plot of *M* parameter vs. Zr (ppm) with superimposed isotherms based on zircon saturation model (Exercise 14.5).

```
GCDkit-> # Before plotting, we need to append results to data (WR)
GCDkit-> addResults("sat.data")
GCDkit-> binary("SiO2", "TZr.sat.C", pch=15)
```

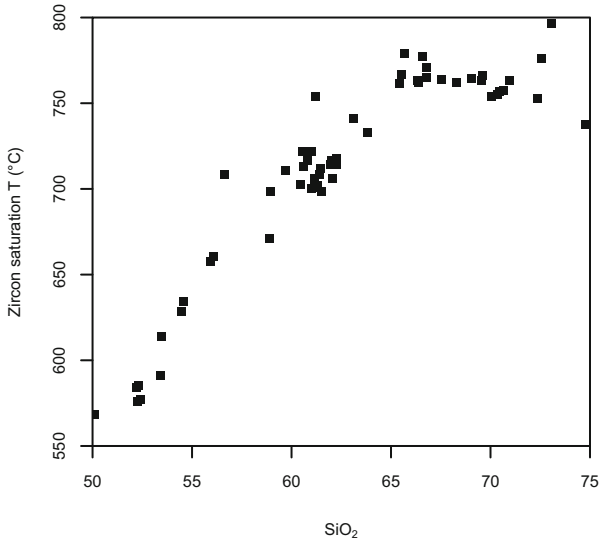


Fig. 14.7 Binary plot of whole-rock silica contents (wt. %) vs. zircon saturation temperatures (Watson and Harrison 1983) for Boggy Plain Suite, Australia (Wyborn 1983) (Exercise 14.5).

References

- Boynton WV (1984) Geochemistry of the rare-earth elements: meteorite studies. In: Henderson P (ed) *Rare Earth Element Geochemistry*. Elsevier, Amsterdam, pp 63–114
- Budd AR, Hazell MS, Sedgmen A, Sedgmen L, Wyborn LAI, Ryburn R (2000) OZCHEM dataset release 1 documentation: AGSO's national whole rock geochemistry database. Australian Geological Survey Organisation, Canberra
- Sun SS, McDonough WF (1989) Chemical and isotopic systematics of oceanic basalts: implications for mantle composition and processes. In: Saunders AD, Norry MJ (eds) *Magmatism in ocean basins*. Geological Society of London Special Publications, vol 42, pp 313–345
- Taylor SR, McLennan SM (1995) The geochemical evolution of the continental crust. *Rev Geophys* 33:241–265
- Watson EB, Harrison TM (1983) Zircon saturation revisited: temperature and composition effects in a variety of crustal magmas types. *Earth Planet Sci Lett* 64:295–304
- Wyborn D (1983) Fractionation processes in the Boggy Plain zoned pluton. Unpublished Ph.D. thesis, Australian National University, Canberra

Chapter 15

Reverse Modelling in R



Exercise 15.1: Fractional crystallization (reversed Ex. 14.2)

Table 15.1 contains trace-element compositions of two tonalites, a primitive WR1 and a differentiated WR2, together with corresponding partition coefficients for the relevant rock-forming minerals.

Table 15.1

	WR1	WR2	Pl	Amp	Ilm	All
La	32.04	1.224	0.4	0.74	0.005	960
Ce	61.9	2.270	0.27	1.52	0.006	940
Nd	25.75	1.170	0.21	4.26	0.0075	750
Sm	3.97	0.158	0.13	7.77	0.01	620
Eu	0.966	0.320	2.15	5.14	0.007	56
Gd	2.3	0.119	0.097	10	0.017	440
Dy	1.16	0.085	0.064	13	0.028	200
Er	0.46	0.057	0.055	12	0.035	100
Yb	0.37	0.101	0.049	8.4	0.075	54
Lu	0.057	0.025	0.046	6	0.1	41



ttg2.data

Let's assume that WR_1 and WR_2 represent pure compositions of a tonalitic melt differentiating by Rayleigh-type fractional crystallization.

- Using the least-square method, estimate the modal composition of the cumulate and the degree of fractional crystallization.



```

> x <- read.table("ttg2.data", sep="\t")
> x <- data.matrix(x)
> dmat <- x[,-(1:2)]-1 # partition coeffs - 1 [Eq. (12.3)]
> # Log ratios of differentiated/primitive magma comp. [Eq. (12.4)]
> cv <- log(x[,2]/x[,1])
> ee <- lsfit(dmat,cv,intercept=FALSE)
> mm <- ee$coeff
> ff <- exp(sum(mm)) # fraction of melt remaining [Eq.(12.7)]
> cat(round((1-ff)*100,1),"% fractional crystallization ","\n")
30 % fractional crystallization

> m <- mm/log(ff)*100 # mineral proportions [Eq. (12.8)]
> print(round(m,1))
  Pl  Amp  Ilm  All
48.5 48.5  2.0  1.0

```



Exercise 15.2: Partial melting

Tables below give selected trace-element contents in a garnet lherzolite and a basaltic magma (Table 15.2) as well as partition coefficients for residual mantle minerals (Table 15.3).

Table 15.2

	Grt_Lherzolite	Magma_A
Rb		4.12
Sr	18.00	93.67
Ni	2000.00	148.68
Nb	0.40	1.62
La	0.25	2.05
Yb	0.40	0.84



[mantle_conc.data](#)

Table 15.3

	Ol	Opx	Cpx	Grt
Rb	0.0001	0.0002	0.0003	0.009
Sr	0.002	0.003	0.7	0.2
Ni	24	5.2	3.4	1
Nb	0.0001	0.34	0.3	0.2
La	0.0004	0.002	0.008	0.008
Yb	0.0015	0.002	0.02	8



[mantle_kd.data](#)

Magma A is formed by batch melting of a garnet lherzolite. Calculate:

- The degree of melting required to form the basaltic magma A .
- The Rb content in the lherzolite prior to melting.
- The mode of the residue after melting.



```
> x <- read.table("mantle_conc.data", sep="\t") # Read rock comp.
> kd <- read.table("mantle_kd.data", sep="\t") # Partition coeffs
> c0 <- x[,1] # Lherzolite
> names(c0) <- rownames(x)
> c1 <- x[,2] # Basalt
> names(c1) <- rownames(x)
```

We should look now for a strongly incompatible element. If successful, the highest C_L/C_0 value would constrain the degree of partial melting through Eq. (12.9).

```
> ratio <- c1/c0
> print(sort(ratio), 3)
      Ni      Yb      Nb      Sr      La
0.0743 2.1000 4.0500 5.2039 8.2000

> ff <- 1/ratio["La"]
> cat("The degree of melting is", round(ff*100,1), "%.", "\n")
The degree of melting is 12.2 %.
```

Also Rb is also strongly incompatible; from Eq. (11.11) follows that if $D \sim 0$, $C_0 = C_L F$:

```
> Rb <- c1["Rb"] * ff
> c0["Rb"] <- Rb
> cat("Rb in the lherzolite is", round(Rb, 2), "ppm", "\n")
Rb in the lherzolite is 0.5 ppm.
```

Least-square solution yields mineral proportions in the residue:

```
> cv <- c0/c1 - ff
> m <- lsfit(kd, cv, intercept=0)$coeff
> m <- m / (1 - ff) # Eq. (12.15)
> print(m, 2)
      Ol      Opx      Cpx      Grt
0.551 0.303 0.097 0.050
```

Part IV Radiogenic Isotopes

As shown in the preceding text, a suite of magmas affected by an open-system process, i.e. interaction with a compositionally dissimilar external component (magma mixing, AFC, hydrothermal alteration, metasomatism...), will generally display regular geochemical patterns. However, such trace-element evidence is often, and major-element variation always, equivocal. The best proofs for operation of open-system processes remain radiogenic isotope ratios which are generally not fractionated during closed-system processes such as melting or crystallization. The magmas formed should preserve the isotopic characteristics of their source. In other words, the radiogenic isotope data are totally transparent to mechanisms of closed-system magmatic differentiation but are very sensitive to mixing or contamination.

Chapter 16

Direct Models

16.1 Binary Mixing

16.1.1 Single Isotopic Ratio

The mixing equation for two end-members, 1 and 2, can be seen as a mean of isotopic ratios (I_1 and I_2), weighted by their respective mass-fraction in the mixture. Marking the mass fraction of the end-member 1 as f_1 , (with $f_1 + f_2 = 1$) and respective concentrations C_1 , C_2 and C_M (Faure 1986):

$$I_M = I_1 \left(\frac{C_1}{C_M} \right) f_1 + I_2 \left(\frac{C_2}{C_M} \right) (1 - f_1) \quad (16.1)$$

Given (Sect. 6.4): $C_M = f_1 C_1 + (1 - f_1) C_2$ (16.2)

$$I_M = \frac{I_1 C_1 f_1 + I_2 C_2 (1 - f_1)}{C_1 f_1 + C_2 (1 - f_1)} \quad (16.3)$$

Eq. (16.3) describes the isotopic ratio as a function of mixing proportion f_1 . However ever, it appears useful to visualize the relationship between elemental concentration (C_M) and isotope ratio (I_M) during mixing, which can be achieved by eliminating f_1 . Equations (16.1) and (16.2) yield:

$$I_M = \frac{C_1 C_2 (I_2 - I_1)}{C_M (C_1 - C_2)} + \frac{C_1 I_1 - C_2 I_2}{C_1 - C_2} \quad (16.4)$$

which is an equation of a rectangular hyperbola in C_M vs. I_M (e.g. Sr vs. $^{87}\text{Sr}/^{86}\text{Sr}$) diagram (Fig. 16.1a).

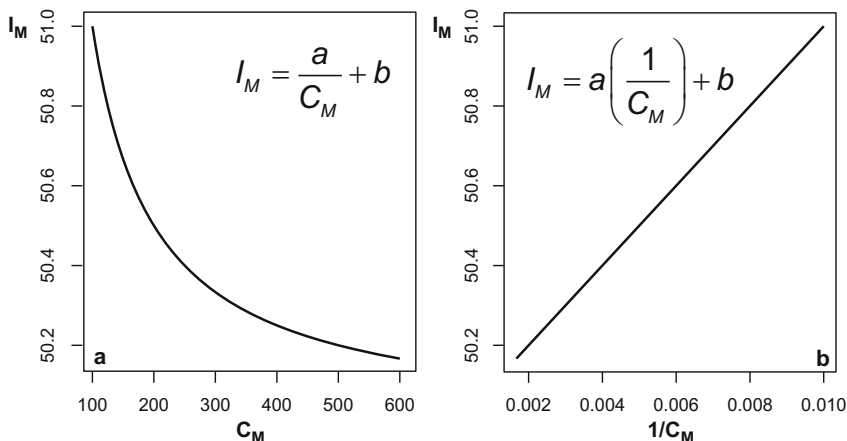


Fig. 16.1 Conversion of a rectangular hyperbola (a) to a straight line (b) by plotting of reciprocal values on the x axis.

In isotope-based modelling of binary mixing, plots such as $1/\text{Sr}$ vs. $^{87}\text{Sr}/^{86}\text{Sr}$ are frequently used, where the mixing hyperbolae change into straight lines (Fig. 16.1b). For a suite of cogenetic igneous rocks, when the slope of this line differs from zero, it indicates the involvement of an open-system process, such as magma mixing or wall-rock assimilation (Briqueu and Lancelot 1979) (Fig. 16.2). On the other hand, samples that originated from the same source by various degrees of closed-system fractionation preserve identical initial isotopic ratios, which in the $1/\text{Sr}$ vs. $^{87}\text{Sr}/^{86}\text{Sr}$ diagram results in a horizontal trend.

The parameter f_i from Eq. (16.3) can be calculated if the isotopic compositions and elemental concentrations for both end-members as well as the isotopic composition of the presumed hybrid are known:

$$f_1 = \frac{c_2(I_2 - I_M)}{I_M(c_1 - c_2) - I_1c_1 + I_2c_2} \quad (16.5)$$



If desired, error propagation in mixing problems can be done using the formulae proposed by Verma (2000).

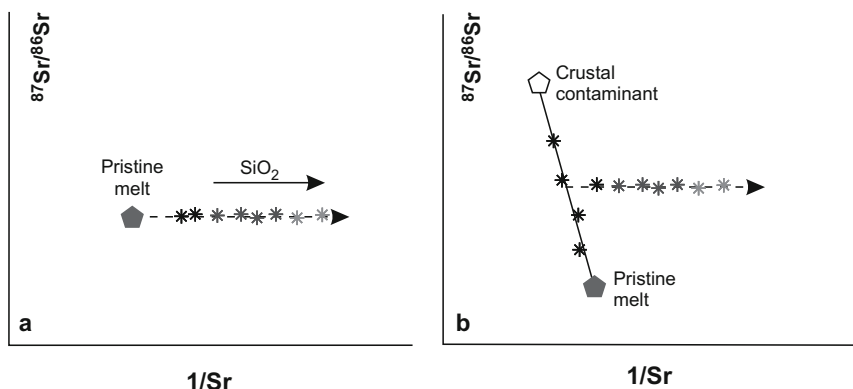


Fig. 16.2 Development of $^{87}\text{Sr}/^{86}\text{Sr}$ composition in a fractionating mantle-derived igneous suite. **a** Closed-system fractional crystallization of a parental magma, **b** Contamination of the pristine melt, followed by closed-system fractionation (after Briquieu and Lancelot 1979).

16.1.2 Pair of Isotopic Ratios

The combination of two isotopic ratios (these may, besides radiogenic, include also stable isotope data, such as $\delta^{18}\text{O}$ values) into a single binary plot is robust in respect to the possible later modification by fractional crystallization or crystal accumulation. It thus provides an insight into the original, open-system generated variation.

In order to perform modelling, one can consider two elements X and Y as well as their isotopic ratios I^X and I^Y that can be obtained from Eq. (16.3). In case of mixing of two end-members, 1 and 2, the exact analytical solution is obtained combining two Eq. (16.5), eliminating f_i (Vollmer 1976; Langmuir et al. 1978).

$$AI_M^X + BI_M^X I_M^Y + CI_M^Y + D = 0 \tag{16.6}$$

When $X = \text{Sr}$ and $Y = \text{Nd}$, $I^X = ^{87}\text{Sr}/^{86}\text{Sr}$ and $I^Y = ^{143}\text{Nd}/^{144}\text{Nd}$, we arrive at:

$$A \left(\frac{^{87}\text{Sr}}{^{86}\text{Sr}} \right)_M + B \left(\frac{^{87}\text{Sr}}{^{86}\text{Sr}} \right)_M \left(\frac{^{143}\text{Nd}}{^{144}\text{Nd}} \right)_M + C \left(\frac{^{143}\text{Nd}}{^{144}\text{Nd}} \right)_M + D = 0 \tag{16.7}$$

Where:

$$A = \left(\frac{^{143}\text{Nd}}{^{144}\text{Nd}} \right)_2 \text{Nd}_2 \text{Sr}_1 - \left(\frac{^{143}\text{Nd}}{^{144}\text{Nd}} \right)_1 \text{Nd}_1 \text{Sr}_2,$$

$$B = \text{Nd}_1 \text{Sr}_2 - \text{Nd}_2 \text{Sr}_1,$$

$$C = \left(\frac{{}^{87}\text{Sr}}{{}^{86}\text{Sr}} \right)_1 \text{Nd}_2 \text{Sr}_1 - \left(\frac{{}^{87}\text{Sr}}{{}^{86}\text{Sr}} \right)_2 \text{Nd}_1 \text{Sr}_2,$$

$$D = \left(\frac{{}^{143}\text{Nd}}{{}^{144}\text{Nd}} \right)_1 \left(\frac{{}^{87}\text{Sr}}{{}^{86}\text{Sr}} \right)_2 \text{Nd}_1 \text{Sr}_2 - \left(\frac{{}^{143}\text{Nd}}{{}^{144}\text{Nd}} \right)_2 \left(\frac{{}^{87}\text{Sr}}{{}^{86}\text{Sr}} \right)_1 \text{Nd}_2 \text{Sr}_1.$$

This equation is that of a hyperbola, unless B is zero, in which case a straight line is obtained. The coefficient B can be further rearranged, defining:

$$\alpha = \frac{(\text{Sr} / \text{Nd})_2}{(\text{Sr} / \text{Nd})_1} \quad (16.8)$$

the special case of a straight line corresponds to $\alpha = 1$ (DePaolo and Wasserburg 1979) (Fig. 16.3), i.e. when the Sr/Nd proportions are equal in both end-members and the mix is not enriched preferentially with one element. Note that also a binary plot of isotopic pairs of the same element, such as ${}^{206}\text{Pb}/{}^{204}\text{Pb}$ vs. ${}^{207}\text{Pb}/{}^{204}\text{Pb}$, will produce a linear correlation as $\alpha = 1$.

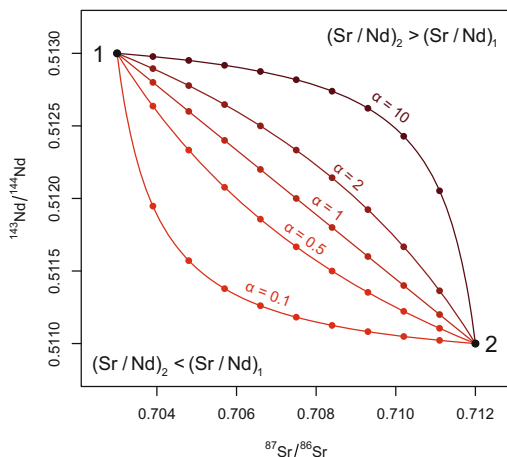


Fig. 16.3 Diagram ${}^{87}\text{Sr}/{}^{86}\text{Sr}$ vs. ${}^{143}\text{Nd}/{}^{144}\text{Nd}$ showing that binary mixing hyperbolae depend on the parameter α [Eq. (16.8)]. Dots show 10 % increments of the end-members, 1 and 2, in the mixture (after DePaolo and Wasserburg 1979).

The general equation of a rectangular hyperbola in $[x, y]$ space with asymptotes x_0 , y_0 and curvature q is:

$$(x - x_0)(y - y_0) = q \quad (16.9)$$

or

$$y = y_0 + \frac{q}{(x - x_0)} \quad (16.10)$$

After rearranging Eq. (16.10), the meaning of the coefficients A , B , C , D in Eq. (16.6) becomes apparent:

$$y_0x - xy + x_0y + q - x_0y_0 = 0 \quad (16.11)$$

$$x_0 = -\frac{C}{B}, \quad y_0 = -\frac{A}{B} \quad (16.12)$$

$$q = x_0y_0 - \frac{D}{B} \quad (16.13)$$

Back to the example of a $^{87}\text{Sr}/^{86}\text{Sr}$ - $^{143}\text{Nd}/^{144}\text{Nd}$ plot [Eq. (16.7)], the asymptotes and curvature of the mixing hyperbola are defined as (Albarède 1995) ($\alpha \neq 1$):

$$x_0 = \frac{\left(\frac{^{87}\text{Sr}}{^{86}\text{Sr}}\right)_1 - \alpha \left(\frac{^{87}\text{Sr}}{^{86}\text{Sr}}\right)_2}{1 - \alpha},$$

$$y_0 = \frac{\left(\frac{^{143}\text{Nd}}{^{144}\text{Nd}}\right)_2 - \alpha \left(\frac{^{143}\text{Nd}}{^{144}\text{Nd}}\right)_1}{1 - \alpha} \quad (16.14)$$

$$q = x_0y_0 + \frac{\alpha \left(\frac{^{87}\text{Sr}}{^{86}\text{Sr}}\right)_2 \left(\frac{^{143}\text{Nd}}{^{144}\text{Nd}}\right)_1 - \left(\frac{^{87}\text{Sr}}{^{86}\text{Sr}}\right)_1 \left(\frac{^{143}\text{Nd}}{^{144}\text{Nd}}\right)_2}{1 - \alpha} \quad (16.15)$$

16.2 AFC Formulation for Isotopes

The model describing the evolution of a trace-element concentration in course of AFC (Sect. 11.4, Fig. 11.7) can be modified for radiogenic isotopes (Fig. 16.4).

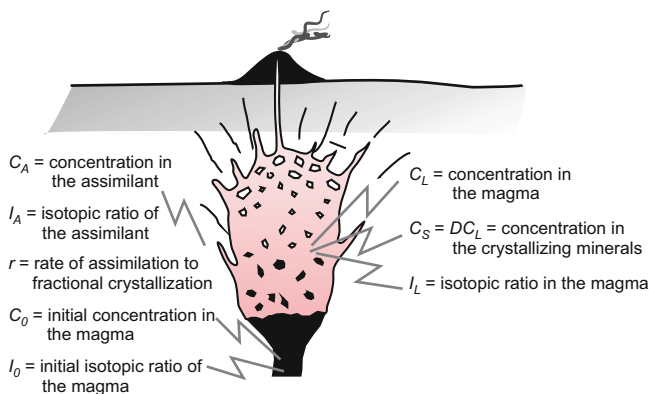


Fig. 16.4 Schematic representation of the AFC process including isotopes (after De Paolo 1981).

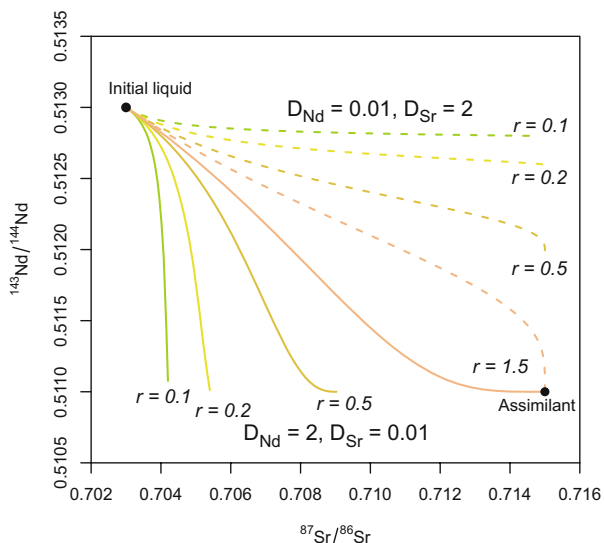


Fig. 16.5 Binary plot $^{87}\text{Sr}/^{86}\text{Sr}$ vs. $^{143}\text{Nd}/^{144}\text{Nd}$ showing the effects of two AFC processes (solid lines: $D_{\text{Nd}} = 2$ and $D_{\text{Sr}} = 0.01$ and dotted lines: $D_{\text{Nd}} = 0.01$ and $D_{\text{Sr}} = 2$), for variable r values (after DePaolo 1981). Note that, due to the endothermic character of assimilation and contamination, r values exceeding unity are very unlikely (Sect. 24.1).

Keeping in mind that the heavy radiogenic isotopes are not fractionated during closed-system crystallization (DePaolo 1981; Albarède 1995):

$$I_L = I_0 + (I_A - I_0) \left(1 - \frac{C_0}{C_L} F^{-z} \right) \tag{16.16}$$

Where I_L , I_0 and I_A are the isotopic ratios (e.g., $^{87}\text{Sr}/^{86}\text{Sr}$) in the differentiated and primitive melt and in the assimilant, and $z = \frac{r + D - 1}{r - 1}$.

In general, AFC processes with constant r and D produce a straight line in the I/C (or C_0/C) vs. I plot. Otherwise, the trends are distinctly curved (Powell 1984; Janoušek et al. 2000) as are, in general, the AFC trends in binary plots involving two isotopic ratios (Fig. 16.5).

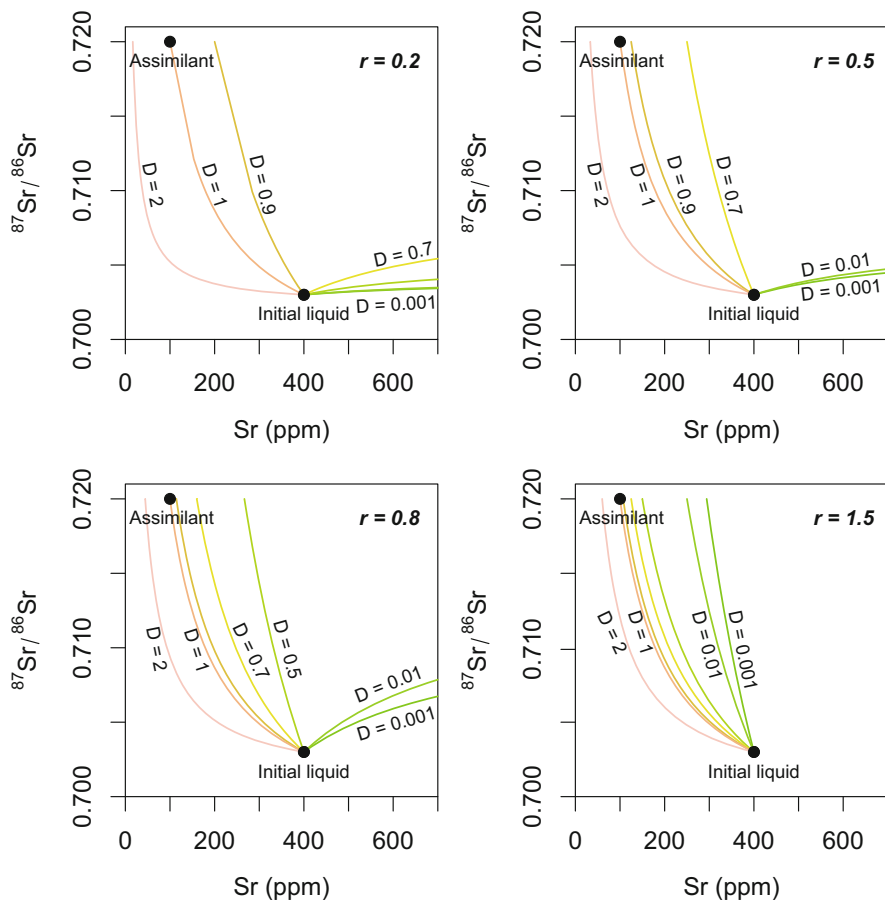


Fig. 16.6 Compositional changes in Sr vs. $^{87}\text{Sr}/^{86}\text{Sr}$ diagrams during AFC with various rate of assimilation to fractional crystallization ($r = 0.2, 0.5, 0.8$ and 1.5). The curves are labelled by the bulk distribution coefficient D_{Sr} ; $D_{\text{Sr}} = 1$ corresponds to simple binary mixing and thus the modelled curve connects both end members, which is otherwise not the case (after DePaolo 1981).

It is worth noting that even a massive assimilation may lead to very limited changes in the isotopic composition of an incompatible element in the melt. In contrast, compatible elements may record large isotopic shifts already at modest assimilation rates (Fig. 16.6). A characteristic feature of AFC is that the composition of the resulting magma does not generally plot onto a tie line between both end members, unlike in the case of binary mixing.

References

- Albarède F (1995) Introduction to geochemical modeling. Cambridge University Press, Cambridge
- Briqueu L, Lancelot J (1979) Rb–Sr systematics and crustal contamination trends for calc-alkaline igneous rocks. *Earth Planet Sci Lett* 43:385–396
- DePaolo DJ (1981) Trace element and isotopic effects of combined wallrock assimilation and fractional crystallization. *Earth Planet Sci Lett* 53:189–202
- DePaolo DJ, Wasserburg GJ (1979) Petrogenetic mixing models and Nd–Sr isotopic patterns. *Geochim Cosmochim Acta* 43:615–627
- Faure G (1986) Principles of isotope geology. John Wiley & Sons, Chichester
- Janoušek V, Bowes DR, Rogers G, Farrow CM, Jelínek E (2000) Modelling diverse processes in the petrogenesis of a composite batholith: the Central Bohemian Pluton, Central European Hercynides. *J Petrol* 41:511–543
- Langmuir CH, Vocke RD, Hanson GN, Hart SR (1978) A general mixing equation with applications to Icelandic basalts. *Earth Planet Sci Lett* 37:380–392
- Powell R (1984) Inversion of the assimilation and fractional crystallization (AFC) equations; characterization of contaminants from isotope and trace element relationships in volcanic suites. *J Geol Soc London* 141:447–452
- Verma SP (2000) Error propagation in equations for geochemical modeling of radiogenic isotopes in two-component mixing. *J Earth Syst Sci* 109:79–88
- Vollmer R (1976) Rb–Sr and U–Th–Pb systematics of alkaline rocks: the alkaline rocks from Italy. *Geochim Cosmochim Acta* 40:283–295

Chapter 17

Reverse Models

17.1 Binary Mixing

Assuming a binary x - y plot of two isotopic ratios (e.g. $^{87}\text{Sr}/^{86}\text{Sr}$ - $^{143}\text{Nd}/^{144}\text{Nd}$), the Eq. (16.11) for the mixing hyperbola can be rearranged to:

$$xy = x_0y + y_0x + q - x_0y_0 \quad (17.1)$$

The mass-balance equation can be written in a matrix form (for p elements):

$$\begin{bmatrix} x_1y_1 \\ x_2y_2 \\ \dots \\ x_py_p \end{bmatrix} = \begin{bmatrix} 1, y_1, x_1 \\ 1, y_2, x_2 \\ \dots \\ 1, y_p, x_p \end{bmatrix} \begin{bmatrix} q - x_0y_0 \\ x_0 \\ y_0 \end{bmatrix} \quad (17.2)$$

and solved for the vector $[q - x_0y_0, x_0, y_0]$ by least-square method (Appendix C).



The detailed treatment of ternary mixing problems can be found, for instance, in Sohn (2013), including the reverse modelling.

17.2 AFC

Reverse solution of the AFC was described by Powell (1984), Mantovani and Hawkesworth (1990) and Aitchison and Forrest (1994). It is straightforward to use the slope S of the mixing line in the I/C vs. I diagram (Powell 1984):

$$I_A = S \left(\frac{r - 1 + D}{r} \right) \frac{1}{C_A} + I_0 - \frac{S}{C_0} \quad (17.3)$$

This can be solved for r :

$$r = \frac{S(1-D)}{S + \left(I_0 - \frac{S}{C_0} - I_A \right) C_A} \quad (17.4)$$



For reverse AFC modelling there is a specialized R package `AFC3D` using an innovative graphical approach (Guzmán et al. 2014).

References

- Aitchison SJ, Forrest AH (1994) Quantification of crustal contamination in open magmatic systems. *J Petrol* 35:461–488
- Guzmán S, Carniel R, Caffè PJ (2014) AFC3D: a 3D graphical tool to model Assimilation and Fractional Crystallization with and without recharge in the R environment. *Lithos* 190–191:264–278
- Mantovani MSM, Hawkesworth CJ (1990) An inversion approach to assimilation and fractional crystallisation processes. *Contrib Mineral Petrol* 105:289–302
- Powell R (1984) Inversion of the assimilation and fractional crystallization (AFC) equations; characterization of contaminants from isotope and trace element relationships in volcanic suites. *J Geol Soc London* 141:447–452
- Sohn RA (2013) A method for inverting ratio-ratio data to estimate end-member compositions in mixing problems. *Chem Geol* 352:63–69

Chapter 18

Forward Modelling in R

18.1 Binary Mixing



Exercise 18.1: Single isotopic ratio

During its ascent, a basaltic magma is contaminated by a host-rock schist.

Table 18.1

	A: schist	B: basalt
Sr	150 ppm	600 ppm
$^{87}\text{Sr}/^{86}\text{Sr}$	0.715	0.703

- Plot a theoretical mixing hyperbola between basalt and schist in the $\text{Sr}-^{87}\text{Sr}/^{86}\text{Sr}$ and $1/\text{Sr}-^{87}\text{Sr}/^{86}\text{Sr}$ diagrams for 5% mixing increments.
- Calculate the $^{87}\text{Sr}/^{86}\text{Sr}$ ratio in a mixture containing 20 % of the schist.
- Determine the proportion of schist in the mixture that has $^{87}\text{Sr}/^{86}\text{Sr} = 0.710$.



```
> c1<- 150
> i1 <- 0.715                                #schist composition
> c2 <- 600
> i2 <- 0.703                                #basalt composition
> # Plot mixing
> windows(width=10,height=6)
> par(mfrow=c(1,2))                          #prepare a two-graph layout
> f1 <- seq(0,1,by=0.05)                     #prop. of schist in mixture
> cm <- c1*f1+(1-f1)*c2
> names(cm) <- f1                            #conc. in mix [Eq.(16.2)]
> im <- i1*c1*f1/cm+i2*c2*(1-f1)/cm          #87Sr/86Sr in mix [Eq. (16.1)]
> srlab <- expression("“^87*Sr/““^86*Sr)
```

```

> plot(cm,im,xlab="Sr (ppm)",ylab=srlab,type="b",pch=19)
> plot(1/cm,im,xlab="1/Sr (ppm)",ylab=srlab,type="b",pch=19)

> # Calculate 20% mixing
> f1 <- 0.2                                #mixing proportion
> im <- (i1*c1*f1+i2*c2*(1-f1))/(c1*f1+c2*(1-f1))
>
>                                           # 87Sr/86Sr [Eq.(16.3)]
> print(im)
[1] 0.7037059

> # Calculate mixing proportion (reverse task)
> im <- 0.710                              #87Sr/86Sr of the mixture
> f1 <- c2*(i2-im)/(im*(c1-c2)-i1*c1+i2*c2) #calc. f1 [Eq. (16.5)]
> print(f1)
[1] 0.8484848

```

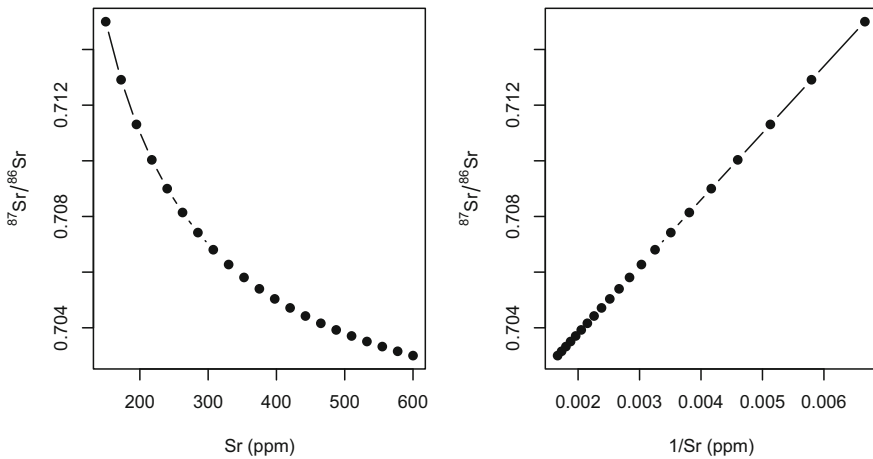


Fig. 18.1 Theoretical mixing hyperbola resulting from contamination of basalt by the surrounding schist (Exercise 18.1).



Exercise 18.2: Pair of isotopic ratios

The same basaltic magma as in Exercise 18.1 is contaminated by schist. However, here, both Sr and Nd isotopic data are available.

Table 18.2

	A: schist	B: basalt
Sr	150 ppm	600 ppm
$^{87}\text{Sr}/^{86}\text{Sr}$	0.715	0.703
Nd	20 ppm	2 ppm
$^{143}\text{Nd}/^{144}\text{Nd}$	0.511	0.513

- Calculate the Sr (ppm), $^{87}\text{Sr}/^{86}\text{Sr}$, Nd (ppm) and $^{143}\text{Nd}/^{144}\text{Nd}$ of mixtures containing 0, 5, 10, ... 100 % of the schist; print the result in a table.
- Plot a theoretical mixing hyperbola in the $^{87}\text{Sr}/^{86}\text{Sr} - ^{143}\text{Nd}/^{144}\text{Nd}$ space.
- Calculate and plot the asymptotes.



```

> windows()
> cx1 <- 150; cx2 <- 600                # Sr, schist and basalt
> ix1 <- 0.715; ix2 <- 0.703          # 87Sr/86Sr, schist and basalt
> f1 <- seq(0,1,by=0.05)              # prop. of schist in mixture
> cmx <- cx1*f1+(1-f1)*cx2            #Sr conc. mix [Eq. (16.2)]
> imx <- ix1*cx1*f1/cmx+ix2*cx2*(1-f1)/cmx
>                                     # 87Sr/86Sr mix [Eq. (16.1)]
> cy1 <- 20; cy2 <- 2                  # Nd in schist and basalt
> iy1 <- 0.511; iy2 <- 0.513         # 143Nd/144Nd, schist/basalt
> cmy <- cy1*f1+(1-f1)*cy2            # Nd conc., mix [Eq. (16.2)]
> imy <- iy1*cy1*f1/cmy+iy2*cy2*(1-f1)/cmy
>                                     # 143Nd/144Nd mix [Eq. (16.1)]
> # Prepare results table
> res <- cbind(cmx,imx,cmy,imy)
> rownames(res) <- f1
> colnames(res) <- c("Sr", "87Sr/86Sr", "Nd", "143Nd/144Nd")
> print(res)
      Sr 87Sr/86Sr  Nd 143Nd/144Nd
0    600.0 0.7030000 2.0 0.5130000
0.05 577.5 0.7031558 2.9 0.5123103
0.1  555.0 0.7033243 3.8 0.5119474...

```

```

> # Plot the mixing hyperbola
> plot(imx,imy,xlab=expression(" "^87*Sr/" "^86*Sr),
+      ylab=expression(" "^143*Nd/" "^144*Nd),type="b",
+      xlim=c(0.7023,0.7152),ylim=c(0.5109,0.5131),pch=19)

> # Calculate and plot asymptotes
> alpha <- (cx2/cy2)/(cx1/cy1)      # calc. alpha [Eq. (16.8)]
> x0 <- (ix1-alpha*ix2)/(1-alpha)  # calc. asymptotes [Eq. (16.14)]
> y0 <- (iy2-alpha*iy1)/(1-alpha)
> print(x0)
[1] 0.7026923
> print(y0)
[1] 0.5109487
> abline(v=x0,lty="dashed")        # draw asymptotes
> abline(h=y0,lty="dashed")

```

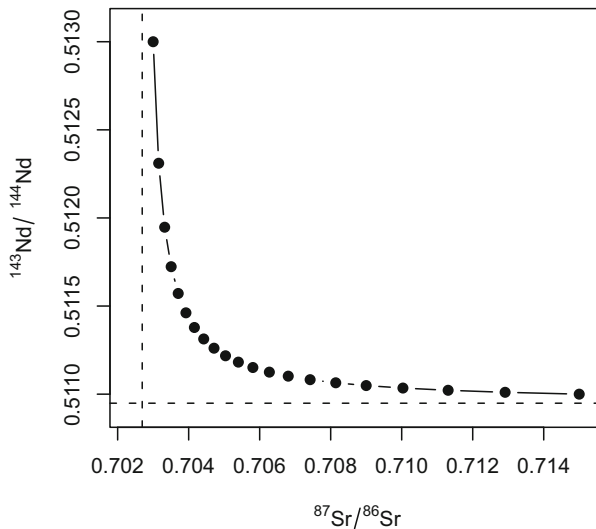


Fig. 18.2 Theoretical mixing hyperbola between basalt and schist. Asymptotes are shown by dashed lines (Exercise 18.2).

18.2 AFC



Exercise 18.3: AFC

Let's assume an AFC process with the following parameters: the parental magma has a $^{87}\text{Sr}/^{86}\text{Sr} = 0.7045$ and contains 150 ppm of Sr; $D_{\text{Sr}} = 3.5$. The contaminant contains 500 ppm of Sr and has a $^{87}\text{Sr}/^{86}\text{Sr}$ ratio of 0.713.

- In the $1/\text{Sr}$ vs. $^{87}\text{Sr}/^{86}\text{Sr}$ diagram, show the effects of up to 60 % crystallization accompanied by assimilation. Plot curves for variable values of the r parameter (0, 0.05, 0.1, 0.2 and 0.5) at 10 % increments of F .



```

> i0 <- 0.704; c0 <- 150 # the initial magma
> ia <- 0.713; ca <- 500 # the assimilant
> dd <- 3.5 # bulk distribution coefficient for Sr
> srlab <- expression("^^87*Sr/"^^86*Sr)
> plot(1/c0,i0,xlim=c(0,0.07),ylim=c(0.7035,0.7135),
+      xlab="1/Sr (ppm)",ylab=srlab,type="n")#draw empty plot

> ee <- c(0,0.05,0.1,0.2,0.5) #vector of r parameters
> for (r in ee){ #repeat for all r
>   z <- (r+dd-1)/(r-1)
>   ff <- seq(0.4,1,by=0.1)
>   x <- c0*ff^-z+r/(z*(r-1))*ca*(1-ff^-z) #Sr [Eq. (11.34)]
>   y <- i0+(ia-i0)*(1-c0/x*ff^-z) #87Sr/86Sr[Eq. (16.16)]
>   points(1/x,y,type="b",pch=19) #plot as a curve
>   text(1/x[1],y[1],pos=3,paste("r =",r),cex=0.8)
> }

> # Plot end members
> points(1/ca,ia,pch=19,cex=1.5,col="darkred") #Contaminant
> text(1/ca,ia,pos=2,"Contaminant",cex=0.8,srt=90)
> text(1/ca,ia,pos=3,expression(r==+infinity),cex=0.8)

> points(1/c0,i0,pch=19,cex=1.5,col="darkblue") #Initial magma
> text(1/c0,i0,pos=1,"Initial magma",cex=0.8)
> lines(c(1/c0,1/ca),c(i0,ia),lty="dashed",lwd=2,col="blue")

```

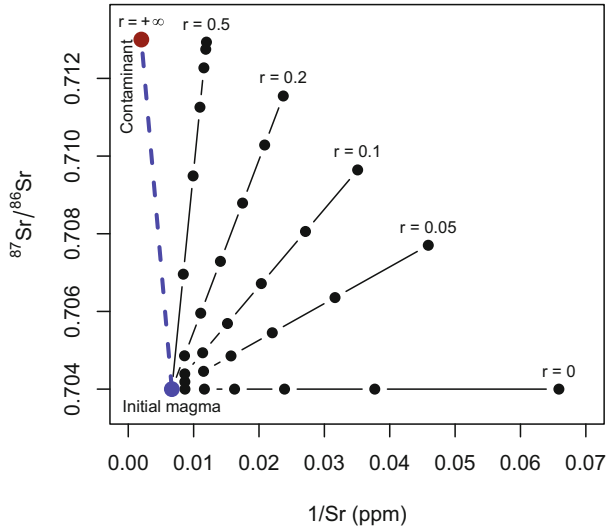


Fig. 18.3 A $1/\text{Sr}$ vs. $^{87}\text{Sr}/^{86}\text{Sr}$ diagram showing effects of up to 60% crystallization of a basaltic magma accompanied by different rates (r) of crustal contamination. A tie line connecting the Initial magma with Contaminant would correspond to binary mixing ($r = \infty$) (Exercise 18.3).

Chapter 19

Reverse Modelling in R



Exercise 19.1: Binary mixing

Pb–Hf isotopic compositions of old and intermediate arc lavas from La Martinique Island in Lesser Antilles reflect binary mixing between depleted-mantle and enriched, plume-derived components (Table 19.1) (Labanieh et al. 2010).

Table 19.1

Sample	$^{206}\text{Pb}/^{204}\text{Pb}$	$^{176}\text{Hf}/^{177}\text{Hf}$
06MT68	18.9866	0.283163
06MT53	19.1900	0.283137
06MT54	19.1876	0.283137
06MT73	19.2678	0.283131
06MT69	19.6896	0.28307
06MT71	19.7037	0.283064
06MT60	19.8770	0.282856
06MT72	19.9352	0.282554
06MT68	18.9866	0.283163



[Martinique.data](#)

- Using the least-square method, fit the data by a mixing hyperbola.
- Determine both the asymptotes and the curvature.
- Plot the data together with the hyperbola and its asymptotes.



```
> z <- read.table("Martinique.data", sep="\t")
> # Fitting the mixing hyperbola
> A <- cbind(1, z[,2], z[,1])           # data matrix [Eq. (17.2)]
> y <- z[,1]*z[,2]                     # left-hand vector [Eq. (17.2)]
```

```

> xa <- lsfit(A,y,intercept=FALSE) # least-square calculation
> xa <- xa$coeff
> names(xa) <- NULL # process the resulting list

> # Determining asymptotes and curvature
> x0 <- xa[2]; y0 <- xa[3] # asymptotes [Eq. (17.2)]
> q <- xa[1]+x0*y0 # curvature [Eq. (17.2)]
> print(x0)
19.99885
> print(y0)
0.2831934
> print(q)
0.00004075364

> # Calculate coordinates of the hyperbola
> xx <- seq(min(z[,1]),max(z[,1]),((max(z[,1])-min(z[,1]))/100))
> yy <- y0+q/(xx-x0) # [Eq. (16.10)]

> # Plotting the mixing hyperbola
> plot(xx,yy,type="l",xlab=expression(""206Pb/"204Pb),
> ylab=expression(""176Hf/"177Hf),
> xlim=c(min(z[,1])-0.01,x0+0.01),
> ylim=c(min(z[,2])-0.00001,y0-0.00001))
> points(z[,1],z[,2],cex=1.5,pch=19) # add data points
> abline(v=x0,lty="dashed") # add asymptotes
> abline(h=y0,lty="dashed")

```

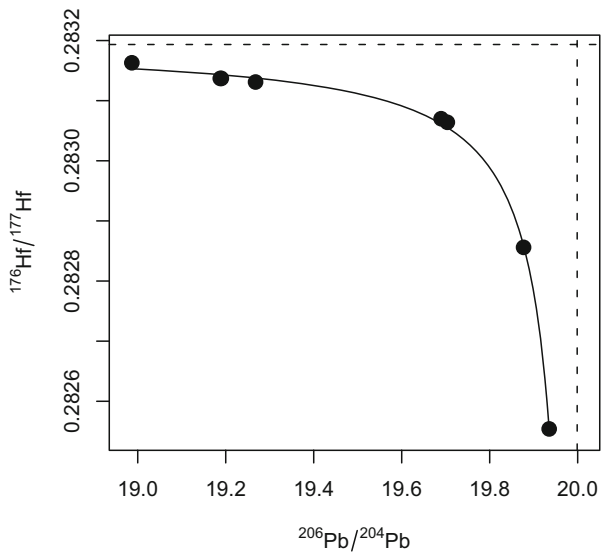


Fig. 19.1 Least-square reverse modelling of binary mixing between depleted-mantle and enriched, plume-derived component using the Pb–Hf isotopic data from La Martinique (Exercise 19.1).

Reference

Labanieh S, Chauvel C, Germa A, Quidelleur X, Lewin E (2010) Isotopic hyperbolas constrain sources and processes under the Lesser Antilles arc. *Earth Planet Sci Lett* 298:35–46

Part V Practical Modelling

In previous chapters, we have seen numerous formulae describing the compositional evolution of a magma undergoing different petrogenetic processes. From a purely mathematical point of view, these equations are relatively simple. However, in any igneous system, there are many unknowns, and several of them must be set or estimated using geological constraints before attempting to (numerically) solve the modelling equations.

It is important to bear in mind that a geochemical model can only test specific hypotheses—i.e., the geologist has to decide on the question to ask, while being aware that the only answer that the model can provide is “yes” (from a geochemical point of view, this mechanism can account for the observed data) or “no” (it is unable to reproduce the dataset). Modelling does not provide answers to “open” questions; thus we can ask, for instance:

- Is it possible to generate this dacite from that basalt, by fractional crystallization of a cumulate made up of amphibole and plagioclase? If so, what is the modal composition of that cumulate?
- Could this granite be derived by partial melting of that sediment? What was the maximum degree of melting allowed by such a source?
- Could assimilation of lower continental crust by ascending basalt yield an andesitic magma of the given composition?
- Could the compositional range observed in this igneous suite be the result of fractionation from a common parent?



Often, a negative answer is actually more useful, as it definitely rules out an assumption. In contrast, a positive answer just indicates that the proposed process is not impossible—it does not demonstrate that it actually happened!

Although there is no universal recipe, a set of tricks can be used. Frequently, there is no pure mathematical solution, and assumptions have to be made. These typically relate to the composition of the primitive magma, or the fractionating mineral phases. Often, a composite approach combining calculations and educated

guesses must be employed. In general, the following steps will be implemented:

- After having demonstrated the existence of a differentiation series (e.g. plotting trends in binary plots), identify and further constrain the process(es) that could have shaped the composition of the suite. This can be done on the basis of:
 - Previous knowledge (literature), analogy with similar occurrences elsewhere, relevant experiments or personal experience.
 - Geological evidence in general, e.g. field relations or petrology.
 - Geochemical evidence, such as interpretation of variation diagrams or isotopic constraints. At this point, one may also apply semi-quantitative tests (e.g. mixing test, determination of compatibility of elements—Chap. 21) that would help in determining what processes were possible or not, and so start constraining them.
- Build a full model, which in turn implies:
 - Choose the process to be modelled: mixing, melting, crystallization...
 - Decide on key variants thereof: modal or non-modal, fractional or batch...
 - Set the key input parameters: composition of the primitive liquid, fractionating phases and their chemistry, partition coefficients...
 - Perform the actual calculations.
- Test the model, i.e. compare the computed result with real data (including all the other available information, such as that coming from geology and petrology). Most often, this leads to refining the existing model.
- Reiterate until the model fits the data satisfactorily.



As a word of caution, one cannot stress strongly enough that it is unsafe to rely on the purely mathematical “best fit”. It is indeed possible that it does not make geological sense, whereas a slightly worse fit (from a numerical perspective) may be more realistic. For instance, modelling can predict the crystallization of an Ol + Qtz cumulate. Such a result is geologically meaningless. On the other hand, an Opx-bearing one is more plausible, even if the numerical fit is worse.

Chapter 20

Choosing an Appropriate Model

Geochemical modelling described in this book is primarily concerned with the interpretation of natural igneous suites. Therefore, any geochemical study must rest upon a sound understanding of their field relations and petrological features. As this text is not a manual of petrology, we will not describe all the relevant tools, but rather point out a few features that may help in deciding on the process to be modelled, even constraining it to some point.

20.1 Evidence for Crystallization

20.1.1 *Final Solidification During Emplacement*

In lava sequences, final solidification after eruption is typically fast and does not affect the chemistry of the suite. However, in low-viscosity magmas such as komatiites, there are well-documented examples of intra-flow differentiation (Arndt 1994) driven by gravity settling of crystals at the bottom of the lava flow (Fig. 20.1a). This process could be adequately modelled using the *incomplete crystal separation* scenario of Sect. 6.1.4 and 11.5.1.

In plutonic complexes, cooling is slower and may be accompanied by segregation of the fractionated liquids from the mush of already formed crystals (Fig. 20.1b), a process that can be enhanced by syn-magmatic deformation (“filter-pressing”, e.g. Sisson and Bacon 1999). One may describe the slow solidification of a pluton in terms of *batch crystallization* (preserving the mass balance, but with changing phase compositions), or of *incomplete crystal separation*.

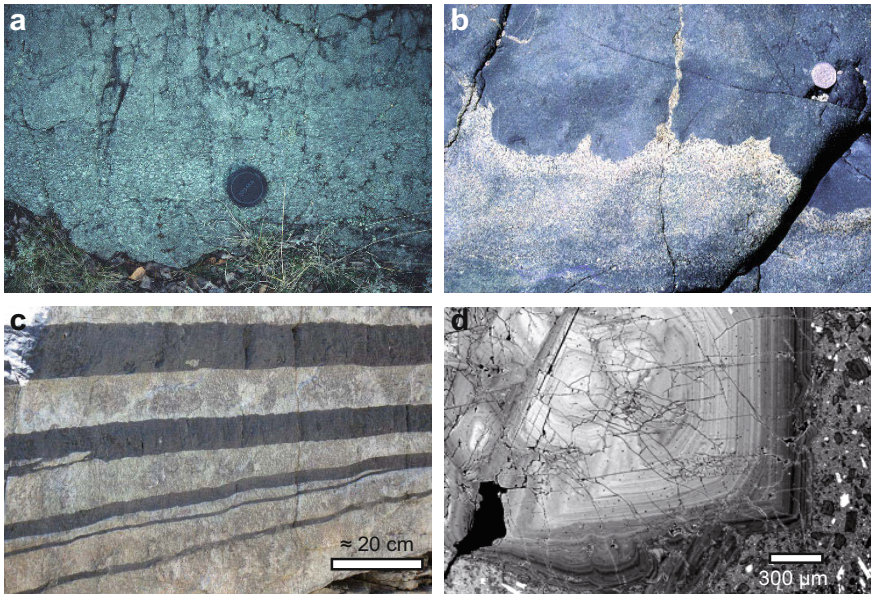


Fig. 20.1 Field evidence for in situ and fractional crystallization. **a** Olivine accumulation at the base of a komatiite flow (Sivikkovaara, Finland) (lens cap for scale). **b** Evidence for late-stage separation of liquids in a crystallizing pluton (Guernsey gabbroic intrusion, Channel Islands, U.K.) (coin for scale). Late felsic melts are extracted from the crystals–liquid mixture (“mush”) below and accumulate against, and even cut through, an overlying layer of already essentially solid material. **c** Cumulate layers of anorthosite and chromitite in the Dwarfs River locality of the Bushveld Complex (South Africa). **d** A back-scattered electron (BSE) view of oscillatory zoning in a plagioclase from Parínacota Volcano, Chile (Ginibre et al. 2002). Although plagioclases commonly show complex zoning patterns that probably reflect stories more complicated than plain crystallization, as a first approximation the composition of this plagioclase becomes more sodic towards the rim, consistent with a crystallization in a magma (Photo G. Wörner).

20.1.2 Fractional Crystallization at Depth

Already at the dawn of geochemistry, geologists recognized the existence of magmatic series, sharing common compositional features (Harker 1909). In these series, the rock compositions change progressively, which is commonly ascribed to evolution by fractional crystallization at depth, in a putative magma chamber.

However, direct evidence for this process is rare, and it is difficult to constrain from geological data. Cumulate layers (such as those observed in layered mafic intrusions; Fig. 20.1c) are an obvious proof for growth and removal of crystals from fractionating parts of the magma chamber. However, whenever cumulate sequences are observed, rocks formed from matching liquids are unlikely to be seen, as melts tend to rise to higher crustal levels, now eroded away. Conversely, when sequences of magmatic rocks crystallized from evolving liquids are preserved, the underlying cumulates are unlikely to be cropping out. In rare, favourable cases it may be possible to observe cumulate enclaves snatched from depth and carried up

by the ascending differentiated magma. Phenocrysts in lava are generally taken as evidence for early fractionation. In particular, their oscillatory or simple continuous zoning patterns (Fig. 20.1d) are an indication for fractional crystallization from a gradually evolving magma.

20.2 Evidence for Melting

The mere presence of igneous rock that had to crystallize from magma is evidence for melting. In that sense every geochemical model should include a stage of partial melting. However, melting processes generally take place at great depth, much deeper than the place where magmas crystallize. Consequently, melting sites can be poorly (if at all) documented at the current exposure level. Therefore, deciphering melting is often tricky and indirect.

20.2.1 *Crustal Anatexis*

Partially molten upper crustal rocks (migmatites) are frequently observed (Fig. 20.2a–c), and there is ample literature describing and interpreting these rocks in terms of field relations, rheology or petrology: see for instance Mehnert (1968) or the reviews in Brown (2007) or Sawyer (2008). A *batch melting* model may seem adequate, and direct observation of the restitic assemblage should make modelling relatively easy.

However, geochemical modelling of migmatites has many pitfalls. One of the critical issues is that the leucosomes seldom have pure melt compositions. Several explanations have been proposed, including reequilibration by diffusion (Fourcade et al. 1992) or “back-reactions” with the melanosome (Kriegsman and Hensen 1998). Alternatively, the leucosomes may be interpreted as early cumulate layers left behind after melt removal (Taylor et al. 2014) or even injected foreign melts (Hasalová et al. 2008). All these processes can be modelled—at the cost of increased complexity.

In addition, the mere existence of felsic intrusions demonstrates that melt has been extracted from migmatites (Brown 2004; Yakymchuk and Brown 2014). Therefore, it is likely that many of them are melt-depleted and thus poorly represent the state of the source during anatexis.

Yet, the presence of migmatites in the right place at the right time does indeed provide crucial evidence for crustal melting processes that could have been potentially involved in the generation of nearby, contemporaneous felsic suites.

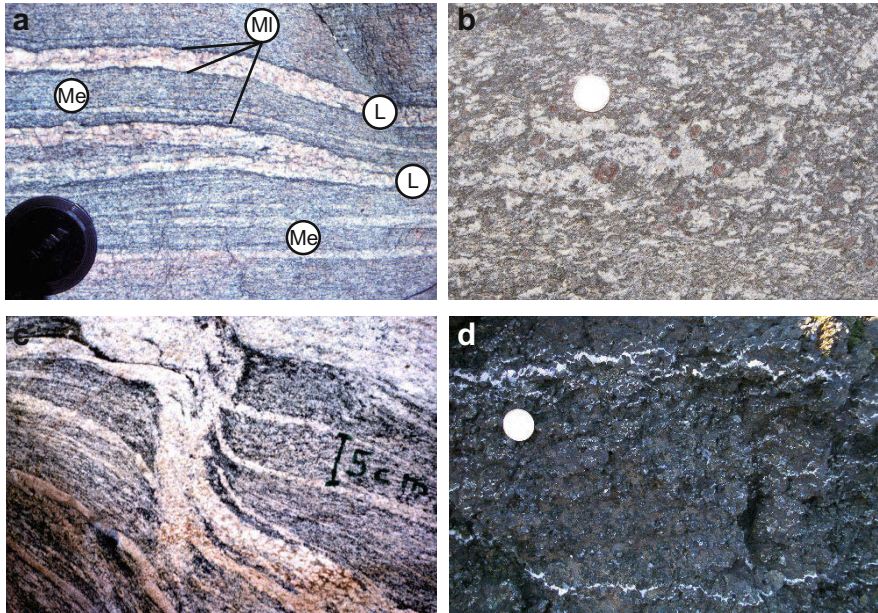


Fig. 20.2 Field evidence for partial melting. **a** Migmatites from the Caicó Block (Rio Grande do Norte, Brazil). A leucosome (L) and matching melanosome (MI, thin black border) are hosted in a mesosome (Me). The mesosome represents a portion of the source not affected by melting, while the leucosome may correspond to the liquid and the melanosome to the restite. Here the melanosome is dominated by biotite, suggesting that the melting reaction was either fluid-present or muscovite breakdown (Stevens et al. 1997). **b** Migmatites from the Southern Marginal Zone of the Limpopo Belt, South Africa. A diffuse network of leucosomes is associated with large crystals of garnet, formed by the biotite-breakdown melting reaction ($Bt + Pl + Qtz + Sil = L + Grt$) (Stevens and van Reenen 1992). **c** Migmatites from Kivijärvi, Finland. An oblique felsic vein is connected to the leucosome, and cuts the foliation, thus demonstrating that melt was being extracted from the migmatite. **d** Thin leucocratic (plagioclase-rich) veins in a lherzolite from the Monte Maggiore ophiolite, Corsica. Small white patches (either interconnected, as in the large vein near the top of the photo, or trapped in the intergranular space, as in the middle) represent small volumes of liquid generated by melting of the surrounding peridotite, which may be regarded as a source for the associated gabbros and basalts from the same ophiolite. As for the lower crustal migmatites, one may ask whether the leucosomes represent trapped in-situ melts or remnants of melt having percolated the peridotite (Photo C. Nicollet).

20.2.2 Melting of the Mantle

Direct evidence for mantle melting is almost never observed (except, perhaps, rare massive peridotites or ophiolite sequences—Fig. 20.2d). Sometimes a suite of mantle xenoliths is found, some of which could represent melt-depleted portions of the source. However, xenolith studies reveal that they mostly come from the mantle above the magma source, being broken apart and carried to the surface by ascending magma (Pearson et al. 2003). As the extraction of low-volume melts from the mantle appears to be an efficient process (Walter 2003), *fractional melting* is often seen as

the most appropriate model, in particular for alkaline sequences. However, for greater degrees of melting (tholeiites), the differences from batch melting become negligible.

20.3 Magma Mixing and Assimilation

20.3.1 *Mixing and Mingling of Magmas*

Field evidence may prove the coexistence of two contrasting magmas: the presence of mafic microgranular enclaves (MME), chilled margins in a mafic magma at its contact with a felsic one, round and lobate liquid–liquid contacts, net veining with a relatively mobile felsic magma invading a nearly solidified mafic one (Fig. 20.1b) or late syn-plutonic dykes often disrupted into enclave swarms (Didier and Barbarin 1991; Hallot et al. 1996; Wiebe and Collins 1998). The mechanism and degree of interaction between two dissimilar magmas would depend, among other factors, on a) thermal energy, reflecting the depth of intrusion and proportion of the hot mafic melt (if small, the system will effectively freeze) and b) relative timing of the mafic melt injection into the felsic magma chamber, related to the degree of crystallinity of the latter (Fig. 20.3).

Hybridization between two magmas is further revealed by microtextural evidence for multistage crystallization (e.g., dendritic plagioclase, acicular apatite, blade-shaped biotite, and quartz/K-feldspar oikocrysts enclosing small quenched crystals), or for exchange of xenocrysts/chemical disequilibria (e.g., amphibole- or pyroxene-rimmed quartz ocelli: Fig. 20.4a, rapakivi and antirapakivi feldspars: Fig. 20.4b, plagioclase with complex resorption history and discontinuous zoning: Fig. 20.4c) (Hibbard 1991; Vernon 1991; Hibbard 1995; Janoušek et al. 2000). Besides standard petrography, optical cathodoluminescence (CL), Nomarski microscopy, or back-scattered electron imagery (BSE) are efficient tools (Marshall 1988; Castro and De la Rosa 1994; Pagel et al. 2000; Janoušek et al. 2004). Compositional mapping can also disclose complex zoning patterns with several episodes of crystallization and resorption (Fig. 20.4d).

All these features demonstrate hybridization between two magmas. However, the strikingly different physical properties of basic and acid liquids (e.g. their great viscosity contrast) tend to make single-stage chemical mixing difficult. The fact that the identity of the two contrasting magmas is preserved does demonstrate that they did not *mix* at the present exposure level, where merely mechanical *mingling* and exchange of earlier formed crystals occurred (Bateman 1995). This may suggest that the scope of mixing was limited. On the other hand, this does not rule out mixing as a significant process at deeper crustal levels with more favourable physical conditions. Alternatively, coexistence of well-mixed regions with poorly homogenized ones (in the form of MME or schlieren) may be due to the chaotic nature of the mixing process (Perugini and Poli 2000). This has been successfully reproduced experimentally on natural materials (e.g. Morgavi et al. 2013).

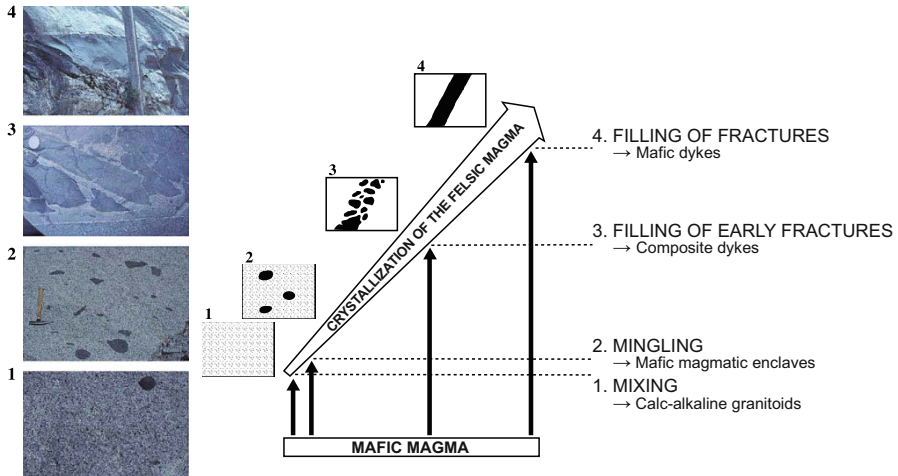


Fig. 20.3 Variable textures in hybrid rocks resulting from injection of mafic magma at different stages of the felsic magma chamber crystallization (Barbarin 2005). Photos are from the Dinkey Creek Pluton, Sierra Nevada, USA. © Elsevier

Mixing and *mingling* can both be modelled by binary mixing equations. However, the scale of the processes does differ. Mixing is primarily diffusion-driven and thus controlled by the surface area of the interfaces between dissimilar liquids. The process should affect large volumes of magma, so the observed rocks may all represent hybrids, and any pure end-members could be totally missing. Mingling, on the other hand, would affect only small volumes (equilibration domains, see Sect. 24.2) of the magmas, and the rocks with end-member compositions are more likely to be preserved.

20.3.2 Assimilation

Striking examples of host-rock xenoliths disaggregating into intrusions are convincing evidence for *assimilation* of country rocks into a pluton (Pitcher and Berger 1972; Clarke et al. 1998; Lackey et al. 2006; Clarke et al. 2007). Assimilation, from a geochemical point of view, is plain mixing, but should be coupled with fractional crystallization into AFC processes. Yet, the scale of such interactions is debatable: do they affect more than the zone located in the immediate vicinity of the xenoliths? Current thinking is that the energy cost of assimilation is so high that a near-solidus pluton cannot provide sufficient heat to assimilate sizeable amounts of rocks at emplacement level (Glazner 2007). However, at depth, in the hot lower crust or in the mantle, the thermal budget is less of an issue and assimilation is more feasible. In the deep crust, such a process has been described as “MASH” (Melting, Assimilation, Storage and Homogenization) (Hildreth and Moorbath 1988; Vernon 2007), modelling of which requires combining several simple mechanisms (Sect. 11.5).

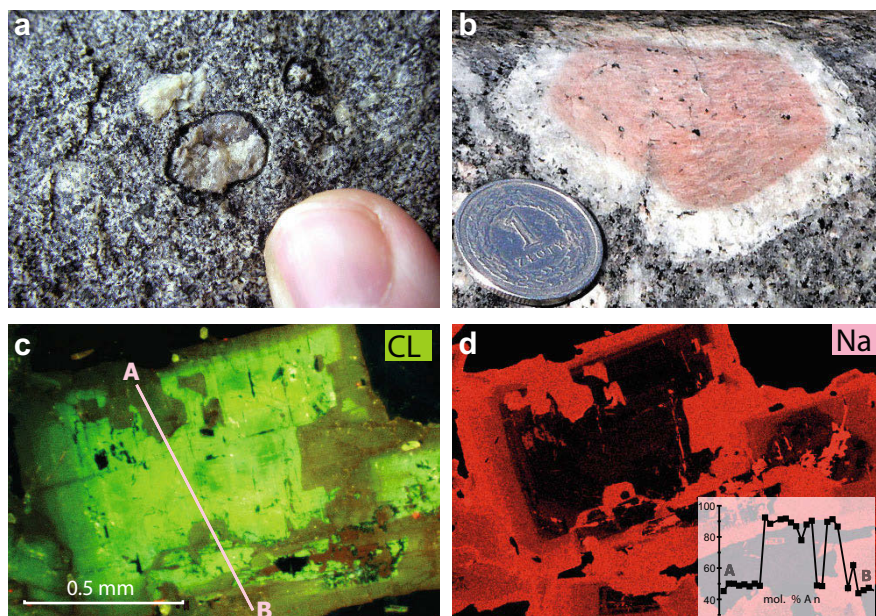


Fig. 20.4 Petrographic evidence for mixing and assimilation processes. **a** Clinopyroxene-rimmed quartz ocelli in the Ploumanac'h granite (France). **b** Rapakivi texture in the Karkonosze granite (Poland); a core of alkali feldspar is rimmed by plagioclase. **c** Zoned plagioclase from hybrid quartz microdiorite, Teletín (Central Bohemian Plutonic Complex), in optical CL. **d** Electron microprobe map of Na distribution in the same crystal; profile A–B is shown in inset (Janoušek et al. 2004).

References

- Arndt NT (1994) Archean komatiites. In: Condie KC (ed) Archean crustal evolution. Developments in Precambrian Geology, vol 11. Elsevier, Amsterdam, pp 11–44
- Barbarin B (2005) Mafic magmatic enclaves and mafic rocks associated with some granitoids of the central Sierra Nevada batholith, California: nature, origin, and relations with the hosts. *Lithos* 80:155–177
- Bateman R (1995) The interplay between crystallization, replenishment and hybridization in large felsic magma chambers. *Earth Sci Rev* 39:91–106
- Brown M (2004) The mechanism of melt extraction from lower continental crust of orogens. *Trans Roy Soc Edinb, Earth Sci* 95:35–48
- Brown M (2007) Crustal melting and melt extraction, ascent and emplacement in orogens: mechanisms and consequences. *J Geol Soc London* 164:709–730
- Castro A, De la Rosa JD (1994) Nomarski study of zoned plagioclases from granitoids of the Seville Range Batholith, SW Spain. Petrogenetic implications. *Eur J Mineral* 6:647–656
- Clarke DB, Henry AS, White MA (1998) Exploding xenoliths and the absence of ‘elephants’ graveyards’ in granite batholiths. *J Struct Geol* 20:1325–1343
- Clarke DB, Paterson SR, Vernon RH (2007) Contaminated granites: preface. *Canad Mineral* 45:1–3
- Didier J, Barbarin B (1991) Enclaves and granite petrology. Elsevier, Amsterdam
- Fourcade S, Martin H, de Brémond d’Ars J (1992) Chemical exchange in migmatites during cooling. *Lithos* 28:43–53

- Ginibre C, Wörner G, Kronz A (2002) Minor- and trace-element zoning in plagioclase: implications for magma chamber processes at Paríacota volcano, northern Chile. *Contrib Mineral Petrol* 143:300–315
- Glazner AF (2007) Thermal limitations on incorporation of wall rock into magma. *Geology* 35:319–322
- Hallot E, Davy P, de Brémond d’Ars J, Auvray B, Martin H, van Damme H (1996) Non-Newtonian effects during injection in partially crystallised magmas. *J Volcanol Geotherm Res* 71:31–44
- Harker A (1909) *A natural history of igneous rocks*. Methuen and Co., London
- Hasalová P, Janoušek V, Schulmann K, Štípská P, Erban V (2008) From orthogneiss to migmatite: geochemical assessment of the melt infiltration model in the Gföhl Unit (Moldanubian Zone, Bohemian Massif). *Lithos* 102:508–537
- Hibbard MJ (1991) Textural anatomy of twelve magma-mixed granitoid systems. In: Didier J, Barbarin B (eds) *Enclaves and granite petrology*. Elsevier, Amsterdam, pp 431–444
- Hibbard MJ (1995) Mixed magma rocks. In: *Petrography to petrogenesis*. Prentice Hall, New Jersey, pp 242–260
- Hildreth W, Moorbath S (1988) Crustal contributions to arc magmatism in the Andes of central Chile. *Contrib Mineral Petrol* 98:455–489
- Janoušek V, Bowes DR, Braithwaite CJR, Rogers G (2000) Microstructural and mineralogical evidence for limited involvement of magma mixing in the petrogenesis of a Hercynian high-K calc-alkaline intrusion: the Kozárovice granodiorite, Central Bohemian Pluton, Czech Republic. *Trans Roy Soc Edinb, Earth Sci* 91:15–26
- Janoušek V, Braithwaite CJR, Bowes D, Gerdes A (2004) Magma-mixing in the genesis of Hercynian calc-alkaline granitoids: an integrated petrographic and geochemical study of the Sázava intrusion, Central Bohemian Pluton, Czech Republic. *Lithos* 78:67–99
- Kriegsman LM, Hensen BJ (1998) Back reaction between restite and melt: implications for geothermobarometry and pressure–temperature paths. *Geology* 26:1111–1114
- Lackey JS, Valley JW, Hinke HJ (2006) Deciphering the source and contamination history of peraluminous magmas using $\delta^{18}\text{O}$ of accessory minerals: examples from garnet-bearing plutons of the Sierra Nevada Batholith. *Contrib Mineral Petrol* 151:20–44
- Marshall DJ (1988) *Cathodoluminescence of geological materials*. Unwin Hyman, Boston
- Mehnert KR (1968) *Migmatites and the origin of granitic rocks*. Elsevier, Amsterdam
- Morgavi D, Perugini D, de Campos CP, Ertel-Ingrisch W, Dingwell DB (2013) Morphochemistry of patterns produced by mixing of rhyolitic and basaltic melts. *J Volcanol Geotherm Res* 253:87–96
- Pagel M, Barbin V, Blanc P, Ohnenstetter D (2000) *Cathodoluminescence in geosciences*. Springer, Berlin
- Pearson D, Canil D, Shirey S (2003) Mantle samples included in volcanic rocks: xenoliths and diamonds. In: Carlson R (ed) *The mantle and core. Treatise on Geochemistry*, vol 2. Elsevier, Amsterdam, pp 171–275
- Perugini D, Poli G (2000) Chaotic dynamics and fractals in magmatic interaction processes: a different approach to the interpretation of mafic microgranular enclaves. *Earth Planet Sci Lett* 175:93–103
- Pitcher WS, Berger AR (1972) *The geology of Donegal: a study of granite emplacement and unroofing*. Wiley-Interscience, New York
- Sawyer EW (2008) *Atlas of migmatites*. The Canadian Mineralogist Special Publication, vol 9. NRC Research Press, Ottawa
- Sisson TW, Bacon CR (1999) Gas-driven filter pressing in magmas. *Geology* 27:613–616
- Stevens G, van Reenen D (1992) Partial melting and the origin of metapelitic granulites in the Southern Marginal Zone of the Limpopo Belt, South Africa. *Precambr Res* 55:303–319
- Stevens G, Clemens JD, Droop GTR (1997) Melt production during granulite-facies anatexis: experimental data from ‘primitive’ metasedimentary protoliths. *Contrib Mineral Petrol* 128:352–370

- Taylor J, Nicoli G, Stevens G, Frei D, Moyen JF (2014) The processes that control leucosome compositions in metasedimentary granulites: perspectives from the Southern Marginal Zone migmatites, Limpopo Belt, South Africa. *J Metam Geol* 32:713–742
- Vernon RH (1991) Interpretation of microstructures of microgranitoid enclaves. In: Didier J, Barbarin B (eds) *Enclaves and granite petrology*. Elsevier, Amsterdam, pp 277–291
- Vernon RH (2007) Problems in identifying restite in S-type granites of southeastern Australia, with speculations on sources of magma and enclaves. *Canad Mineral* 45:147–178
- Walter M (2003) Melt extraction and compositional variability in mantle lithosphere. In: Carlson R (ed) *The mantle and core. Treatise on Geochemistry*, vol 2. Elsevier, Amsterdam, pp 363–394
- Wiebe RA, Collins WJ (1998) Depositional features and stratigraphic sections in granitic plutons: implications for the emplacement and crystallization of granitic magma. *J Struct Geol* 20:1273–1289
- Yakymchuk C, Brown M (2014) Consequences of open-system melting in tectonics. *J Geol Soc London* 171:21–40

Chapter 21

Semi-Quantitative Geochemical Approach

Even without embarking on developing a proper geochemical model, it is possible to devise several geochemical tests that can help in selecting a model, or in constraining some of its parameters.

21.1 Assessing Trace-Element Compatibility

As noted already in Sect. 10.2, the concept of compatibility and incompatibility of a trace element is a relative one. For instance, let's consider the behaviour of Yb. During peridotite melting, leaving a residue made of olivine ($K_{D_{Yb}}^{Ol/L} = 0.0015^1$), orthopyroxene ($K_{D_{Yb}}^{Opx/L} = 0.05$) and clinopyroxene ($K_{D_{Yb}}^{Cpx/L} = 0.28$), $D_{Yb} \ll 1$ and Yb would show a strongly incompatible behaviour. In contrast, for eclogite melting the residue consists of clinopyroxene ($K_{D_{Yb}}^{Cpx/L} = \sim 1.0$) and garnet ($K_{D_{Yb}}^{Gr/L} = 21$); consequently, $D_{Yb} \gg 1$ and Yb would be strongly compatible as soon as more than 5% garnet is present.

In silica-rich magmas, most elements tend to become compatible due to the complex main rock-forming and accessory mineral assemblages involved. Even elements such as REE (strongly incompatible in basic magmas) are hosted by accessory minerals (allanite, monazite, xenotime, etc.). Of course, this effect is taken to the extreme in highly differentiated systems, such as pegmatites.

The first step in any study is, therefore, to assess the behaviour of each element in the system. The simplest approach is to plot binary diagrams of a differentiation index vs. the investigated elements. A positive correlation characterizes incompatible, and a negative one compatible elements. In basic suites, commonly used differentiation indexes are MgO, Cr, Ni or mg#, while in intermediate to acid associations, SiO₂ is preferred. Still, it must be kept in mind that diagrams involving major elements, especially SiO₂, suffer from the constant sum effect (Sect. 3.1.2).

¹ K_D values are from Rollinson (1993).

21.2 Order of (In)Compatibility

Regardless of the process involved, the largest changes in elemental concentrations are observed for D values very different from 1. This idea was developed for incompatible elements by Schiano et al. (1993). In a suite of rocks related by a single petrogenetic process (such as fractional crystallization or partial melting), there is a correlation between D and the *variability* of the dataset, defined as:

$$V_{\alpha} = \frac{\sigma(\alpha)}{\bar{\alpha}} \quad (21.1)$$

with $\sigma(\alpha)$ and $\bar{\alpha}$ referring respectively to the standard deviation, and the mean of the concentrations, of the element α .

For incompatible elements, the order of increasing variability then mimics the increasing incompatibility of individual elements (i.e. the smaller D , the higher the variability). Likewise for compatible elements, variability correlates with compatibility (large D results in high variabilities): elements with D very different from 1 (very compatible or very incompatible) have highest variabilities². Several applications of this approach can be found in Schiano et al. (1993). For instance, one may plot the variability of a dataset against that in a reference rock suite (typically MORBs). Elements plotting away from the 1:1 line have D values different in the two sets (often because other minerals were involved, in the melting source crystallizing assemblage). Similarly, when plotting a spidergram normalized to the likely source, if all the elements are arranged in the order of compatibility established from the dataset, any anomalies reveal deviation of the source composition from the normalization values.



Exercise 21.1: Order of (in)compatibility

File `chpuy.data` contains analyses³ for melt inclusions in olivine crystals from the *Chaîne des Puys Quaternary volcanoes of central France* (Jannot 2005). We shall investigate the genesis of these magmas from their mantle source; we focus on the set of elements present in Hofmann's (1988) Primitive Mantle composition, for which the variability in MORBs was calculated by Schiano et al. (1993).



[chpuy.data](#)
[hofmann.data](#)

² Thus, this approach originally developed for incompatible elements will also work for compatible ones, but the two groups must be treated independently.

³ Major elements were corrected for reequilibration with the host olivine.

- Calculate the variability V_a for all elements [Eq. (21.1)] and print in descending order.
- Plot a diagram comparing the variability in this dataset with that in MORBs (Schiano et al. 1993).
- Display a spiderplot normalized to the Primitive Mantle, but with elements arranged in the order of increasing compatibility (= variability) in the inclusions.



```

> chpuy <- read.table("chpuy.data", sep="\t")
> s <- apply(chpuy, 2, sd, na.rm=T) # calculate even for missing values
> m <- apply(chpuy, 2, mean, na.rm=T)
> variability <- s/m # Eq. (21.1)
> print(rev(sort(variability)), 2)
   Cr   Th   Ba   Rb   La   Ce  P2O5   Sm   Nd   Eu   Nb
0.706 0.292 0.262 0.245 0.235 0.198 0.194 0.190 0.187 0.174 0.165 ...
> hofmann <- read.table("hofmann.data", sep="\t")
> hofmann <- as.matrix(hofmann)
> # Select elements for which we do have the MORB variability data
> v.el <- colnames(hofmann)[!is.na(hofmann["V.MORB",])]
> x.data <- hofmann["V.MORB", v.el]
> plot(x.data, variability[v.el], xlim=c(0, 0.5), ylim=c(0, 0.5), pch=15,
+      xlab="Variability, MORB", ylab="Variability, Ch. Des Puy")

```

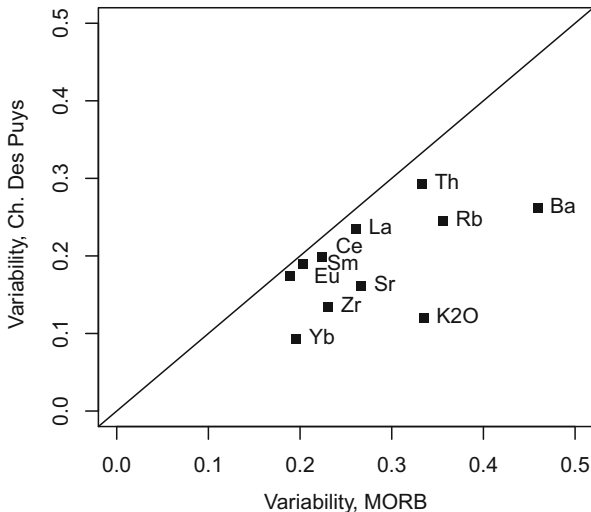


Fig. 21.1 A plot comparing the variability in MORBs with that in the studied dataset (Exercise 21.1). Some elements (notably Ba and K₂O) have very different variabilities in MORBs and in the investigated suite, demonstrating their distinct behaviour in the two datasets. This is an effect of phlogopite and/or amphibole that was presumably present in the mantle source of the Chaîne des Puy basalts.

```
> text(x.data,variability[v.el],v.el,pos=4,offset=0.5)
> abline(0,1)
> # Order the elements in decreasing incompatibility
> v.ordered <- rev(sort(variability [colnames(hofmann)]))
> # Select the data and normalization values
> data <- chpuy[,names(v.ordered)]
> norm <- hofmann["PM",names(v.ordered)]
```

Spider plot – Prim. mantle (Hofmann 1988) [CP order]

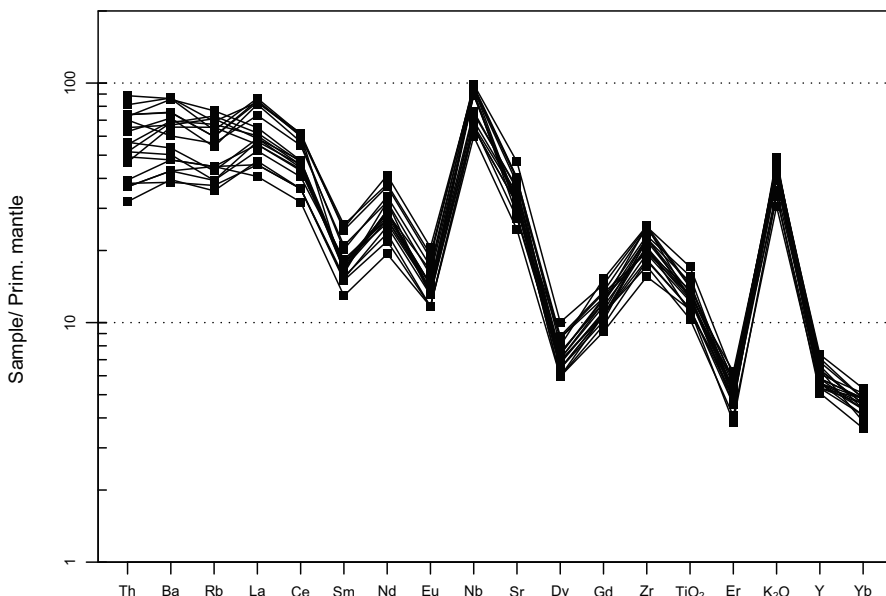


Fig. 21.2 Spiderplot for Chaîne des Puys melt inclusions, normalized to Primitive Mantle (Hafmann 1988) but with elements arranged in order of compatibility determined for the inclusions data. Prominent anomalies for Nb, Sr, Zr and K₂O show that the source of lavas differed from the Primitive Mantle (the former most likely contained amphibole and/or phlogopite).

The plotting is best done using *GCDkit* (for a plain R approach, see Exercise 3.4).

```
GCDkit-> norm <- t(as.matrix(norm))
GCDkit-> rownames(norm) <- "Prim. mantle (Hofmann 1988) [CP order]"
GCDkit-> spider(data,norm,pch=15,ymin=1,ymax=200)
GCDkit-> print(results)
```

	ThN	BaN	RbN	LaN	CeN
Chaumont11	70.11070	60.17524	56.04334	73.30184	54.96221
Chaumont2	51.66052	50.25624	39.23034	57.01254	45.59365...

21.3 Process Identification

For major elements, the three main petrogenetic processes (melting, crystallization and mixing) are governed by mass-balance relationships (Sect. 6.5). This results in a linear trend in any binary plot of major-element compositions.



A linear trend in a binary plot of two major elements, or their oxides (including Harker plots), indicates no specific petrogenetic process! This can be generalized, in p -dimensional space, for p major elements.

For trace elements, melting is commonly regarded as a batch process and crystallization as fractional. Mixing, on the other hand, still follows linear laws. As shown in Part III, these three processes are described by contrasting equations:

$$C_L = \frac{C_0}{D + F(1 - D)}, \quad \frac{C_L}{C_0} = F^{(D-1)} \quad \text{and} \quad C_L = f_1 C_1 + (1 - f_1) C_2.$$

In a binary plot of two trace elements, the resulting curves have different shapes⁴.

21.3.1 Mixing vs. Crystallization/Melting

Recognition of mixing is, theoretically, straightforward. Mixing is controlled by mass balance and yields linear trends in any element vs. element diagram (and hyperbolae in plots involving at least one ratio, see Table 11.1), whereas the two other processes generate curved trends (except in a major–major plot). A straight line in a trace–trace (or major–trace) diagram is therefore *no indicator of fractionation*, but rather points to mixing (unless D is close to 0, in which case the fractionation/batch curves both collapse to $C_L = C_0/F$, i.e. a straight line).

Obviously, isotopes are the tool of choice to spot mixing—at least between two isotopically contrasting compositions. However, open-system processes such as magma mixing or assimilation are frequently accompanied with, or followed by, fractional crystallization/accumulation that modifies the binary mixing-related elemental distribution, often beyond recognition. Even in such cases, the isotope ratios should escape unaffected, still ‘seeing through’ such modifications (Part IV).

21.3.2 Crystallization vs. Melting in a Log–Log Diagram

In Chap. 11, it has been shown that the behaviour of incompatible elements during both crystallization and melting is roughly similar. Indeed, they are all expressed

⁴ But see Sect. 24.3.1 for a discussion on the feasibility of distinguishing between processes.

by equations such that when $D \rightarrow 0$, then $C_L \rightarrow C_0/F$. On the other hand, fractional crystallization is extremely efficient at depleting compatible elements in a magma, whereas partial melting has little effect on these.

This relation is usually described in a $\log(\alpha)$ vs. $\log(\beta)$ diagram, where α is incompatible and β compatible. From *Rayleigh's Law* we derive for each element:

$$\log C_L - \log C_0 = (D-1) \log F \quad (21.2)$$

$$\log F = \frac{\log C_L - \log C_0}{D-1} \quad (21.3)$$

Combining two Eq. (21.3), for α and β , gives:

$$\log C_L^\beta = \frac{D_\beta - 1}{D_\alpha - 1} \log C_L^\alpha + \left(\log C_0^\beta - \frac{D_\beta - 1}{D_\alpha - 1} \log C_0^\alpha \right) \quad (21.4)$$

In a $\log(C_\alpha)$ vs. $\log(C_\beta)$ diagram, this is a straight line whose slope is:

$$\frac{D_\beta - 1}{D_\alpha - 1} \quad (21.5)$$

Since $D_\alpha \sim 0$ and $D_\beta \gg 1$, the slope is steep negative⁵, close to $-D_\beta$.

Likewise, the *fractional melting* equation (instantaneous liquids, Eq. 11.13) can be expressed for elements α and β , transformed in log coordinates and combined into:

$$\begin{aligned} \log C_L^\beta = & \left(\frac{D_\alpha (1 - D_\beta)}{D_\beta (1 - D_\alpha)} \right) \log C_L^\alpha + \log C_0^\beta + \log \frac{1}{D_\beta} + \\ & + \left(\frac{D_\alpha (1 - D_\beta)}{D_\beta (1 - D_\alpha)} \right) \left(\log \frac{1}{D_\alpha} - \log C_0^\alpha \right) \end{aligned} \quad (21.6)$$

The result is again a straight line, whose slope is:

$$\left(\frac{D_\alpha (1 - D_\beta)}{D_\beta (1 - D_\alpha)} \right) \quad (21.7)$$

⁵ Note that the scales should be the same on both axes; indeed when the scales are too dissimilar the slope of the line is distorted.

Since $D_\alpha \sim 0$ and $D_\beta \gg 1$, the slope is shallow negative, close to:

$$\left(\frac{D_\alpha (-D_\beta)}{D_\beta} \right) \approx -D_\alpha. \quad (21.8)$$

The *batch melting* equation is not exponential, and therefore cannot be expressed by linear relations in log coordinates. Nevertheless, the equation generates a curve, again with a shallow slope.

As a result, in a $\log(\alpha = \text{incompatible})$ vs. $\log(\beta = \text{compatible})$ plot, fractional crystallization generates an almost vertical trend while partial melting (both fractional and batch) would result in a nearly horizontal one (Fig. 21.3).

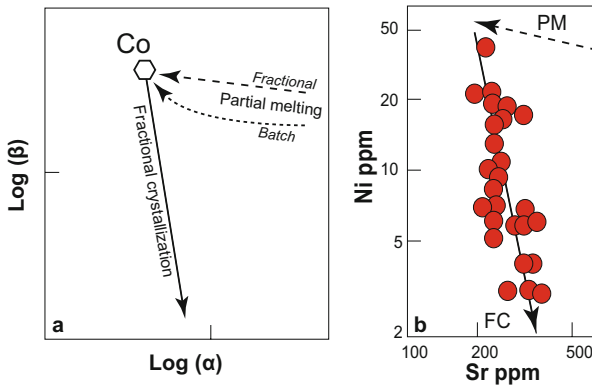


Fig 21.3 a In a $\log(\alpha = \text{incompatible})$ vs. $\log(\beta = \text{compatible})$ diagram, fractional crystallization produces an almost vertical trend whereas partial melting results in a nearly horizontal one. **b** Plot $\log(\text{Sr})$ vs. $\log(\text{Ni})$ showing that the Archaean TTG from eastern Finland (red circles) evolved by fractional crystallization (FC) and not by partial melting (PM) (adapted from Martin 1987).

These diagrams are generally used to determine the main (or the latest) mechanism that shaped the geochemical characteristics of a rock suite. However, they can also help in proposing more complex scenarios (Fig. 21.4). In this case, each successive melt batch from the same source fractionated independently.

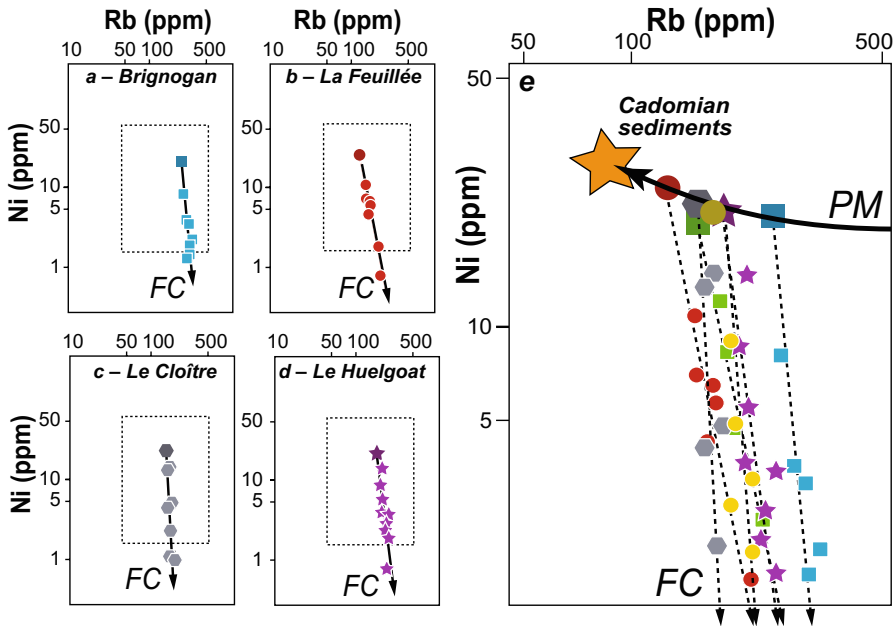


Fig. 21.4 a–d Log(incompatible = Rb) vs. log(compatible = Ni) plots for Cadomian and Hercynian granites from Brittany. Six individual granitic suites (four of which are plotted here) define fractional crystallization (FC) trends, specific to each pluton. **e** The parental melts of each pluton (darker, bigger symbols), however, plot along a batch melting trend (PM), the source being local metasediments (Georget 1986).

21.3.3 Crystallization vs. Melting Using Incompatible Elements

Minster and Allègre (1978) proposed an alternative treatment, based only on incompatible elements and specifically focusing on low-degrees of mantle melting (i.e. basalts). Element α , as previously, is strongly incompatible, and thus $D_\alpha \ll F \ll 1$. Element γ is moderately incompatible, $D_\gamma \approx F \ll 1$. In this case, combining Rayleigh's equations for α and γ yields:

$$\frac{C_L^\alpha}{C_L^\gamma} = \frac{C_0^\alpha}{C_0^\gamma} F^{(D_\alpha - D_\gamma)} \quad (21.9)$$

Since D_α and D_γ are small, Eq. (21.9) becomes:

$$\frac{C_L^\alpha}{C_L^\gamma} \approx \frac{C_0^\alpha}{C_0^\gamma} \quad (21.10)$$

The ratio of two incompatible elements is not affected by fractional crystallization.

For batch partial melting, the resulting equation is not so simple:

$$\frac{C_L^\alpha}{C_L^\gamma} = \frac{D_\gamma - D_\alpha}{(1 - D_\alpha)C_0^\gamma} C_L^\alpha + \frac{C_0^\alpha}{C_0^\gamma} \frac{1 - D_\gamma}{1 - D_\alpha} \tag{21.11}$$

Nevertheless, since we are dealing with two elements with different degrees of incompatibility, $D_\alpha \ll D_\gamma$, Eq. (21.11) becomes:

$$\frac{C_L^\alpha}{C_L^\gamma} \approx \frac{D_\gamma}{C_0^\gamma} C_L^\alpha + \frac{C_0^\alpha}{C_0^\gamma} (1 - D_\gamma) \tag{21.12}$$

which in a C_L^α vs. C_L^α / C_L^γ plot represents a straight line with a slope of D_γ / C_0^γ .

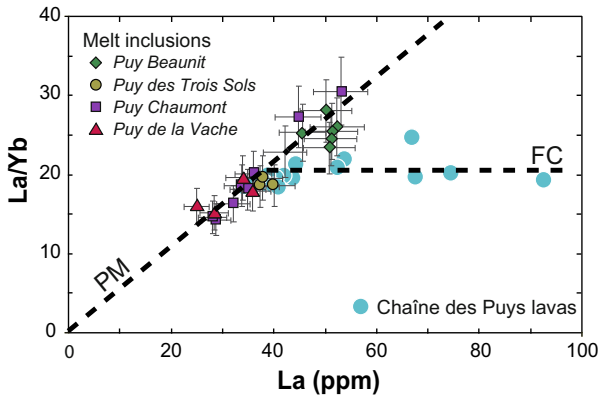


Fig. 21.5 A diagram La vs. La/Yb for compositions of whole rocks and melt inclusions in olivines from the Quaternary Chaîne des Puys volcanoes (Central France) (same dataset as Exercise 21.1). Two distinct trends are clearly apparent. The steeper line, defined by melt inclusions and the most primitive lavas, reflects mantle melting (PM). Its intercept at La_0/Yb_0 is very low (as typical of a mantle source). The horizontal line, formed by the more differentiated lavas, represents fractional crystallization (FC) of the primary melt (redrawn after Jannot 2005).

Therefore, in such a diagram, partial melting and fractional crystallization produce contrasting trends (Fig. 21.5). In addition, for elements with similar C_0 , the slope of the melting line depends on the D value, thus allowing a qualitative assessment of their relative degree of incompatibility.

21.4 Mixing Test

In binary plots of major-element oxides, it is tempting to interpret any linear data array in terms of binary mixing (Wall et al. 1987). However, during this process, all the elements should be affected by exactly the same degree of mixing f_j .

This can be checked by a simple graph, also known as the “mixing test” (Fourcade and Allègre 1981). Equation (6.23) can be rearranged as:

$$(C_M - C_2) = f_1(C_1 - C_2) \quad (21.13)$$

Thus, in a $C_1 - C_2$ vs. $C_M - C_2$ diagram, the points corresponding to each individual element should plot along a straight line of slope f_1 , passing through the origin (see Fig. 21.6 for an example). This equation is yet another expression of mass balance, and therefore, for *major elements*, a similar geometry is observed also as a result of fractional crystallization or partial melting. However, when dealing with *trace elements*, crystallization and melting produce curved trends. As they may pass through the origin, caution is required especially if all the plotted elements have $D \sim 1$, in which case both partial melting and fractional crystallization reduce to simple mass balance.

With these limitations, the mixing test provides a powerful check to determine whether a given rock composition can be explained as a mixture between two known endmembers. The test on the other hand *cannot* be used when the compositions were modified by subsequent processes, such as fractional crystallization.



Exercise 21.2: Major-elements based mixing test

In the Central Bohemian Plutonic Complex (CBPC), Amp and Cpx-bearing monzonites and monzogabbros are associated with the Kozárovec granodiorite (Janoušek et al. 2000). In addition, the granodiorite contains small net-veined bodies and enclaves of Bt–Amp quartz monzonite. Table 21.1 gives representative compositions of all three main rock types.



[kozamix.data](#)

Table 21.1 Compositions of typical rock types in the Kozárovec Pluton (CBPC)

	1: granodiorite	M: quartz monzonite	2: monzogabbro
SiO ₂	64.60	59.58	49.21
TiO ₂	0.57	0.72	1.02
Al ₂ O ₃	14.99	14.8	13.69
Fe ₂ O ₃	1.27	1.69	2.47
FeO	2.79	4.08	6.96
MnO	0.08	0.14	0.15
MgO	2.37	4.11	8.53
CaO	3.44	5.33	9.74
Na ₂ O	3.12	2.84	1.89
K ₂ O	4.34	4.19	3.61

- Using major elements, test whether the quartz monzonite (M) could correspond to a hybrid between granodiorite (1) and monzogabbro (2).
- If so, determine the proportion of granodiorite in the mixture.



```

> x <- read.table("kozamix.data", sep="\t")
> mix1 <- x[,1]-x[,3] # C1-C2, x-coordinate
> mix2 <- x[,2]-x[,3] # CM-C2, y-coordinate
> plot(mix1,mix2,xlim=c(-10,16),ylim=c(-10,16),pch=16,cex.lab=1.3,
+      xlab=expression(C[1]-C[2]),ylab=expression(C[M]-C[2]))
> abline(h=0) # horizontal line through 0
> abline(v=0) # vertical line
> text(mix1,mix2,rownames(x),adj=c(1,0),pos=3) # label by oxide names
> lq <- lsfit(mix1,mix2,intercept=FALSE) # calculate least squares
> abline(lq,lty="dashed") # plot the best fit line
> print(lq$coeff) # slope = f1 [Eq. (21.13)]
      X
0.6841038
    
```

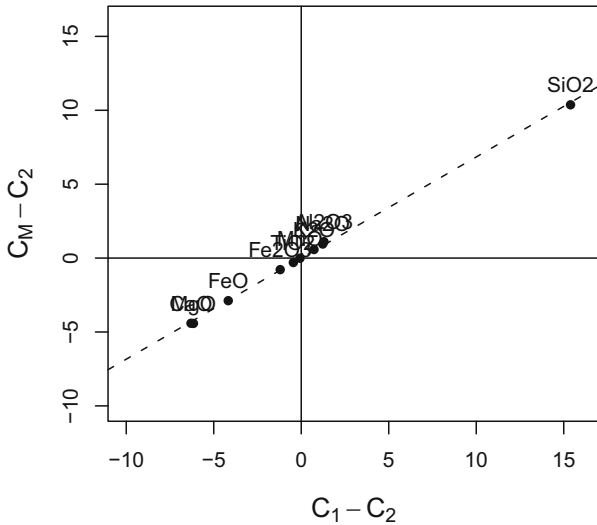


Fig. 21.6 Major-element based mixing test for the Kozárovec quartz monzonite (Exercise 21.2); C_1 , C_2 and C_M correspond to wt. % oxide in the acid end-member (granodiorite), basic end-member (monzogabbro), and suspected hybrid (quartz monzonite); the slope of the regression line gives the estimated proportion of the acid component f_1 (68.4 %).

21.5 Identifying Fractionating Minerals Using Log-Log Plots

For Rayleigh-type fractionation, one may identify controlling phases using log-log plots of whole-rock trace-element concentrations, in which the originally exponential trends are converted to linear ones [Eq. (21.2)]. This enables plotting fractionation vectors, either for pure mineral phases, or any combination thereof.

A clever choice consists in using compatible elements, whose content sharply decreases during fractional crystallization. Of course, such an approach requires the prior determination, for the investigated system, of the compatible/incompatible character of all elements (see Sect. 21.1).



Exercise 21.3: Fractionation vectors

The file `blatna.data` contains Ba and Sr concentrations (ppm) from granodioritic rocks of the Blatná suite, Central Bohemian Plutonic Complex (Janoušek et al. 2010). Table 21.2 summarizes partition coefficients between amphibole, biotite, K-feldspar and plagioclase and dacitic to rhyolitic melts (Hanson 1978).

Table 21.2 Partition coefficients for selected minerals in dacitic to rhyolitic melts (Hanson 1978)

Mineral	Sr	Ba
Amp	0.22	0.044
Bt	0.12	6.36
Kfs	3.87	6.12
Pl	4.4	0.31



`blatna.data`
`hanson.data`

- Plot the analyses in a binary graph of Ba vs. Sr (with logarithmic coordinates).
- Superimpose vectors portraying 10% fractional crystallization of each individual rock-forming mineral.



```
> WR <- read.table("blatna.data", sep="\t") # Read whole-rock data
> kd <- read.table("hanson.data", sep="\t") # Partition coefficients
> # Binary plot (plain R)
> plot(WR[, "Ba"], WR[, "Sr"], xlab="Ba", ylab="Sr", log="xy", pch=15,
+       ylim=c(250, 550))
```

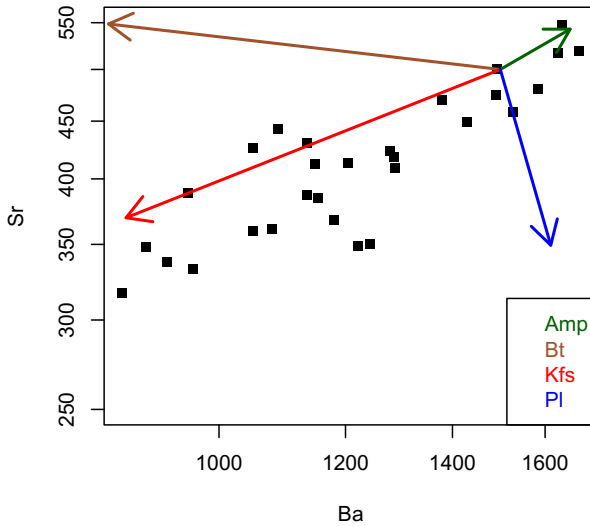


Fig. 21.7 Trace-element modelling of fractional crystallization in the Blatná suite. The arrows portray the effects of 10% fractionation of the minerals indicated (Exercise 21.3). The observed trend can be accounted for by up to *ca.* 15% fractionation of an assemblage dominated by K-feldspar, or by a plagioclase–biotite mix in the right proportions. Geological constraints or other diagrams must be used to decide between these two possibilities.

```

> Ba0 <- 1500
> Sr0 <- 500
> Ba <- Ba0*0.9^(kd[,"Ba"]-1)
> Sr <- Sr0*0.9^(kd[,"Sr"]-1)
> cols <- c("darkgreen","sienna","red","blue")
> arrows(Ba0,Sr0,Ba,Sr,col=cols,lwd=1.5)
> legend("bottomright",text.col=cols,legend=rownames(kd))

```

References

- Fourcade S, Allègre CJ (1981) Trace-elements behavior in granite genesis—a case-study the calc-alkaline plutonic association from the Querigut complex (Pyrenées, France). *Contrib Mineral Petrol* 76:177–195
- Georget Y (1986) Nature et origine des granites peralumineux à cordiérite et des roches associées. Exemple des granitoïdes du Massif Armoricaïn (France): pétrologie et géochimie, Mémoires et documents du Centre Armoricaïn d'Etude Structurale des Socles, vol 9, Rennes
- Hanson GN (1978) The application of trace elements to the petrogenesis of igneous rocks of granitic composition. *Earth Planet Sci Lett* 38:26–43
- Hofmann AW (1988) Chemical differentiation of the Earth: the relationship between mantle, continental crust, and oceanic crust. *Earth Planet Sci Lett* 90:297–314
- Jannot S (2005) Genèse et évolution des magmas primitifs de la Chaîne des Puys (Massif Central): une approche par l'étude des inclusions fluides. Unpublished PhD thesis, Université Blaise-Pascal, Clermont-Ferrand

- Janoušek V, Bowes DR, Braithwaite CJR, Rogers G (2000) Microstructural and mineralogical evidence for limited involvement of magma mixing in the petrogenesis of a Hercynian high-K calc-alkaline intrusion: the Kozárovec granodiorite, Central Bohemian Pluton, Czech Republic. *Trans Roy Soc Edinb, Earth Sci* 91:15–26
- Janoušek V, Wiegand BA, Žák J (2010) Dating the onset of Variscan crustal exhumation in the core of the Bohemian Massif: new U–Pb single zircon ages from the high-K calc-alkaline granodiorites of the Blatná suite, Central Bohemian Plutonic Complex. *J Geol Soc London* 167:347–360
- Martin H (1987) Petrogenesis of Archaean trondhjemites, tonalites and granodiorites from eastern Finland; major and trace element geochemistry. *J Petrol* 28:921–953
- Minster J, Allègre C (1978) Systematic use of trace elements in igneous processes. Part III: inverse problem of batch partial melting in volcanic suites. *Contrib Mineral Petrol* 68:37–52
- Rollinson HR (1993) Using geochemical data: evaluation, presentation, interpretation. Longman, London
- Schiano P, Allègre CJ, Dupré B, Lewin E, Joron J-L (1993) Variability of trace elements in basaltic suites. *Earth Planet Sci Lett* 119:37–51
- Wall VJ, Clemens JD, Clarke DB (1987) Models for granitoid evolution and source compositions. *J Geol* 95:731–749

Chapter 22

Constraining a Model

After completing the previous tasks, enough information should have been gathered to decide on the likely processes shaping the composition of the suite. This chapter will discuss setting different parameters for subsequent calculations.

22.1 Choosing an Appropriate Strategy

First of all, one has to decide on “variants” of the model, e.g., batch vs. fractional processes. The choice between these will be based on a balance between added complexity (related to the number of free parameters that will have to be set), and geological realism. Quite possibly, the best strategy is to test several variants of the models, and see (i) whether they produce results that are significantly different, and (ii) which one provides a better match with the data.

After that, a correct treatment has to be chosen for each element. Is it a major (mass balance only), a dilute trace (partition coefficient) or an ESC-type (solubility-controlled) element? Again, the choice will be guided primarily by petrology, especially by the nature of the minerals present. For instance, when a system only contains small amounts of K_2O , e.g. during a partial melting of a phlogopite-bearing peridotite, it is possible to consider that K_2O behaves as a major element since it is a stoichiometric component in phlogopite. However, this would imply knowing the phlogopite composition, which may be difficult to constrain. On the other hand, K_2O can be treated as a trace element, by assuming that $K_{D_{K_2O}}^{Phl/L}$ is constant. This scenario leads to fewer assumptions and simplifies the computing procedure (for instance by ignoring major elements and focussing on traces). We shall return to this question in Exercise 22.1 and compare the results of different equations when dealing with accessory minerals.

Finally, one must decide on the use of a forward or reverse approach. The underlying logic is not the same. A forward model will be handy to test a hypothesis (“can this cumulate account for the liquid line of descent as observed in the host lavas?”). Reverse models would rather help in constraining an otherwise poorly known process (“which cumulate modal composition may generate such trends?”).

22.2 Constraining a Fractionation or Melting Model

All the equations established in parts II and III relate C_L , C_0 , F and D ; D itself is a function of the mineral proportions in the solid (restite or cumulate) and of the partition coefficients for each of the mineral phases. Some of these parameters can be set from geological or geochemical constraints; the others can be calculated by various modelling techniques.

22.2.1 *The Differentiated Liquid(s)/Melt: C_L*

Determining the value of C_L is generally straightforward: in most cases, it is given by input data as the chemistry of the rock studied. The aim of our model is to explain its composition as a product of crystallization or melting.

However, it is commonplace to sample and analyse many rocks (e.g. a full differentiation series in a volcanic province). In this case, as it would be tedious and impractical to model the chemistry of every single rock, one has to carefully select which composition(s) will be investigated. This can be done on geological grounds (the most typical lithology) or using geochemical arguments (the “extreme” composition or, in case of a multi-stage process, that corresponding to an inflexion of the differentiation trend). The logic is then that any rock falling between C_0 , and the selected C_L , is assumed to have formed by the same process, albeit with a different value of F .

Most of the modelling approaches developed in this book aim at predicting the composition of melts. Consequently, it is necessary to be sure that the investigated rocks do represent pure liquids. This is for instance not the case for leucosomes in migmatites (whose compositions seldom match that of any realistic anatectic melt) and maybe even granites (that commonly appear to represent mixtures of liquid and solid material) as well as phenocryst-rich lavas (obviously a blend between melt and crystals). Treating such rocks as pure melts is therefore not a rigorous approach: their modelling requires additional components (such as mixing with cumulates or portions thereof). However, a “pure melt” approach may (or may not) be appropriate as a first-order approximation.

22.2.2 *The Primitive Liquid/Source: C_0*

C_0 is the concentration of the given element in the source (melting problem), or in the primitive magma (crystallization). Unfortunately, C_0 is only rarely accessible. For instance, in the case of melting, the source normally remains at depth, such that it cannot be sampled (except perhaps in tilted or strongly faulted crustal sections). Moreover, in most cases, the source (or the primitive liquid) has disappeared, as by definition it has been modified by the melting (or fractionation) process. Its chemistry can still be constrained, though.

Empirical/geological constraints

In a magmatic suite that evolved by fractional crystallization, the least differentiated magma is commonly regarded as being the parental liquid. Whether this composition is the primitive magma in a petrological sense, is open to discussion (but frequently tends to be a reasonable approximation).

For melting, it is often possible to find equivalents of the likely source elsewhere (low-grade equivalents along strike, mantle xenoliths...). On the other hand, one of the modelling targets is to determine which (if any), among these potential sources is the most plausible. One must think twice about facts that could be considered as obvious. For instance, using unmelted (mesosome) enclaves in migmatites is not advisable: if a rock escaped melting, it probably reflects a peculiar, more refractory composition, and not at all that of the likely source.

Numerical/graphical constraints

Rarely, it is conceivable that the same source gave rise to several independent magma batches that subsequently evolved following different fractionation paths. For instance, this is the case of subduction-zone magmas primarily generated by metasomatized mantle melting, and that, depending on their depth of emplacement, the water content, etc., differentiate following distinct crystallization paths. Then the trends defined by each suite would intersect in a single point, corresponding to the common parental liquid (Fig. 22.1).

In a completely closed system (a small magma chamber for instance, such as a small layered mafic complex), if one assumes that no magma has been lost during crystallization, the primitive liquid is the sum of the compositions of all the rocks present in the complex weighted by their relative abundances (McBirney and Noyes 1979).

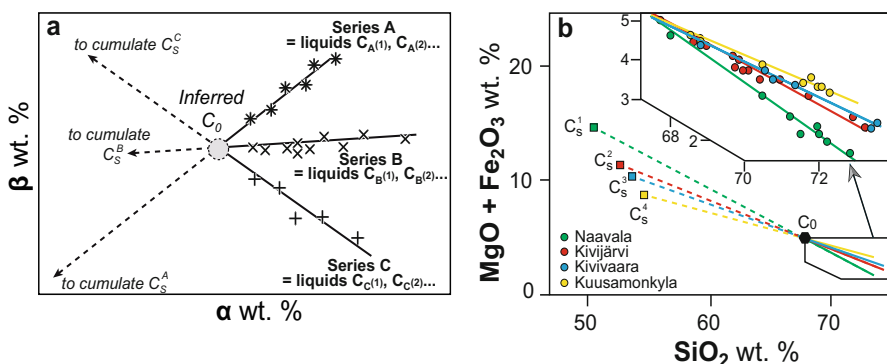


Fig. 22.1 a Theoretical diagram showing three magmatic series differentiated from the same parental liquid C_0 , but with cumulates of different modal composition. In this case all differentiation trends intersect at the C_0 composition. b Example of four suites of Archaean TTG from Eastern Finland, whose differentiation trends converge at about 67.5 wt. % SiO_2 , the composition considered as being that of the parental magma. After Martin (1985, 1987).

22.2.3 Composition of the Solid Phases (Cumulate/Restite)

The nature of the solid phases involved in melting or crystallization is critical. However, these may be the most difficult parameters to determine: the number of possible minerals and the range of their compositions are vast.

Geological constraints

Often, geological information can be incorporated into the model:

- In the most favourable case, remnants of the solid (i.e., cumulate enclaves or fragments of the restite) can be found, and their compositions (and maybe mineral chemistries and proportions) directly measured.
- In lavas, the compositions of phenocrysts in the less differentiated members of the fractionation series are commonly regarded as a good approximation of the chemistries of the crystallizing phases.
- Sometimes, ideal minerals, or minerals with an arbitrary composition from the literature, can be used. This applies mostly to simple phases: e.g., the composition of plagioclase will be similar in all andesitic magmas.
- Experimental data on systems of relevant composition may constrain the chemical/modal compositions of the solid phases in equilibrium with the melt.
- Phase-equilibrium modelling predicts the composition of all the phases stable in the system (melt and solid). Of course, this approach solves the whole problem (if P, T and the system's chemistry are fixed, the proportions and compositions of all phases are calculated). Then there is no need for further mass-balance modelling of major elements (see Next step box below).



Crystallization and melting result from changing intensive parameters, especially temperature. Recent thermodynamic models are able to predict the amount and composition of all phases, including melt, in a system of given bulk composition and P–T conditions. Thus, instead of guessing or geochemically constraining the composition of solid phases, it is possible to use more realistic models, assessing more precisely the nature, chemistry and amount of solid phases. Gone also is the assumption of a constant composition (mode and mineral chemistry) of the cumulate (respectively restite) during fractionation or melting—an unlikely, if not impossible proposition in a multivariant system, in which by definition a change in e.g. T is accompanied by changes in composition. Technically, the most commonly used thermodynamic databases are:

- MELTS (Ghiorso and Sack 1995) and pMELTS (Ghiorso and Sack 1995; Ghiorso et al. 2002) are able to deal with mafic liquids (komatiites to basalts), at mantle conditions. They do not predict realistic compositions for water-present systems, shallow depths (crustal) or felsic liquids. Rhyolite-MELTS (Gualda et al. 2013) is identical to MELTS, but has been adjusted to model K-feldspar and quartz. However, it is not able to assess equilibria involving large amounts of hydrous phases (e.g. biotite or amphibole) and should therefore be used primarily for differentiation of rhyolites or dry basalts (MORBs).

- THERMOCALC (Holland and Powell 1998, 2011), initially developed for (high-T) metamorphic equilibria in the continental crust; a melt model (White et al. 2001, 2007) has been added, which provides modest, but improving, provides modest, but improving, abilities to deal with crustal melting and granitic liquids. itic liquids.

Several programs are available to perform such calculations. They differ in terms of their minimization strategies, the databases and mineral models they incorporate, and the output format. The most commonly used software includes:

- MELTS, bundled with its own database. This programme is effective for predicting the evolution of a liquid composition along a given P–T path, including options for fractionation, etc. (melts.ofm-research.org).
- THERMOCALC also relies on its own database. It is designed to draw pseudo-sections and phase diagrams, but retrieving the phase compositions is a bit more difficult (www.metamorph.geo.uni-mainz.de/thermocalc).
- PERPLE_X (Connolly and Pettrini 2002) can use any mineral model, and many of them are bundled in the default distribution (e.g. Berman 1990; Tajčmanová et al. 2009), including THERMOCALC models. PERPLE_X is very good at generating gridded output mapping the system properties (phase proportions, phase compositions...) in P–T space. On the other hand, modelling fractionation along a P–T path is more involved (www.perplex.ethz.ch).
- Theriak/Domino (de Capitani and Petrakakis 2010) is similar to PERPLE_X albeit with slightly less accessible output (phase compositions) and fewer calculation options. It can also use all sorts of models but the set coded in the existing data files is restricted to a handful of databases. Preparing new models is fairly difficult (titan.minpet.unibas.ch/minpet/theriak/theruser.html).

Geochemical constraints

In fractional crystallization (respectively melting), the geometric relations imposed by the lever rule imply that the cumulate (respectively restite), the initial liquid (respectively source) and the fractionated liquids (respectively melt) must be linearly aligned in any n -dimensional space ($2 \leq n \leq$ number of major elements). Therefore, we know in which portion of the diagram(s) the solid composition lies. In the common situation when C_L is known and C_0 inferred, C_0 , C_S and C_L are aligned on the linear trend, and C_S plots on the opposite side from C_L .

This approach can be used to rule out one phase. In Fig. 22.2, the fractionation trend points towards hornblende, whereas biotite plots far away. Therefore, it is very unlikely that biotite played any significant role in shaping this trend.

A more elaborate analysis is illustrated in Fig. 22.3, where the composition of the primitive and most differentiated liquids are assessed graphically. We can constrain the position of the cumulate as being on the left-hand side of the best-fit trends, between the most basic composition and the intersection with the horizontal axes. The strongest constraint is provided by the SiO_2 – K_2O diagram; there the intersection with the x-axis occurs at $\text{SiO}_2 = 50\%$, further restricting the range of permissible cumulate compositions. As the lavas are basalts to basaltic andesites, the fractionating phases were probably plagioclase, amphibole and/or pyroxene(s)

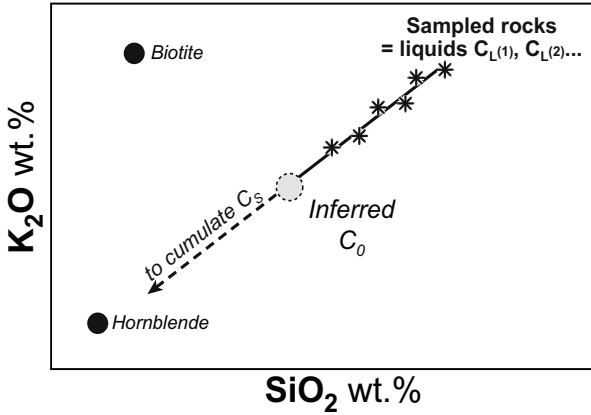


Fig. 22.2 Evolution of a suite of cogenetic liquids. It cannot result from biotite fractionation (its projection does not align with the trend) but can be driven by homblende crystallization.

with iron oxides. None of these contains K_2O (as also suggested by the step positive trend in the SiO_2-K_2O plot), so we can additionally assume $C_s^{K_2O} = 0$.

Taken together, we can constrain the cumulate composition on the dashed line at $K_2O = 0$, which yields $SiO_2 \sim 50$ wt. % (red circle labelled C_s). Knowing this silica value and using the other diagrams, the composition of the cumulate for all elements can be inferred.

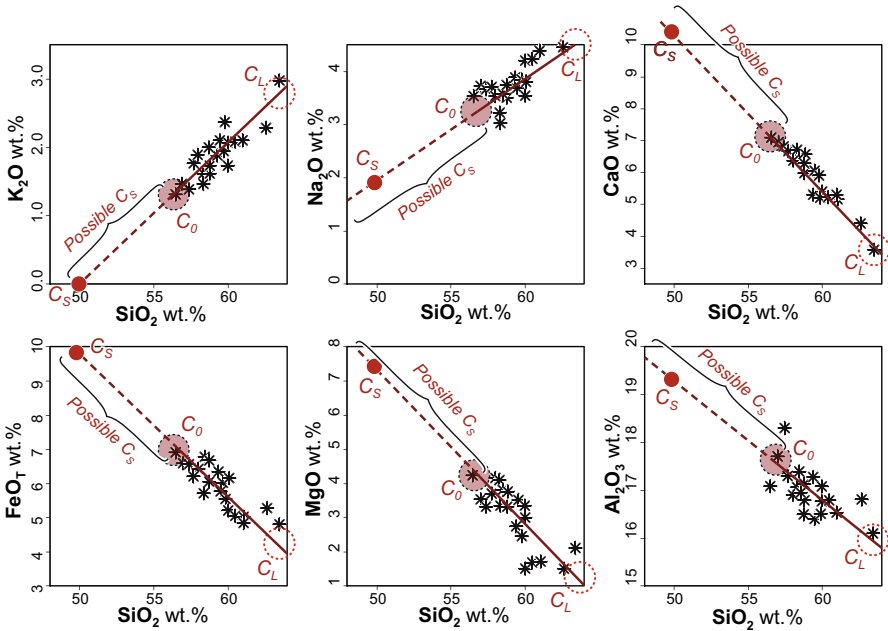


Fig. 22.3 Harker plots showing a series of calc-alkaline lavas (black asterisks), and a possible graphical interpretation (red circles and the thick line). For explanation see text.

22.2.4 Partition Coefficients

Measuring partition coefficients involves analysing mineral/melt pairs in chemical equilibrium, which is not a straightforward task. Some 25 years ago, most K_D measurements were done on phenocrysts in natural lavas, although it is not guaranteed that the crystals grew in equilibrium with the surrounding matrix. In addition, it is difficult to ensure that the matrix composition is representative of that of the melt. The only way to proceed consisted in analysing mineral and matrix separated from the same rock. This was not only a tedious process, but also it was impossible to take into account problems such as phenocrysts zoning, or presence of inclusions (especially of accessory minerals). It is thus not surprising that most determinations from that era gave extremely scattered and often inconsistent results (Rollinson 1993; Shaw 2006). More modern (roughly since the 1990s), in-situ analyses by ion probe or LA ICP-MS suffer less from these adverse effects. In addition they permit one to study experimental charges, for which the system parameters are better known (by definition).

Reliable and exhaustive databases of K_D values are found, for instance in Rollinson (1993) and on the GERM website (earthref.org/KDD).



The lattice strain model as a tool to calculate K_D values

Fitting a foreign atom in a crystal network involves deforming (straining) the lattice to accommodate the oversized/undersized cation. Therefore, the degree of compatibility depends primarily on the size of the ion relative to the site.

Blundy and Wood (1994 and subsequent work) tried to model the partition coefficients using the concept of “lattice strain”. In their formulation, the partition coefficient K_{D_i} of an ion of radius r_i , in a site of size r_0 , can be expressed as:

$$K_{D_i} = D_0 e^{\frac{-4\pi E \mathcal{N} [r_0(r_i - r_0)^2/2 + (r_i - r_0)^3/3]}{RT}}$$

where E is the site’s Young modulus (empirically determined, as is r_0), \mathcal{N} is the Avogadro number, R the gas constant and T the temperature (in K).

So far this approach has been used for several simple minerals (clinopyroxene and garnet, primarily). Smith and Asimow (2005) attempted to derive an internally consistent set for all minerals involved in mantle melting.

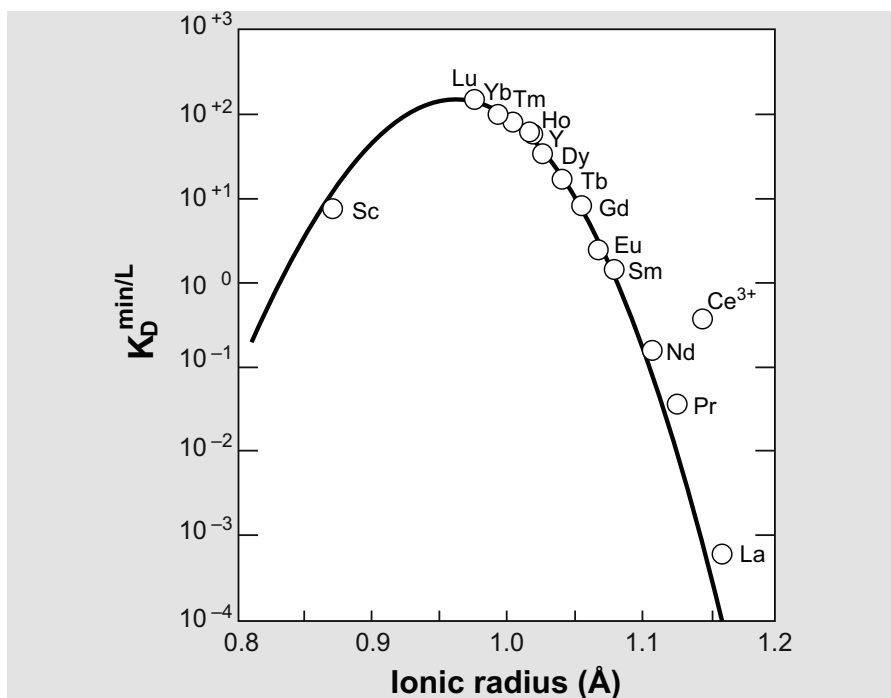


Fig 22.4 The lattice strain model applied to zircon–melt partition coefficients in a peralkaline rhyolite at 700 °C. The fit is excellent for trivalent lanthanides, except Ce^{3+} , which is due to the presence of both Ce^{3+} and Ce^{4+} in the melt (Blundy and Wood 2003)

22.3 Dealing with Accessory Minerals

As shown in Chap. 13, modelling the behaviour of accessory minerals poses a special challenge. They contain large amounts of elements that only appear in traces in the whole rock; yet, a mass-balance based model is not adequate, because of their low modal abundances. The common approach, based on saturation equations, is not easy to implement. This section presents several alternatives.

22.3.1 Assessing the Role of Accessory Minerals

The possible role of accessory minerals (e.g. in fractionation) is documented by:

- Presence of accessories in thin section (optical microscope, CL, BSE), especially if clearly magmatic (euhedral, magmatically zoned...) (Fig. 22.5).
- Models fitting analytical data for all elements, but inconsistent for the ones most likely to be controlled by accessories (Zr...).
- Negative correlations between a differentiation index (SiO_2 , mg#...) and whole-rock contents of elements such as Zr, LREE, etc. (Fig. 22.6).

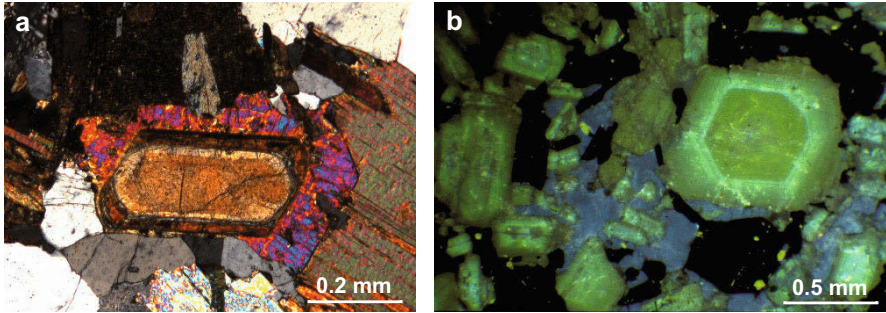


Fig. 22.5 Petrological identification of accessory minerals. **a** Optical microscope (cross-polarized light) image of a zoned allanite, rimmed by pistacite, in Karkonosze granite, Poland (*Photo E. Slaby*). **b** Optical CL image of the Kozárovce granodiorite, Central Bohemian Plutonic Complex (Janoušek et al. 2000). Apart from plagioclase (ochre/dull yellow) and K-feldspar (blue), the technique reveals tiny bright yellow apatites concentrated mainly in hornblende (euhedral-subhedral, non-luminescent mineral).

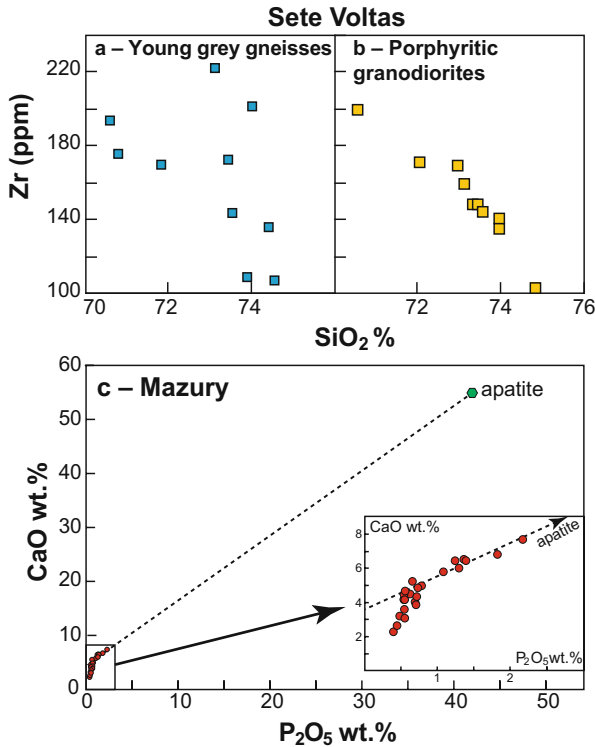


Fig. 22.6 Identifying the role of accessory minerals fractionation. **a–b** In the Sete Voltas Archaean plutonic suites (Brazil) (Martin et al. 1997), young grey gneisses show no correlation between SiO₂ and Zr (a), whereas a strong negative correlation is observed in the porphyritic granodiorites (b), implying zircon fractionation. **c** P₂O₅ vs. CaO diagram discloses the role played by apatite during the differentiation of the Mazury granitoid Complex (Poland) (Duchesne et al. 2010). For P₂O₅ > 0.7 wt. %, data plot on a trend pointing towards the apatite composition.

22.3.2 Modelling with Accessories

The modelling approaches described so far have aimed at establishing equations linking the compositions of the melt with those of the solid phases. Integrating accessory minerals in such models is not straightforward, because the solubility laws are expressed in a different form. Nevertheless, the mass-balance equation can be written to include the behaviour of an accessory mineral:

$$C_0 = f_L C_L + f_S C_S + f_{Acc} C_{Acc} \quad (22.1)$$

With f_{Acc} denoting its mass fraction and C_{Acc} the content of the element under consideration. If f_S and f_L refer to the mass fractions of the solid (other than the accessory phase) and liquid, respectively:

$$f_L + f_S + f_{Acc} = 1 \quad (22.2)$$

Since, by definition, accessory minerals occur in very small amounts, f_{Acc} is negligible compared to the other proportions. Then $f_L + f_S \approx 1$ and the notation can be simplified to the familiar form:

$$\begin{aligned} C_0 &= F C_L + (1 - F) C_S + f_{Acc} C_{Acc} \\ &= F C_L + (1 - F) D C_L + f_{Acc} C_{Acc} \end{aligned} \quad (22.3)$$

with D being the bulk distribution coefficient for all the mineral phases other than the accessory mineral. This equation can be used in two alternative ways:

- It is possible to express C_{Acc} as a function of C_L , writing $K_D^{Acc/L} = C_{Acc} / C_L$. This partition coefficient can be approximated as a constant or parameterized as a function of P , T , F ... (see Next step box, Sect. 11.2.4). This amounts to treating the accessory mineral as any other cumulate (or residual) phase.
- One may assume that the composition of the melt (C_L) is given by the solubility law, and it is therefore known. In this case, the equation has two unknowns, F and f_{Acc} . The system reacts to any change in F (melt fraction) by crystallizing/dissolving the accessory mineral, keeping C_L buffered. Thus the C_L is modelled independently for the accessory-controlled ESC, and remaining elements.

Using K_D

It is possible to define empirical values of $K_D^{Acc/L}$ for various accessory minerals. Stoichiometric zircon, for example, has 497,644 ppm Zr. In a felsic melt, capable of crystallizing this mineral, Zr contents typically range from 100 to 1000 ppm. Consequently, $K_{D_zr}^{Zrn/L}$ can be set between 500 and 5000 (Fig. 22.7). This value can only be an approximation since, as we discussed (Sect.13.1) partition coefficients

for minerals controlled by solubility are not constant, but a function of C_L and T (see Exercise 22.1).

Owing to their large K_D values, such accessory phases have a disproportionate effect on the final value of D . Not all elements are equally affected, though. The situation can be rather bad for Zr, Hf, and some of the REE depending on the stability of monazite, allanite or (less commonly) xenotime.

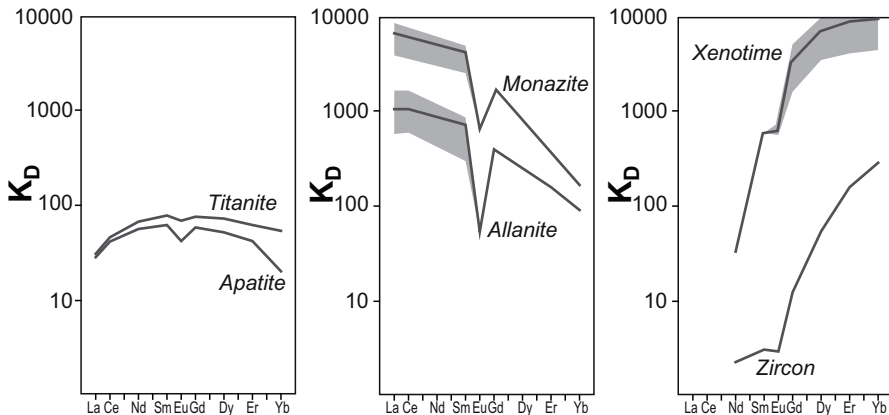


Fig. 22.7 Empirical partition coefficients for REE in typical accessory minerals of felsic igneous rocks. Strictly speaking, it is not possible to draw such a diagram for e.g. LREE in monazite or allanite, as they are not dilute components in these minerals and K_D is a function of concentration. However, these diagrams use a log scale, such that the variations of K_D (suggested by the grey fields) are reasonably small. Data sources: apatite and zircon: Nagazawa (1970); titanite: Simmons and Hedge (1978); allanite: Mahood and Hildreth (1983); monazite: Fleischer and Altschuler (1969); xenotime: Āmli (1975).

For instance, in a dacitic magma, all main rock-forming minerals have partition coefficients for LREE (i.e. La) less than unity (Mahood and Hildreth 1983; Nash and Crecraft 1985; Bacon and Druitt 1988; Sisson and Bacon 1992). However, if only 0.1 wt. % of allanite crystallizes, since $K_D^{All/L} \approx 1000$, $m_{All} K_D^{All/L} = 1$ and La becomes compatible, irrespective of the nature of the other 99.9 % of minerals.

A related trick is to take advantage of the fact that many accessories occur as inclusions in rock-forming minerals (zircon in biotite for instance). Thus they will fractionate (or melt) only when their host is involved. Instead of explicit modelling, one may simply adjust the K_D value of the host phase. This would be a sum of the K_D values for the host and the accessory, weighted by their mass fractions:

$$K_D^{(Host+Acc)/L} = (1 - m_{Acc}) K_D^{Host/L} + m_{Acc} K_D^{Acc/L} \quad (22.4)$$

Using saturation equations

By definition, as long as buffered by the presence of an accessory mineral, the melt composition obeys the saturation law. The strongest control on saturation is typically exerted by the temperature. For modelling, it is thus necessary to know

how T varies as a function of F , or conversely. This is where coupling thermodynamic and geochemical models (Next step box, Sect. 22.2.3) is of particular use.

Alternatively, one can assume that the liquid was saturated throughout its evolution (or a relevant portion thereof) (Evans and Hanson 1993; Hoskin et al. 2000). Then, the saturation temperature of individual samples can be calculated, and curves of T vs. chemical parameters established.

Effects on other elements

Another issue with accessory minerals such as zircon is that the K_D values are high not only for their stoichiometric components, but also for a range of other elements. For instance, zircon (ZrSiO_4) can form solid solution with hafnon (HfSiO_4), thorite (ThSiO_4), coffinite (USiO_4), but it is also able to contain up to 4.4 wt. % REE_2O_3 or 10 wt. % Y_2O_3 (Hoskin and Schaltegger 2003). This translates to a very high K_D (although Henry's law is not applicable in this situation): ca. 1000 for Hf, and exceeding 100 for HREE (Fig. 22.7), higher than in most rock-forming minerals (even garnet has K_D for HREE lower than 50). This effect must also be taken into account, by adding to the cumulate (or restite) the relevant amount of accessory minerals for further trace-element based calculations.

For zircon, knowing the whole-rock concentration C_0^{Zr} and the saturation value $(C_L^{\text{Zr}})_{\text{sat}}$, the mass-balance relationship holds between C_0 , C_L and the zircon crystals. The excess Zr, available to form zircon grains, is $C_0 - (C_L^{\text{Zr}})_{\text{sat}}$. The mass proportion of zircon crystallizing is then:

$$m_{\text{Zrn}} = \frac{C_0^{\text{Zr}} - (C_L^{\text{Zr}})_{\text{sat}}}{C_{\text{Zrn}}^{\text{Zr}}} \quad (22.5)$$

with $C_{\text{Zrn}}^{\text{Zr}} = 497,644$ ppm in stoichiometric zircon. The resulting m_{Zrn} value (typically small) should be integrated into the calculation of D for other elements.



The situation is more complex when several accessory minerals play a role (e.g., monazite and zircon) as they will “compete” for the trace elements available! The solubility equations must then be solved simultaneously.



Exercise 22.1: Modelling with accessory minerals

We shall develop a (forward) model accounting for the evolution of a rock suite undergoing fractional crystallization. The concentration of Zr (and potentially any other trace element hosted by zircon) will be modelled using several approaches (solubility or ad-hoc values of K_D), that will be compared.

The dataset used here is synthetic, calculated by adding random noise to a Rayleigh fractional crystallization curve (see details in Sect. 24.3). Therefore we “know” that we can model the evolution of these rocks by fractionating up to 58 % ($F = 0.42$) of a cumulate specified in Table 22.1 (in real life, we would need to first establish this, see Exercise 9.1 or Worked example 1, Chap. 25):

Table 22.1 Mineral proportions and mineral–liquid partition coefficients used in Exercise 22.1

	Amp	Pl	Ilm	Zrn	
Prop. in cumulate	0.5	0.45	0.05		
K_D	Zr	0.02	0.01	10^{-5}	3100
	Y	5	0.05	10^{-5}	200



noisy.data
mincomp.data
kd.data

As already seen, the zircon saturation equation [Eq. (13.1)] is temperature dependent. Based on experimental data on fractionation of andesites (e.g. Almeev et al. 2013; Blatter et al. 2013; Nandedkar et al. 2014), we will use the following (totally empirical!) equation to link composition and chemistry:

$$T(^{\circ}\text{C}) = 1020 - \frac{\text{SiO}_2 - 56}{16} \times 300 \quad (22.6)$$

- Plot a binary diagram $\text{SiO}_2 - \text{Zr}$.
- Add the curve corresponding to the zircon saturation.
- Assuming zircon K_D values given in Table 22.1, draw a curve for zircon mass proportion of 0.002 (i.e. 0.2 wt. %).



Clearly, it is not possible to calculate Zr saturation independently from the rest of the bulk composition, so we need to build a full forward model (see exercises 8.1 to 8.3, 14.2). The code, taking advantage of *GCDkit* functions, also demonstrates how to incorporate different laws (mass balance, partition coefficients and saturation-based) in a single model. As the primitive magma C_0 we use sample *a13* that has the lowest SiO_2 content of 55.9 %.

```
GCDkit-> loadData("noisy.data", sep="\t")      # Read whole-rock data
GCDkit-> mjrs <- c("SiO2", "Al2O3", "FeOt", "MgO", "MnO", "CaO", "Na2O",
+               "K2O", "TiO2")
GCDkit-> trc <- c("Zr", "Rb", "Y")
GCDkit-> c0.1 <- WR["a13", c(mjrs, trc)]
GCDkit-> mincomp <- read.table("mincomp.data", sep="\t") # Mineral data
```

```
GCDkit-> mincomp <- as.matrix(mincomp)
GCDkit-> minprop1 <- c(0.45,0.5,0.05,0)
GCDkit-> names(minprop1) <- c("Pl", "Amp", "Mt", "Zrn")
GCDkit-> cs.1 <- as.vector(minprop1%%mincomp)
GCDkit-> names(cs.1) <- colnames(mincomp)
GCDkit-> kd <- read.table("kd.data", sep="\t") # Kd data
GCDkit-> kd <- as.matrix(kd)
```

We need to link temperature and chemistry for saturation calculations, so we have an auxiliary function calculating T as a function of SiO_2 :

```
GCDkit-> t.c <- function(si) {
GCDkit->     z <- 1020-(si-56)/16*300 # Eq. (22.6)
GCDkit->     return(z)
GCDkit-> }
```

The core of the model is the following function that returns the composition of the evolved liquid (C_L) for a given value of F , with and without accounting for zircon saturation. The function calculates:

- Mass balance for major elements;
- Ordinary (Rayleigh-type) partitioning of trace elements, without saturation;
- Zr saturation values (using the *Saturation* plugin of *GCDkit*). If the Zr concentration estimated by partitioning is lower, the system is not saturated. Otherwise, the excess Zr should form zircon: we set the Zr concentration of the melt to the saturation value, and recalculate the D and C_L for remaining elements¹.

```
GCDkit-> cl.f <- function(ff,c0,cs,minprop) {
GCDkit->   # Major elements
GCDkit->   maj <- (c0[mjrs]-(1-ff)*cs[mjrs])/ff
GCDkit->   # Trace elements (omitting solubility)
GCDkit->   D <- minprop%%kd # D values, not accounting for Zrn sat!
GCDkit->   tr <- c0[trc]*ff^(D[1,trc]-1)
GCDkit->   # Saturation values
GCDkit->   milcats <- millications(maj[mjrs])
GCDkit->   sat.data <- zrSaturation(milcats,T=t.c(maj["SiO2"]),
+     Zr=WR["al3","Zr"]) # call Saturation plugin
GCDkit->   Zr.sat <- sat.data["Zr.sat"]
```

¹ This is actually a slight approximation, as the trace-element content for each step is calculated relative to C_0 . A more precise approach would be an iterative calculation, whereby the concentration for each step is obtained based on that from the previous step. The resulting model, however, is not very different, such that this more complex approach is not justified by the improvement in accuracy.

```

GCDkit-> M <- sat.data["M"]
GCDkit-> # Correction for Zrn
GCDkit-> if(tr["Zr"]<=Zr.sat){
GCDkit->   tr.c <- tr
GCDkit->   zrc.prop <- 0
GCDkit-> }else{
GCDkit->   zr.excess <- tr["Zr"]-Zr.sat
GCDkit->   zrc.prop <- zr.excess/497644
GCDkit->   m.pr <- minprop
GCDkit->   m.pr["Zrn"] <- zrc.prop
GCDkit->   m.pr <- m.pr/sum(m.pr)
GCDkit->   D.c <- m.pr*%kd
GCDkit->   tr.c <- c0[trc]*ff^(D.c[1,trc]-1)
GCDkit->   tr.c["Zr"] <- Zr.sat
GCDkit-> }
GCDkit-> z <- c(maj,M,Zr.sat,zrc.prop,tr,tr.c)
GCDkit-> names(z) <- c(mjrs,"M","Zr.sat","Zrn.prop",
+   paste(trc,"nosat",sep="_"),trc)
GCDkit-> return(z)
GCDkit-> }

```

The rest is simple; we define a range of F values and `sapply` the above function to them. A nice feature of this approach is that we model C_L compositions for all elements (major and traces) simultaneously, based on the same assumptions. Thus the model is internally consistent and can be plotted on any diagram.

```

GCDkit-> f.1 <- seq(1,0.42,by=-0.01)
GCDkit-> qq <- sapply(f.1,cl.f,c0=c0.1,cs=cs.1,minprop=minprop1)
GCDkit-> fwd.mod <- t(qq)

```

For instance, let's investigate the effect of zircon saturation:

```

GCDkit-> binary("SiO2","Zr",pch=15,ymax=300)
GCDkit-> lines(fwd.mod[, "SiO2"],fwd.mod[, "Zr_nosat"],lty="dashed",
+   col=2)
GCDkit-> lines(fwd.mod[, "SiO2"],fwd.mod[, "Zr"],col=2)

```

We can also look at the (apparent) $K_{D_z}^{Zrn/L}$:

```

GCDkit-> print(497644/fwd.mod[, "Zr"])

```

As expected, its value changes during fractionation; the average of ca. 3080 justifies our choice of 3100 for the simplified calculation.

Now, for comparison, we will calculate a fractionation curve (for the portion of the diagram above zircon saturation level—i.e. above ca. 66 % SiO₂). First, we find

the saturation point, i.e. the last step for which the Zr content is the highest². This becomes the new C_0 , which is plotted.

```
GCDkit-> j <- which.max(fwd.mod[, "Zr"])
GCDkit-> c0.2 <- fwd.mod[j,]
GCDkit-> points(c0.2["SiO2"], c0.2["Zr"], cex=2, pch=8, col="purple")
```

The range of F values must also be redefined, relative to the new source. Since this composition was obtained for $f.1[j] = 0.54$, we have $F_{\text{new}} = F_{\text{old}}/0.54$ and the new range of F values will be from $0.54/0.54 = 1$ to $0.42/0.54 = 0.78$. We can use the previous function, `cl.f`: it will give extra information, so we will keep only what is needed. Before invoking it, we must modify the mineral proportions by adding the required amount of zircon. Finally, we plot the curve on top of the previous diagram.

```
GCDkit-> zrc.amount <- 0.002
GCDkit-> f.2 <- f.1[j:length(f.1)]/f.1[j]
GCDkit-> minprop2 <- minprop1
GCDkit-> minprop2["Zrn"] <- zrc.amount
GCDkit-> minprop2 <- minprop2/sum(minprop2)
GCDkit-> qq <- sapply(f.2, cl.f, c0=c0.2, cs=cs.1, minprop=minprop2)
GCDkit-> fwd.mod2 <- t(qq)
GCDkit-> lines(fwd.mod2[, "SiO2"], fwd.mod2[, "Zr_nosat"], col="purple")
```

By invoking the previous code repeatedly (changing the value for `zrc.amount`) or, even better, wrapping it in a function taking `zrc.amount` as a parameter, we generate Fig. 22.8a. The same code (replacing “Zr” by “Y”) provides Fig. 22.8b.

The best fit is obtained for a zircon mass fraction of 0.25 % (2.5×10^{-3}) (solid curve). Using a saturation model, the amount of zircon varies from 10^{-5} to 5×10^{-4} , i.e. is orders of magnitude lower. Therefore, the effect of this approach is more pronounced on other elements. The effect of zircon on Y is visible, but tiny, and likely to be drowned in analytical uncertainties.

This exercise demonstrates several points, some of which will be addressed latter:

- The need to model simultaneously major and trace elements (obvious in the case of Zr solubility!), as opposed to simply drawing curves on a diagram;
- The fact that elaborate models (here, based on solubility) do not necessarily provide a better match to the data than simple ones (here, a Rayleigh law); especially if the data, like all natural datasets, are noisy;
- The effect of accessory phases on other elements is noticeable, but normally negligible (even with large K_D). This is a result of their low modal abundance.

² We could also look for the last step with a predicted amount of zircon equal to 0.

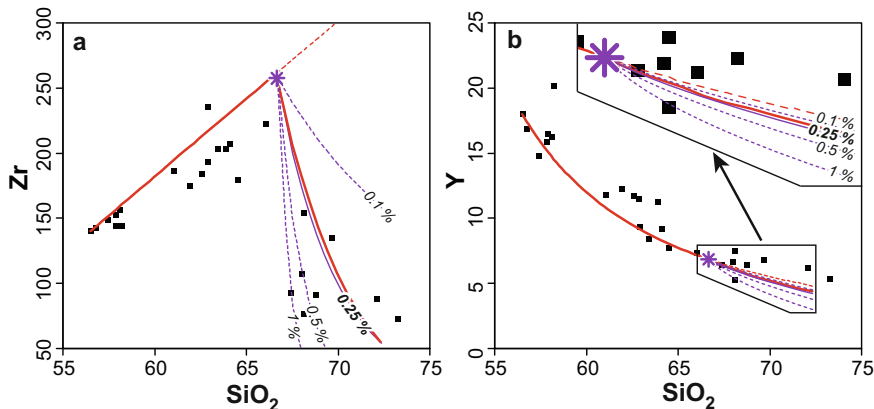


Fig. 22.8 **a** Comparing models based on zircon solubility (red), with those using a K_D approach (here with $K_{D_z}^{Zr^{ni/L}} = 3100$, purple). Various mass proportions of zircon (1, 0.5, 0.2 and 0.1 wt. %) are labelled on the curves. The C_0 for these models is the purple star. The dashed red curve portrays the evolution with no zircon at all (beyond the saturation point). Squares correspond to the actual dataset (*noisy.data*). **b** Effects of the same models on Y concentration.

22.4 Constraining the End-Members of a Mixing Model

Whenever a rock, or a suite of rocks, is suspected to have been generated by mixing, the challenge consists in identifying two (or more) suitable end-members. The most obvious strategy is to use the compositions of the extreme (the most/least silicic) rock types found in the studied series. This can, however, be misleading. It may well be that even these extreme compositions are hybrid already. Likewise, it is possible that the most basic rock represents, for instance, a mixture between cumulate and mafic liquid. Alternatively, the most acid composition may correspond to fluid-rich igneous rocks, or melts of the country rock, having nothing to do with processes occurring at deeper crustal levels. Special attention must be paid to mafic microgranular enclaves (MME). Many geologists consider them as possible end-member for mixing in granites. However, MME may undergo chemical and isotopic exchange with the remaining host magma or late-magmatic fluids. This affects especially the mobile elements and, among the radiogenic isotopes, Sr. Thus, the utility of the MME in petrogenetic studies may be limited (Pin et al. 1990; Elburg 1996).

For these reasons, it is not uncommon to invoke hypothetical end-members, such as a theoretical mantle melt (even if no basalt is preserved). Such a composition can be deduced from experimental petrology, or calculated using direct modelling approaches.

When using isotopes, recognition and quantification of open-system processes requires the existence of an isotopic contrast between the end-members. Some isotopic systems in a particular case are more prone to contamination, others not. If the concentration of the given element in the magma, compared to the assimilant,

is high, the isotopic composition will be essentially buffered until high degrees of contamination. For example, Bohemian Variscan lamprophyres and ultrapotassic intrusions have high Sr and Nd contents that rendered them resistant to crustal assimilation during intrusion. For this reason, their crust-like Sr–Nd isotopic signature must reflect enriched mantle source or its contamination by a deeply subducted felsic crust (Janoušek et al. 2010).

References

- Almeev R, Holtz F, Ariskin AA, Kimura JI (2013) Storage conditions of Bezymianny Volcano parental magmas: results of phase equilibria experiments at 100 and 700 MPa. *Contrib Mineral Petrol* 166:1389–1414
- Åmli R (1975) Mineralogy and rare earth geochemistry of apatite and xenotime from the Gloseheia granite pegmatite, Froland, southern Norway. *Amer Miner* 60:607–620
- Bacon CR, Druitt TH (1988) Compositional evolution of the zoned calc-alkaline magma chamber of Mount Mazama, Crater Lake, Oregon. *Contrib Mineral Petrol* 98:224–256
- Berman RG (1990) Mixing properties of Ca – Mg – Fe – Mn garnets. *Amer Miner* 75:238–344
- Blatter DL, Sisson TW, Hankins WB (2013) Crystallization of oxidized, moderately hydrous arc basalt at mid- to lower-crustal pressures: implications for andesite genesis. *Contrib Mineral Petrol* 166:861–886
- Blundy J, Wood B (1994) Prediction of crystal melt partition coefficients from elastic moduli. *Nature* 372:452–454
- Blundy J, Wood B (2003) Mineral–melt partitioning of uranium, thorium and their daughters. In: Bourdon B, Henderson GM, Lundstrom CC, Turner SP (eds) *Uranium-series geochemistry*. Mineralogical Society of America Reviews in Mineralogy and Geochemistry, vol 52, pp 59–123
- Connolly JAD, Petrini K (2002) An automated strategy for calculation of phase diagram sections and retrieval of rock properties as a function of physical conditions. *J Metamorph Geol* 20:697–708
- de Capitani C, Petrakakis K (2010) The computation of equilibrium assemblage diagrams with Theriak/Domino software. *Amer Miner* 95:1006–1016
- Duchesne J-C, Martin H, Bagiński B, Wiszniewska J, Vander Auwera J (2010) The origin of ferroan–potassic A-type granitoids: the case of the hornblende–biotite granite suite of the Mesoproterozoic Mazury Complex, northeastern Poland. *Canad Mineral* 48:947–968
- Elburg MA (1996) Evidence of isotopic equilibration between microgranitoid enclaves and host granodiorite, Warburton Granodiorite, Lachlan Fold Belt, Australia. *Lithos* 38:1–22
- Evans OC, Hanson GN (1993) Accessory-mineral fractionation of rare-earth element (REE) abundances in granitoid rocks. *Chem Geol* 110:69–93
- Fleischer M, Altschuler ZS (1969) The relationship of the rare earth composition of minerals to geological environment. *Geochim Cosmochim Acta* 33:725–732
- Ghiorso MS, Sack RO (1995) Chemical mass-transfer in magmatic processes. 4. A revised and internally consistent thermodynamic model for the interpolation and extrapolation of liquid–solid equilibria in magmatic systems at elevated temperatures and pressures. *Contrib Mineral Petrol* 119:197–212
- Ghiorso MS, Hirschmann MM, Reiners PW, Kress VC (2002) The pMELTS: a revision of MELTS for improved calculation of phase relations and major element partitioning related to partial melting of the mantle to 3 GPa. *Geochem Geophys Geosyst* 3:1–35
- Gualda GAR, Ghiorso MS, Lemons RV, Carley TL (2013) Rhyolite-MELTS: a modified calibration of MELTS optimized for silica-rich, fluid-bearing magmatic systems. *J Petrol* 53:875–890

- Holland TJB, Powell R (1998) An internally consistent thermodynamic dataset for phases of petrological interest. *J Metamorph Geol* 16:309–343
- Holland TJB, Powell R (2011) An improved and extended internally consistent thermodynamic dataset for phases of petrological interest, involving a new equation of state for solids. *J Metamorph Geol* 29:333–383
- Hoskin PWO, Schaltegger U (2003) The composition of zircon and igneous and metamorphic petrogenesis. In: Hancher JM, Hoskin PWO (eds) *Zircon*. Mineralogical Society of America and Geochemical Society Reviews in Mineralogy and Geochemistry, vol 53, pp 27–62
- Hoskin PWO, Kinny PD, Wyborn D, Chappell BW (2000) Identifying accessory mineral saturation during differentiation in granitoid magmas: an integral approach. *J Petrol* 41:1365–1396
- Janoušek V, Bowes DR, Braithwaite CJR, Rogers G (2000) Microstructural and mineralogical evidence for limited involvement of magma mixing in the petrogenesis of a Hercynian high-K calc-alkaline intrusion: the Kozárovce granodiorite, Central Bohemian Pluton, Czech Republic. *Trans Roy Soc Edinb, Earth Sci* 91:15–26
- Janoušek V, Holub FV, Magna T, Erban V (2010) Isotopic constraints on the petrogenesis of the Variscan ultrapotassic magmas from the Moldanubian Zone of the Bohemian Massif. *Mineral Spec Pap* 37:32–36
- Mahood GA, Hildreth EW (1983) Large partition coefficients for trace elements in high-silica rhyolites. *Geochim Cosmochim Acta* 47:11–30
- Martin H (1985) Nature, origine et évolution d'un segment de croûte continentale archéenne: contraintes chimiques et isotopiques. Exemple de la Finlande orientale. *Mémoires et Documents du Centre Armoricaïn d'Etude Structurale des Socles*, vol 1, Rennes
- Martin H (1987) Petrogenesis of Archaean trondhjemites, tonalites and granodiorites from eastern Finland; major and trace element geochemistry. *J Petrol* 28:921–953
- Martin H, Sabaté P, Peucat J-J, Cunha JC (1997) Crustal evolution in the early Archaean of South America: example of the Sete Voltas Massif, Bahia state, Brazil. *Precambr Res* 83:35–62
- McBirney AR, Noyes RM (1979) Crystallization and layering of the Skaergaard intrusion. *J Petrol* 20:487–554
- Nagazawa H (1970) Rare Earth concentrations in zircon and apatite and their host dacite and granites. *Earth Planet Sci Lett* 9:359–364
- Nandedkar R, Ulmer P, Müntener O (2014) Fractional crystallization of primitive, hydrous arc magmas: an experimental study at 0.7 GPa. *Contrib Mineral Petrol* 167:1–27
- Nash WP, Crecraft HR (1985) Partition coefficients for trace elements in silicic magmas. *Geochim Cosmochim Acta* 49:2309–2322
- Pin C, Binon M, Belin JM, Barbarin B, Clemens JD (1990) Origin of microgranular enclaves in granitoids—equivocal Sr–Nd evidence from Hercynian rocks in the Massif Central (France). *J Geophys Res* 95:17821–17828
- Rollinson HR (1993) *Using geochemical data: evaluation, presentation, interpretation*. Longman, London
- Shaw DM (2006) *Trace elements in magmas: a theoretical treatment*. Cambridge University Press, Cambridge
- Simmons EC, Hedge CE (1978) Minor-element and Sr-isotope geochemistry of Tertiary stocks, Colorado mineral belt. *Contrib Mineral Petrol* 67:379–396
- Sisson TW, Bacon CR (1992) Garnet/high-silica rhyolite trace element partition coefficients measured by ion microprobe. *Geochim Cosmochim Acta* 56:2133–2136
- Smith P, Asimow P (2005) *Adiabat_1ph*: a new public front-end to the MELTS, pMELTS, and pHMELTS models. *Geochem Geophys Geosyst* 6: doi: 10.1029/2004GC000816
- Tajčmanová L, Connolly J, Cesare B (2009) A thermodynamic model for titanium and ferric iron solution in biotite. *J Metamorph Geol* 27:153–165
- White RW, Powell R, Holland TJB (2001) Calculation of partial melting equilibria in the system CaO–Na₂O–K₂O–FeO–MgO–Al₂O₃–SiO₂–H₂O (CNKFMASH). *J Metamorph Geol* 19:139–153
- White RW, Powell R, Holland TJB (2007) Progress relating to calculation of partial melting equilibria for metapelites. *J Metamorph Geol* 25:511–527

Chapter 23

Numerical Tips and Tricks

Geochemical modelling is an art as much as a science. In many cases, in addition to the geological constraints discussed above, some numerical tricks—mostly related to the behaviour of the compositional space—may provide substantial help.

23.1 The Size of the Geochemical Space

It is vital to remember that a 2D graphical representation (such as a binary diagram) is a projection of the p -dimensional space onto a plane. An important skill for geochemists is to find the right viewing angle (projection) that best emphasizes the features of interest.

As an illustration, let's consider a binary diagram, where the geochemical data define a straight or a curved trend. Without further examination of the data (in the full p -dimensional space), it is not possible to decide whether this corresponds to an actual evolution (Fig. 23.1a), or to an artefact resulting from the projection of a more or less flat cloud of data onto the X–Y plane (Fig. 23.1b). By the same logic we can interpret a triangular data array on the X–Y plane. If, in 2D, data points fall in a small section of a plane (a triangle) defined by three end-members, it may correspond to a legitimate ternary mixing (Fig. 23.1c). Or it reflects a meaningless, essentially random 3D distribution (Fig. 23.1d).

Clearly, there are better viewing angles. In Fig. 23.1b for instance, projecting the data in an X–Z or Y–Z plane, or even better, from a direction perpendicular to the data plane, would reveal the whole compositional range. On the other hand, looking at the same data “from the top” (projected on the X–Y plane) makes them appear as a line. This notion underlies the concept of Principal Component Analysis (PCA), which is essentially a numerical technique that defines the directions in the geochemical space in which the dataset has the highest variance. These directions are called the first, second etc. principal components, and each of them is associated with a proportion of the total variance of the data.



Principal component analysis (PCA) in R/GCDkit

GCDkit can calculate and plot PCA for the current dataset, from the menu *Calculations|Statistics|Principal components*. Several other options for statistical treatment of the dataset are present in the same menu; the underlying R functions are described in Reimann et al. (2008).

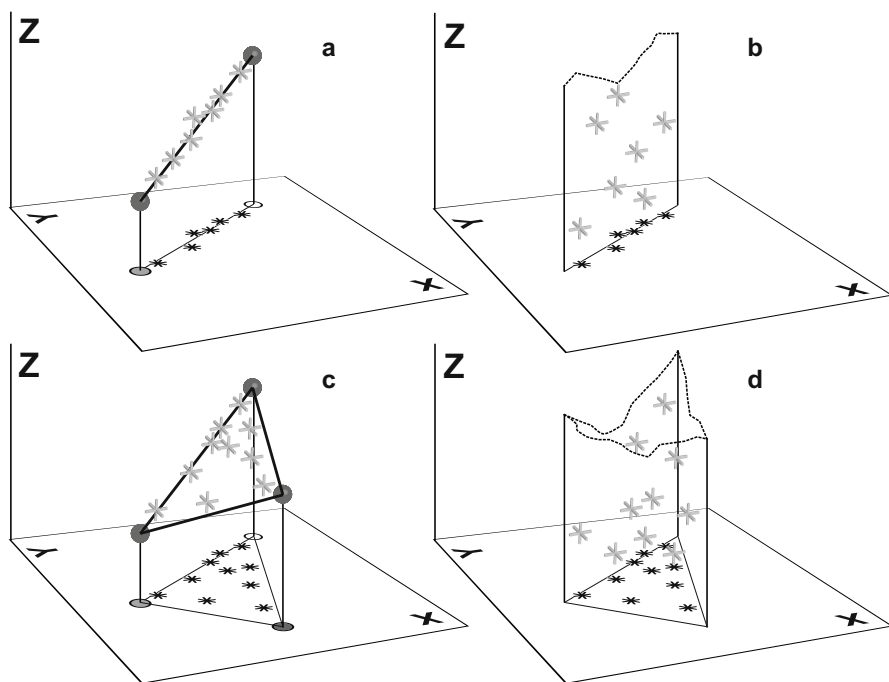


Fig. 23.1 A straight line in a X vs. Y binary diagram may (a) or may not (b) correspond to a true binary mixing array in the underlying p -dimensional space (here, $p = 3$). In the same way, a triangle may (c) or may not (d) reflect a mixing between three end members in the full p -dimensional space ($p = 3$).

When PCA is applied to geochemical datasets from igneous rocks, the first component often reflects differentiation (it is positively correlated to SiO_2 , and negatively to MgO and FeO). Experimenting with your own datasets will reveal that the first three or four principal components generally carry up nearly all of the total variance of the dataset. Practically, this indicates that it is not possible to decipher more than three or four components of the geochemical signal, for instance end members in mixing.



Projections and compositional space

More detailed analysis of the geometric properties of the p -dimensional compositional space is frequently used in metamorphic petrology. Even though it has been successfully applied e.g. to isotopic systematics of oceanic basalts (Allègre et al. 1987; Iwamori and Nakamura 2012), such an approach is not so common in igneous petrology. Good presentation of this topic including the meaning and use of various projections, the interpretation of compositions as vectors and the application of linear algebra to rock compositions, can be found for instance in chapter 6 of Spear (1994), or in the program *C-space* (Torres-Roldan et al. 2000) and accompanying documentation.

23.2 Reducing the System

Whenever a mineral is the only, or main, host for a specific element (e.g. Ti in ilmenite), the amount of this phase in the fractionating solid assemblage can be determined independently. Moreover, its chemical inventory can be subtracted and the “remaining” bulk composition adjusted accordingly. From a mathematical point of view, this amounts to removing one equation (for the element used), and one unknown (the given mineral mass fraction) from the system.

Likewise, if a mineral is a simple oxide (quartz, rutile), the relevant element can be adjusted independently from the others. This is equivalent to reducing n (number of minerals) by 1.

23.3 Colinearity

It is common for several mineral assemblages to share the same bulk composition. For instance, a mixture of 1 Fo + 1 Qtz is chemically equivalent to 2 En :



Therefore, if a solution is reached using En , (numerically) an equally valid one can be obtained with $Fo + Qtz$ (Fig. 23.2). Of course, this example is rather silly from a petrological point of view, since forsterite and quartz do not coexist. More realistically, the chemical composition of an amphibole is equivalent to that of an assemblage of plagioclase + pyroxene + water. Consequently, when a model fits data for a plagioclase + pyroxene cumulate, amphibole (\pm a smaller amount of plagioclase) would yield a comparably good solution. Which one is the more realistic depends on petrological, not numerical, considerations (see Chap. 25 for an example of practical application of this).

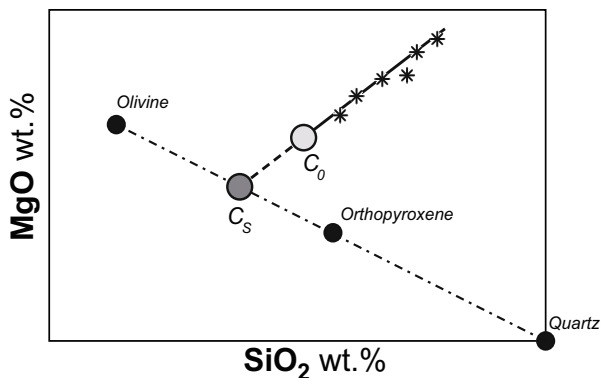


Fig. 23.2 Olivine, orthopyroxene and quartz are linearly aligned. Here, a fractionation trend is controlled by a cumulate with composition of C_S , falling on the line between quartz and olivine. C_S can be expressed equally well as a mixture of olivine + orthopyroxene, or olivine + quartz, but the second option is petrologically unlikely as these two minerals do normally not coexist.

23.4 Breaking Minerals into End Members

When modelling major-element behaviour, a common trick involves breaking down minerals into their end-members. For instance plagioclase is treated as two phases (pure Ab and An); similarly titanomagnetite is considered as a mixture of pure magnetite and rutile. This approach removes the need to make an assumption on the composition of the solid solution as this will come out as a result of the model (see Chap. 25 for an application). An additional benefit pertains to overdetermined systems, i.e. when there are more equations (p) than unknowns (n) (Sec. 7.2). This trick artificially increases the number of unknowns, bringing the system closer to $n = p$ for which there is an exact solution. However, this approach is limited by the fact that if the number of unknowns exceeds that of equations ($n > p$), the system becomes underdetermined and cannot be solved (Appendix C).

23.5 Coupling Majors and Traces

A common issue related to geochemical modelling as presented in many papers, is that they are based on a restricted number of elements. Most often the computed model really boils down to a curve on a diagram. In this case, the model satisfactorily predicts the behaviour of the elements or isotopic systems taken into account, but does not provide any information on the remaining ones. Thus it is impossible to assess the internal consistency of the proposed scenario.

For instance, modelling based solely on isotopes could lead to a conclusion that a basalt has been contaminated by ~50 % of continental crust, but this is unrealistic because such a magma would not be basaltic anymore. Another classical example is that of trace-element modelling indicating that a parental magma differentiated by e.g. 50% fractional crystallization of amphibole. However, parental magma containing 5 % MgO cannot crystallize 50 % amphibole containing 15 % MgO (the computed value for C_L^{MgO} would be negative, here -5 %). In other words, the system does not contain enough MgO to precipitate 50 % of amphibole. This issue is not obvious from trace elements alone (as the laws are multiplicative), but becomes clear from major elements (that use subtractive equations).

On the other hand, we have also discussed the fact that major and trace elements carry different information. Most importantly, processes cannot be distinguished using majors only (Sect. 21.3). Therefore, it is vital to build internally-consistent models accounting for the largest possible range of elements (and isotope ratios). Major and trace elements should be coupled. For instance, a forward model should calculate simultaneously the composition in major (via mass balance) and trace elements, using the same mineral proportions in both cases.

¹ Note that the phase rule is not violated, as the increase in number of components is a pure numerical exercise—physically, the phases were solid solutions.

A common strategy involves a mixed approach, solving the reverse problem for major elements (least-square method), and using the mineral proportions as the input into a forward model for traces (see Martin 1987 for an example of this approach, or the Part VI).

This Space Left Blank for Your Own Tricks

References

- Allègre CJ, Hamelin B, Provost A, Dupré B (1987) Topology in isotopic multispace and origin of mantle chemical heterogeneities. *Earth Planet Sci Lett* 81:319–337
- Iwamori H, Nakamura H (2012) East–west mantle geochemical hemispheres constrained from independent component analysis of basalt isotopic compositions. *Geochem J* 46:e39–e46
- Martin H (1987) Petrogenesis of Archaean trondhjemites, tonalites and granodiorites from eastern Finland; major and trace element geochemistry. *J Petrol* 28:921–953
- Reimann C, Filzmoser P, Garrett R, Dutter R (2008) *Statistical data analysis explained: applied environmental statistics with R*. Wiley, Chichester
- Spear FS (1994) *Metamorphic phase equilibria and pressure–temperature–time paths*. Mineralogical Society of America Monographs. Mineralogical Society of America, Washington
- Torres-Roldan RL, Garcia-Casco A, Garcia-Sanchez PA (2000) CSpace: an integrated workplace for the graphical and algebraic analysis of phase assemblages on 32-bit Wintel platforms. *Comput Geosci* 26:779–793

Chapter 24

Common Sense in Action

One of the most commonly heard complaints about geochemical modelling—and indeed, one of the worst problems of this approach—is that it is very easy to get bogged down in numerical subtleties and lose touch with the underlying geological reality. Most importantly, a geochemical model is developed in order to understand and quantify a geological process. Thus any sound model must rest on a solid geological understanding of the problems involved. In here, we discuss some of the limitations of geochemical modelling applied to geological problems.

24.1 Physical Constraints

Modelling based on mass balance describes the evolution of igneous rocks in purely chemical terms—i.e. focussing on conservation of mass. Equally important, however, is the conservation of energy, in other words, physical constraints. Currently, comprehensive models coupling chemical and physical models are not routinely used; yet one should, at least, make sure that a proposed geochemical model is not grossly inconsistent with physics.

24.1.1 Thermodynamic Constraints

Thermodynamic constraints are probably some of the most often ignored physical controls in geochemical modelling.

Melting, for instance, is a strongly endothermic process, such that its magnitude (F) is strongly controlled by the available heat supply (Thompson and Connolly 1995; Henk et al. 2000; Annen et al. 2006; Sawyer et al. 2011; Bea 2012).

Assimilation involves physical disruption of the assimilated rock, and its subsequent melting. Both are very expensive processes in terms of energy. The sophisticated AFC equations with many parameters can be easily tweaked to yield solutions nicely reproducing the observed variation. Still, they may be geologically unrealistic (Roberts and Clemens 1995), as they ignore the constraints imposed by conservation of energy. In fact, the range of physically permissible parameters during AFC is restricted (see Sect. 11.4, including the Next step boxes). The rate of assimilation

to fractional crystallization (r) is governed by the thermal state of the assimilated (Reiners et al. 1995); it tends to be low for cold upper crustal rocks and higher for hotter deeper ones. Nevertheless, r is unlikely to be higher than about 1, as the amount of heat required in order to melt a mass of country rock roughly equals the heat released by crystallization of the same mass of magma (De Paolo 1981; Taylor and Sheppard 1986).

24.1.2 Mechanical (Rheological) Constraints

There are also several mechanical issues related to the rheology of partially molten system (Arzi 1978; Rosenberg 2001). Depending on the interplay between the many parameters such as viscosity, temperature, strain rate and melt fraction, solid–liquid segregation may be more or less efficient. Note also that most of these parameters are not independent of each other, but are somehow related to the chemical properties we are trying to model! This has important implications for the feasibility of generating differentiated magmas (Vigneresse and Burg 2004).

Crystallization

In a liquid-dominated system (Newtonian viscous medium), the speed of gravitational settling of particles (crystals) is expressed by Stokes' (1901) law:

$$v_s = \frac{2r_p^2 g \Delta\rho}{9\eta} \quad (24.1)$$

where v_s is the sinking velocity, r_p the particle's radius, g gravitational constant, $\Delta\rho$ the density difference between the particle and the melt, and η the viscosity.

In a non-Newtonian fluid, the critical radius below which a crystal would not sink solely under the effect of gravity is (McBirney and Noyes 1979):

$$r_{crit} = \frac{3\sigma_y}{g\Delta\rho} \quad (24.2)$$

where σ_y is the yield strength of the fluid. In a typical felsic magma, $\eta = 10^5$ Pa.s, $\sigma_y = 10$ Pa and $\rho_{magma} = 2300 \text{ kg.m}^{-3}$ (Turcotte and Schubert 1982). The critical radius for a zircon ($\rho = 4650 \text{ kg.m}^{-3}$; Anthony et al. 2014) is ca. 1.3 mm: it is unlikely that it would reach this size. Therefore, gravitational settling is unable to extract this mineral out of the magma from which it crystallized. A biotite has a lower density ($\rho = 3000 \text{ kg.m}^{-3}$; Anthony et al. 2014), but typically a larger size; its critical radius is 4.4 mm, a perfectly feasible size for a biotite in a felsic magma. The sinking velocity of a 5 mm biotite is, from Eq. (24.1), $3.8 \times 10^{-7} \text{ m.s}^{-1}$ (ca. 12 m/yr). Crystal/liquid segregation would be possible but sluggish.

A mafic or ultramafic melt has a much lower viscosity: ca. 1 Pa.s in komatiites, 50–100 Pa.s in basalts (Spera 2000). Under these conditions, a 1 mm olivine

($\rho = 3400 \text{ kg.m}^{-3}$; Anthony et al. 2014) may reach a sinking velocity of 1–2 mm/s in a komatiitic magma.

Pure gravitational settling is appropriate for magma chambers subject to no external stress: a situation possible for e.g. mafic layered intrusions (McBirney and Noyes 1979), but very unlikely for large felsic bodies (Bouchez 1997). In the latter case crystal–liquid segregation may be assisted by processes such as filter-pressing or magma flow (Bachmann and Bergantz 2004, 2008).

Melting

The key issue that governs melt extraction from the partially molten source is the connectivity of the melt network. This is controlled by the wetting angle of the melt phase in its solid matrix (Laporte 1994). A wetting angle below 60° would result in an interconnected melt network even for low melt fractions (Fig. 24.1a); whereas higher wetting angles would yield melt in small, isolated pockets at grain boundaries (Fig. 24.1b). Experimental data show that the wetting angles tend to be low for minerals such as olivine, but higher for quartz and feldspars (Laporte 1994). Therefore in mafic systems, the melt is easily segregated from its residue; in felsic rocks, melt segregation is much more difficult to achieve.

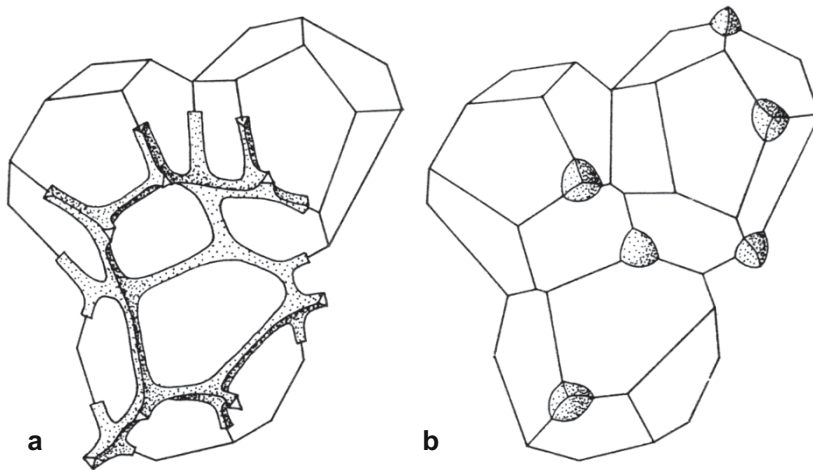


Fig. 24.1 Wetting angle and melt network connectivity. **a** With a wetting angle $< 60^\circ$, melt forms an interconnected network along grain boundaries. **b** When the wetting angle is $> 60^\circ$, melt concentrates in isolated pockets at the grain corners (Laporte 1994). © Springer

Again, melt segregation could be assisted by deformation (Vigneresse and Burg 2004). Felsic systems are therefore likely to behave in a dual way: at low melt fractions, melt is not extracted; at higher melt fractions, the melt pockets become interconnected, the system switches to a liquid-like behaviour and the resulting mush will be mobile as a whole, but still not efficiently segregating solids from liquids.

In summary, for mafic systems it is very easy to achieve melt/crystal separation, be it during crystallization or melting. Fractional processes are perfectly feasible, and low-melt fraction (F) liquids may exist. In felsic systems, liquid/solid segregation is more difficult, and may only exist if assisted by deformation. Low- F liquids are less likely to be observed, and batch processes are more feasible.

24.2 Scale and Speed of Processes—Approach to Equilibrium

Chemical equilibrium is attained when the reactants and products of a reaction are present in concentrations that do not change with time. Thermal equilibrium occurs when there are no temperature changes in the system. In both cases, this does not preclude a dynamic balance of heat or material fluxes between components of the system.

Perfect equilibrium is never achieved in nature. It is however possible to break down a continuous process into a succession of infinitesimal equilibrium states, between which parameters (temperature, concentration...) vary only slightly. For each step, the system can be treated as in equilibrium, which implicitly assumes that it reacts sufficiently fast to the changes.

In geochemical modelling, the term “equilibrium” is used to imply such a situation, i.e. a system reacts to (temperature-induced mostly) changes more quickly than is the rate of heating or cooling. This tends to be a sound assumption, because heat diffusion¹ is sluggish in natural materials (e.g. Turcotte and Schubert 1982), whereas the kinetics of mineral reactions is strongly temperature-dependent, and therefore reasonably fast at igneous temperatures (Spear 1994). However, there may be situations where this assumption fails—in particular when the anatexis was short-lived, the system dry or cold, the source infertile and/or some of its components incapable of equilibrating with the melt. Some minerals are refractory and difficult to re-equilibrate; others may have failed to communicate with the melt, having been shielded by such refractory, or newly grown peritectic, phases (Watson and Harrison 1984). Also the solubility of accessories, often hosting a significant proportion of trace elements and radiogenic isotopes, is limited (Chap. 13). This is shown e.g., by the common occurrence of inherited zircon in low- T , anatectic granites (Miller et al. 2003).

In all these scenarios, equilibrium is not attained, primarily because the chemical process is slower than the rate of temperature change. However, one may note that this definition largely relies on equilibration time, itself a function of the system size. From this observation is derived the concept of “equilibration volume”, i.e. the portion of a system that is small enough to allow equilibrium. This notion, although not new (Blackburn 1968) is increasingly used as a tool to decipher complex metamorphic textures, such as partially reacted assemblages or

¹ Of course, if heat advection or convection are significant, disequilibrium, in the sense discussed here, is much more likely.

phenocrysts preserved from igneous protolith (e.g. Tinkham and Ghent 2005 amongst others). In effect, a very similar approach is used for igneous rocks. In a “non-modal” melting model, one assumes that only a part of the system (although its spatial extent is not explicitly specified) was involved in melting. “Dis-equilibrium”² approaches (i.e. models based on melting or crystallization affecting only a portion of a rock) have been successfully used to account for trace-element (Barbero et al. 1995; Villaros et al. 2009) or isotopic (Knesel and Davidson 1996; Farina and Stevens 2011; McLeod et al. 2012) characteristics of melts, primarily during (relatively low-T) crustal melting.

From this it is clear that the notion of equilibrium (from an igneous perspective) is very strongly dependent on the scale of observation. Pushing the reasoning to the absurd, it is clear that equilibrium is not attained at the scale of the whole mantle (melts generated there are not in equilibrium with a bulk mantle composition). As one looks at smaller volumes, equilibrium becomes more likely. On the other hand, there is in general little point in considering equilibrium volumes that are too small (a few grains). The resulting melts are likely to be eventually mixed and homogenised, and any such subtle chemical variations erased.

The size of the equilibration volume to consider for geochemical modelling of magmatic rocks has to be decided on a case-by-case basis. Depending on the temperature of the processes studied, duration, presence of fluids etc., it may range from a few mm³ (similar to equilibration domains in metamorphic petrology), through a hand-specimen, to that of a rock unit.

24.3 Is Your Model Worth Your Efforts?

In general, the more complex the model, the longer it will take to develop. It is, therefore, important to think beforehand whether it is worth the added complexity, and how precise or detailed an answer is needed. In addition, complex models tend to require more input data: fewer parameters of a simple scenario are likely to be much better constrained than many of a complex one. Finally, a model is not built for its own sake, but for comparison with real data. If they are of poor quality (be it for analytical problems, or limited understanding of the geology involved), modelling will fail to discriminate between possible solutions.

² Depending on the context, the opposite to “equilibrium” can be either “disequilibrium” or “fractional”, which is why the term “equilibrium” is not used in this book to describe a class of models (see Warning box at beginning of Chap. 11). Fractional melting (or crystallization) is not a disequilibrium process, as the system still reacts sufficiently fast to the changes to be regarded as in equilibrium at any point in time!

24.3.1 *How Well Can We Discriminate Between Models?*

In the preceding text, different equations were written in order to describe various situations that are encountered during melting, crystallization or mixing. In theory, individual processes do produce distinct trends in geochemical plots. However, in many cases the difference is less than the scatter in the dataset. All natural datasets are intrinsically noisy due to: a) analytical errors, b) variable alteration of individual samples, that is hard to totally avoid, c) limited sample size vs. that of possible heterogeneities (accumulated crystals, incompletely mixed magma batches, etc.), and/or d) multistage, complex genesis. The latter may reflect superposition of several processes, such as melting of different portions of a source, crystallization, variable contamination, crystal accumulation or metasomatic redistribution of elements by fluids.

In general, geochemists try to model only the dominant process(es), thus simplifying the problem by ignoring the other mechanisms. However, all of them affect to varying degrees the whole-rock compositions, and introduce some additional variability in the dataset. When these variations are large, they are easily recognizable and we try to incorporate them in a more complex model. When they are small, they are easily considered as natural noise and overlooked.

In order to discuss whether it is practicable to distinguish between different models, we have built a synthetic dataset (the same as used for Exercise 22.1)³. The advantage is that, unlike for natural data, the true evolution line is known, and it is possible to compare models against it. This dataset has been generated by calculating the theoretical evolution of a calc-alkaline basaltic magma, crystallizing Pl + Amp + Mt, with Zrn added using the saturation concept. “Sample” compositions were obtained by randomly modifying the ideal composition based on a normal distribution ($2\sigma = 5\%$ for majors and 10% for traces). These computed values scatter around the actual model curve like natural datasets do.

Figure 24.2 compares the difference between three principal petrogenetic models (fractional crystallization, melting and mixing), with the noise of our synthetic dataset. Clearly, processes are efficiently distinguished only when considering elements with contrasting behaviour and with D values very different from 1 (if $D = 1$, all equations collapse to linear). Even so, the fit between the true model (Rayleigh fractionation) and the data is satisfactory, but not great—there is significant scatter around the curve. The use of a log scale does not make a difference: Rayleigh curves are linearized (cf. Fig. 24.2c and f), but when the D values are too similar or too close to 1 (cf. Fig. 24.2a–b with d–e), this does not help.

In the light of this, one may question the use of elaborate models such as AFC or fractional melting. While they may be intellectually satisfying, in that they arguably incorporate geologically more realistic processes, they may not be distinguishable on geochemical grounds, and may actually bring no further insight! Likewise, the use of complex solubility equations (Sect. 22.3) may, or may not

³ The code generating this dataset is given in full on the [Web site](#).

generate a better model than simpler approaches. Therefore, it is wise to start with using basic equations, and resort to more complex models only when needed.

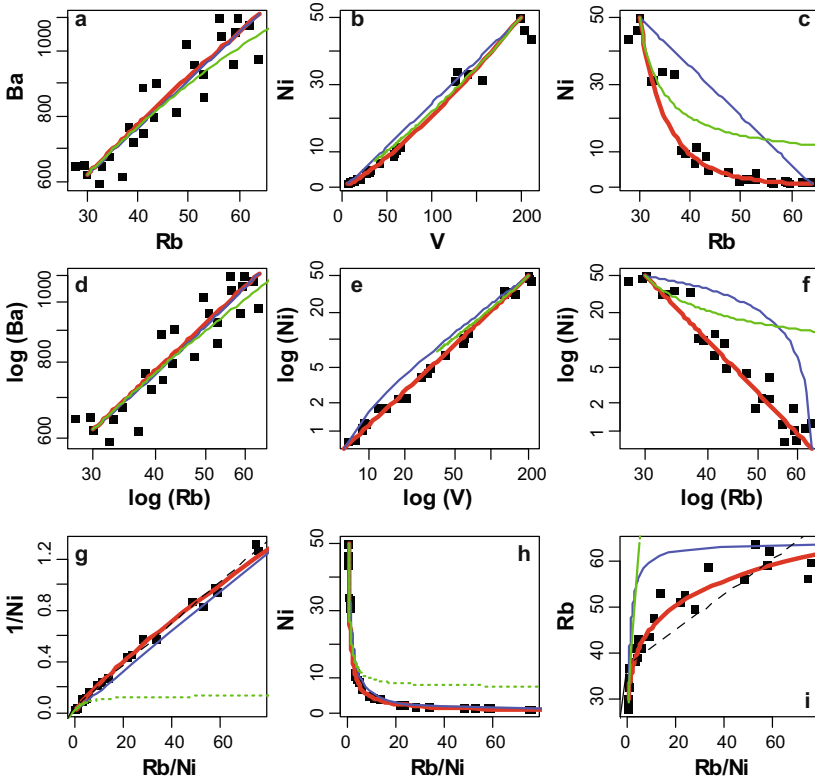


Fig. 24.2 Effects of analytical noise and projection used to represent the data. The dataset plotted (*noisy.data*, black squares) was calculated by adding random noise to a Rayleigh fractionation evolution (thick red curve, i.e. the “true” model). The blue and green curves correspond to mixing and batch melting models. In many cases, a poor choice of axes leads to diagrams where distinct models are not distinguishable. The dashed line in (i) is a linear fit to the dataset.

24.3.2 Dangerous Projections

Sometimes, the graphical representation used to show modelling results is misleading. Consider, for instance, popular ratio diagrams such as the ones on Fig. 24.2g–i⁴. In theory, of course, such a projection is appropriate to distinguish between a mixing trend (a straight line), and a crystallization or melting curve. However, the use of a ratio-based projections (and even worse, the fact that both

⁴ Such a diagram was recently spotted by one of the authors in a presentation that shall remain anonymous.

axes have a common denominator) creates an apparent linear correlation (Chayes 1971; Le Maître 1982; Rock 1988; Rollinson 1993). In Fig. 24.2g, fitting a straight line to the data gives an excellent result, with an R^2 value of 0.99. Even the obviously poorer fit of Fig. 24.2i (dashed line) still has a R^2 of 0.74. Most geochemists would confidently assume such values to be hard evidence for a linear relationship, and hence favour a mixing model; whereas the data were actually generated by fractional crystallization.

24.3.3 K_D vs. C_0 —What Should You Improve First?

During fractional crystallization modelling, the importance of accurate K_D should not be overestimated. In Fig. 24.3, we compare the effects of inaccuracy on the value of D (a), and of C_0 (b), again using the noisy dataset as in Fig. 24.2. Both panels show the real value for C_0 and the real fractionation curve, as well as the dataset that we are trying to reproduce.

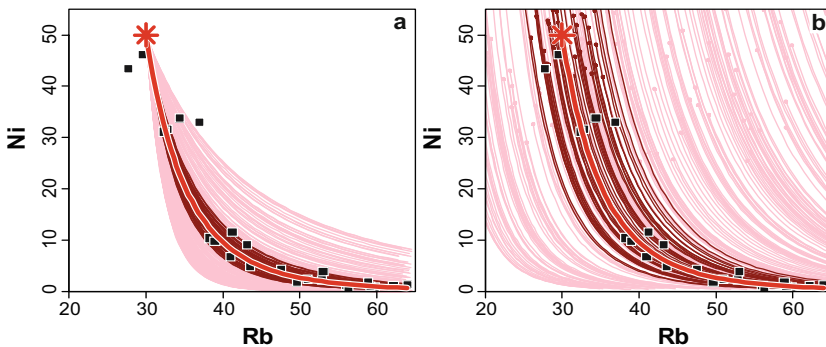


Fig. 24.3 Simulation of the effects imposed on Rayleigh-type fractionation curves by uncertainties in D (a) and C_0 (b). In both plots, the thick red curve is calculated using the “real” value for C_0 (Rb = 30 ppm and Ni = 50 ppm; red star) and D ($D_{Rb} = 0.025$ and $D_{Ni} = 6.6$). The black squares represent the “noisy” dataset. For explanation, see text.

Figure 24.3a investigates the effect of errors on D . Fifty dark red curves were generated by randomly choosing D_{Ni} and D_{Rb} within 20 % of the true value, i.e. $1.2 \times D_{real} > D > D_{real}/1.2$. The resulting scatter is noticeable, but not higher than the typical dispersion of whole-rock analyses from magmatic series. An error of this magnitude will most likely be drowned by other uncertainties (sampling, analytical, etc.). Two hundred pink curves were calculated by choosing D values such that $2 \times D_{real} > D > D_{real}/2$. Here the scatter is worse, although the overall shape of the fractionation curve is preserved. This suggests that there is little to gain in refining D beyond a certain point.

In Fig. 24.3b we investigate the effect of uncertainties of the same magnitude on C_0 . Quite clearly, an error of 20 % still gives acceptable results, although much

worse than in Fig. 24.3a. On the other hand, curves generated by an error of a factor of two cover the whole diagram.

In general, it must be kept in mind that the composition of a melt is also a function of the source (or primitive liquid) composition (C_0) and F —parameters for which there are considerable uncertainties. Even though K_D is a source of error, it is perhaps not the worst offender in most models. It seems more important to ensure that the ratios between individual K_D are right, as this would eventually control the ratio in the melt. Indeed, many geochemists would rely more on ratios (such as Zr/Nb, Nb/Ta, etc.) than on absolute values. On the other hand, a good determination of C_0 is more crucial, as it can easily lead to meaningless results. This is perhaps more important during partial melting, as modelling relies on a selection of a possible, although rarely known, source; whereas the primitive liquid of a fractionating series is generally observed. In other words, the most important aspect of modelling is to get the geology right, and to understand what is actually melting (or fractionating)!

24.4 Back to the Field!

In a sense, the most critical input parameter in any model remains the geological understanding. There is, for instance, little point in trying to build a model for a dataset that includes rock units of distinct ages. Therefore, modelling should be endured on a well-designed dataset, including only relevant data. This may involve heart-breaking decisions, such as discarding some of your precious analyses. In any case, such a judgement can only be made on the basis of geological understanding of the studied region.

Finally, one cannot stress strongly enough that the ultimate test for a model is its geological consistency. Therefore, models that invoke sources absent from the studied area; that predict volumes of rocks not matching the observed distribution; that require thermal regimes totally at odds with the local record, or impossibly high melt amounts are of no use. Although such models may pass the geochemical tests, reproduce observed compositions and otherwise seem satisfactory at first glance, one must keep in mind that geological data in the broadest sense are just as valuable as geochemical ones. Indeed, the ultimate goal of modelling is to provide an explanation for all the observations, regardless of their origin, and shed some light onto the evolution of existing rocks in their geological context.

And so, as a final word of caution, perhaps unexpected in a text on geochemical modelling, we would like to encourage you to return again and again to the observation of field relationships, geological maps, samples and thin sections...

If you don't understand it—map it!

—An anonymous geologist

References

- Annen C, Blundy JD, Sparks RSJ (2006) The sources of granitic melt in Deep Hot Zones. *Trans Roy Soc Edinb, Earth Sci* 97:297–309
- Anthony JW, Bideaux RA, Bladh KW, Nichols MC (2014) Handbook of Mineralogy (web version). Mineralogical Society of America. <http://www.handbookofmineralogy.org>
- Arzi AA (1978) Critical phenomena in the rheology of partially melted rocks. *Tectonophysics* 44:173–184
- Bachmann O, Bergantz GW (2004) On the origin of crystal-poor rhyolites: extracted from batholithic crystal mushes. *J Petrol* 45:1565
- Bachmann O, Bergantz GW (2008) Rhyolites and their source mushes across tectonic settings. *J Petrol* 49:2277–2285
- Barbero L, Villaseca C, Rogers G, Brown P (1995) Geochemical and isotopic disequilibrium in crustal melting: an insight from the anatectic granitoids from Toledo, Spain. *J Geophys Res* 100:15745–15765
- Bea F (2012) The sources of energy for crustal melting and the geochemistry of heat-producing elements. *Lithos* 153:278–291
- Blackburn W (1968) The spatial extent of chemical equilibrium in some high-grade metamorphic rocks from the Grenville of southeastern Ontario. *Contrib Mineral Petrol* 19:72–92
- Bouchez J-L (1997) Granite is never isotropic: an introduction to AMS studies of granitic rocks. In: Bouchez J-L, Hutton DHW, Stephens WE (eds) *Granite: from segregation of melt to emplacement fabrics*. Kluwer Academic Publications, Dordrecht, pp 95–112
- Chayes F (1971) *Ratio correlation: a manual for students of petrology and geochemistry*. University of Chicago Press, Chicago
- De Paolo DJ (1981) Trace element and isotopic effects of combined wallrock assimilation and fractional crystallization. *Earth Planet Sci Lett* 53:189–202
- Farina F, Stevens G (2011) Source controlled $^{87}\text{Sr}/^{86}\text{Sr}$ isotope variability in granitic magmas: the inevitable consequence of mineral-scale isotopic disequilibrium in the protolith. *Lithos* 122:189–200
- Henk A, von Blanckenburg F, Finger F, Schaltegger U, Zulauf G (2000) Syn-convergent high-temperature metamorphism and magmatism in the Variscides: a discussion of potential heat sources. In: Franke W, Haak V, Oncken O, Tanner D (eds) *Orogenic processes: quantification and modelling in the Variscan Belt*. Geological Society of London Special Publications, vol 179, pp 387–399
- Knesel KM, Davidson JP (1996) Isotopic disequilibrium during melting of granite and implications for crustal contamination of magmas. *Geology* 24:243–246
- Laporte D (1994) Wetting behavior of partial melts during crustal anatexis: the distribution of hydrous silicic melts in polycrystalline aggregates of quartz. *Contrib Mineral Petrol* 116:486–499
- Le Maître RW (1982) *Numerical petrology*. Elsevier, Amsterdam
- McBirney AR, Noyes RM (1979) Crystallization and layering of the Skaergaard intrusion. *J Petrol* 20:487–554
- McLeod CL, Davidson JP, Nowell GM, de Silva SL (2012) Disequilibrium melting during crustal anatexis and implications for modeling open magmatic systems. *Geology* 40:435–438
- Miller CF, McDowell SM, Mapes RW (2003) Hot and cold granites? Implications of zircon saturation temperatures and preservation of inheritance. *Geology* 31:529–532
- Reiners PW, Nelson BK, Ghiorso MS (1995) Assimilation of felsic crust by basaltic magma: thermal limits and extents of crustal contamination of mantle-derived magmas. *Geology* 23:563–566
- Roberts MP, Clemens JD (1995) Feasibility of AFC models for the petrogenesis of calc-alkaline magma series. *Contrib Mineral Petrol* 121:139–147

- Rock NMS (1988) Numerical geology. A source guide, glossary and selective bibliography to geological uses of computers and statistics. Lecture Notes in Earth Sciences, vol 18. Springer, Berlin
- Rollinson HR (1993) Using geochemical data: evaluation, presentation, interpretation. Longman, London
- Rosenberg CL (2001) Deformation of partially molten granite: a review and comparison of experimental and natural case studies. *Int J Earth Sci* 90:60–76
- Sawyer EW, Cesare B, Brown M (2011) When the continental crust melts. *Elements* 7:229–234
- Spear FS (1994) Metamorphic phase equilibria and pressure–temperature–time paths. Mineralogical Society of America Monographs. Mineralogical Society of America, Washington
- Spera FJ (2000) Physical properties of magma. In: Sigurdsson (ed) Encyclopedia of volcanoes. Academic Press, San Diego, pp 171–189
- Stokes GG (1901) Mathematical and physical papers, vol 3. Cambridge University Press, Cambridge
- Taylor HP, Jr, Sheppard SMF (1986) Igneous rocks: I. Processes of isotopic fractionation and isotope systematics. In: Valley JW, Taylor HP, Jr, O’Neil JR (eds) Stable isotopes in high temperature geological processes. Mineralogical Society of America Reviews in Mineralogy, vol 16, pp 227–271
- Thompson AB, Connolly JAD (1995) Melting of the continental crust: some thermal and petrological constraints on anatexis in continental collision zones and other tectonic settings. *J Geophys Res* 100:15565–15579
- Tinkham DK, Ghent ED (2005) Estimating PT conditions of garnet growth with isochemical phase-diagram sections and the problem of effective bulk-composition. *Canad Mineral* 43:35–50
- Turcotte DL, Schubert G (1982) Geodynamics: applications of continuum physics to geological problems. John Wiley and Sons, New York
- Vigneresse JL, Burg J-P (2004) Strain-rate dependent rheology of partially molten rocks. In: Grocott J, McCaffrey KJW, Taylor G, Tikoff B (eds) Vertical coupling and decoupling in the lithosphere. Geological Society of London Special Publications, vol 227, pp 327–336
- Villaras A, Stevens G, Moyen J-F, Buick IS (2009) The trace element composition of S-type granites: evidence for disequilibrium melting and accessory phase entrainment in the source. *Contrib Mineral Petrol* 158:543–561
- Watson EB, Harrison TM (1984) Accessory minerals and the geochemical evolution of crustal magmatic systems: a summary and prospectus of experimental approaches. *Phys Earth Planet Inter* 35:19–30

Part VI Worked Examples

Geochemical modelling is never conducted in isolation, but with the goal of understanding the geological evolution of a specific rock unit. Therefore, it is strongly dependent on regional geology and petrological descriptions and can be endeavoured only after such a complex study. In this part, although space does not allow presenting a full geological description, we nevertheless try to demonstrate how a model is grounded on such observations.

Different rock units pose different challenges in terms of modelling. The observables and the unknowns for instance are not the same. The processes may differ, and contrasting physical properties of mafic and felsic systems, lavas and intrusive units, call for different strategies. Here we illustrate two different approaches, on intermediate lavas on the one hand, and felsic (anatectic) melts on the other.

Chapter 25 deals with the evolution of a calc-alkaline differentiation series, from recent Andean volcanoes in Ecuador. We show that fractional crystallization was the dominant process, and that all the lavas in the volcano are related by fractionation from a common parent. The differentiation story is modelled here as a two-step process, with distinct cumulate compositions. We also explore some uncertainties of the modelling exercise and discuss the range of possible solutions permissible by geochemistry.

Chapter 26 presents a different challenge, modelling of crustal partial melting to form a migmatitic complex. In this environment, the melts are not well extracted from their solid residue. They are poorly homogenised and their composition largely reflects the variability of the available sources. On the other hand, field relations allow to directly constrain the local melt amount. Finally, increasing melt fractions correspond to successive melting reactions, and thus a residue with an evolving composition. We propose, therefore, a strategy based on describing the evolution of melt's composition for a given source as a function of the melt amount (and therefore of the nature of the residue), and of the source's composition. We bracket the possible range of melts between the compositions derived from two end-member sources.

Chapter 25

Differentiation of a Calc-Alkaline Series: Example of the Atacazo-Ninahuilca volcanoes, Ecuador¹

25.1 Geological Setting

In Ecuador, South America, the Nazca Plate is being subducted under the South American Plate (Fig. 25.1). It also carries an oceanic plateau (the Carnegie Ridge), generated by the magmatic activity of the Galapagos hot spot, into the subduction zone. The Ecuador volcanic arc, known as the Northern Volcanic Zone of the Andes, is made up of over 50 Quaternary volcanoes.

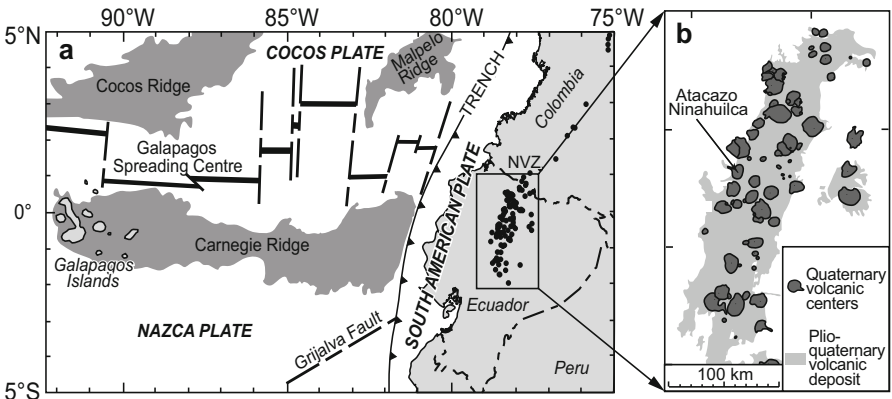


Fig. 25.1 **a** Simplified geodynamic setting of the Northern Volcanic Zone of the Andes. Black circles represent volcanic edifices while the dark grey fields are for oceanic plateaux (adapted from Gutscher et al. 1999). **b** Geographical position of the fifty-five Quaternary volcanoes in the Ecuador volcanic arc, with the position of the Atacazo-Ninahuilca Complex also marked.

One of these is the Atacazo-Ninahuilca Complex that consists of two main units:

¹ Based on the work by S. Hidalgo (Hidalgo 2006; Hidalgo et al. 2012).

- The *Atacazo*, made of lava flows and domes emplaced between 220 and 71 ka. Their composition ranges from andesites to dacites, which generally contain 30–50 vol. % phenocrysts of plagioclase, clinopyroxene, orthopyroxene, hornblende and Fe–Ti oxide (Fig. 25.2).
- The younger *Ninahuilca* erupted from 71 to 2.32 ka. The volcanic activity consisted mainly of dome emplacement and pumice eruptions. The lavas are dacites containing 20–40 % phenocrysts of plagioclase, hornblende, orthopyroxene, biotite and Fe–Ti oxide.



Fig. 25.2 Lavas from Atacazo volcano. A dark grey groundmass contains common plagioclase phenocrysts (white), as well as less abundant phenocrysts of pyroxene, amphibole and Titanomagnetite (Photo S. Hidalgo).

25.2 Data Exploration and Implications

25.2.1 Isotopic Data



[atacazo.data](#)

First we navigate to the right directory and import the data file `atacazo.data` into *GCDkit*:

```
GCDkit-> loadData("atacazo.data")
```

As it contains columns $^{87}\text{Sr}/^{86}\text{Sr}$ and $^{143}\text{Nd}/^{144}\text{Nd}$, the isotope plugin will start, and ask about the age of emplacement (here 0.1 Ma, close enough to zero to make no difference). Selecting *Append Sr-Nd isotopic data* from the Sr–Nd plugin menu, or running the corresponding command, allows subsequent plotting of $^{87}\text{Sr}/^{86}\text{Sr}_i$ and ϵ_i^{Nd} like any other variable from WR:

```
GCDkit-> addResultsIso()
```

```
GCDkit-> multiple("SiO2",c("87Sr/86Sri","EpsNdi"))
```

```
GCDkit-> plateLabelSlots(pos="topleft",style="") #labels a, b
```

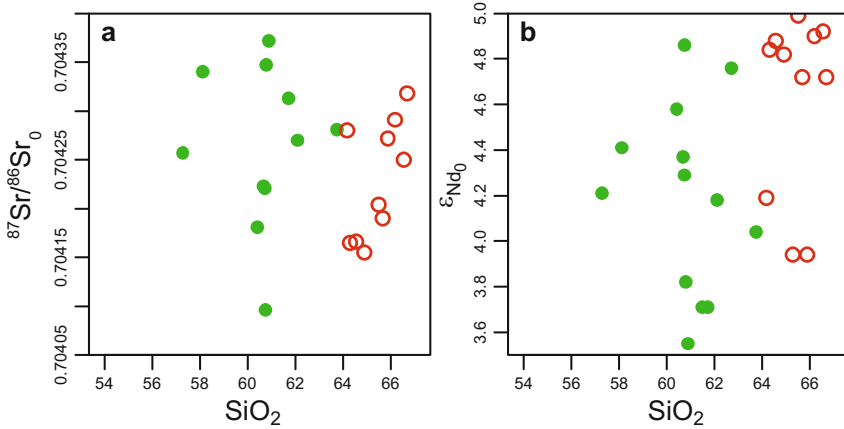


Fig. 25.3 SiO_2 vs. $^{87}\text{Sr}/^{86}\text{Sr}_0$ (a) and ϵ_0^{Nd} (b) plots showing that both Atacazo (filled green circles) and Ninahuilca (open red circles) Sr and Nd isotopic ratios are homogeneous and mutually comparable; they vary over a very small range and are not correlated with SiO_2 .

The Sr and Nd isotopic ratios vary in the same range in both Atacazo and Ninahuilca lavas (Fig. 25.3) and, as demonstrated by Hidalgo (2006), they are not correlated with SiO_2 . Thus it can be concluded that the late crustal contamination played a limited, if any, role during magmatic differentiation. If contamination occurred, it was in the source, earlier on. Also recent O isotopic investigations confirmed negligible crustal contamination (Hidalgo et al. 2012).

25.2.2 Major Elements

Fifty-five samples from Atacazo and 54 from Ninahuilca were analyzed for major and trace elements. All iron was determined as Fe_2O_3 .

We create Harker plots (Fig. 25.4) using `Plot|Multiple plots...`, i.e. the command:

```
GCDkit-> multiple("SiO2", "Al2O3, Fe2O3, MgO, CaO, Na2O, K2O")
```

In Harker diagrams, all oxides show nice correlations with SiO_2 (Fig. 25.4). They are negative (CaO , Fe_2O_3 and MgO) or positive (Na_2O and K_2O). For Al_2O_3 the trend starts with a (poorly defined) positive slope and bends to a negative one at ca. 64 wt. % SiO_2 . For most elements, Ninahuilca and Atacazo lavas plot on the same trends. However, for Al_2O_3 and MgO (Fe_2O_3 to a lesser degree), an inflection occurs between the compositions from both volcanoes. Such a pattern cannot be achieved by binary mixing; the differentiation mechanisms were either partial melting or fractional crystallization (with a changing cumulate composition).

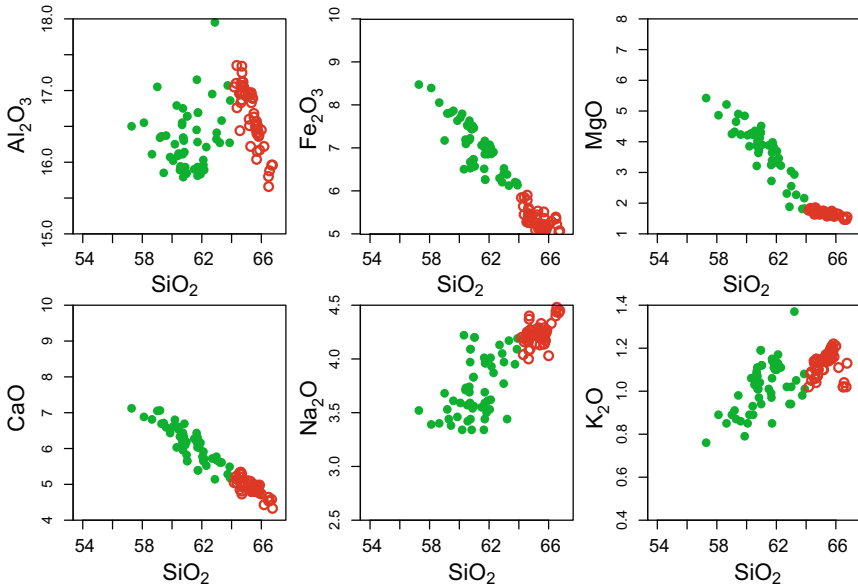


Fig. 25.4 Harker plots for the Atacazo (green, solid) and Ninahuilca (red, open) lavas.

25.2.3 Trace Elements

In Fig. 25.5, TiO_2 and selected trace elements are plotted against SiO_2 (as a differentiation index). This has been done using the following code:

```
GCDkit-> multiple("SiO2", "TiO2,Rb,Ba,La,Yb,Th,Cr,Ni,V")
GCDkit-> plateOYLim() # to set zeroes as minima to all y axes
```

Most often, Atacazo and Ninahuilca data do not fall on a single straight trend in SiO_2 vs. trace-element diagrams. Rather, they tend to form inflexed lines. This again rules out binary mixing. In addition, the content of some elements (Rb, Ba, La and Th) increases in the course of differentiation: they are incompatible during this process. In contrast, Yb, Cr, Ni and V are anti-correlated with SiO_2 , thus pointing to their compatible behaviour.

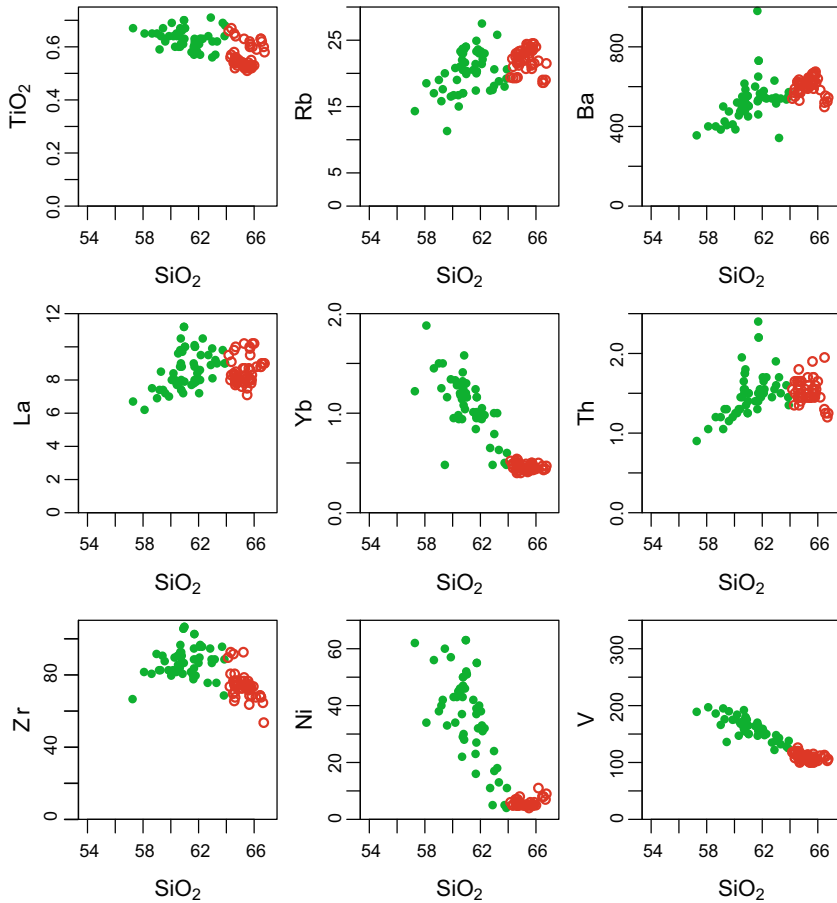


Fig. 25.5 Titanium oxide (wt. %) and selected trace-element contents (ppm) plotted against SiO_2 (same symbols as in Fig. 25.3)

Figure 25.6 is a plate filled by three binary plots (*Plot|Plate of several plots*, or equivalent command). For instance, for the second plot, the *GCDkit* code is (note the choice of plotting limits to ensure the same scale on the x and y axes):

```
GCDkit-> multiplePerPage(3, nrow=1, ncol=3, title=NULL)
GCDkit-> Plate(2) # Selects the second slot
GCDkit-> binary("Ba", "Cr", log="xy", xmin=5, ymin=5, xmax=1100,
+             new=F) ...
```

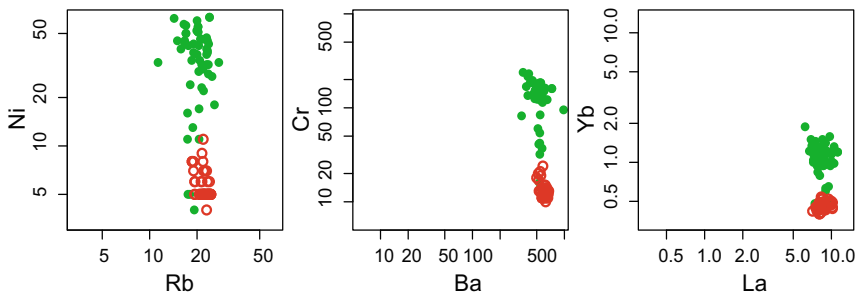


Fig. 25.6 $\log(\text{incompatible})$ [Rb, Ba, La] vs. $\log(\text{compatible})$ [Ni, Cr, Yb] diagrams. The Atacazo-Ninahuilca magmas plot along almost vertical trends, indicating that the differentiation was probably driven by fractional crystallization (same symbols as Fig. 25.3).

In $\log(\text{incompatible})$ vs. $\log(\text{compatible})$ diagrams (Fig. 25.6), the trends defined by the Atacazo-Ninahuilca magmas are always almost vertical, which is typical of fractional crystallization (see Sect. 21.3).

25.3 Geochemical Modelling

Some of the binary plots of SiO_2 vs. major or trace elements are inflexed (Figs 25.4 and 25.5). Consequently, we will model differentiation as a two-step process. During each of them, the cumulate composition remains constant, but it changes in between. For each step, the composition of the parental magma (C_D) is approximated by the least differentiated lava, while the most differentiated one represents the evolved liquid (C_L). During the first step, we model fractionation of ATAC-4 to ATAC-58, and in the second of ATAC-58 to NINA-54.

The mineral compositions in the datafile are taken from phenocrysts in the more primitive lavas (Hidalgo 2006). However, the plagioclase can be very variable and prone to reequilibration: therefore, we use two pure end-members (Ab and An) instead, to be subsequently recombined. The same holds for the Fe–Ti oxide that we treat as a ‘solid solution’ of magnetite with rutile, irrespective of the actual mineral present (Ti-magnetite).

Partition coefficients are compiled from the literature (mostly Rollinson 1993). Two sets of values are present for amphibole, as its K_D does vary significantly between mafic and intermediate liquids.



atacazo.data
atacazo_mins.data
atacazo_kd.data

The data (and other useful definitions) are loaded as follows:

```
GCDkit-> loadData("atacazo.data")
```



```
GCDkit-> min.tab <- read.table("atacazo_mins.data", sep="\t")
GCDkit-> kd.tab <- read.table("atacazo_kd.data", sep="\t")
GCDkit-> mjrs <- c("SiO2", "Al2O3", "Fe2O3", "MgO", "CaO", "Na2O", "K2O",
+               "TiO2")
GCDkit-> trc <- c("La", "Ce", "Nd", "Sm", "Eu", "Gd", "Dy", "Er", "Yb", "Rb",
+               "Ba", "Th", "Nb", "Sr", "Zr", "Y", "V", "Cr", "Ni")
```

The full code supplied on the Web page defines four functions. The first:

```
rev.maj <- function(c0.lab, cL.lab, min.set, norm=F) {...
```

calculates reverse models based on majors; since this is pure mass balance, it would also work for melting (see exercises 9.1 and 9.2). The function:

```
rev.tr.fc <- function(c0.lab, cL.lab, min.set) {...
```

computes reverse fractional crystallization models based on trace elements (see Exercise 15.1). These two functions return a list with components *ff* (melt fraction), *cS* (cumulate composition) or *dd* (bulk distribution coefficient), *r.sq* (the sum of squared residuals, ΣR^2), and *m* (mineral proportions). The function:

```
fwd.mod <- function(c0.lab, m, ff, norm=F, eqn="FC") {...
```

is designed for forward modelling of major and trace elements, in the course of either melting or fractional crystallization. This is similar to, although more complete than, the exercises 8.1–3, 14.2, 14.3, 22.1. The function returns a list with *cS*, *cL* (fractionated liquid composition) and *dd*.

The following arguments are required by these functions:

- *c0.lab*, *cL.lab*: names of the existing samples with C_0 and C_L compositions,
- *min.set*: a character vector containing the names of the minerals to be considered, they must match those from the K_D and mineral composition files,
- *m*: a named vector containing the mineral proportions (0–1), the names must match those from the K_D and mineral composition files,
- *ff*: the value of F (melt amount; 0→1),
- *norm*: logical, indicating whether all the major-element data should be normalized to 100 % before calculation,
- *eqn*: "FC" or "PM", the model type to be used for forward calculations.

In addition, the following variables are required in the system:

- *WR*: the (*GCDkit*) numeric matrix of whole-rock compositions,
- *min.tab*: a data frame/matrix with mineral compositions,
- *kd.tab*: a data frame/matrix with partition coefficients.

Finally, we define an auxiliary function to recombine the two plagioclase end-members into a plagioclase solid solution:

```
GCDkit-> plagio <- function(an,ab){
GCDkit->   mw.an <- mw["Ca"]+2*mw["Al"]+2*mw["Si"]+8*mw["O"]
GCDkit->   mw.ab <- mw["Na"]+mw["Al"]+3*mw["Si"]+8*mw["O"]
GCDkit->   total.plag <- ab+an
GCDkit->   an_pct <- an/mw.an/(an/mw.an+ab/mw.ab)*100
GCDkit->   res <- c(total.plag,an_pct)
GCDkit->   names(res) <- c("total.plag","an_pct")
GCDkit->   return(res)
GCDkit-> }
```

25.3.1 First Step: Atacazo

The phenocryst assemblage in Atacazo samples includes two pyroxenes, as well as amphibole. However, from a major-element point of view $\text{Opx} + \text{Cpx} + \text{Pl} = \text{Amp}$ (colinearity, see Sect. 23.3). It is therefore very likely that Cpx- and Amp-bearing solutions would both yield a satisfactory fit for major elements. The difference is however important in petrological terms (as it will reflect evolution under different H_2O contents or redox conditions). Fortunately, the K_D for pyroxene and amphibole are markedly different (in particular for HREE: $K_{D_{\text{Yb}}}^{\text{Opx/L}} = 0.88 \approx K_{D_{\text{Yb}}}^{\text{Cpx/L}} = 0.90 \neq K_{D_{\text{Yb}}}^{\text{Amp/L}} = 4.2$), and thus the trace elements should provide further vital clues.

Model Atacazo—1cpx

For calculation we use the previously defined functions:

```
GCDkit-> c0.lab <- "ATAC-4"
GCDkit-> cL.lab <- "ATAC-58"
GCDkit-> min.set.1cpx <- c("Cpx","Opx","Ab","An","Rt","Mt")
GCDkit-> mod1cpx <- rev.maj(c0.lab,cL.lab,min.set.1cpx,norm=T)
GCDkit-> print(mod1cpx,3)
$ff
  F
0.531...
```

Ab and An can be recombined into ca. 53 wt. % of $\sim\text{An}_{54}$ plagioclase:

```
GCDkit-> print(plagio(mod1cpx$m["An"],mod1cpx$m["Ab"]),2)
total.plag   an_pct
   0.53      54.45
```

The trace-element model is computed, including the associated ΣR^2 :

```
GCDkit-> cL1cpx <- fwd.mod(c0.lab,mod1cpx$m,mod1cpx$ff)$cL[trc]
GCDkit-> print(sum(((WR[cL.lab,trc]-cL1cpx[trc])/WR[cL.lab,trc])^2))
[1] 15.27383
```

Table 25.1 Summary of various models calculated for Step 1

Type of model	Minerals present	Mineral proportions (wt. %), F	ΣR^2 (majors)	ΣR^2 (traces)
Reverse majors + forward traces	Cpx	Cpx: 14.7, Opx: 25.8, Pl(An_{54}): 52.7, Mt: 6.8; $F = 0.531$	0.08	15.27
	Cpx + Amp	Cpx < 0, Opx < 0, Amp > 100	(0.44) ^a	(13.9)
	Amp	Opx: 18.4, Pl(An_{52}): 45.9, Mt: 2.4, Amp: 33.3; $F = 0.483$	0.07	0.44
	Amp + Zrn	Opx: 18.4, Pl: 45.9, Mt: 2.4, Amp: 33.3, Zrn: 0.008; $F = 0.483$	0.07	0.35
Reverse traces	Cpx	Pl < 0		(1.86)
	Cpx + Zrn	Pl < 0		(1.84)
	Cpx + Amp	Opx: 14.9, Pl: 38.7, Mt: 2.6, Cpx: 4.2, Amp: 39.7; $F = 0.544$		0.14
	Cpx + Amp + Zrn	Opx: 14.8, Pl: 40.0, Mt: 2.4, Cpx: 4.0, Amp: 38.8, Zrn: 0.65; $F = 0.533$		0.11
	Amp	Opx: 14.4, Pl: 41.1, Mt: 3.3, Amp: 41.2; $F = 0.535$		0.14
	Amp + Zrn	Opx: 14.4, Pl: 42.3, Mt: 3.1, Amp: 40.2, Zrn: 0.64; $F = 0.523$		0.12

^a Whenever there is a numerical solution, it is accompanied by a ΣR^2 value. However, when the solution makes no geological sense, ΣR^2 brings no information. In such a case it is in brackets. The full code for the exercise is supplied on the [Web page](#).

Modelling the first stage (Atacazo), with a Cpx-bearing cumulate yields excellent fit ($\Sigma R^2 = 0.08$) for major elements. The cumulate consists of an assemblage Cpx + Opx + Pl (An_{54}) + Ti-Mt. The model requires 46.9 wt. % of cumulate ($F = 0.531$) to be removed from the melt (Table 25.1).

The trace-element model is plotted (Fig. 25.7):

```
GCDkit-> foo <- rbind(WR[c0.lab,trc],WR[cL.lab,trc],cL1cpx[trc])
GCDkit-> spider(foo,"Boynton",ymin=1,ymax=100,col=c("red",
+ "darkblue","blue"),pch=c(15,16,1),new=F)
GCDkit-> spider(foo,"^Primitive Mantle..McDonough 1995",ymin=1,ymax=
+ 500,col=c("red","darkblue","blue"),pch=c(15,16,1),new=F)
```

Unfortunately, this model is unable to predict correctly the REE behaviour (Fig. 25.7). In particular, the HREE segment for C_L is significantly different from that observed. In fact, the model foresees that HREE should be incompatible during differentiation (e.g., $D_{Yb} = 0.53$), whereas the qualitative analysis demonstrated that Yb is compatible. The model fails, because a phase with high K_D for HREE should have been included (in this case, amphibole is the most likely candidate²).

² Adding zircon does not help here, unless unrealistically high amounts of this mineral are invoked. The calculation is skipped to save space, see Exercise 22.1 for a very similar case.

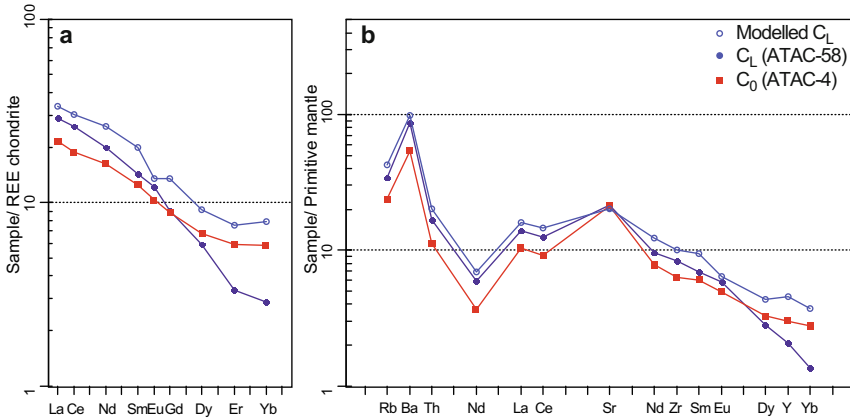


Fig. 25.7 Chondrite-normalized REE patterns (a: Boynton 1984) and Primitive Mantle-normalized multi-element diagram (b: McDonough and Sun 1995), showing that a clinopyroxene-bearing cumulate cannot account for the trace-element variation in the Atacazo lavas.



Robustness and unicity of models

Assessing whether a model is robust to small changes in input parameters is not easy. Likewise, it is important to decide whether the solution generated is mathematically unique. This can be investigated using the Monte Carlo method, i.e. calculating many models by tweaking the input parameters, and examining the model’s response. As an illustration, we examine the effects of changing mineral proportions on ΣR^2 : is our best-fit model significantly better than any other combinations of minerals? We generated 1,000 models by randomly setting cumulate mineral proportions and calculating the ΣR^2 value (Fig. 25.8).

It can be seen that ΣR^2 decreases towards the “true” value (that determined previously by least-squares). The resulting data cloud has only one minimum, suggesting that there is a unique solution, at least with this set of minerals.

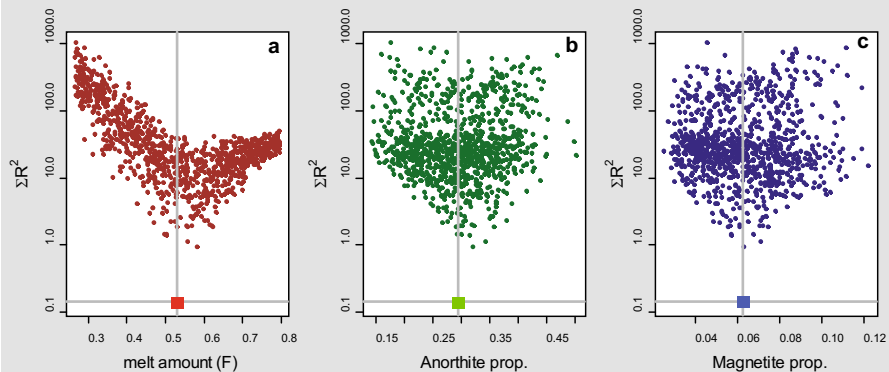


Fig. 25.8 Dependency of ΣR^2 on several parameters. One thousand models were calculated by randomly selecting a set of parameters (F and mineral proportions). Three of these parameters (melt fraction F , anorthite and magnetite proportions) are plotted against ΣR^2 . In each panel, the grey lines and big squares show the best-fit values.

Model Atacazo—1amp

As previously, we invoke our script with:

```
GCDkit-> min.set.lamp <- c("Opx", "Ab", "An", "Rt", "Mt", "Amp")
GCDkit-> modlamp <- rev.maj(c0.lab, cL.lab, min.set.lamp, norm=T)
GCDkit-> print(modlamp, 3)
$ff
  F
0.483..
```

The plagioclase can be recombined to 45.9 % of labradorite (An₅₂).

We then calculate the trace-element contents, with and without zircon:

```
GCDkit-> cLlamp <- fwd.mod(c0.lab, modlamp$m, modlamp$ff) $cL[trc]
GCDkit-> zr.added <- 0.008/100
GCDkit-> ee <- c(modlamp$m, zr.added)
GCDkit-> min.prop.lampzrc <- ee/sum(ee)
GCDkit-> names(min.prop.lampzrc) <- c(min.set.lamp, "Zrn")
GCDkit-> cLlampzrc <- fwd.mod(c0.lab, min.prop.lampzrc,
+   modlamp$ff) $cL[trc]
```

Finally, we plot the model (Fig. 25.9):

```
GCDkit-> foo <- rbind(WR[c0.lab, trc], WR[cL.lab, trc], cLlamp[trc],
+   cLlampzrc[trc])
GCDkit-> spider(foo, "Boynton", ymin=1, ymax=100, col=c("red",
+   "darkblue", "blue", "royalblue"), pch=c(15, 16, 1, 6), new=F)
GCDkit-> spider(foo, "^Primitive Mantle..McDonough 1995", ymin=1,
+   ymax=500, col=c("red", "darkblue", "blue", "royalblue"),
+   pch=c(15, 16, 1, 6), new=F)
```

When clinopyroxene is replaced by amphibole, modelling also provides good results for major elements ($\Sigma R^2 = 0.07$; Table 25.1). The cumulate consists of Amp + Opx + Pl (An₅₂) + Ti-Mt. On the other hand, attempting to calculate a model with both Amp and Cpx gives a meaningless result (negative values for m that do not correspond to realistic peritectic reactions).

The fit for trace elements (Fig. 25.9) is better than that obtained using a Cpx-bearing cumulate. Still, the modelled Zr content of the differentiated liquid (122 ppm) is significantly higher than in the sample ATAC-58 (88 ppm). This gives a vital clue: our calculation does not take into account the role of zircon fractionation. By trial and error, the amount of zircon extracted to adjust Zr contents³ can be determined as 0.008 wt. %. This amount is very low, and does not influence major-element behaviour; the other trace elements are affected only marginally.

³ The Zr content is calculated here by using a $K_D^{Zr/L}(Zr)$ of 3750 (see Exercise 22.1).

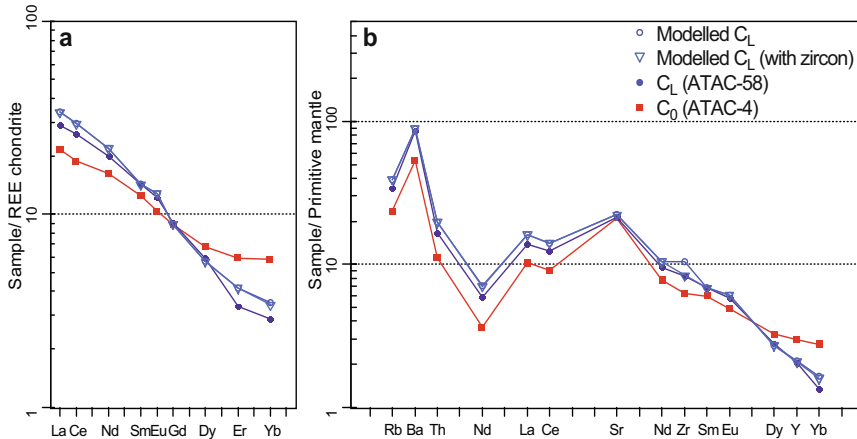


Fig. 25.9 Chondrite-normalized REE patterns (**a**: Boynton 1984) and Primitive Mantle normalized multi-element diagram (**b**: McDonough and Sun 1995), showing the results of modelling the differentiation of Atacazo lavas with an amphibole-bearing cumulate, with or without zircon.

It is worth realizing that the major-element model(s) are not very discriminant. Both models calculated have given good to excellent numerical results. It is even possible to generate a range of other models, numerically slightly worse but still with $\Sigma R^2 < 0.1$, i.e. very acceptable (Fig. 25.8). This is partly a result of our strategy—by breaking down both plagioclase and Fe–Ti oxide into end-members, we are actually significantly loosening the constraints on the model. Still, all of the models are broadly similar in petrological terms (the cumulate includes about 50 % of a fairly calcic Pl, some 5 % of Fe–Ti oxides, and either two pyroxenes or Opx + Amp). The discrimination between the two contrasting scenarios (Amp vs. Cpx) is possible only by using trace elements.

Of course, a reverse approach⁴ can also be used for trace elements (Sect. 12.1 and Exercise 15.1). It leads to the same conclusion (Table 25.1): an Amp-free cumulate cannot account for the observed trace-element compositions. The “best” models derived from majors and traces yield essentially similar proportions of cumulus minerals: c. 15–20 % Opx, 40–45 % Pl, 30–40 % Amp and 2–3 % Ti-Mt. Up to 4 % Cpx has no major effect on the fit. Realistically, the subtle differences between the models have no geological significance!

25.3.2 Second Step: *Ninahuilca*

Ninahuilca magmatic evolution is modelled by differentiating the most evolved Atacazo magma. In this case we choose to use the actual chemistry of ATAC-58,

⁴ NB the K_D values used here are similar for different ‘minerals’ of the K_D table (e.g., Ab and An). This is fine for the forward models but causes the reverse code (function `rev.tr.fc`) to behave erratically. The K_D table must be adjusted to remove these duplicates. Of course, the reverse model is then unable to break down the plagioclase into the two end-members.

rather than the modelled composition of the differentiated liquid of Step 1. The final liquid of Step 2 is taken as NINA-54. The main difference from the previous model is that orthopyroxene does not crystallize anymore, but small amounts of biotite enter the cumulate. The fractionating assemblage is thus: Amp + Bt + Pl (An_{66}) + Ti-Mt (Table 25.2).

The function calls are very similar to those made previously (note the use of “amp2” instead of “amphibole”, to invoke the second set of K_D values):

```
GCDkit-> c0.lab <- "ATAC-58"; cL.lab <- "NINA-54"
GCDkit-> min.set.2 <- c("Ab", "An", "Rt", "Mt", "amp2", "Bt")
GCDkit-> mod2 <- rev.maj(c0.lab, cL.lab, min.set.2, norm=T)
GCDkit-> print(mod2, 3)
$ff
  F
0.868...
GCDkit-> cL2 <- fwd.mod(c0.lab, mod2$m, mod2$ff)$cL[trc]
GCDkit-> zr.added <- 0.12/100
GCDkit-> ee <- c(mod2$m, zr.added)
GCDkit-> min.prop.2zrc <- ee/sum(ee)
GCDkit-> names(min.prop.2zrc) <- c(min.set.2, "Zrn")
GCDkit-> cL2zrc <- fwd.mod(c0.lab, min.prop.2zrc, mod2$ff)$cL[trc]
GCDkit-> foo <- rbind(WR[c0.lab, trc], WR[cL.lab, trc], cL2[trc],
+ cL2zrc[trc])
GCDkit-> spider(foo, "Boynton", ymin=1, ymax=100, col=c("darkblue",
+ "darkgreen", "green", "chartreuse2"), pch=c(15, 16, 1, 6),
+ new=F)
GCDkit-> spider(foo, "^Primitive Mantle..McDonough 1995", ymin=1,
+ ymax=500, col=c("darkblue", "darkgreen", "green",
+ "chartreuse2"), pch=c(15, 16, 1, 6), new=F)
```

Table 25.2 The two models calculated for Step 2

Type of model	Zircon present?	Mineral proportions (wt. %), F	ΣR^2 (majors)	ΣR^2 (traces)
Reverse majors + forward traces	No	Pl(An_{66}): 63.9, Amp: 19.0, Bt: 8.0, Mt: 9.1; $F = 0.868$	0.02	0.91
	Yes	Pl(An_{66}): 63.9, Amp: 19.0, Bt: 8.0, Mt: 9.1, Zrn: 0.12; $F = 0.868$	0.02	0.23

Again, fractionation of zircon allows a better adjustment of Zr values (Fig. 25.10); however, compared with previous models, its amount increases to 0.12 wt. %. As this model predicts a low degree of crystallization (13.2 %), the compositional changes of the residual magma are very limited. In this case the uncertainties in partition coefficients are probably of the same order of magnitude as the observed changes. Also, the predicted plagioclase is probably too calcic (An_{66}) for such silica content (dacites). Consequently, the limit of reliable modelling is reached.

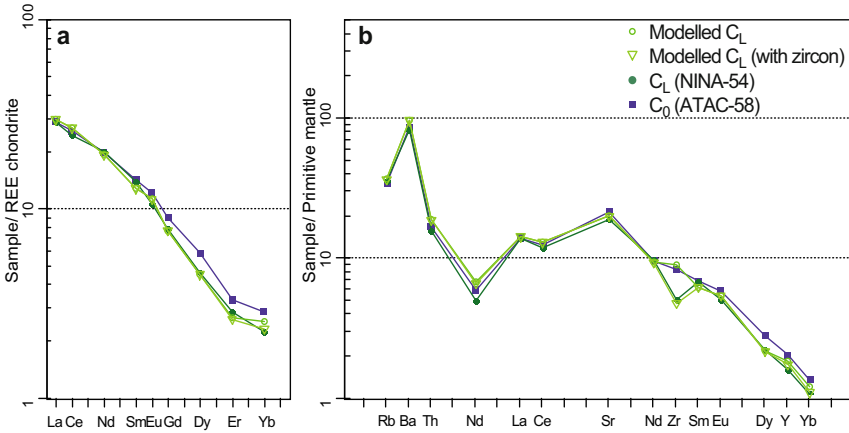


Fig. 25.10 Chondrite-normalized REE patterns (a: Boynton 1984) and Primitive Mantle normalized multi-element diagram (b: McDonough and Sun 1995), showing the results of modelling the differentiation of sample ATAC-58.

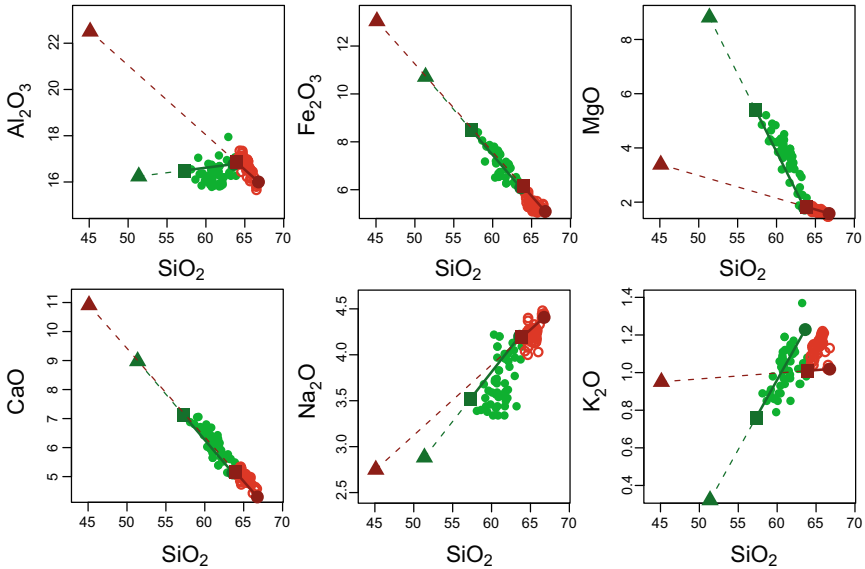


Fig. 25.11 Harker diagrams (wt. %), summarizing the results of the two-step model for major elements. In addition to the sample compositions (same symbols as in Fig. 25.3), the first step (ATAC-4 to ATAC-58, Amp + Zrn version) is plotted in dark green and the second (ATAC-58 to NINA-54, with Zrn) in dark red. Squares are C₀ (ATAC-4 and ATAC-58 respectively); triangles are the cumulates, C_S; large circles are calculated compositions of the differentiated liquids, C_L. The C_S to C₀ segments of the models are dashed, the C₀ to C_L segments solid.

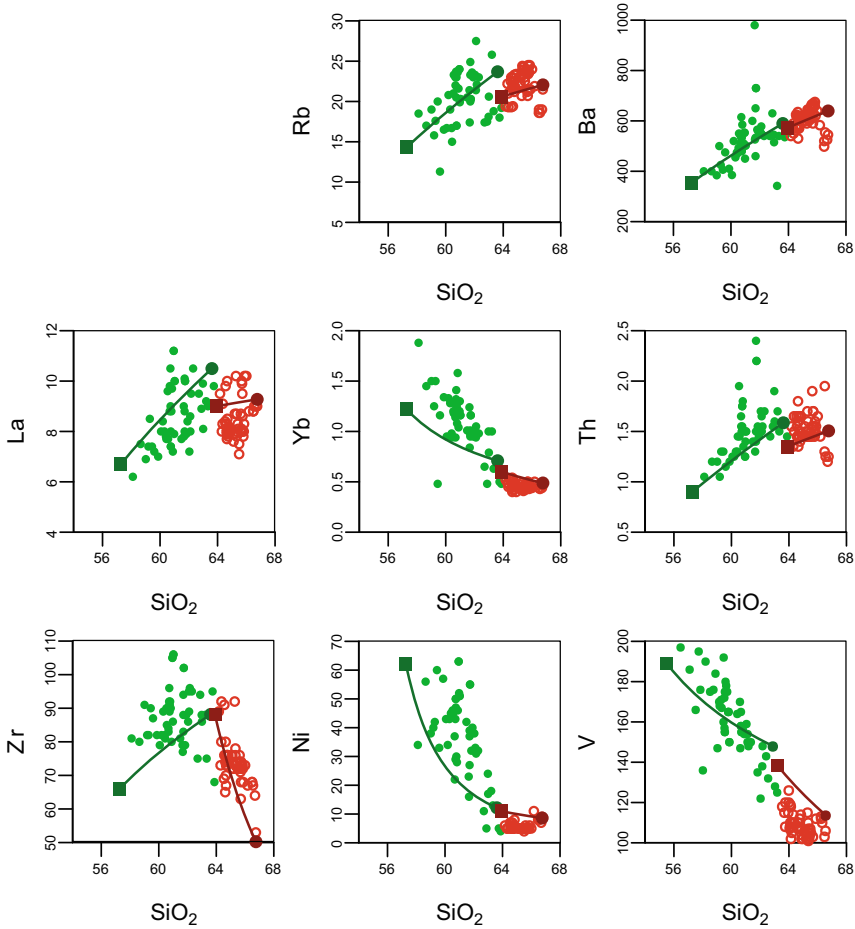


Fig. 25.12 Binary plots of silica (wt. %) vs. selected trace elements (ppm), summarizing the results of the two-step model for trace elements. Same caption as Fig. 25.11. Top left slot is intentionally left empty, to facilitate comparison with Fig. 25.5.

25.4 Summary

The preferred model is summarized in Figs. 25.11 and 25.12. Examining these diagrams reveals that our model is perhaps not ideal. There are many ways to improve it. One could for instance try different mineral compositions (if the phenocrysts are indeed compositionally variable), or change partition coefficients (within the range of permissible values). One may settle for different mineral proportions, estimated with other approaches (e.g., using the reverse modelling of traces). One may also question the choice of C_0 for each step: for example,

ATAC-4 has the lowest SiO_2 , but is out of the main trend for Zr and Yb. Finally, one could also build the model for the second stage using as a primitive magma, $C_0(2)$, the outcome of the first step ($C_L(1)$) rather than an existing composition. The tools provided here will allow the critical readers to investigate these options, and many more, for themselves!

References

- Boynton WV (1984) Geochemistry of the rare-earth elements: meteorite studies. In: Henderson P (ed) Rare Earth Element geochemistry. Elsevier, Amsterdam, pp 63–114
- Gutscher MA, Malavieille J, Lallemand S, Collot J-Y (1999) Tectonic segmentation of the North Andean margin: impact of the Carnegie Ridge collision. *Earth Planet Sci Lett* 168:255–270
- Hidalgo S (2006) Les interactions entre magmas calco-alcalins “classiques” et adakitiques: exemple du complexe volcanique Atacazo-Ninahuilca (Equateur). Unpublished PhD. thesis, Université Blaise-Pascal, Clermont-Ferrand
- Hidalgo S, Gerbe MC, Martin H, Samaniego P, Bourdon E (2012) Role of crustal and slab components in the Northern Volcanic Zone of the Andes (Ecuador) constrained by Sr–Nd–O isotopes. *Lithos* 132:180–192
- McDonough WF, Sun SS (1995) The composition of the Earth. *Chem Geol* 120:223–253
- Rollinson HR (1993) Using geochemical data: evaluation, presentation, interpretation. Longman, London

Chapter 26

Progressive Melting of a Metasedimentary Sequence: the Saint-Malo Migmatitic Complex, France¹

26.1 Geological Setting

The Saint-Malo Massif belongs to the high-T belt of the Cadomian Orogen (Brun and Balé 1990). Figure 26.1 shows that it consists of three main lithological and metamorphic units (Brun and Martin 1977), which are, from S to N, (i) greenschist-facies micaschists and gneisses, (ii) amphibolite-facies gneisses, and (iii) migmatites. The metamorphic event, culminating in anatexis, has been dated at ca. 540 Ma (Peucat and Martin 1985; Peucat 1986).

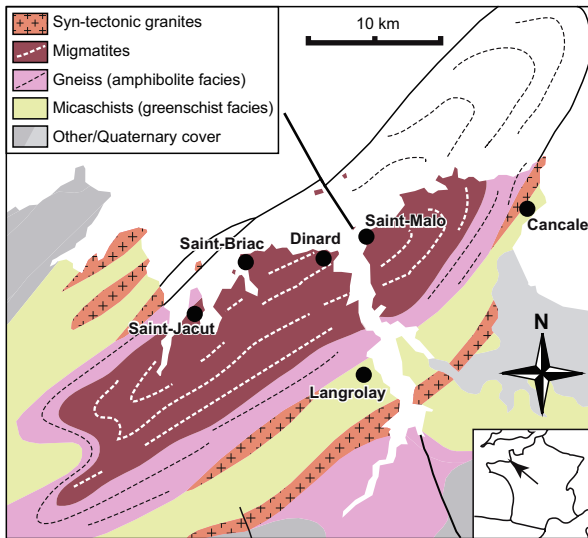


Fig. 26.1 Simplified geological map of the Saint-Malo Massif showing the geographical distribution of the main lithologies; the degree of metamorphism increases northwards, i.e. towards the core of the dome (redrawn after geological map of France and Martin 1980). Inset: sketch map of France for orientation; arrow shows the location of the Saint-Malo Massif.

¹ Adapted from Brown (1979), Martin (1977, 1979, 1980) and Weber et al. (1985).

The micaschists and gneisses correspond to metamorphosed immature sedimentary rocks whose compositions vary widely, from pelitic schists to graywackes (Martin 1979). All the stages of their progressive migmatization can be followed across the metamorphic zones into the migmatitic core. Similarly, in the migmatite zone, all the stages of partial melting can be observed in the field, from metatexites, through banded diatexites and nebulitic diatexites to anatectic granites (Fig. 26.2). The melting pressures were estimated at $\sim 3\text{--}4$ kbar, with temperature increasing from ca. 650 to nearly 750 °C (Martin 1979).

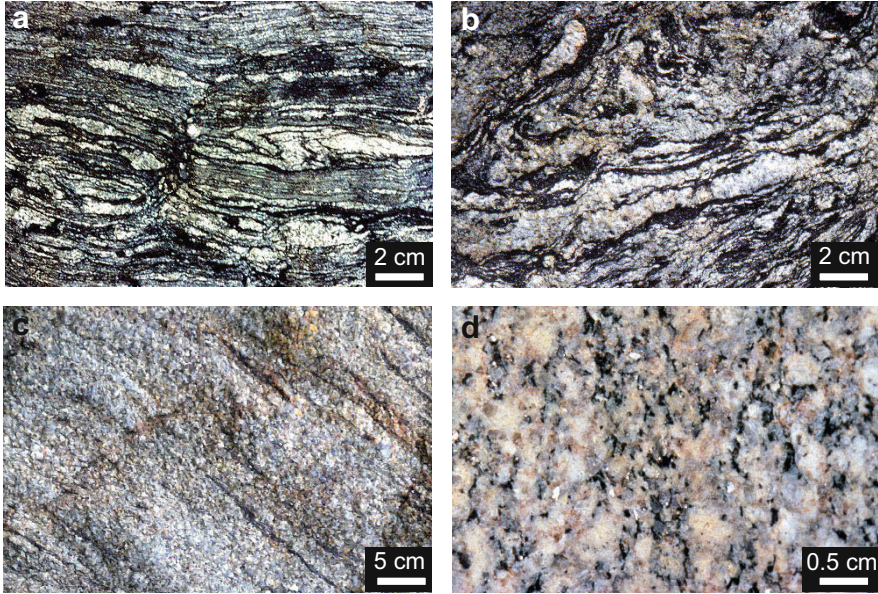



Fig. 26.2 Field photos of Saint-Malo migmatites, showing different stages of partial melting: **a** metatexites ($F \approx 29\%$); **b** banded diatexites ($F \approx 47\%$); **c** nebulitic diatexites ($F \approx 76\%$); **d** anatectic granite ($F \approx 96\%$).

26.2 Major and Trace Elements

Two samples of unmelted gneisses were analyzed, corresponding to end-members of the rock types around the migmatitic dome: QFG (quartzo-feldspathic gneiss) and MRG (mica-rich gneiss). Amongst the migmatites, 17 samples were taken and their leucosomes extracted. Two main assumptions were made: (i) the leucosomes represent chilled melts, and therefore can be modelled as such, and (ii) no melt escaped the system, and thus the proportion of leucosome on a given outcrop (estimated by image analysis) corresponds to F . Both assumptions are questionable. First, leucosomes commonly do *not* represent true melt compositions (Sect. 20.2). Second, melt *does* commonly escape migmatites, and thus the proportion of leucosomes is unlikely to reflect the melt fraction during melting. However, we use these hypotheses as a first

approximation, if only as a reference point for further, more advanced models. It turns out in this specific example that such an approach may lead to very reasonable results—the real point of geochemical modelling.

 `stmalo.data`

After loading the data file, we colour the data points according to the degree of melting, as one of the main features that we will model. The two samples of unmelted gneisses, having a value of 0 for `Melt_frac`, remain grey.

```
GCDkit-> loadData("stmalo.data")
GCDkit-> assignColVar("Melt_frac", "reds")
```

As previously (Chap. 25), binary plots of silica vs. major-element oxides and trace elements are plotted using:

```
GCDkit-> multiple("SiO2", "Al2O3, Fe2O3, MgO, CaO, Na2O, K2O") # Fig. 26.3
GCDkit-> multiple("SiO2", "Rb, Sr, Zr, Ni, Cr, V") # Fig. 26.4
GCDkit-> plate0YLim() # to set zeroes as minima to all y axes
```

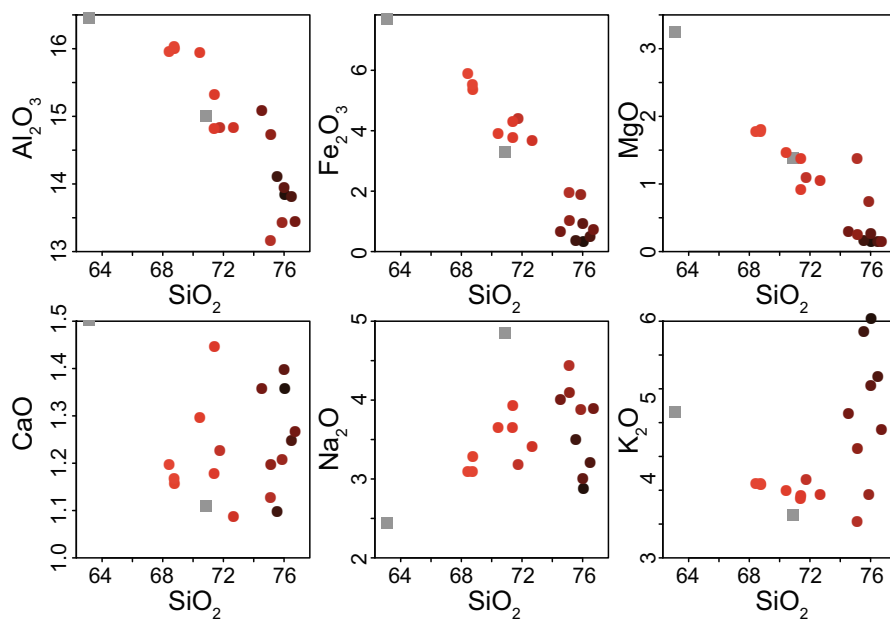


Fig. 26.3 Harker diagrams; many show considerable scatter (CaO, Na₂O, K₂O) while in others, the data define a crude general trend. Unmelted samples = grey squares; leucosomes = circles, colour-coded by the melt fraction (the brighter red, the higher).

When plotted in binary plots where SiO₂ has been selected as the index of differentiation, both major (Fig. 26.3) and trace (Fig. 26.4) elements generally scatter

around a very rough trend. In the worst cases (e.g. CaO, Sr), it is hard to honestly define it. This poses a challenge to modelling and calls for adequate strategies.

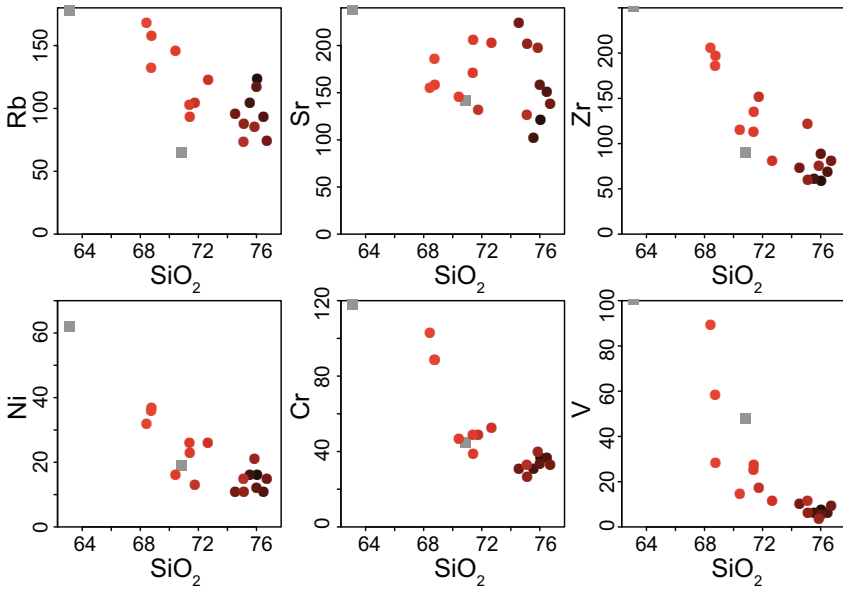


Fig. 26.4 Trace elements plotted against SiO_2 . These diagrams mostly do not define real trends but scatter widely.

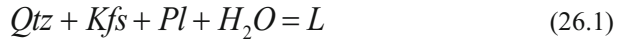
26.3 Geochemical Modelling

Unlike in Chap. 25, the nature of the petrogenetic process operating is not in doubt here: partial melting was responsible for the observed variations. However, the large data scatter precludes any reliable attempt at classical petrogenetic modelling, using an evolution from a single source. Very probably it reflects the fact that the source of melts was a heterogeneous metamorphosed sedimentary pile, whose composition varied widely. Each stratum had its own mineralogical and chemical composition, and the system behaved as if several different sources melted together.

Consequently, we propose a different modelling approach. We use a pure forward approach, and model melting of two gneisses having very contrasted compositions (biotite-rich and quartz–feldspathic). They may be regarded as end-member compositions involved in melting: the resulting liquids will thus delineate the range of possible melts. In addition, during prograde metamorphism each of the gneisses would encounter a series of melting reactions (Clemens and Vielzeuf 1987; Stevens and Clemens 1993), each with different reactants and products. Thus the modal composition of the restite would change during melting, affecting the behaviour of all elements.

26.3.1 Mode Evolution During melting

The first reaction on the prograde path is the relatively low-T (~650 °C) water-present melting:



During fluid-present melting of rocks with excess plagioclase, this mineral can be consumed by melting on the plagioclase–quartz cotectic:



In the modelled compositions, white mica is rare. Thus, the next significant melting reaction is incongruent melting of biotite, at relatively low T (~720–750 °C):



Based on experimental data, it is possible to constrain the stoichiometry of each of the successive melting reactions for both rock types (Table 26.1) (Martin 1980; Weber et al. 1985). Consequently we can describe the evolution of the mode of the rock during melting. Starting from the initial mode of a rock, we subtract for each 1% melt increment minerals in proportions defined by the stoichiometry of the successive melting reactions, given in Table 26.1. Figure 26.5 represents mineral proportions as a function of F ; mineral proportions may be expressed relative to the full system (Fig. 26.5a–b), or to the restite (m ; Fig. 26.5c–d). We are using the same trick as in Chap. 25, breaking down the plagioclase to its end-members to account for compositional changes of this phase during (multi-variant) melting.

Table 26.1 Stoichiometry of the successive melting reactions. Note that the sum of all reactants is equal to the sum of the products (closed-system behaviour)

	From	To	Reactants	Products
Mica-rich gneiss (MRG)				
Stage 1	$F = 0$	$F = 0.25$	0.32 Qtz + 0.42 Kfs + 0.26 Pl(An ₂₅) (+ H ₂ O)	1 Melt
Stage 2	$F = 0.26$	$F = 0.30$	0.5625 Qtz + 0.125 Pl(An ₂₅) + 0.125 Bt + 0.375 Sil	1 Melt + 0.1875 Crd
Stage 3	$F = 0.31$	$F = 0.75$	0.333 Qtz + 0.333 Pl(An ₂₅) + 0.333 Bt	1 Melt
Stage 4	$F = 0.76$	$F = 1$	0.17 Pl(An ₂₅) + 0.79 Bt + 0.04 Crd	1 Melt
Quartzo-feldspathic gneiss (QFG)				
Stage 1	$F = 0$	$F = 0.37$	0.34 Qtz + 0.30 Kfs + 0.36 Pl(An ₁₁) (+ H ₂ O)	1 Melt
Stage 2	$F = 0.38$	$F = 0.68$	0.49 Qtz + 0.51 Pl(An ₁₁) (+ H ₂ O)	1 Melt
Stage 3	$F = 0.69$	$F = 1$	0.53 Pl(An ₁₁) + 0.47 Bt	1 Melt

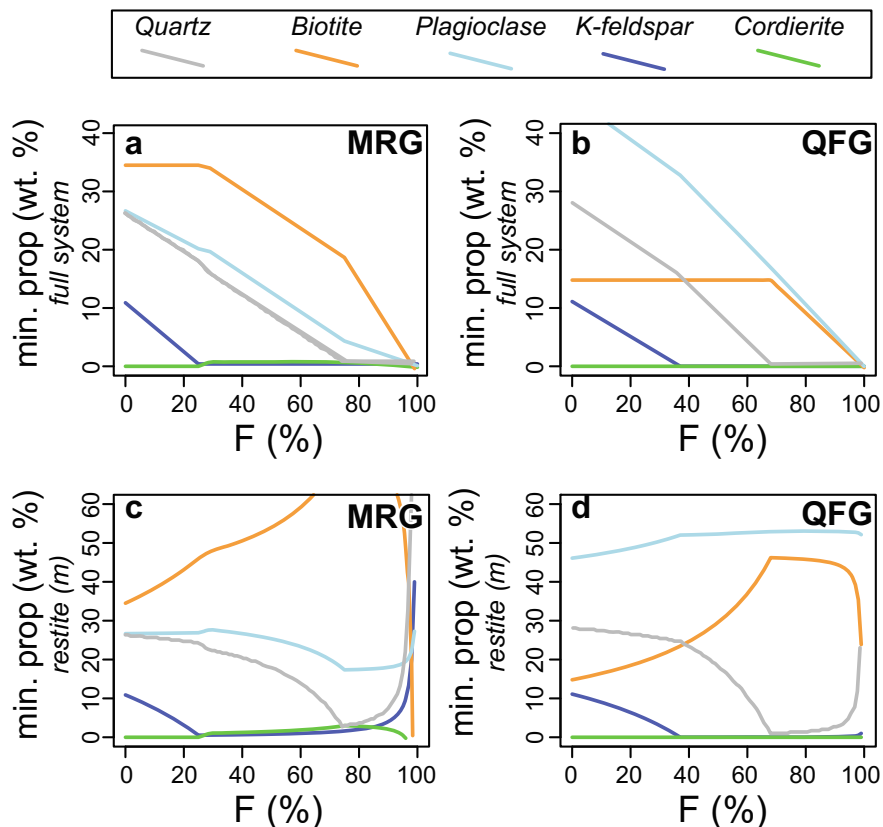


Fig. 26.5 Mineral proportions as a function of the degree of melting, for MRG (a and c) and QFG (b and d) compositions. Panels **a** and **b** show the proportions relative to the whole system (including melt): as F increases, the proportions of all reactant decrease, but the proportion of peritectic minerals (cordierite) rises. Panels **c** and **d** show the proportions in the restite (m), used for further calculations. Although the proportions of e.g. feldspars do decrease in absolute terms, as they are incorporated into the melt, for F values above ca. 80 % other minerals (biotite) get into the melt at a faster rate such that the relative amount of feldspar in the restite does increase.

For convenience, the stoichiometry of the melting reactions is defined in a datafile. The first line contains the original (pre-melting) mode, and each subsequent one corresponds to one melting stage with its stoichiometric coefficients (negative for reactants and positive for products), normalized to 100 units of melt. Column F_{\max} represents the maximum value of F for the given stage.



stmalo_stc_mrg.data
stmalo_stc_qfg.data

We define a function that would calculate the mode of the system for each melt increment, as a function of the initial mode, the stoichiometry of the reaction and the degree of melting (F). As long as the stoichiometric coefficients remain constant, this can be calculated relative to the original mode m_0 . For this calculation we treat the melt fraction as a “mineral” phase:

```
GCDkit-> mins <- c("Qtz", "Kfs", "Ab", "An", "Bt", "Sil", "Crd")
GCDkit-> mm <- c(mins, "Melt")
GCDkit-> melt.mode <- function(m0, stc, ff) {
GCDkit->     m <- m0[mm]+ff/100*stc[mm]
GCDkit->     return(m)
GCDkit-> }
```

For the mica-rich gneiss (MRG) for instance, we load the file and prepare the data:

```
GCDkit-> stc.tab <- read.table("stmalo_stc_mrg.data", sep="\t")
GCDkit-> stc.tab <- as.matrix(stc.tab)
```

Next, we are looking for the mode of the residue for each 1% melt increment; this corresponds to several successive stages of melting with different melting reactions. We must, therefore, cycle first through each stage (this will be done using a `for` loop) and then for each melting increment (for this purpose we shall use the function `sapply`, as we have done in Chap. 25). Each stage corresponds to one line of `stc.tab` (2 to 5, in the case of composition MRG). The number of melt increments within a stage is given by the difference between F_{\max} for this stage, and F_{\max} at the end of the previous stage; for this purpose we generate a vector `f.r` with values ranging from 1 to the required number of elements (melt increments).

We first initialize a matrix `res` (to the pre-melting mode). We need `drop=F` because `res` must be a one-row matrix and not a vector, otherwise we cannot extract the subset `res[nrow(res), mm]` below.

```
GCDkit-> res <- stc.tab["m0", mm, drop=F] # initialize res
```

Then we loop through each stage, updating `res` before moving on:

```
GCDkit-> for(i in 2:5){ # corresponding to lines of stc.tab
GCDkit->     f.r <- seq(1, stc.tab[i, "Fmax"]-stc.tab[i-1, "Fmax"], 1)
GCDkit->     stc <- stc.tab[i, mm]
GCDkit->     m0 <- res[nrow(res), mm] # The last line of prev stage
GCDkit->     ee <- t(sapply(f.r, FUN=function(z) {
GCDkit->         melt.mode(m0, stc, z)
GCDkit->     }))
GCDkit->     res <- rbind(res, ee) # update res before the next step
GCDkit-> }
```

It is convenient to also have the values of the total Pl amount stored in `res`:

```
GCDkit-> Pl <- res[, "Ab"]+res[, "An"]
GCDkit-> mode.mrg <- cbind(res, Pl)
```

In the same way, we generate `mode.qfg` for the QFG composition. The full code is supplied on the [Web page](#).

Plotting is done by first creating an empty graph; and then adding lines to it, e.g.:

```
GCDkit-> plot(1,1,ylim=c(0,40),xlim=c(0,100),pch="",xlab="F",
+           ylab="min. prop. in full system")
GCDkit-> lines(mode.mrg[, "Melt"],mode.mrg[, "Qtz"],lwd=1.5,col="grey")
GCDkit-> lines(mode.mrg[, "Melt"],mode.mrg[, "Kfs"],lwd=1.5,col="blue")
Etc. # Fig. 26.5a
```

In the case of the plots showing proportions in the residue, we must normalize to the bulk rock (i.e. divide by $1-F$):

```
GCDkit-> plot(1,1,ylim=c(0,60),xlim=c(0,100),pch="",xlab="F",
+           ylab="min. prop. in residue (m)")
GCDkit-> lines(mode.mrg[, "Melt"],mode.mrg[, "Qtz"]/
+           (100-mode.mrg[, "Melt"])*100,lwd=1.5,col="grey")
Etc. # Fig. 26.5c
```

26.3.2 Major and Trace Elements

Given the composition of the source (C_0), the mode of the restite (m), the melt fraction (F) and mineral compositions for relevant solid phases, it is possible to calculate the major-element composition of the melt using mass-balance. The additional knowledge of partition coefficients allows calculating its trace-element composition as well.



Partition coefficients varying as a function of plagioclase composition

Separating plagioclase into albite and anorthite may allow using different partition coefficients for each end-member: by changing the relative proportions of these components, we could obtain K_D varying as a function of the plagioclase composition.



[stmalo_mins.data](#)
[stmalo_kd.data](#)

For this purpose, we will use the function `fwd.mod` defined in Chap. 25 as:

```
fwd.mod <- function(c0.lab,m,ff,norm=F,eqn="FC") {...
```

Thus demonstrating the versatility of our function and the way we can re-use our previous work! We first prepare the required data:

```
GCDkit-> min.tab <- read.table("stmalo_mins.data",sep="\t")
GCDkit-> kd.tab <- read.table("stmalo_kd.data",sep="\t")
GCDkit-> mjrs <- c("SiO2","Al2O3","Fe2O3","MgO","CaO","Na2O","K2O",
+               "TiO2")
GCDkit-> trc <- c("Rb","Sr","Zr","Ni","Cr","V")
```

We will then apply the function `fwd.mod` to each line of the matrix `mode.mrg` containing the modal proportions:

```
GCDkit-> c0.lab <- "MRG"
GCDkit-> melts.mrg <- t(apply(mode.mrg,1,function(z){
GCDkit->     m <- z[mins]/(100-z["Melt"])
GCDkit->     ff <- z["Melt"]/100
GCDkit->     ee <- fwd.mod(c0.lab,m,ff,eqn="PM")$cL
GCDkit->     return(ee)
GCDkit-> })))
```

We do the same for QFG, and plot our model on top of the data (Fig. 26.6). The full code is supplied on the [Web page](#).

Figure 26.6 shows that, both for major and trace elements (except Zr), the compositions of the leucosomes evolve in a restricted band, limited by the models calculated by the end-member compositions MRG and QFG. Such behaviour leads to the conclusion that the scatter in leucosome compositions reflects the source heterogeneity and that partial melting of the Saint-Malo gneisses perfectly accounts for the leucosome compositions.

In this case, the main process shaping the chemistry is the evolution of the restite mode during melting. It is constrained by experimental data, with the numbers tweaked to get a consistent evolution (i.e. such that the mode of each phase ends up at 0 for $F = 1$). This is the most critical parameter and time-consuming part of the modelling exercise. The interested reader may investigate (by editing the files `stmalo_stc_qfg.data` and `stmalo_stc_mrg.data`) the effects of various melting models on the composition of the liquids. It turns out that it is fairly difficult to propose a series of stoichiometric coefficients that (i) are realistic with regard to what we know about melting reactions, (ii) are internally consistent, and (iii) lead to a decent fit between the model and the observations.

A model is set to answer a specific question. In this case it has been “can progressive melting of QFG and MRG lithologies (with coefficients defined in Table 26.1) account for the observed leucosome compositions?”. The answer is “yes”.

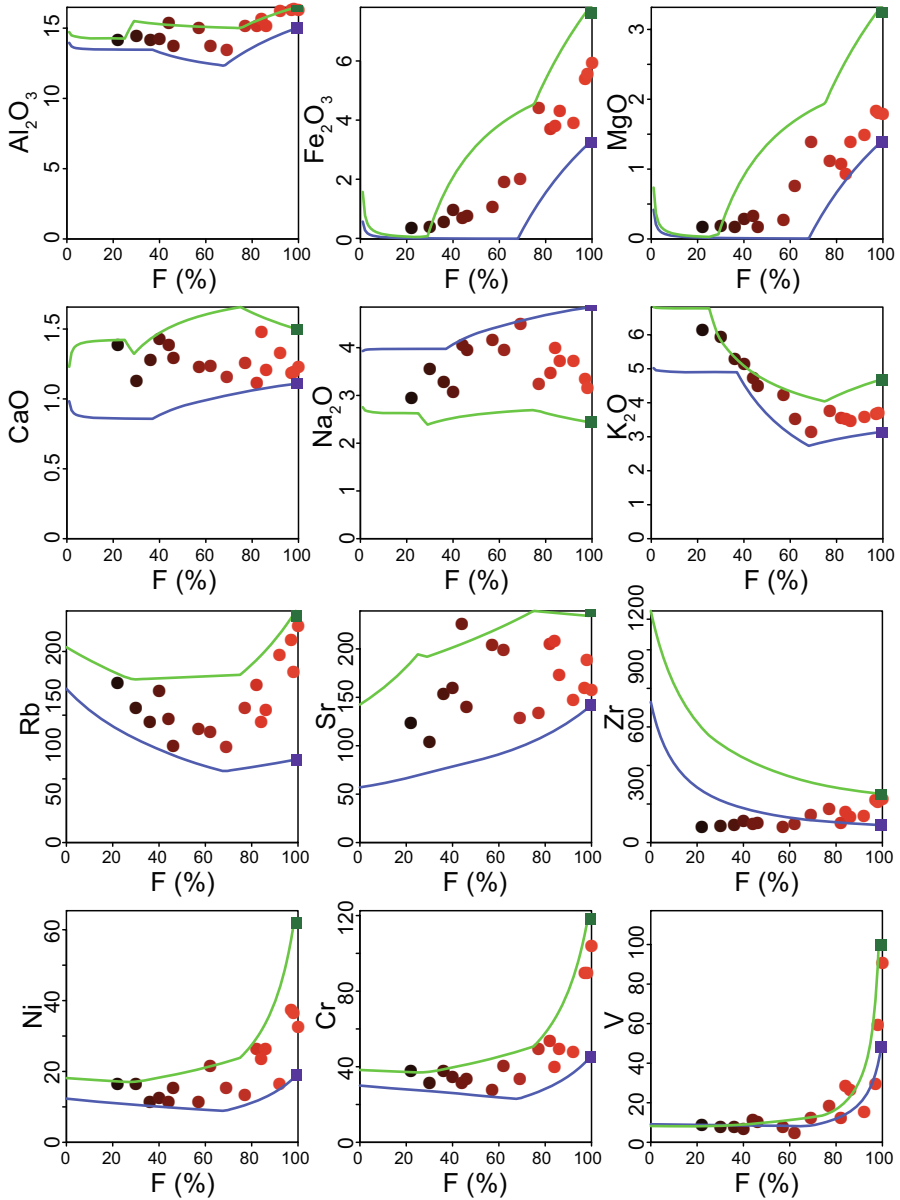


Fig. 26.6 Results of numerical modelling for both major and trace elements. The green curve corresponds to MRG source and the blue one to QFG. The squares show the C_0 values of these two sources.

26.3.3 Zircon

Again, Zr is the only element for which our model does not fit observations: we modelled it as an incompatible element, whereas it shows a compatible behaviour (Fig. 26.4). As shown in Exercise 22.1, several alternatives are available to deal with this problem. Whereas a saturation-based approach would be more rigorous, we add here, for simplicity, a small proportion of zircon to the restite with a set K_D of 3800.

The only difference from Chap. 25 is that in here, `mode.mrg` and `mode.qfg` do not store the mineral proportions in the cumulate (m), but in the whole system. Therefore we must recalculate the whole-system value corresponding to the desired m , by multiplying by $I-F$. We can then re-run the function `fwd.mod` to get the new C_L . All of this occurs in a function `melts.with.zrn` that requires arguments `c0.lab` (name of the composition to use for C_0), `litho.mode` (the matrix that contains the successive modes during melting) and `m.zrn` (the amount of zircon added, in wt. %). We must first change the list of minerals in the system (`mins2`), before defining the function:

```
GCDkit-> mins2 <- c(mins,"Zrn")
GCDkit-> melts.with.zrn <- function(c0.lab,litho.mode,m.zrn){
GCDkit->   Zrn <- m.zrn*(100-litho.mode[, "Melt"])/100
GCDkit->   corrected.mode <- cbind(litho.mode,Zrn)
GCDkit->   corrected.melt <- apply(corrected.mode,1,function(z){
GCDkit->     m <- z[mins2]/(100-z["Melt"])
GCDkit->     ff <- z["Melt"]/100
GCDkit->     ee <- fwd.mod(c0.lab,m,ff,eqn="PM")$cL
GCDkit->     return(ee)
GCDkit->   })
GCDkit->   corrected.melt <- t(corrected.melt)
GCDkit->   return(corrected.melt)
GCDkit-> }
```

To further refine our model, we compare the evolution for several zircon amounts:

```
GCDkit-> zr.props <- c(0.01,0.02,0.05,0.1,0.5,1)
```

And for each of those, we apply the function we just defined; for instance for composition MRG we calculate a matrix `zr.mrg` that contains the Zr contents of the melts as a function of F and the amount of zircon:

```
GCDkit-> zr.mrg<-sapply(zr.props,function(i){
GCDkit->   z <- melts.with.zrn("MRG",mode.mrg,i)
GCDkit->   return(z[, "Zr"])
GCDkit-> })
GCDkit-> colnames(zr.mrg) <- zr.props
```

We do the same for QFG, calculating the matrix `zr.qfg`.

The plotting routine that generates the plate shown in Fig. 26.7 is:

```
GCDkit-> multiplePerPage(6,nrow=2,ncol=3,title=NULL)
GCDkit-> for(i in 1:6){
GCDkit-> zr.added <- zr.props[i]
GCDkit->   screen(i)
GCDkit->   binary("Melt_frac*100","Zr",xmin=0,xmax=100,ymax=400,ymin=0,
+             xlab="F",main=paste("Zrn prop. =",zr.added,
+             "wt. %"),new=F)
GCDkit->   points(100,WR["MRG","Zr"],pch=15,cex=2,col="darkgreen")
GCDkit->   points(100,WR["QFG","Zr"],pch=15,cex=2,col="darkblue")
GCDkit->   lines(mode.mrg[,"Melt"],zr.mrg[i],lwd=1.5,col="green")
GCDkit->   lines(mode.qfg[,"Melt"],zr.qfg[i],lwd=1.5,col="blue")
GCDkit-> }
```

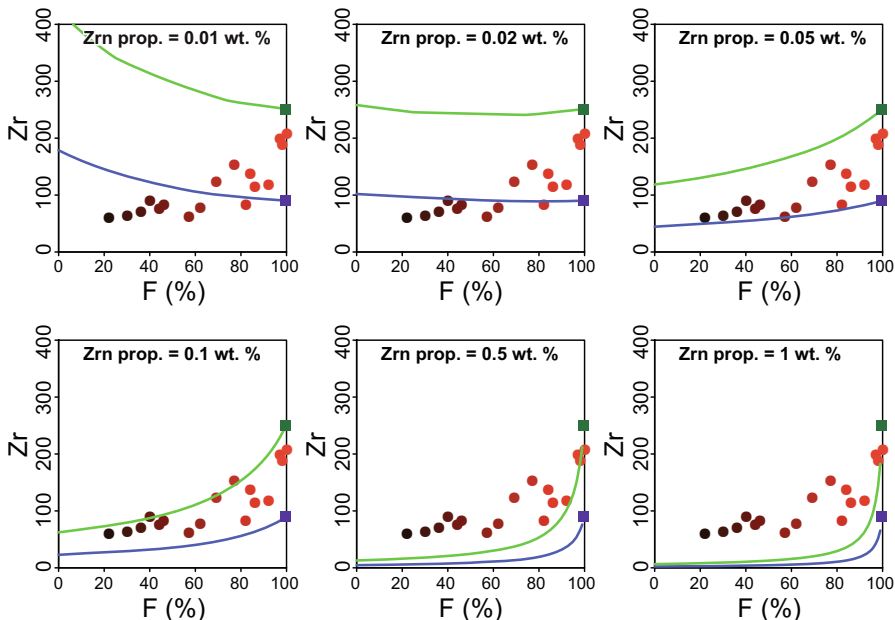


Fig. 26.7 Evolution of Zr concentrations in the melt, taking into account the role of zircon, for various values of m_{Zrn} . Values of about 0.05 to 0.1 wt. % give the best fits.

As expected, Fig. 26.7 shows that the simple expedient of adding a small amount of zircon (0.05 to 0.1 wt. %) to the restite is sufficient to alter the model so that it does fit the observed compositions.



An alternative approach using phase equilibria (pseudosections)

This example is amenable to a treatment using phase-equilibrium modelling, since we are dealing with melting of metasediments for which good thermodynamic models are available. Using the program PERPLE_X (Connolly 2005; www.perplex.ethz.ch) with mineral models mostly from Thermocalc (Powell and Holland 1988; White et al. 2001, 2007; Holland and Powell 2011)², we calculated P–T and T–X (X representing the H₂O content in the rock) pseudosections at 3.5 kbar for MRG and QFG compositions. The output gives the proportions and the composition of each phase, including melt. Phase proportions are plotted as a function of F in Fig. 26.8, for different scenarios regarding water availability. The melt compositions (for major elements) predicted by the model are presented in Fig. 26.9. Finally, trace-element compositions can be calculated in each case, using a batch melting equation, since we know C_0 (the trace-element composition of the source, MRG or QFG); F (the melt amount, calculated by PERPLE_X) and D , itself a function of the K_D and the mineral proportions m (from PERPLE_X). They are plotted also in Fig. 26.9. Figures 26.8–9 can be compared to Figs 26.5–6.

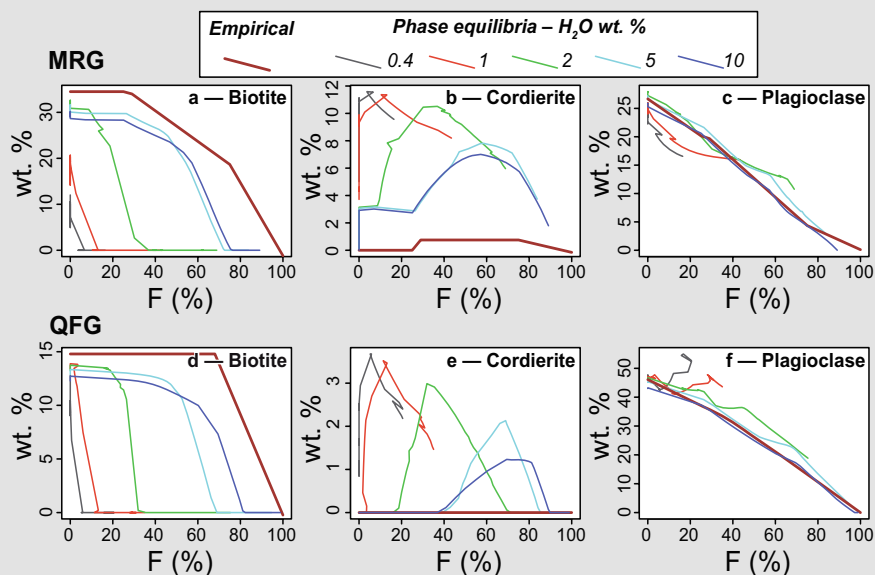


Fig. 26.8 Evolution of phase proportions for MRG (a–c) and QFG (e–f) compositions. The empirical model proposed here is the thick brown line, whereas the thinner lines are derived from phase-equilibrium modelling for various water contents (fully dry to 10 wt. % H₂O). Our empirical model resembles the water-saturated systems. Note however that the empirical model generally predicts more biotite, but less cordierite than phase equilibria; in the latter case, orthopyroxene (not shown) is also predicted as a peritectic mineral.

² Specifically the mineral models used are Bio(TCC), Opx(HP), Mica(CHA1), hCrd, feldspar, Gt(WPH), Ilm(WPH) and melt(HP) using PERPLE_X 6.6.8 and June 2013 datafiles.

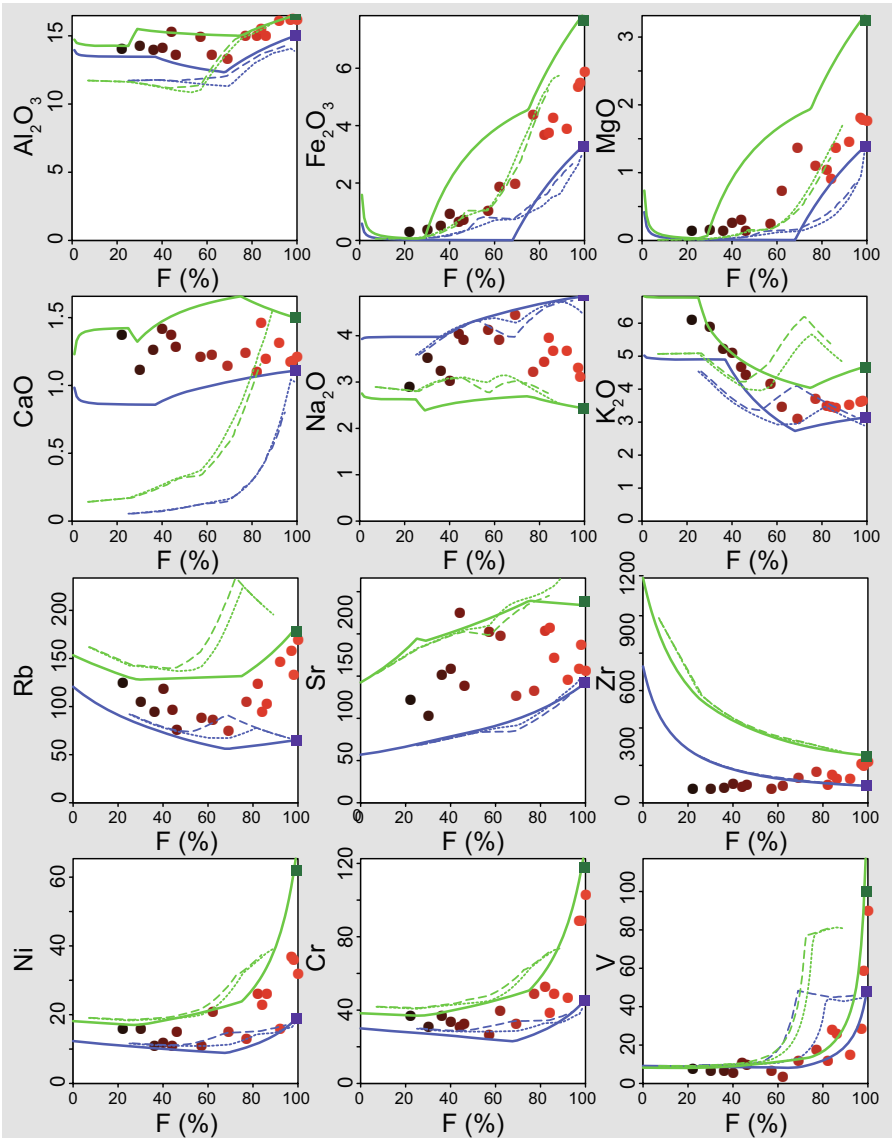


Fig. 26.9 Comparison of the chemical evolution in melt for empirical model (solid line) and as derived from phase-equilibrium modelling at water-saturated conditions (dashed and dotted lines, 5 and 10 wt. % H₂O respectively). Green are MRG and blue QFG compositions. The two approaches give comparable results, both providing a reasonable fit to the major-element data. The only significant difference is for CaO, where the phase equilibria predict contents much lower than the empirical approach. Possible explanations include that (i) the melt model used for phase-equilibria modelling is unable to deal properly with CaO or (ii) the leucosomes are enriched in CaO compared to actual melts (Nicoli et al. 2013; Taylor et al. 2014). For traces, the consistency between the two approaches is even better. The main difference appears for Rb, as a result of the increased biotite stability in the empirical compared to phase-equilibria modelling (cf. Fig. 26.8).

References

- Brown M (1979) The petrogenesis of the St. Malo migmatite belt, Armorican Massif, France, with particular reference to the diatexites. *Neu Jb Mineral, Abh* 135:48–74
- Brun J-P, Balé P (1990) Cadomian tectonics in Northern Brittany. In: D’Lemos RS, Strachan RA, Topley CG (eds) *The Cadomian Orogeny*. Geological Society of London Special Publications, vol 55, pp 95–114
- Brun JP, Martin H (1977) Relations métamorphisme-déformation au cours de l’évolution dynamique d’un dôme migmatitique: le Massif de Saint-Malo (France). *Bull Soc Géol France* 20:91–101
- Clemens JC, Vielzeuf D (1987) Constraints on melting and magma production in the crust. *Earth Planet Sci Lett* 86:287–306
- Connolly JAD (2005) Computation of phase equilibria by linear programming: a tool for geodynamic modeling and its application to subduction zone decarbonation. *Earth Planet Sci Lett* 236:524–541
- Holland TJB, Powell R (2011) An improved and extended internally consistent thermodynamic dataset for phases of petrological interest, involving a new equation of state for solids. *J Metamorph Geol* 29:333–383
- Martin H (1977) Contribution à l’étude de l’anatexie: le Massif de Saint-Malo (Massif armoricain). Mobilisation des éléments durant la fusion. Proposition d’un modèle. Unpublished PhD thesis, Université de Rennes I, Rennes
- Martin H (1979) Geochemical behaviour of major and trace elements during incongruent melting of biotite in the Saint-Malo migmatites. *Neu Jb Mineral, Mh* 509–524
- Martin H (1980) Comportement de quelques éléments en traces au cours de l’anatexie: exemple du Massif de Saint-Malo (Bretagne, France). *Can J Earth Sci* 17:927–941
- Nicoli G, Stevens G, Moyen J-F, Taylor J (2013) Leucosome formation by disequilibrium melting and melt loss: perspectives from the South Marginal Zone (SMZ) of the Limpopo Belt, South Africa. *Mineral Mag* 77:1846
- Peucat J-J (1986) Behavior of Rb–Sr whole rock and U–Pb zircon systems during partial melting as shown in migmatitic gneisses from the St-Malo Massif, N.E. Brittany, France. *J Geol Soc London* 143:875–886
- Peucat J-J, Martin H (1985) Are Rb–Sr thin slab migmatite ages meaningful? *Neu Jb Mineral, Abh* 152:1–21
- Powell R, Holland TJB (1988) An internally consistent thermodynamic dataset with uncertainties and correlations: 3. Applications to geobarometry, worked examples and a computer program. *J Metamorph Geol* 6:173–204
- Stevens G, Clemens J (1993) Fluid-absent melting and the roles of fluids in the lithosphere: a slanted summary? *Chem Geol* 108:1–17
- Taylor J, Nicoli G, Stevens G, Frei D, Moyen JF (2014) The processes that control leucosome compositions in metasedimentary granulites: perspectives from the Southern Marginal Zone migmatites, Limpopo Belt, South Africa. *J Metamorph Geol* 32:713–742
- Weber C, Barbey P, Cuney M, Martin H (1985) Trace element behaviour during migmatization. Evidence for a complex melt–residuum fluid interaction in the St-Malo migmatitic dome (France). *Contrib Mineral Petrol* 90:52–62
- White RW, Powell R, Holland TJB (2001) Calculation of partial melting equilibria in the system CaO–Na₂O–K₂O–FeO–MgO–Al₂O₃–SiO₂–H₂O (CNKFMASH). *J Metamorph Geol* 19:139–153
- White RW, Powell R, Holland T (2007) Progress relating to calculation of partial melting equilibria for metapelites. *J Metamorph Geol* 25:511–527

Appendix A

R Syntax in a Nutshell

Here we give an overview of the syntax and basic usage of the R language. We describe how to start and stop an R session, obtain help and find documentation. An account of the main object types and their manipulation in direct (i.e. command line) mode is followed by text on arguably the strongest point—graphics. The Appendix is closed by a section on writing true R programs (batch mode). The text is partly based on the pdf file ‘*An Introduction to R*’, available from the *Help* menu.

This text does not intend to be a replacement for a proper R course. Apart from the help system and pdf manuals included with the R distribution, the reader can find additional information in an increasing number of books and web sites.

Importantly, information concerning the current state of the R project, binaries, source codes and documentation are obtainable from the dedicated website (www.r-project.org) and the Comprehensive R Archive Network (CRAN, cran.r-project.org). CRAN, which is mirrored at many servers worldwide, also provides a distribution channel for user-contributed packages that add new functionality to the core of the R system.

Chapter 1

Direct Mode

1.1 Basic Operations

1.1.1 Starting and Terminating the R Session

In Windows, double clicking the file *RGUI.EXE* or the associated shortcut opens the “*R Console*”, a text window for the entry of commands and display of textual output (Fig. A1.1). The system prints a number of messages, the most important of which is the last line with a prompt, showing that the R environment is awaiting commands. Apart from the *R Console*, one or more windows for graphical output and help pages may be displayed.

To end an R session, one can invoke the menu item *File|Exit* or type `q()`. Alternatively, one can terminate the session by closing the *R Console* window.¹

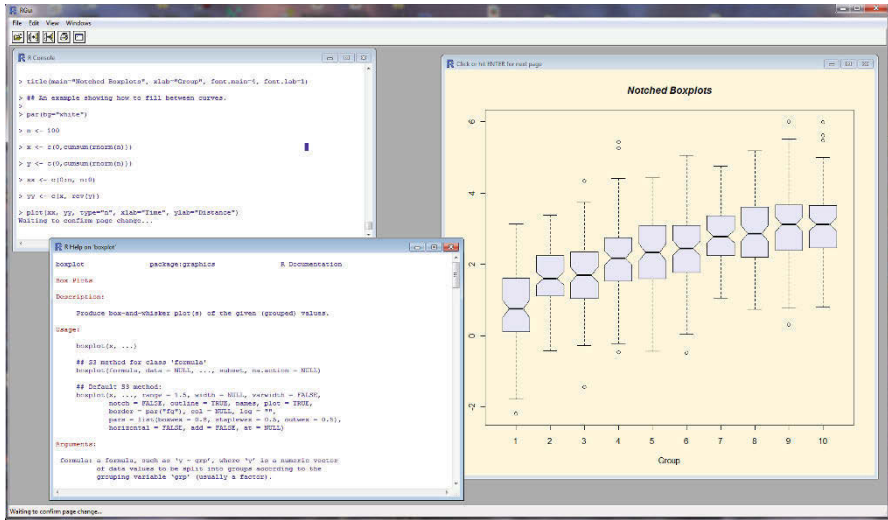


Fig. A1.1 Screenshot of a typical R session.

1.1.2 Seeking Help and Documentation

The R environment provides help in several forms—including plain text (displayed in the Console) or HTML (viewed using a web browser).

```

> help(plot) # text help on a function called 'plot'
> ?plot      # equivalent, a shortcut

```

Commands related to 'plot':

```

> apropos(plot)

```

Examples of correct usage of 'plot':

```

> example(plot)

```

An HTML browsable help window can be obtained from the menu option *Help|R language (html)* or by:

```

> help.start()

```

¹Note that the system may ask you, upon closing, whether you want to save the current workspace (i.e., memory image with all the variables). For beginners probably the best option is 'No', ensuring that the R environment starts afresh the next time.

R is distributed together with PDF documents, which can be invoked from the menu item *Help|Manuals*. There are several documents available, including ‘Writing R Extensions’, ‘R Data Import/Export’, ‘The R Language Definition’ and ‘R Installation and Administration’. At this stage the most appropriate will be ‘An Introduction to R’ which outlines the basics of the R language.

Other good sources of information are the many books about R (e.g., Maindonald and Braun 2003; Murrell 2005; Crawley 2007; Chambers 2009; Adler 2012; van den Bogaard and Tolosana-Delgado 2013), or the related S language (Becker et al. 1988; Chambers and Hastie 1992; Chambers 1998) as the two languages share most of their syntax. CRAN contains a list of published monographs (www.r-project.org/doc/bib/R-books.html) as well as links to numerous contributed documents or manuals, both general and specific. The R Journal, an open-access refereed journal, features short to medium length articles on various R applications, R programming and add-on packages. The community meets at annual useR! conferences. Moreover, there exist e-mail discussion groups dedicated to help users (*R-help*), to announce new versions and further progress in the R project (*R-announce*, *R-packages*) and to facilitate communication among developers (*R-devel*). Further information, including the archive of the e-mail discussion groups, is available on CRAN.

Lastly, there exist numerous blogs dedicated to the R project, most of them accessible from the R-bloggers web page, www.r-bloggers.com. A useful starting point to search for a topic is RSeek, www.rseek.org.

1.2 Fundamental Objects of the R Language

1.2.1 Commands

The R environment can be utilized in **direct mode**, typing commands straight into the *Console* and getting an immediate response. Alternatively, the whole R code can be prepared in advance as a plain text file and run at once in **batch mode**. The commands (functions) in R are entered either individually, each on a single line, or are separated by a semicolon (;). More complex statements consisting of several lines of code are enclosed in braces {}. Each command is followed by brackets with parameters (or empty, if none are required or default values are desired). Typing just the command name returns a listing of the function’s definition.



The R language is case sensitive. Commands are typed in lowercase and the environment distinguishes between lower and upper case letters in variable names. The latter cannot start with a digit and may contain any symbols apart from the hash mark (“#”). Note however that it is not wise to use, for instance, accented characters.

It is also important to note that several words are reserved by the system and cannot be used as variable names. For details, see `?Reserved`.

Direct Mode

In the simplest case, commands are entered and the result displayed:

```
> (15+6)*3
[1] 63
```

The numerical values can be assigned to a named variable. Perhaps confusingly, R does not use “=” as an assignment operator. Instead, an arrow “<-” is implemented, corresponding to a combination of “<” (less than) and “-” (minus) characters²:

```
x <- 5
```

In direct mode, the content of a variable is displayed by typing its name:

```
x
[1] 5
```

If an incomplete command is entered, R displays a prompt “+” giving the opportunity to add what is needed.

```
> (15+6
+ ) * 3
[1] 63
```

The R environment automatically records a command history. The previous commands can be recalled using the vertical arrow keys, edited and re-used, as desired. The history can be displayed by the namesake function:

```
history()
```

Batch Mode

A sequence of R commands or program can also be prepared beforehand in the form of a plain text file. This can be written by any editor ranging from *Notepad*, to more sophisticated word processors. In the latter case the file may need to be exported as Plain/*ASCII* text. However, the most useful seem to be text editors designed especially for programmers as they often provide extra functionality such as line numbering, syntax checking/highlighting and brackets matching (*WinEdt*, *Tinn-R*, *Notepad++*, etc.)

Commonly used suffixes for R program scripts are “*r*” or “*R*”. The script can be run from the menu *File|Source R code* or using the command `source`:

```
> source("myprogram.r")3
```

The program can be stopped by pressing the `ESC` key or from the menu *Misc|Stop current computation*. Optional comments start with a hash mark:

```
> # My comment
```

² In fact the “=” also works as an assignment operator, however it is considered to degrade the code readability. We prefer using the arrow notation throughout the book.

³ Assuming that the code resides in the current working directory; otherwise the full path needs to be specified or directory changed.



Note that in batch mode the content of a variable must be displayed using the commands `print` or `cat` (this Appendix, Chap. 3.1). Unlike in direct mode, typing the mere variable name does not suffice here.

```
> e <- 1.602
> print(e)
[1] 1.602
```

The usage of batch mode (and graphical capabilities) of R is best demonstrated by running some built-in demos, such as:

```
> demo(graphics)
> demo(image)
```

1.2.2 Handling Objects in Memory

R stores data using a variety of **object types** including vectors, arrays, matrices (two-dimensional arrays), factors, data frames, lists and functions (Table A1.1). To display the current list of user objects, use the menu *Misc|List objects* or:

```
> ls()
```

Unnecessary objects can be removed with the function `rm`:

```
> rm(x, y, junk)
```

All user R objects can be deleted using the menu item *Misc|Remove all objects*.

Table A1.1 Overview of the most important object types in the R language

Object	Characteristics	Possible modes	Can have several modes?
Vector	one-dimensional collection of elements	numeric, character, complex, logical	No
Factor	each element is set to one of several discrete values, or levels (a categorical variable)	numeric, character	No
Array	multidimensional collection of elements	numeric, character, complex, logical	No
Matrix	two-dimensional array	numeric, character, complex, logical	No
Data frame	like a matrix but every column can be of a different mode	numeric, character, complex, logical	Yes
List	consists of an ordered collection of objects (components) that can be of various modes (recursive, i.e. list can itself consist of lists)	numeric, character, complex, logical, function, expression, formula	Yes
Function	fundamental piece of code, typically dedicated to a single task, with defined input parameters (arguments) and output values	–	–

All the objects are stored in memory, and not automatically saved to disc. When quitting the R environment, you are given the opportunity to save the current workspace, i.e. all the objects created during the given session. If you accept, they are written to a file `.RData` in the current directory and reloaded automatically the next time R is started. Different R sessions may therefore be maintained in separate directories.

1.2.3 *Attributes to Objects*

Every object possesses several properties, called attributes. The two most important of these are *length* and *mode*. Some object types, or in R jargon **classes**, can have more **modes**. For the given object, the mode (logical, numeric, complex or character) can be displayed using the namesake function:

```
> mode(10)
[1] "numeric"
```

1.3 Numeric Vectors

1.3.1 *Assignment*

Assignment of several items to a vector is done using the combine function *c*:

```
> x <- c(10.4, 5.6, 3.1, 6.4, 21.7)
> y <- c(x, 0, x)
> y
[1] 10.4 5.6 3.1 6.4 21.7 0.0 10.4 5.6 3.1 6.4 21.7
```

1.3.2 *Vector Arithmetic*

For vectors, calculations are made using basic arithmetic operators: `+` `-` `*` `/` `^`. The use of these operators for two vectors of the same length is intuitive. In other cases, the elements of the shorter vector are recycled as often as necessary. For instance, for the `x` vector defined above, we can calculate:

```
> x*2
[1] 20.8 11.2 6.2 12.8 43.4
> x*c(1,2)
[1] 10.4 11.2 3.1 12.8 21.74
```

1.3.3 Names

Each vector may have an attribute `names` (the lengths of the vector itself and its names must be matching!). For instance:

```
> x <- c(3,15,27)
> names(x) <- c("Op $x$ ", "Cp $x$ ", "P1")
> x
Op $x$  Cp $x$  P1
 3 15 27
```

1.3.4 Generating Regular Sequences

Regular sequences with step 1 or -1 can be generated using the colon operator ("`:`"). It has the highest priority within an expression, higher than the other operators (`+*`/`^`).

```
> 1:9
[1] 1 2 3 4 5 6 7 8 9
> 9:1
[1] 9 8 7 6 5 4 3 2 1
> 1:9*2
[1] 2 4 6 8 10 12 14 16 18
> 1:(9*2)
[1] 1 2 3 4 5 6 7 8 9 10 11 12 13 14 15 16 17 18
```

seq(from, to, by)

Yields a sequence of numbers with an arbitrary step (`by`):

```
> seq(30,22,-2)
[1] 30 28 26 24 22
```

rep(x, times)

Repeats the argument `x` specified a number of `times`:

```
> x <- c(3,9)
> rep(x,5)
[1] 3 9 3 9 3 9 3 9 3 9
```

⁴ NB that this is not a dot (scalar) product, but simply a result of an element-wise multiplication.

1.3.5 Functions to Manipulate Numeric Vectors

The R language contains a number of functions. Only those most important for manipulation of numeric vectors are presented in Table A1.2. Information about others and the whole range of available parameters can be found in the R documentation.

Table A1.2 Basic functions for numeric vectors manipulation

Function	Explanation
<code>abs(x)</code>	absolute value
<code>sqrt(x)</code>	square root
<code>log(x)</code>	natural logarithm
<code>log10(x)</code>	common (base 10) logarithm
<code>log(x, base)</code>	logarithm of the given base
<code>exp(x)</code>	exponential function
<code>sin(x)</code>	
<code>cos(x)</code>	trigonometric functions
<code>tan(x)</code>	
<code>min(x)</code>	minimum
<code>max(x)</code>	maximum
<code>which.min(x)</code>	index of the minimal element of a vector
<code>which.max(x)</code>	index of the maximal element of a vector
<code>range(x)</code>	range of elements in x ; equals to $c(\min(x), \max(x))$
<code>length(x)</code>	number of elements (= length) of a vector
<code>rev(x)</code>	reverses the order of elements in a vector
<code>sort(x)</code>	sorts elements of a vector (ascending)
<code>rev(sort(x))</code>	sorts elements of a vector (descending)
<code>round(x, n)</code>	rounds elements of a vector to n decimal places
<code>sum(x)</code>	sum of the elements of a vector
<code>mean(x)</code>	mean of the elements of a vector
<code>prod(x)</code>	product of the elements of a vector

1.4 Character Vectors

Character vectors are collections of text strings, i.e. sequences of characters delimited by the double quote symbol, e.g., "granite". They use `\` – backslash as the escape sequence for special characters, including `"\t"` – tab and `"\n"` – new line.

paste(x, y, ..., sep="")

Merges two (or more) character vectors, one by one, the elements being separated by string `sep`:

```
> paste("Gabbro", "olivine and", "pyroxene", sep=" with ")
[1] "Gabbro with olivine and with pyroxene"
```

substring(x, start, stop)

Extracts a part of vector `x` starting at position `first` and ending at `last`:

```
> x <- c("Plagioclase", "Biotite", "Muscovite")
> substring(x, 1, 4)
[1] "Plag" "Biot" "Musc"
```

strsplit(x, split)

Splits the strings in `x` into substrings based on the presence of `split`. Returns a list (see this Appendix, Chapter 1.8):

```
> x <- c("Plagioclase", "K-feldspar")
> strsplit(x, "a")
[[1]]
[1] "Pl" "giocl" "se"

[[2]]
[1] "K-feldsp" "r"
```

1.5 Logical Vectors

Logical vectors consist of elements that can attain only two logical values: TRUE or FALSE. These can be abbreviated as T and F, respectively.



In the R language, the symbol name `F` is reserved as an abbreviation for logical FALSE. For this reason, it is not advisable to name any variable `F`. The same applies, of course, to `T`.

1.5.1 Logical Operators

The logical vectors are typically produced by comparisons using operators `<` (smaller than) `<=` (smaller or equal to) `>` (greater than) `>=` (greater or equal to) `==` (equals to) `!=` (does not equal to). For instance:

```
> x <- c(1, 12, 15, 16, 13, 0)
> x > 13
[1] FALSE FALSE TRUE TRUE FALSE FALSE
```

The result can be assigned to a vector of the mode `logical`:

```
> temp <- x>13
> temp
[1] FALSE FALSE TRUE TRUE FALSE FALSE
```

Boolean arithmetic combines two or more logical conditions using the logical operators: `and(&)`, `or(|)`, `not(!)` with or without brackets:

```
> x <- c(1,12,15,16,13,0)
> c1 <- x>10
> c2 <- x<15
> c1
[1] FALSE TRUE TRUE TRUE TRUE FALSE
> c2
[1] TRUE TRUE FALSE FALSE TRUE TRUE
> c1 & c2 # logical "and"
[1] FALSE TRUE FALSE FALSE TRUE FALSE
> c1 | c2 # logical "or"
[1] TRUE TRUE TRUE TRUE TRUE TRUE
> !c1 # negation
[1] TRUE FALSE FALSE FALSE FALSE TRUE
```

1.5.2 Missing Values (NA, NaN)

Within R, missing data are represented by a special value `NA` (not available). Some operations which give no meaningful result in the circumstances will return its special form, `NaN` (not a number):

```
> sqrt(-15)
[1] NaN
```

Moreover, division by zero gives $+\infty$ (`Inf`).

```
> 1/0
[1] Inf
```

is.na(x)

Tests for the presence of missing values in each of the elements of the vector `x`:

```
> x <- c(5,9,-4,12,-6,-7)
> is.na(sqrt(x))
[1] FALSE FALSE TRUE FALSE TRUE TRUE
```

1.6 Arrays, Matrices, Data Frames

Several kinds of table-like objects exist in R. *Data frames* are data objects to be processed by statistics, with “observations” as columns (elements/oxides in geo-

chemistry) and “cases” (samples) in rows. They can contain columns of any mode, even mixed modes; thus they are not intended for matrix operations.

For such purpose, *matrices* should be used. All elements of a matrix can only be of a single mode (numeric, most commonly). Arrays are generalized matrices: they must have a single mode but can have any number of dimensions. Although superficially similar, these three types of objects must not be confused.



Depending on the exact content of the file, many file reading operations (such as `read.table`) would generate a data frame: it is the user’s responsibility to convert it to a matrix if it is to be used later for calculations.

matrix(data = NA, nrow = 1, ncol = 1, byrow = FALSE)

This command defines a matrix of `nrow` rows and `ncol` columns, filled by the `data` (if `data` has several elements, they will be used down columns, unless an extra parameter `byrow=TRUE` is provided). For instance:

```
> x <- matrix(1:12,3,4)
> x
      [,1] [,2] [,3] [,4]
[1,]    1    4    7   10
[2,]    2    5    8   11
[3,]    3    6    9   12

> x <- matrix(1:12,3,4,byrow=TRUE)
> x
      [,1] [,2] [,3] [,4]
[1,]    1    2    3    4
[2,]    5    6    7    8
[3,]    9   10   11   12
```



The default behaviour for filling a matrix with data—as well as matrix division by a vector—proceeds along columns, not rows!

array(data = NA, dim = length(data))

Defines a new data array and fills it with `data`. The argument `dim` is a vector of length one or more, giving maximal dimensions in each of the directions.

1.6.1 Matrix/Data Frame Operations

Matrices can be subject to scalar operations using the common operators (`+-*/^`). Similar to vectors, the shorter component is recycled as appropriate. Useful functions for matrix/data frame manipulations are summarized in Table A1.3.

Table A1.3 Basic matrix/dataframe-related functions

Function	Explanation
<code>nrow(x)</code>	number of rows
<code>ncol(x)</code>	number of columns
<code>rownames(x)</code>	row names
<code>colnames(x)</code>	column names
<code>rbind(x, y)</code>	binds two objects (matrices or data frames) of the same <code>ncol</code> (or vectors of the same length) as rows
<code>cbind(x, y)</code>	binds two objects (matrices or data frames) of the same <code>nrow</code> (or vectors of the same length) as columns
<code>t(x)</code>	transposition
<code>apply(X, MARGIN, FUN)</code>	applies function <code>FUN</code> (for vector manipulations) along the rows (<code>MARGIN = 1</code>) or columns (<code>MARGIN = 2</code>) of a data matrix <code>X</code>
<code>x%*%y</code>	matrix multiplication (does not work on data frame!)
<code>solve(A)</code>	matrix inversion (see Appendix C)
<code>dix(x)</code>	diagonal elements of a matrix

It is worth noting that matrix multiplication is performed using the `%*%` operator. Of the functions presented in the table, some explanation is required for `apply`:

apply(X, MARGIN, FUN, ...)

If `X` is a matrix, it is split into vectors along rows (if `MARGIN = 1`) or columns (if `MARGIN = 2`). To each of these vectors is applied the function `FUN` with optional parameters... passed to it.

For instance, we can calculate row sums of a matrix:

```
> x <- matrix(1:12, 3, 4, byrow=TRUE)
> apply(x, 1, sum)
[1] 10 26 42
```

1.7 Indexing/Subsetting of Vectors, Arrays and Data Frames

In real life, one often needs to select some elements of a vector or a matrix, fulfilling certain criteria. This data selection functionality can be achieved using logical conditions or logical variables placed in square brackets after the defined object name. Subsets can be also used on the left hand side of the assignments when replacement of selected elements by certain values is desired.

1.7.1 Vectors

Subsets of a vector may be selected by appending to the name of the vector an index vector in square brackets. For example, first create a named vector:

```
> x <- c(1,12,15,NA,16,13,0,NA,NA)
> names(x) <- c("Pl", "Bt", "Mu", "Q", "Kfs", "Ky", "Ol", "Px", "C")
> x
Pl Bt Mu Q Kfs Ky Ol Px C
 1 12 15 NA 16 13 0 NA NA
```

Index vectors can be of several types: logical, numeric (with positive or negative values), and character:

1. Logical vector

```
> x[x>10] # all elements of x higher than 10 (or NA)
Bt Mu <NA> Kfs Ky <NA> <NA>
12 15 NA 16 13 NA NA
> x[!is.na(x)] # all elements of x that are available
Pl Bt Mu Kfs Ky Ol
 1 12 15 16 13 0
```

2. Numeric vector with positive values

```
> x[1:5] # the first five elements
Pl Bt Mu Q Kfs
 1 12 15 NA 16
> x[c(1,5,7)] # 1st, 5th and 7th elements
Pl Kfs Ol
 1 16 0
```

3. Numeric vector with negative values (specifies elements to be excluded)

```
> x[-(1:5)] # all elements except for the first five
Ky Ol Px C
13 0 NA NA
```

4. Character vector (referring to the element names)

```
> x[c("Q", "Bt", "Mu")]
Q Bt Mu
NA 12 15
```

1.7.2 Matrices/Data Frames

Elements of a matrix are presented in the order [row, column]. If nothing is given for a row or column, it means no restriction. For instance:

```
> x[1,] # (all columns) of the first row
> x[,c(1,3)] # (all rows) of the first and third columns
> x[1:3,-2] # all columns (apart from the 2nd) of rows 1-3
```

If the result is a single row or column, it is automatically converted to a vector. To prevent such a behaviour, one can supply an optional parameter `drop=F`, e.g.:

```
> x[1,,drop=F] # (all columns) of the 1st row, keep as matrix
```

Moreover, matrices can be manipulated using index arrays. This concept is best explained on an example. Let's assume a matrix defined as:

```
> x <- matrix(1:20,4,5)
```

If the elements `[1,3]`, `[2,2]` and `[3,1]` in `x` are to be replaced by zeroes, create an index array `i` containing the elements' coordinates:

```
> i <- matrix(c(1,2,3,3,2,1),3,2)
```

```
> i
```

```
      [,1] [,2]
[1,]    1    3
[2,]    2    2
[3,]    3    1
```

```
> x[i]
```

```
[1] 9 6 3
```

```
> x[i] <- 0
```

```
> x
```

```
      [,1] [,2] [,3] [,4] [,5]
[1,]    1    5    0   13   17
[2,]    2    0   10   14   18
[3,]    0    7   11   15   19
[4,]    4    8   12   16   20
```

The situation for multidimensional arrays is analogous—just the appropriate number of dimensions is higher.

1.8 Lists

Lists are ordered collections of other objects, known as components, which do not have to be of the same mode or type. Thus lists can be viewed as very loose groupings of R objects, involving various types of vectors, data frames, arrays, functions and even other lists. Components are numbered and hence can be addressed using their sequence number given in double square brackets, `x[[3]]`. Moreover, components may be named and referenced using an expression of the form `list_name$component_name`. Subsetting is similar to that of other objects, described above.

```
list.name <- list(component_name_1=, component_name_2=...)
```

Builds a list with the given components.

Here is a simple real-life example of a list definition:

```
> x1 <- c("Luckovice", "9 km E of Blatna", "disused quarry")
> x2 <- "melamonzonite"
> x3 <- c(47.31, 1.05, 14.94, 7.01, 8.46, 10.33)
> names(x3) <- c("SiO2", "TiO2", "Al2O3", "FeO", "MgO", "CaO")
> luckovice <- list(ID="Gbl-4", Locality=x1, Rock=x2, major=x3)
> luckovice
$ID
[1] "Gbl-4"
$Locality
[1] "Luckovice" "9 km E of Blatna" "disused quarry"
$Rock
[1] "melamonzonite"
$major
  SiO2 TiO2 Al2O3 Fe2O3   FeO  MgO  CaO
47.31  1.05 14.94  2.23  7.01  8.46 10.33
```

As well as some examples of subsetting:

```
> luckovice[[1]]
[1] "Gbl-4"

> luckovice$Rock # or luckovice[[3]]
[1] "melamonzonite"

> luckovice[[2]][3]
[1] "disused quarry"

> luckovice$major[c("SiO2", "Al2O3")]
  SiO2 Al2O3
47.31 14.94
```

1.9 Coercion of Individual Object Types

R is generally reasonably good at dealing seamlessly with data types, converting them on the fly when needed and being able to use the same operators on different data types. When necessary, there are a series of functions for testing the mode or type of an object:

is.numeric(x), **is.character(x)**, **is.logical(x)**, **is.matrix(x)**, **is.data.frame(x)**

At times there is a need to explicitly convert between data types/modes using functions such as:

as.numeric(x), **as.character(x)**, **as.expression(x)**

Less straightforward are:

as.matrix(x), **as.data.frame(x)**

which attempt to convert an object *x* to a matrix or data frame, respectively. A more user-friendly way of converting data frames to matrices is provided by the function `data.matrix` that converts all the variables in a data frame *x* to numeric mode and then binds them together as the columns of a matrix.

1.10 Factors

Factors are vector objects used for discrete classification (grouping) of components in other vectors of the same length, matrices or data frames. In statistical applications, these often serve as categorical variables.

1.10.1 Basic Usage of Factors

factor(x)

The (unordered) factors are set by the function `factor` where `x` is a vector of data, usually containing a small number of discrete values (known as levels). In this case the levels are stored in alphabetical order. For instance:

```
> x <- c("Pl", "Bt", "Pl", "Pl", "Kfs", "Pl", "Bt", "Pl", NA)
> factor(x)
[1] Pl   Bt   Pl   Pl   Kfs  Pl   Bt   Pl   <NA>
Levels: Bt Kfs Pl
```

ordered(x, levels)

This function defines a special type of factor in which the order of levels is specified explicitly using the `levels` parameter. Following the previous example:

```
> ordered(x, c("Pl", "Kfs", "Bt"))
[1] Pl   Bt   Pl   Pl   Kfs  Pl   Bt   Pl   <NA>
Levels: Pl < Kfs < Bt
```

levels(x)

Returns all possible values (levels) of the factor `x`.

1.10.2 Conversion of Numeric Vectors to Factors

In some cases it is advantageous to divide the total range of a numeric vector `x` into a certain number of discrete ranks (groups), and code the values in `x` according to the rank they fall into. If each of these ranks is labelled by identifying text, the result is a factor of the same length as the original vector.

cut(x, breaks, labels)

The function `cut` splits a numeric vector `x` into a number of ranks and classifies its items accordingly. The argument `breaks` either defines cut-off values or a desired number of intervals. Parameter `labels` may provide names for individual ranks. For an example of use, see Part I, Exercise 2.7.

1.10.3 Frequency Tables

table(...)

This function counts the number of occurrences of the given level within the factor. A pair of factors defines a two-way cross-classification (a frequency-contingency table) (Part I, Exercise 2.8).

1.10.4 Using Factors to Handle Complex Datasets

Examples of using factors to deal with complex geochemical datasets are given in Part I, exercises 2.5 and 2.6, the relevant syntax is presented here.

tapply(x, INDEX, FUN, ...)

The components of the vector `x` are split into several (non-empty) groups of values, based on levels of the factor `INDEX` (or list of two factors) of the same length. Then a function `FUN` is applied to each of the groups, optionally with further arguments (...) passed to it. The vector and the factor used for grouping collectively form a so-called ragged array, since the group sizes are typically variable.

aggregate(x, by, FUN, ...)

Applies function `FUN` to each of the variables (columns) of a numeric matrix or data frame `x` respecting grouping given by factor (or list of factors) `by`. Each of the variables in `x` is split into subsets (rows) of identical combinations of the components of `by`, and `FUN` is applied to each such a subset. Again, further arguments can be passed to `FUN`, as desired, via the ... argument.

by(data, INDICES, FUN, ...)

A data frame `data` is split by rows into data frames subset by the values of `INDICES` (a factor or list of factors). The function `FUN` is applied to each such subset (data frame) with further arguments in ... passed to it. In fact the function `by` is an object-oriented wrapper for `tapply` designed to deal with data frames.

1.11 Data Input/Output, Files

1.11.1 Reading Data

The tools for data handling and editing available in R are fairly limited and thus it is a good idea to prepare them beforehand in a dedicated application, such as a spreadsheet or database program.

Several packages are available on CRAN to help communicate with databases using SQL or ODBC protocols. Moreover there is a package interfacing to Windows applications (including MS Excel) via the DCOM interface. If you require any of these sophisticated tools, see the “R Data Import/Export” pdf documentation file.

In many situations it will be sufficient to import plain text files. The most powerful of the functions available for this purpose is:

```
read.table(filename, header = FALSE, sep = "", na.strings = "NA",
  check.names = TRUE, quote = "\"", dec = ".", fill = !blank.lines.skip)
```

This function imports a data file specified by ‘filename’, in which the individual items are separated by separator `sep`. The common separators are “,” – comma, “\t” – tab, and “\n” – new line. The parameter `dec` specifies a character interpreted as a decimal point. Note that the result is a data frame (and not a matrix), even if the file contains only numerical values. If matrix operations are to be employed, the data object must be explicitly converted.



Unless the full path is specified, the file is searched for in the current working directory. The directory can be queried with the `getwd()` command and set with the `setwd(dir)` function or the menu option *File|Change dir...*

A parameter worth resetting to `FALSE` is `check.names` as it determines whether the row and column names are to be syntactically checked to be valid R names. When `TRUE`, R will replace e.g. accented characters and slashes (“/”) with dots.

There is a useful convention; if the first row in the data file has one item less than the following ones, it is interpreted as column names and every first item in subsequent rows as a respective row name. The file might look as follows:

```
SiO2 → TiO2 → Al2O3 → Fe2O3 → FeO
Li1 → 51.73 → 1.48 → 16.01 → 1.03 → 7.06
Li2 → 51.88 → 1.48 → 15.93 → 0.99 → 6.85 ...
```

In order to read a text file in which the lengths of rows are all the same, but column names are present, one can employ `header=TRUE, row.names = 1`).

Parameter `na.strings` specifies text strings to be interpreted as missing values, e.g., `na.strings=c("b.d.", "-", "NA")`.



It is fairly common for a file exported from a spreadsheet such as MS Excel to have all trailing empty fields and their separators omitted. To read such files set `fill = TRUE` or simply copy and paste the data from a spreadsheet to your text editor directly using the Windows clipboard.

readClipboard()

In its simplest form, this function reads the text from the Windows clipboard.

1.11.2 Sample Data Sets

R and its packages contain numerous sample datasets that can be attached to the current session using the function `data(...)`. For instance:

```
> data(islands)
```

Then documentation is available using the `help` command:

```
> ?islands
```

1.11.3 Saving Data

```
write.table(x, file = "", append = FALSE, sep = " ", na = "NA", dec = ".",  
            row.names = TRUE, col.names = TRUE)
```

This function writes an object `x` (a matrix, a data frame, or an object that can be converted to such) to the specified `file`, separating the individual items by `sep`. As for `read.table`, one can specify the strings representing the missing values and the decimal point. Moreover, there are logical parameters determining whether row and/or column names are to be stored (`row.names`, `col.names`) and whether to `append` the data without erasing those possibly already present.

```
writeClipboard(str)
```

Writes the text specified by the character vector `str` to the Windows clipboard.

Chapter 2

Graphics

A key benefit of using R is the large range of functions for the production and export of (near) publication-quality diagrams. They can be divided into two types; *high-level functions* that open a new graphical window and set up a coordinate system of the brand new graph (Table A1.4) and *low-level functions* that annotate pre-existing plots (Table A1.5). Note also that some of the functions (e.g., `curve`) can show both types of behaviour depending on the given arguments.

2.1 Obtaining and Annotating Binary Plots

```
plot()
```

This is a key plotting function. For two numeric vectors, it produces a binary plot [`plot(x, y)`]. If one vector is shorter, it is recycled as appropriate.



A quick peek at objects, classes and methods...

There are special methods of `plot` to handle many types of R objects. A factor for instance produces a barplot of its individual levels whereas an object created by hierarchical clustering plots as a dendrogram. This is a consequence of R being an object-oriented language whereby a function can be used on any type of data (`class`) for which the method (e.g., `plot` or `print`) has been defined.

Often it is possible to plot most objects directly, without the need to restructure the data; the appropriate `x` and `y` values are extracted as required. Developers can extend the capabilities by creating new classes and associated methods.

Table A1.4 An overview of the selected high-level graphical functions in R

Function	Purpose
<code>plot(x, y)</code>	binary plot <code>x</code> vs. <code>y</code> (two numeric vectors)
<code>curve(expr, from, to)</code>	curve specified by <code>expr</code> (written as a function of <code>x</code>) in the interval <code>from-to</code>
<code>contour(x, y, z)</code>	contour plot (<code>x</code> and <code>y</code> specify a regular grid, <code>z</code> the values)
<code>filled.contour(x, y, z)</code>	filled contour plot (<code>x</code> and <code>y</code> specify a regular grid, <code>z</code> the values)
<code>boxplot(x)</code>	“box-and-whiskers” plot
<code>coplot(formula)</code>	conditioning plot; if <code>formula = y~x z</code> , bivariate plots of <code>x</code> vs. <code>y</code> for each level of the factor <code>z</code>
<code>pairs(x)</code>	matrix of all possible bivariate plots between columns of <code>x</code> (matrix or data frame)
<code>hist(x)</code>	histogram of frequencies for <code>x</code>
<code>pie(x)</code>	circular pie-chart

When calling the function `plot`, and indeed many other graphical functions, a number of additional parameters can be specified to modify the appearance of the plot. Some are fairly universal (e.g., `col` or `pch`), but others are restricted or may behave unexpectedly. An overview of the most commonly used graphical parameters is given in Table A1.6. If in doubt, the manual page of the particular plotting function should be consulted. Colours may be arranged into collections called palettes. The codes for available plotting symbols, standard colours and preview of palettes are in Fig. A1.2.



The complete set of graphical parameters supported by many standard R functions can be obtained using `?par`. For detailed explanation, and other topics related to R graphics, see the monograph of Murrell (2005).

Table A1.5 An overview of the most useful low-level graphical functions in R

Function (basic use)	Explanation
<code>points(x, y, type="p")</code>	adds extra data points at $[x, y]$
<code>text(x, y, labels)</code>	adds text specified by <code>labels</code> at $[x, y]$
<code>mtext(text, side)</code>	places <code>text</code> at margins, outside the plotting region on <code>side</code> (1 = bottom, 2 = left, 3 = top, 4 = right)
<code>contour(x, y, z, add=TRUE)</code>	contour plot (<code>x</code> and <code>y</code> specify the regular grid, <code>z</code> the values)
<code>lines(x, y, type="l")</code>	joins the points with straight line segments
<code>curve(expr, add=TRUE)</code>	adds a curve specified by <code>expr</code> (a function of <code>x</code>)
<code>arrows(x0, y0, x1, y1)</code>	arrows from $[x_0, y_0]$ to $[x_1, y_1]$
<code>abline(a, b)</code>	straight line defined by intercept (<code>a</code>) and slope (<code>b</code>)
<code>abline(v=x), abline(h=y)</code>	vertical or horizontal straight line(s)
<code>grid(nx, ny=nx)</code>	grid with <code>nx</code> cells horizontally and <code>ny</code> vertically
<code>rect(xleft, ybottom, xright, ytop)</code>	rectangle given left, bottom, right and top limits
<code>polygon(x, y)</code>	polygons whose vertices are given in <code>x</code> and <code>y</code>
<code>axis(side, at, labels)</code>	custom axis; <code>side</code> = 1 for <code>x</code> , 2 for <code>y</code> ; <code>at</code> = values to be annotated by <code>labels</code>
<code>box(which)</code>	box around the plotting region (<code>which</code> = "plot") or "figure", "inner", "outer"
<code>legend(x, y, legend, lty, lwd, pch)</code>	adds a legend at the point $[x, y]$
<code>title(main, sub, xlab, ylab)</code>	main title/subtitle or axes labels to the plot

palette(value)

This function serves to view or manipulate a colour palette. Optional parameter `value` is the name of palette predefined in standard R. For instance:

```
> ee <- palette(heat.colors(5))
> ee
[1] "red"      "#FF5500" "#FFAA00" "yellow"   "#FFFF80"
```

abline(a = NULL, b = NULL, h = NULL)

This command is used to draw a straight line. For instance:

```
> abline(a, b)           # slope b, intercept a
> abline(h=y)           # horizontal line(s)
> abline(v=1:5, lty="dotted") # vertical dotted grid lines
```

Table A1.6 An overview of the main graphical parameters

Parameter	Meaning	Example
adj	text justification relative to the coordinates $[x, y]$	0 – left, 1 – right, 0.5 – centered
asp	aspect ratio y/x	asp = 1
axes	logical, should the axes be drawn?	axes = FALSE
bg	background colour	bg = "khaki"
cex	relative character size expansion (of text or symbols)	cex = 2
cex.main, cex.sub	size of plot's title, subtitle	
cex.lab, cex.axis	size of axes labels, tick labels	
col	plotting colour	col = 0, col = "red"
las	style of axis labels	0 – parallel to the axes, 1 – horizontal 2 – perpendicular, 3 – vertical
log	which of the axes is/are logarithmic?	log = "xy", log = "" 1 – "solid" 2 – "dashed" 3 – "dotted" 4 – "dotdash"
lty	line type (a number or text string)	
lwd	relative line width	lwd = 2
main	main title of the diagram (top)	main = "My diagram"
mar	outer margins of a plot in lines of text c(bottom, left, top, right)	mar = c(4, 4, 0, 0)
mfcol=c(nr, nc) mfrow=c(nr, nc)	splits the plotting window into nr rows and nc columns, the graphs are filled by columns (mfcol) or rows (mfrow)	mfcol = c(2, 1) mfrow = c(2, 1)
pch	plotting character; a numeric code or a single alphanumeric symbol	pch = 7, pch = "Q"
pos	position of the text relative to the coordinates $[x, y]$	1 – below, 2 – left, 3 – above, 4 – right
pty	type of plot region to be used	"s" – square, "m" – maximal
srt	rotation of the text in degrees	srt = 90
sub	subtitle of the diagram (bottom)	sub = "for thesis"
type	type of the diagram	"p" – points, "l" – lines, "b" – both, "o" – overplot, "n" – none (no plotting)
xaxs, yaxs	scaling style for axes (default is <i>extended</i> : plotted symbols cannot crash with axes)	"r" – extended range "i" – exact scaling
xlab, ylab	labels for x and y axes	xlab = "SiO2[wt.%]"
xlim, ylim	limits of the x and y axes	xlim=c(50, 70)

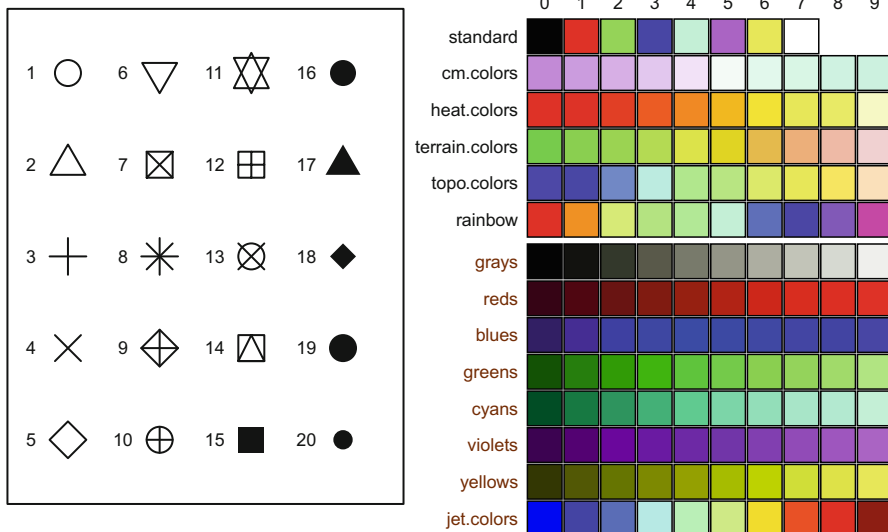


Fig. A1.2 Plotting symbols and colours available through the parameters `pch` and `col` (the first row, labelled ‘standard’)⁵ as well as some examples of palettes built-in plain R (black names) and *GCDkit* (brown names).

lm(formula)

A function for fitting linear models. The simplest form of `formula` is “`y~x`”, i.e. `y` as a function of `x`, performing a linear regression. To see details of the resulting object use the function `summary`. Note that `abline` has a method for plotting thus generated linear fits.

text(x, y, labels)

This low-level function displays the given text at coordinates `[x, y]`. It is especially useful to label individual data points of the binary diagrams (in combination with the `pos` parameter). For example, using data from the calc-alkaline Sázava suite of the Variscan Central Bohemian Plutonic Complex (Janoušek et al. 2004):

```

> sazava<- read.table("sazava.data", sep="\t")
> plot(sazava[, "SiO2"], sazava[, "Ba"], xlab=expression(SiO[2]),
+      cex=1.5, ylab="Ba", pch=16, main="Sazava", xlim=c(45, 75))
> abline(h=seq(0, 1500, 500), lty="dotted", col="gray")
> abline(v=seq(40, 80, 10), lty="dotted", col="gray")
> text(sazava[, "SiO2"], sazava[, "Ba"], rownames(sazava), pos=4,
+      col="red")
    
```

⁵ Standard codes correspond to "black", "red", "green3", "blue", "cyan", "magenta", "yellow" and "white". Function `colors()` displays all the symbolic names available (657 of them!).

We can also produce a linear fit, and assign the result to an arbitrary variable `ee`:

```
> ee <- lm(sazava[, "Ba"] ~ sazava[, "SiO2"])
> ee
Call:
lm(formula = sazava[, "Ba"] ~ sazava[, "SiO2"])
```

```
Coefficients:
(Intercept)  sazava[, "SiO2"]
-1680.45      43.67
```

and the object `ee` is ready to be plotted by the function `abline` (Fig. A1.3):

```
> abline(ee, lwd=2, lty="dashed", col="blue")
```

If we want to know the details, we can display the whole list `ee` using:

```
> summary(ee)
[Output intentionally omitted]
```

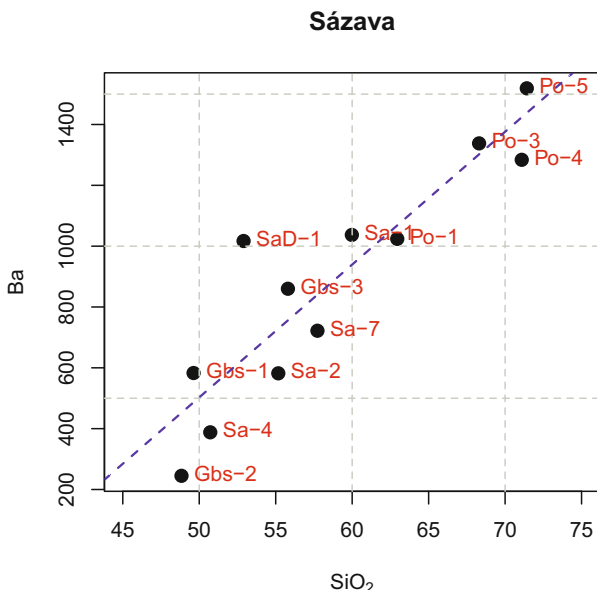


Fig. A1.3 Binary plot SiO₂ (wt. %) vs. Ba (ppm) for the Sázava suite of the CBPC. Linear fit was plotted by `abline`, as were the grid lines.

grid(nx, ny)

A convenience function creating better-looking grids with spacing `nx` and `ny` in the `x` and `y` axis directions.

curve(expr, from = NULL, to = NULL, add = FALSE)

A function for adding a curve (if `add=TRUE`) specified by an expression (`expr`; written as a function of `x`). Optionally, the range of the `x` axis can be also set, using the parameters `from` and `to`. For example:

```

> sazava <- read.table("sazava.data", sep="\t")
> plot(sazava[, "Rb"], sazava[, "Sr"], xlab="Rb (ppm)",
+       ylab="Sr (ppm)", pch=sazava[, "Symbol"], cex=2,
+       xlim=c(0, 70), ylim=c(0, 650), xaxs="i", yaxs="i")
> abline(0, 5, col="red", lwd=1.5, lty="dashed")
> curve(x^2, add=TRUE, col="blue", lwd=1.5, lty="dotted",
+       from=0, to=25)

```

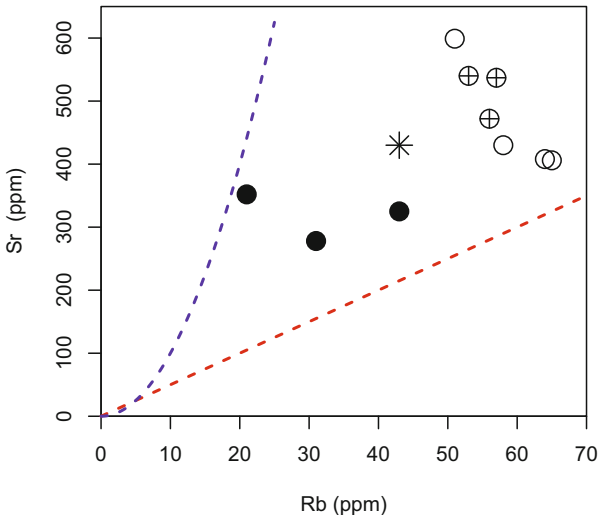


Fig. A1.4 Binary plot Rb (ppm) vs. Sr (ppm) for the Sázava suite. The red trend is linear, created by `abline`, while the blue one is parabolic, drawn by `curve`.

points(x, y, type = "p")

Function `points` adds new data points with coordinates `[x, y]` to an existing plot. The argument `type` controls how they are displayed (as points, lines, etc.).

lines(x, y)

Adds straight line segments; `x` and `y` are vectors of corresponding coordinates.

legend(x, y = NULL, legend, fill = NULL, col, pch, lty, lwd, inset = 0)

Adds a legend at `[x, y]`. If `y = NULL`, the position (`x`) can be specified by a single keyword such as "bottomright" or "center". The explanatory text is given by a character vector `legend`; the attributes for the symbols can be `fill` (colours to fill boxes), `pch` (plotting characters), `col` (colours of plotting characters or lines), `lty` (line types) or `lwd` (line widths). The numeric argument `inset` defines a distance from the margins as a fraction of the plot region size.

2.2 Additional High-level Plotting Functions

Here we show examples of the most useful of the other high-level functions for plotting boxplots, correlation matrices, histograms and such alike (Table A1.4).

boxplot(x)

Creates a “box-and-whiskers” plot, i.e. a diagram, in which each variable (column of a data frame/matrix *x*) is represented by a rectangle (its horizontal sides correspond to the 1st and 3rd quartiles a horizontal line denotes a median). Two vertical lines join extremes (minimum and maximum); outliers⁶ are plotted as tiny circles.

```

> sazava <- read.table("sazava.data", sep="\t")
> oxides <- c("MgO", "CaO", "Na2O", "K2O")
> boxplot(sazava[,oxides], col=c("khaki", "gray", "red", "blue"))

```

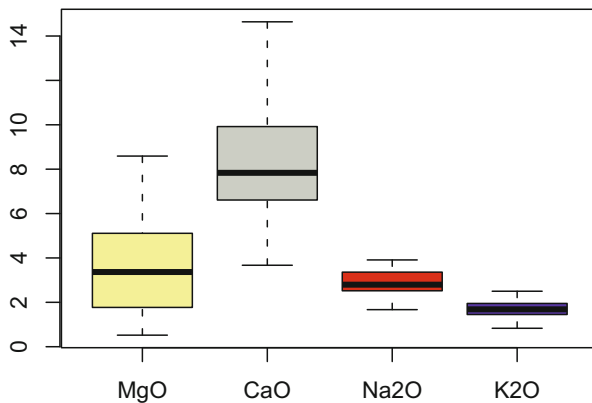


Fig. A1.5 Boxplot of selected oxides from the Sázava suite.

summary(x)

Information similar to `boxplot` but in textual form gives:

```

> summary(sazava[,oxides])
MgO           CaO           Na2O
Min.  :0.520   Min.   : 3.670   Min.   :1.670
1st Qu.:2.033   1st Qu.: 6.718   1st Qu.:2.525
Median :3.365   Median : 7.835   Median :2.795 ...

```

pairs(x)

A scatterplot matrix for all possible combinations of columns in matrix *x*:

```

> pairs(sazava[,oxides], pch=15, col="darkred")

```

⁶ For details on the underlying calculations, see `?boxplot.stats`.

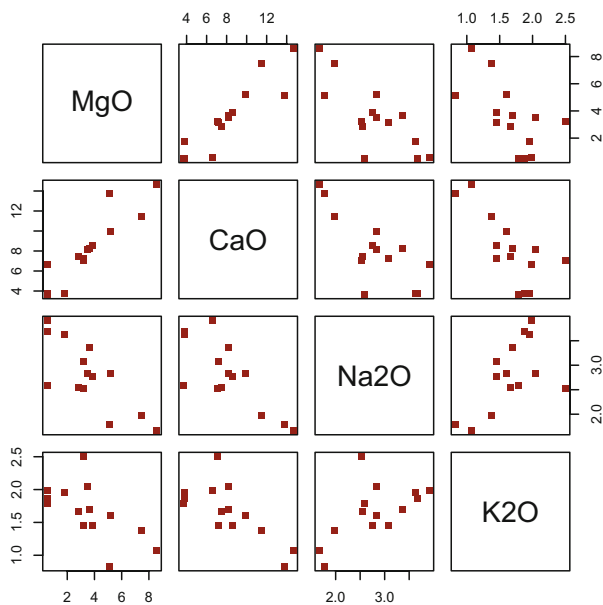


Fig. A1.6 Correlation plots obtained by `pairs` for selected oxides from the Sázava suite.

hist(x)

Produces a histogram of frequencies of the vector `x`:

```
> hist(sazava[, "Sr"], xlab="Sr", ylab="frequency",
+       xlim=c(100, 700), col="darkred", density=5, angle=45)
> box()
```

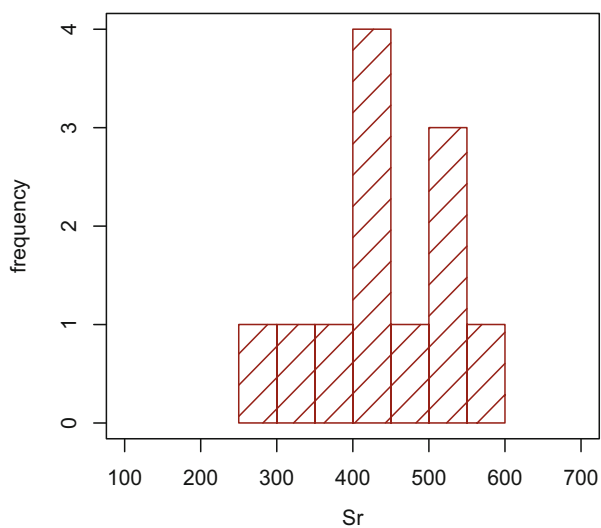


Fig. A1.7 Histogram of frequencies for Sr contents (ppm) in the Sázava suite.

coplot(y~x|z)

Conditioning plot; in this form it displays a set of bivariate plots of x vs. y for each level of the factor z .

```
> coplot(sazava[, "CaO"]~sazava[, "SiO2"]|sazava[, "Intrusion"],
+       cex=1.5,xlab=expression(SiO[2]),ylab="CaO",
+       pch=sazava[, "Symbol"],col=sazava[, "Colour"])
```

Given : WR[, "Intrusion"]

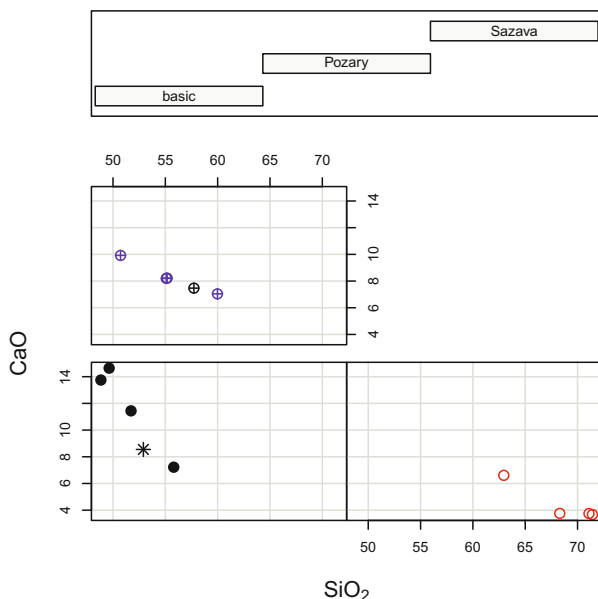


Fig. A1.8 Coplot showing SiO_2 -CaO variations in individual rock types within the Sázava suite.

contour(z, add = FALSE)

Creates a contour plot, or adds contour lines to a pre-existing plot (if `add=TRUE`) based on a data matrix z ⁷. A simple use will be demonstrated on isohypses of the Maunga Whau volcano, as given in the `volcano` dataset (see `?volcano`):

```
> data(volcano)
> contour(volcano,col="blue")
```

filled.contour(z, color.palette = cm.colors)

Creates a filled contour plot, in which the values of z are represented by individual colours from the `color.palette`. Another example using `volcano` dataset:

```
> filled.contour(volcano,color.palette=terrain.colors,asp=1)
```

⁷ NB that the data must be prepared in a regular grid and that the function does not perform any interpolation such as kriging. In this form, both coordinates are normalized from 0 to 1. The real ones can be provided by the optional arguments x and y .

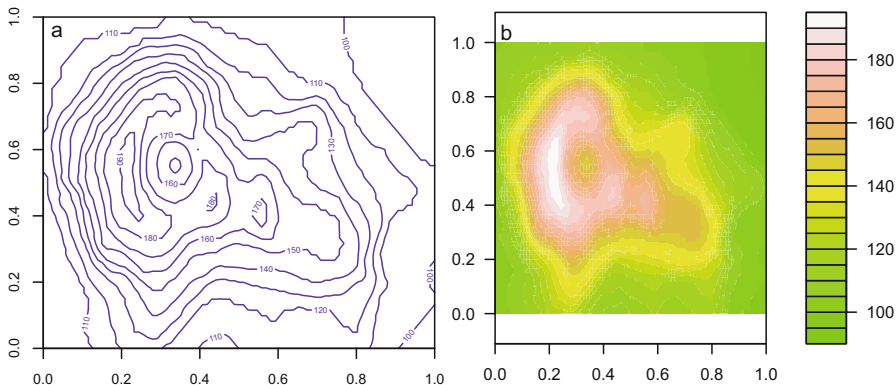


Fig. A1.9 Contour plots for the Maunga Whau volcano, New Zealand, plotted using `contour` (a) and `filled.contour` (b) functions.

2.3 Creating Custom Layouts and Axes

To gain more control of the plotting window, use the graphical parameters function `par` to create multi figure plots and the `axis` function to fine-tune style and placement of axes.

`par(mfrow = c(nrow, ncol))`

`par(mfcol = c(nrow, ncol))`

Create multi figure layouts by splitting the graphical window into a matrix of *nrow* × *ncol* plotting regions to be sequentially filled by plotted graphs (row wise—`mfrow` or column wise—`mfcol`).

Arbitrary sized plotting regions can be configured using the `fig` option to `par`.

`axis(side, at, labels)`

The `plot` function can be called with a parameter `axes=FALSE` such that no axes are drawn. This is a prelude to the command `axis`, to define a custom layout. The arguments `side = 1` for bottom (x), `2` left (y), `3` top, `4` right; `at` – a vector with values to be labelled; `labels` – character vector with the text labels. For example:

```
> plot(1,1,xlim=c(0,3),ylim=c(-1,1),axes=FALSE,
+      xlab="custom X",ylab="custom Y",type="n")
> axis(1,0:3,c("A","B","C","D"))
> axis(2,-1:1,c("I","II","III"))
> box()
```

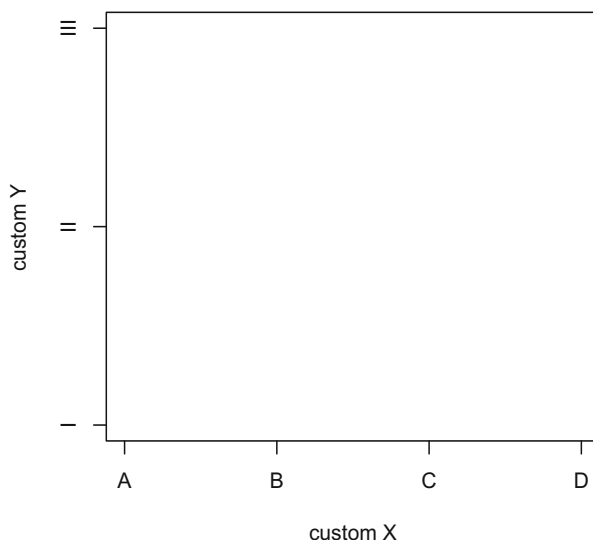


Fig. A1.10 Custom axes created and annotated using the function `axis`.

In order to produce true publication quality diagrams, R includes a powerful way of coding mathematical expressions that can be plotted on diagrams, e.g. as text or in axis labels (Murrell and Ihaka 2000). For this purpose the functions `expression` and `as.expression` are used.

`expression(...)`, `as.expression(x)`

Return a vector of type "expression" containing its unevaluated arguments.

```
> expression(SiO[2])
expression(SiO[2])
> plot(1,1,xlab=expression(SiO[2]))
expression and as.expression are used.
```

Some examples of valid expressions related to geochemical plotting are (details in the following Next step box):

Expression	Meaning
<code>TiO[2]</code>	TiO_2
<code>FeO^T</code>	FeO^T
<code>Al[2]*O[3]</code>	Al_2O_3
<code>epsilon[Nd]</code>	ϵ_{Nd}
<code>30*degree</code>	30°

`parse(text = NULL)`

A function that returns a parsed, but unevaluated expression. The most common use—in conjunction with the function `as.expression`—is to convert character string(s) with mathematical annotations to expressions ready for plotting.

```
> x <- "SiO[2]"
```

```
> parse(text=as.expression(x))
expression(SiO[2])
```

substitute(expr)

This function returns the unevaluated expression `expr`, substituting any variables therein by their values. For instance:

```
> sazava <- read.table("sazava.data", sep="\t")
> sr.mean <- mean(sazava[, "Sr"], na.rm=TRUE)
> text(1,0,as.expression(substitute(italic(bar(x)[Sr]) == m,
+ list(m=sr.mean))))
```

results in: $\bar{x}_S = 443$

An additional example is useful if dealing with isotopes:

```
> age <- 350
> text(1,0,as.expression(substitute(" ^87Sr/" ^86Sr[m],
+ list(m=age))))
```

as it gives: $^{87}Sr / ^{86}Sr_{350}$.



Mathematical annotations to plots

The fairly complex syntax used by `as.expression` and `expression` is based on the typesetting package TeX. The table below summarizes selected features; see `?plotmath` and `example(plotmath)` for details.

Syntax	Meaning	Result
<code>x + y</code> , <code>x - y</code>	x plus y, x minus y	$x + y$ $x - y$
<code>x*y</code>	juxtapose x and y	xy
<code>x %/% y</code> , <code>x %%*% y</code>	x divided by y, x times y	$x \div y$ $x \times y$
<code>x/y</code>	x slash y	x/y
<code>x %+-% y</code>	x plus or minus y	$x \pm y$
<code>x[2]</code> , <code>x^2</code>	x subscript 2, x superscript 2	x_2 x^2
<code>frac(x,y)</code> , <code>over(x,y)</code>	x over y	$\frac{x}{y}$
<code>x == y</code>	x equals y	$x = y$
<code>bar(x)</code>	x with bar	\bar{x}
<code>x*degree</code>	x degrees	x°
<code>sqrt(x)</code> , <code>sqrt(x,y)</code>	square root of x, y th root of x	\sqrt{x} $\sqrt[y]{x}$
<code>sum(x[i], i==1,n)</code>	sum x[i] for i equals 1 to n	$\sum_{i=1}^n x_i$
<code>plain(x)</code> , <code>bold(x)</code> , <code>italic(x)</code> , <code>bolditalic(x)</code>	sets typeface for x	
<code>alpha-omega</code> , <code>Alpha-Omega</code>	lower and upper case Greek letters	

2.4 Exporting Graphs from R and Graphical Devices

Graphs can be exported to a word processor, a desktop publishing or a graphical package (e.g. Adobe Illustrator or CorelDraw) for further editing. They can be copied to the Clipboard or saved into a file by right-clicking the graphical window and selecting *Save as...* Alternatively, corresponding items in the menu *File* of the graphical window can be invoked. There are a wealth of formats to choose from, including the most popular vector (PostScript, PDF, WMF) and bitmap (TIF, PNG, BMP, JPG) ones. Of course, for further editing or publishing, vector formats are to be preferred. PostScript and PDF are generated in a quality superior to the Windows Metafile (WMF) format.

As a useful alternative, the graphical output can be redirected to one of the many supported graphical devices (Table A1.7).

Table A1.7 Selected devices available in R

Function	Description	Type
<code>windows()</code>	a graphical window (Windows)	–
<code>quartz()</code>	a graphical window (Mac OS X)	–
<code>x11()</code>	a graphical window (Linux)	–
<code>postscript(file)</code>	PostScript (see also <code>?ps.options</code>)	Vector
<code>pdf(file)</code>	Adobe PDF (Portable Document Format)	Vector
<code>win.metafile(filename)</code>	Windows Metafile (WMF)	Vector
<code>png(filename)</code>	bitmap (lossless compression, less common)	Raster
<code>tiff(filename)</code>	bitmap (lossless uncompressed, widely accepted)	Raster
<code>jpeg(filename)</code>	bitmap (lossy compression, small files)	Raster

dev.off()

Close the current graphical window.

graphics.off()

Close all the opened graphical windows.

2.5 Interaction with Plots

The ability to interact with graphics makes it possible, for instance, to select outliers and label them with sample names. Or one can pick samples for further processing, such as setting end members for numerical modelling. Clearly these functions are only useful for interactive plotting devices.

locator()

The locator returns the coordinates of one or more points clicked on by the left mouse button. Identification is stopped by pressing the right mouse button and selecting *Stop*.

identify(x, y, labels)

This function annotates the plot with `labels` for each given `[x, y]` coordinate. Usually only useful when there are a small number of data points.

Chapter 3

Programming in R

This chapter deals with preparing R scripts to be run in batch mode. We shall learn to control the output to the screen and input from the keyboard, to build conditional statements and loops as well as to program simple user-defined functions.

3.1 Input and Output

print(x)

Prints the contents of an object `x`, nicely formatted.

cat(..., file="", sep="")

This function displays the contents of one or more R objects in a less sophisticated way, but enabling much more control over the output format⁸:

```
> x <- 5.8
> cat("The result is ", x, " N/m.\n")
The result is 5.8 N/m.
```

readline(prompt)

Displays the `prompt` and then reads input from the keyboard:

```
> x <- readline("Enter x:\n")
Enter x:
> 5.8
> x
[1] "5.8"
```

This example shows that keyboard input is always in the form of a character vector of length 1. If required it has to be coerced to a numeric value using the function `as.numeric`:

```
> x <- as.numeric(x)
> x
[1] 5.8
```

⁸Note that this function does not append a newline character that must be added explicitly to the output string as `"\n"`.

3.2 Conditional Execution

Conditional execution of R code can be achieved using:

if(*condition*) *expression1* **else** *expression2*

If *condition* evaluates to TRUE, *expression1* is executed, otherwise *expression2* is run. Complicated commands may be grouped together in braces:

```
> x <- 6
> y <- 0.5
> if(x>2 & y<1){
>   print(x)
>   print(y)
> }else{
>   cat("Warning, x<=2 or y>=1!\n")
> }
```

3.3 Loops

Sometimes it is useful to run some chunk of code repetitively in a loop. Due to the powerful indexing in R, loops are needed considerably less often than in any conventional programming language. They can be built using the statement:

for(*variable in expression1*) *expression2*

expression2 is a chunk of R code, usually grouped in braces to be executed once for each of the values of the control *variable*. The range of possible values for the *variable* is specified by a vector, *expression1*. See the example, which calculates and prints the square roots of the sequence of numbers 1, 3, 5, 7, and 9:

```
> for(f in seq(1,10,by=2)){
>   cat("Square root of",f,"is",sqrt(f),"n")
> }
Square root of 1 is 1
Square root of 3 is 1.732051
Square root of 5 is 2.236068
Square root of 7 is 2.645751
Square root of 9 is 3
```



Try to avoid loops if possible. Their execution in R tends to be time consuming and there are, usually, other alternatives. For instance here, thanks to the recycling rules in R, we can write:

```
> x <- seq(1,10,by=2)
> ee <- paste("Square rootof",x,"is",sqrt(x),"n")
> cat(ee)
```

Commands `apply`, `tapply` or `sapply` (below) are commonly a better approach.

while(*condition*) *expression*

In this case, `expression` will be executed as long as the `condition` remains valid (i.e. is `TRUE`).

repeat *expression*

This command is used in conjunction with a `break` statement (this is not a function and thus no brackets are required). In fact, the `break` statement can be used to terminate any loop, if necessary. The `next` statement can be invoked to discontinue one particular cycle and skip to the next one.

3.4 User-defined Functions

User-defined functions provide a stylish way of extending the set of the available commands. In fact, much of R itself is written in R! The function definition looks like:

function.name <- **function** (*argument1*, *argument2*, ...) *expression*

The `expression` is a chunk of R code, usually grouped in braces. In order to avoid confusion, the last statement should be `return(z)`, where `z` is an expression or variable name giving the value(s) to be returned by the function⁹.

For example, we can write a user-defined function calculating a geometric mean, defined as the n^{th} root of the product of n numbers, and use it on some data:

$$S = \sqrt[n]{\prod_{i=1}^n x_i}$$

```
> geo.mean <- function(x) {
>   z <- prod(x)^(1/length(x))
>   return(z)
> }
> sazava<- read.table("sazava.data", sep="\t")
> geo.man(sazava[, "SiO2"])
[1] 57.49363
```

3.4.1 Arguments to Functions

There are two possibilities for providing arguments to an R function. First, you can pass them in the order matching the function's definition. The second is to

⁹ If more values need to be returned, they can be assembled into a list object.

supply the arguments in the form `argument.name = value` in an arbitrary sequence.

When writing a user-defined function, one can provide default values as in the following example:

```
> my.plot <- function(x, y, symb="+", colour="red") {
>   plot(x, y, pch=symb, col=colour)
> }
```

And such a function then can be called in a number of ways¹⁰, for instance:

```
> my.plot(x, y)                #red crosses
> my.plot(x, y, "o")          #red circles
> my.plot(x, y, colour="blue") #blue crosses
```

But it is also obvious that:

```
> my.plot(x, y, "blue")
```

will not work as intended because the third parameter will be interpreted as parameter `symb`, i.e. a plotting character and a red ‘b’ will be plotted.

args(name)

Displays the arguments to an existing function specified by `name`, e.g.:

```
> args("my.plot")
function (x, y, pch = "+", col = "red")
```

3.4.2 Assignments in Functions

Importantly, the variables used within a user-defined function (in the example of the function calculating a geometric mean these were `x` and `z`) are local (in R jargon, limited to the function’s “environment”). This means that any assignments done within the function are temporary, being lost after the evaluation is done. Therefore, such assignments do not affect the value of the variable with the same name in the calling environment.

In (rare) cases when it is desirable to alter the value of a variable globally (in the `.GlobalEnv` environment), this can be done with the “super assignment”:

```
> x <<- "Hello"
```

¹⁰Note that in R, most of the arguments to the functions have been given sensible defaults appropriate to most of the applications. Thus the ordinary user does not need to specify all of them, or to even be aware of their existence.

3.5 An Alternative to Loops—*sapply*

If loop-like execution of code seems unavoidable, often a more time-efficient solution can be made using functions such as `apply`, `tapply` or `sapply`.

`sapply(x, FUN)`

Applies a function `FUN` over a vector `x`. This means, that the function is run once for each of the values that are present in the vector `x`. An example (the same as given for `for` loops, but quicker and more compact):

```
> sapply(seq(1,10,by=2),sqrt)
[1] 1.000000 1.732051 2.236068 2.645751 3.000000
```

Of course, the function `FUN` can also be a user-defined one.



Anonymous functions

A strategy, often employed in R, is to use an anonymous function. So called, as it is not named and not visible outside the `sapply` statement:

```
> sapply(seq(1,10,by=2),function(i){
>   z <- paste("Square root of ",i," is ",round(sqrt(i),6))
>   return(z)
> })
```

References

- Adler J (2012) R in a nutshell. O'Reily, Sebastopol
- Becker RA, Chambers JM, Wilks AR (1988) The new S language. Chapman & Hall, London
- Chambers JM (1998) Programming with data. Springer, New York
- Chambers JM (2009) Software for data analysis: programming with R. Springer, Berlin
- Chambers JM, Hastie TJ (1992) Statistical models in S. Chapman & Hall, London
- Crawley MJ (2007) The R book. John Wiley & Sons, Chichester
- Janoušek V, Braithwaite CJR, Bowes DR, Gerdes A (2004) Magma-mixing in the genesis of Hercynian calc-alkaline granitoids: an integrated petrographic and geochemical study of the Sázava intrusion, Central Bohemian Pluton, Czech Republic. *Lithos* 78:67–99
- Maindonald J, Braun J (2003) Data analysis and graphics using R. Cambridge University Press, Cambridge
- Murrell P (2005) R graphics. Chapman & Hall/CRC, London
- Murrell P, Ihaka R (2000) An approach to providing mathematical annotation in plots. *J Comp Graph Stat* 9:582–599
- van den Bogaard P, Tolosana-Delgado R (2013) Analyzing compositional data with R. Springer, Berlin

Appendix B

Introduction to *GCDkit*

Processing whole-rock data in igneous geochemistry is often a tedious and error-prone activity, whether it includes simple recalculations and plotting or advanced modelling as described in this book. *GCDkit* is a freeware package tailored to facilitate such work. It is designed for a Windows edition of the open-source R language (R in short), but may also be installed under a suitable Windows emulator on Linux and MacOS systems. It comprises tools written to solve a comprehensive set of (geochemist's) real-life tasks, and (mostly thanks to the underlying R) the code can be examined and explored. Expandability is almost unlimited.

Chapter 1

First Steps with *GCDkit*

1.1 Installation

Installation of *GCDkit* is as simple as for any other Windows application. There is just one catch: since it is a package for R, the **R environment (the Rgui) has to be installed first, followed by *GCDkit***. *GCDkit* simply has to 'find' R in the system. Please follow the instructions at its website (www.gcdkit.org). While these can vary over time, in general you have to:

- Check which version of R is needed at the *GCDkit* website (www.gcdkit.org),
- Download the appropriate Windows version of R (cran.r-project.org),
- Install R by running the installer,
- Download the *GCDkit* installer from www.gcdkit.org/download,
- Install *GCDkit* by running it.

Administrator's rights are necessary for the installation in the Windows system, otherwise the process fails¹.

It is also good to check the website from time to time for patches fixing known bugs or other issues. If there is one, you can download and install a patch by dragging-and-dropping the file onto the main *GCDkit* window.

¹ For installation without admin rights (with some limitations) see the download page.



This text is based on version 4.0 of *GCDkit*.

1.2 *GCDkit* Overview: The User Interface

When installed, *GCDkit* is started by double clicking its *hammer & test-tube* icon.

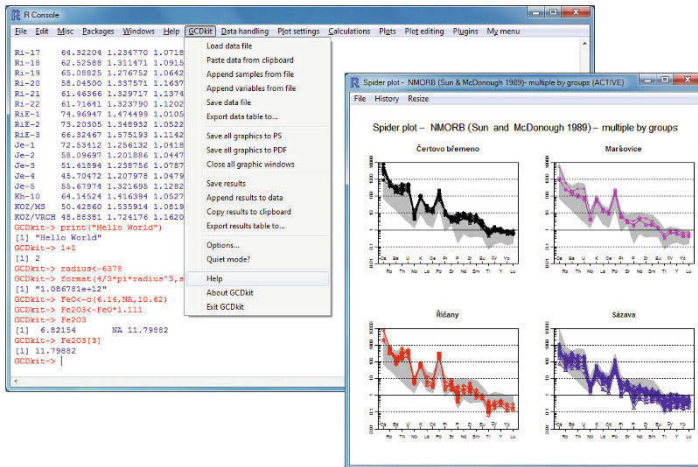


Fig. A2.1 Screenshot of principal parts of the *GCDkit* interface—*R-Console* with text input and output, an opened menu and a graphical window with a plot.

As seen in Fig. A2.1, the program starts with a single window, *R-Console*. This presents a standard command line interface, where the operator enters R commands (in red), and the output result is displayed (in blue). If you type `print("Hello")` or simply `1+1`, you get the expected result. In the same way any of innumerable R or *GCDkit* functions can be entered, as described in more detail in Appendix A and in a number of online and printed resources.

Furthermore, there is a series of pull-down menus at the top of the *R-Console*. The first six entries (from *File* to *Help*) refer to the R system and are almost of no importance to us. The remaining belong to *GCDkit* itself, and are covered by this Appendix. A further set of menu items is available on top of the graphical windows and within right-click context menus. Invoking each menu entry triggers one or more functions. This implies that *GCDkit* functionality is accessible both by pull-down menus as well as from the text console. The former is more straightforward and intuitive; the latter is trickier but brings more flexibility and power. Fig. A2.2 summarizes some basic operations in both interactive and text mode.

<i>GCDkit</i> degustation menu	
#Menu	shows how to work with <i>GCDkit</i> in interactive mode; parameters are defined in pop-up dialogs
#R-console	shows use of functions in text mode with example parameters; type ?function for help
Import data file:	
Menu:	<i>GCDkit</i> Load data file
R-console:	loadData("Sazava.data") # *.data, *.csv, *.xls, *.xlsx, *.mdb
	#Correct data format necessary, see Appendix II, Chapter 1.3; set working directory by gcdOptions()
Plot binary diagram:	
Menu:	Plots Binary plot
R-console:	binary("SiO2", "K2O", log="xy")
Plot ternary diagram:	
Menu:	Plots Ternary plot
R-console:	ternary("Na2O+K2O", "FeO", "MgO", grid=T, ticks=F)
Plot Harker-style diagrams:	
Menu:	Plots Multiple plots ... 1 vs. majors
R-console:	multiple("SiO2", y="MgO, Na2O+K2O, (FeO+MgO)/MgO, 3*Rb")
	#any available compound and simple formula applies
Plot predefined diagram (classification, geotectonic):	
Menu:	Plots Classification... or Plots Geotectonic...
R-console:	plotDiagram("TAS") or plotPlate("Wood")
	#check ?plotDiagram and ?plotPlate for applicable parameters
Plot spidergram (including REE patterns):	
Menu:	Plots Spider plots for selected samples
R-console:	spider(WR, "Boynton", 0.1, 1000, pch="*", col="red")
Split data into groups (for plotting, numerical exploration etc):	
Menu:	Data handling Set groups by... ... label
R-console:	groupsByLabel("Intrusion") #more options available
Retouch plot: #not applicable for multiple and statistical diagrams	
	Zoom in: Plot editing Zoom... ...in or figZooming()
	Add legend: Plot editing Add... legend or figLegend()
	Label samples: Plot editing Identify points or figIdentify() #end by Esc
	Add contours: Plot editing Add contours or addContours()
Assign plotting symbols and colours to samples:	
Menu:	Plot settings Symbols/colours by groups
R-console:	assignSymbGroup()
	#confirm changes by closing the spreadsheet window
	#can be predefined in the source file in columns "Symbols" and "Colours"
Perform normative mineral calculation (norm):	
Menu:	Calculations Norms...
R-console:	results<-CIPW(WR) #more norms available
	#results can be copied into clipboard via menu <i>GCDkit</i> Copy results to clipboard
Obtain basic statistical description:	
Menu:	Calculations Statistics Majors summary All/selection
R-console:	summaryAll("SiO2, MgO, Rb", show.boxplot=T, show.hist=T)

Fig. A2.2 Suggestions of simple tasks to start with *GCDkit*; multiple other options and procedures are available for more advanced users.

GCDkit is (apart from I/O functions) responding in two ways: textual information is displayed in the *Console*, whereas plots pop-up in separate graphical windows. The most recent plot (labelled *ACTIVE*) can be in most cases further edited as described later. Any graphical window can be saved to a selected format or to the clipboard (from context menu or *GCDkit|Save all graphics to...*). Also the text output displayed on the *Console* can be saved using *GCDkit|Save results*.

Documentation is gathered in the help system available from the menu item *GCDkit|Help...* In addition to its obvious purpose to assist in using the software, it also briefly documents the geochemical background and provides appropriate references. The help system opens in a web browser and, apart from documentation for individual functions (mimicking the menu structure), it also contains several *.pdf manuals. Documentation is also available in standard R ways, i.e. in the system help or by typing a function name preceded by a question mark.



***GCDkit* is mutating.** Menus, plots and tools available depend on the type of loaded data. If some of the features described below are missing, it is most likely because the appropriate data are absent.

1.3 Working with Data

1.3.1 Data Format

Any session inevitably has to start by data preparation. The native data format is based on a simple table with samples (cases) in rows and compounds (numerical variables) with textual metadata (labels) in columns. The columns can be presented in arbitrary order. A unique name for each sample and compound should be stored in the first column and row, respectively. In order to be properly handled by the system, the major-element oxides and trace elements must be labelled solely by their chemical formulae (SiO_2 , Sr etc.) and given in wt. % and ppm, respectively.

Plotting colour, symbol and symbol size for each sample can be specified in columns headed 'Colour', 'Symbol' and 'Size'. Additional textual or numerical information for each sample, such as locality, rock name, age, or isotopic composition may be stored in additional columns (Fig. A2.3). Further details are provided in the documentation (type `?loadData`); example files are also available.

As seen from the explanation above, data are of two categories: numerical and descriptive (textual). Both are treated differently. It is vital to understand how the system recognizes the categories:

- Data in any column with correct oxide or element name (including variants for total Fe, H_2O^+ , $\text{Mg}\#$...) are considered as numerical; any text therein is imported as a missing value.

- Data in columns labelled ‘Symbol’, ‘Colour’ and ‘Size’ are considered as symbol plotting parameters (this Appendix, Sect.1.4.1).
- Data in any other column containing at least some text (except permitted strings for missing values) are treated as textual (descriptive).
- Data in any other column containing strictly numbers (with, or without, permitted strings for missing values) are treated as numerical.

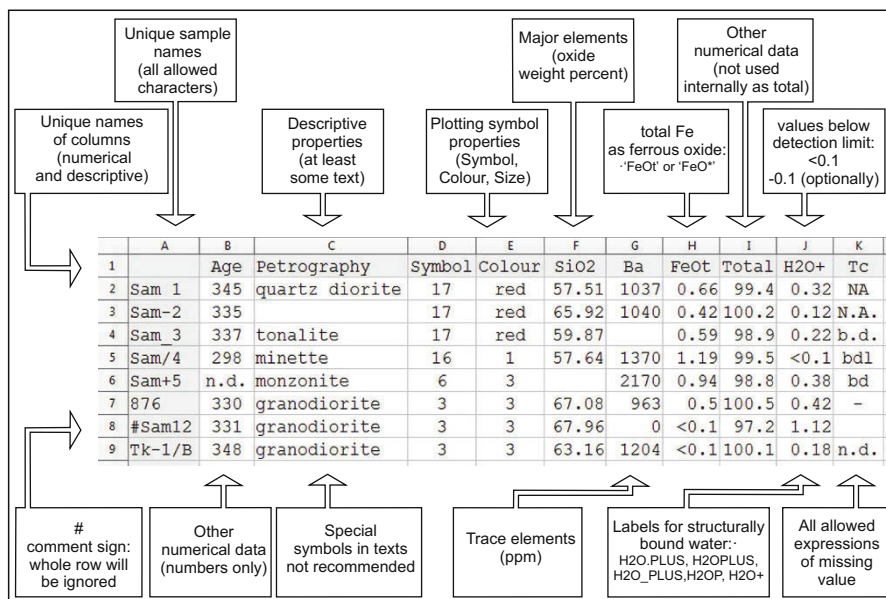


Fig. A2.3 Commented example of a correctly formatted input file.

Some common formatting mistakes are highlighted in Fig. A2.4. There are no doubt many more possibilities to spoil the input; this is a field of unlimited creativity.



In the following text and in *GCDkit*, **Variable** refers to the name of a column (and the data within it) recognized as numerical. **Label** is a term reserved for names of the remaining descriptive columns.

1.3.2 Loading Data

There are several ways of introducing data into *GCDkit*. The basic one leads through menu *GCDkit|Load data file*, which invokes a file selection dialogue to find the desired *.data file (and other formats). However, more popular has

	A	B	C	D	E	F	G	H	I	J	K
1		Petrography	Age	Symbol	Farbe	SiO ₂	FeO _t		Rb (ppm)	Ba	Ba
2	Sam 1	kfemenny diorit	345	17	red	57.51	0.66		254	1037	987
3	Sam-2		335	17	red	65.92	0.42		118	1040	1120
4	Sam 3	tonalite	337	17	red	59.87	0.59		187		770
5	Sam 3	minette	298	16	1	57.64			228	1370	
6	Sam+5	monzonite	none	6	3		0.94		635	2170	2498
7	876	granodiorite	330	3	3	67.08	0.5		140	963	699
8											
9	Tk-1/B	granodiorite	348	3	3	63.16	<0.1		142	1204	n.d.

Fig. A2.4 Examples of common formatting mistakes.

proved to be pasting via the Windows clipboard: just copy the pre-formatted data from the spreadsheet programme (both Excel and OpenOffice family work), and select from the menu *GCDkit*|Paste data from clipboard. If successful, the *R-Console* displays the metadata summary, a listing of loaded plugins and a report of data processing finished by the ‘...done!’ statement. If something goes wrong, the problem is most probably in the data format.

In addition, *GCDkit* is able to read Excel (*.xls, *.xlsx) and Access files. It can also import formats of other geochemical programs, such as MinPet, IgPet, NewPet, or of online geochemical databases (GeoRoc, Navdat or PetDB).

There are two potentially dangerous dialogues during data loading, where a wrong answer can harm the imported data:

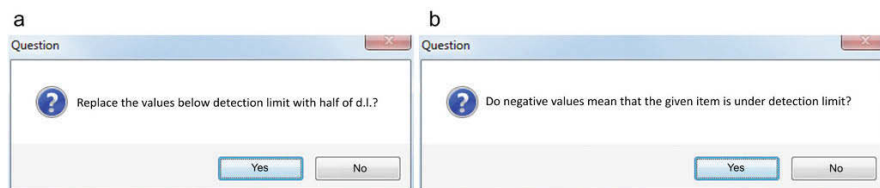


Fig. A2.5 Dialogues controlling the fate of ‘below detection’ and negative values.

The first window (Fig. A2.5a) asks whether the values below the known detection limit (such as ‘< 0.1’) should be replaced by its half (Sect. 2.1). Such replacement can be legitimate if statistical treatment is desired. Otherwise the values should be treated as missing (answer ‘No’).

The other question (Fig. A2.5b) concerns the meaning of negative values. Answering ‘Yes’ marks them as below detection limit and they are dealt with in ac-

cordance with the previous paragraph. If there are legitimate negative values in the file (e.g. isotopic δ values), the answer should be ‘No’.



***GCDkit* does not alter the original data file.** The system creates its own internal copy and any subsequent changes to the data (merging, subsetting, adding variables etc.) should be saved manually.

1.3.3 Merging Data

Closely related are two helpful tools for data appending and merging, an arduous job if done manually.

One dataset should already be loaded in both cases. The option *GCDkit|Append samples from file* adds new samples to existing data, introducing columns and empty values where necessary (Fig. A2.6a). If data overlap occurs (i.e. files contain lines with identical sample names), both are preserved with modified names.

On the other hand, the option *GCDkit|Append variables from file* adds columns with new data to existing samples. If any column appears in both merged files, both are preserved with modified labels (Fig. A2.6b).

a

	Locality	SiO2	TiO2	Rb	file
Sam1	Loc1	70	5	NA	File1
Sam2	Loc2	70	5	NA	File1
Sam3.x	Loc3	70	5	NA	File1
Sam3.y	Loc-3	69	NA	150	File2
Sam4	Loc-4	69	NA	150	File2

b

	Locality.x	SiO2.x	TiO2	Locality.y	SiO2.y	Rb
Sam1	Loc1	70	5	NA	NA	NA
Sam2	Loc2	70	5	Loc-2	69	150
Sam3	Loc3	70	5	Loc-3	69	150
Sam4	NA	NA	NA	Loc-4	69	150

Fig. A2.6 Schema of merging two datasets: appending samples (a) and appending variables (b).

1.3.4 Choosing Data

It is not always desirable to work with the whole dataset. *GCDkit* has several tools for this purpose.

1) In order to explore thoroughly part of the original dataset, one can use *Data handling|Select subset by...* to make a subset of the original dataset. The subset is available as the ‘main’ dataset from now on, until *Select whole data set* in the *Data handling|Select subset by...* menu is clicked, restoring the original data.

2) When specifying input data for a new plot or calculation, only a temporary selection is made. The selection criteria are ‘forgotten’ once the procedure (plotting, calculation) is completed, and the master dataset remains untouched.

3) Temporary selection of displayed data can also be made *after* a plot has been generated (menu *Plot editing*, see below).

1.3.5 Grouping

Samples can be assigned to groups based on several criteria. This allows many functions throughout the system to split the dataset into coherent subsets, which facilitates the comparisons of, say, analyses from individual intrusions.

Tools for assigning the data to groups, found in menu *Data handling|Set groups by...*, are listed in Table A2.1.

Table A2.1 Methods of group definition

Grouping method	Comment
<i>label</i>	values of any of the descriptive labels (locality, rock type, ...)
<i>numerical variable</i>	range of the variable (e.g. SiO ₂) split by arbitrary intervals
<i>classification diagram</i>	samples are classified by diagram and groups assigned accordingly
<i>cluster analysis</i>	the method and number of clusters may be chosen
<i>outline</i>	polygons are defined within a plot using mouse, analyses falling within are assigned to appropriate groups, the rest to group ‘unclassified’
<i>merge groups</i>	existing groups are listed in a spreadsheet and new names may be specified; groups with identical new names will be merged

1.4 Plotting

There are several plot categories with different behaviour. First, most of the single geochemical plots are generated by an internal *GCDkit* system called Figaro, which also includes tools for subsequent plot changes (available in menu *Plot editing*). Second, so-called plates act as a platform for the arbitrary combination of more Figaro plots arranged over a regular grid, which can be edited collectively as well as individually. Third, there are the mainly statistically oriented ones, which are native to R and cannot be edited by *GCDkit* tools. All graphics without exception may be exported in several vector or bitmap formats.

Most plotting functions are gathered in the *Plots* menu entry, but some are also in the *Calculations|Statistics* and elsewhere (Table A2.2). Actual plotting is preceded by series of pop-up windows, which vary from case to case, but the overall logic remains the same: what variables to plot (e.g. x, y axis), what samples to use and further plot details, if any.

How to select a variable for plotting or calculation

A dialogue box requesting variable selection pops up in various situations. Here are examples of the available responses:

- SiO₂ – complete name of variable,
- O – part of the variable name—the system offers a clickable list of matching variable names (all oxides and Os in this case),
- 5 – the sequential number of a variable listed in the *R-Console* (fifth here),
- (Na₂O+K₂O)/K₂O – simple equation; variables can be combined with:
 - brackets
 - arithmetic operators +, -, *, /, ^
 - R numerical functions (*sqrt*, *sum*, *mean*, *min*, *exp* etc.)
 - numbers and constants,
- [empty] – entering an empty field invokes a list of all variables.

It is good to notice that with each pop-up window the *R-Console* displays supplementary information, such as available compounds or samples.

Each plot opens in a separate window and remains available for saving until closed by the user. Note that too many opened windows may cause *GCDkit* to crash, so it is wise to close unnecessary windows from time to time (either individually or by *GCDkit|Close all graphic windows* entry).

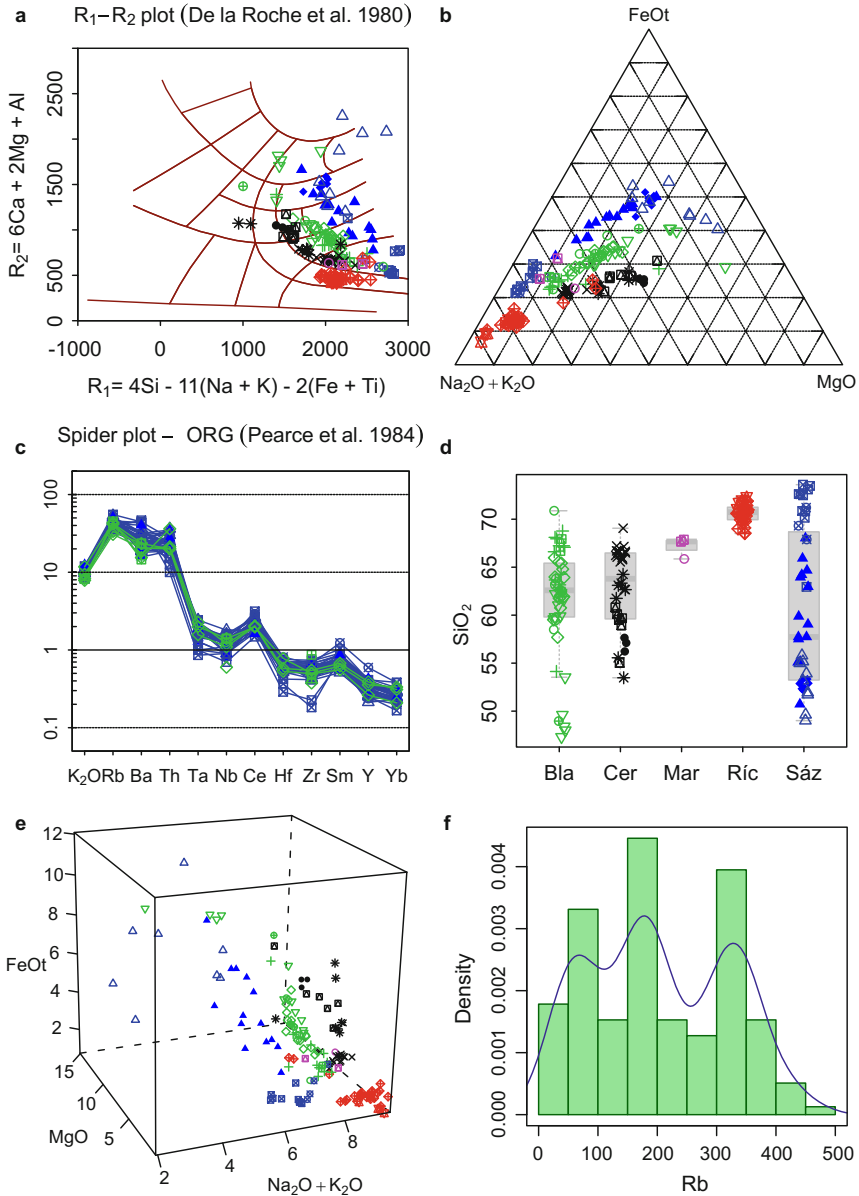


Fig. A2.7 Examples of *GCDkit*-generated plots. **a** Classification diagram (plotDiagram("LarocheVolc"); figRemove()). **b** Ternary diagram (ternary("Na2O+K2O", "FeOt", "MgO", grid=TRUE)). **c** Spider plot normalized by average Oceanic Ridge Granites (ORG) composition of Pearce et al. (1984) (spider(WR, chondrit="ORG", pch=labels\$Symbol, col=labels\$Col)). **d** Strip boxplot, sorted by groups (stripBoxplot("SiO2")). **e** 3D plot (threeD("Na2O+K2O", "MgO", "FeOt")). **f** Probability density plot (summarySingle("Rb"))

Table A2.2 Overview of basic plot types available in *GCDkit*

Menu item	multi?	vars	stats?	edit?	Note
<i>Plots</i> <i>Binary plot</i>	N	2	N	Y	generic xy plot
<i>Plots</i> <i>Ternary plot</i>	N	3	N	Y	generic triangle plot; x + y + z sums to 100%
<i>Plots</i> <i>3D plot</i>	N	3	N	N	generic 3D plot; can be rotated
<i>Plots</i> <i>xyz plot with circles</i>	N	3	N	N	xy plot with symbol size and colour according to z
<i>Plots</i> <i>Binary boxplot</i>	N	2	Y	N	xy plot with boxplots for each axis
<i>Plots</i> <i>Anomaly plot</i>	N	3	Y	N	xy plot with symbol and its size according to z
<i>Plots</i> <i>Multiple plots ... 1 vs. majors or 1 vs. traces</i>	Y	≥3	N	Y	Harker-style series of plots with common x axis
<i>Plots</i> <i>Multiple plots ... Copley</i>	Y	3	N	N	conditioning plot; several xy plots split according to z
<i>Plots</i> <i>Spider plots ... selected samples</i>	N	var	N	Y	spiderplot, multiple normalizing schemes
<i>Plots</i> <i>Spider plots ... summary boxplot</i>	N	var	Y	N	spiderplot with boxplot or box and percentile plot for each element
<i>Plots</i> <i>Spider plots ... double normalized</i>	N	var	N	Y	spiderplot as above renormalized to unity for a chosen element
<i>Plots</i> <i>Profiler</i>	N	≥1	N	Y	profile of one or more variables
<i>Plots</i> <i>Classification ...</i>	N	var	N	Y	various whole-rock chemistry based classification diagrams
<i>Plots</i> <i>Geotectonic ...</i>	var	var	N	Y	various whole-rock chemistry based geotectonic diagrams
<i>Calculations</i> <i>Statistics</i> <i>Single variable all/selection</i>	Y	1	Y	N	boxplot, percentile, histogram, probability density plot
<i>Calculations</i> <i>Statistics</i> <i>Single variable by group</i>	Y	1	Y	N	boxplot by group, probability density plot
<i>Calculations</i> <i>Statistics</i> <i>Majors summary</i>	Y	≥2	Y	N	boxplot and probability density plot for more variables
<i>Calculations</i> <i>Statistics</i> <i>Stripplot by groups</i>	N	1	Y	N	1D scatterplots for groups with jitter added for better visibility
<i>Calculations</i> <i>Statistics</i> <i>Plot summary by element ...</i>	N	2	Y	N	binary plot with group means and whiskers spanning ±1σ
<i>Calculations</i> <i>Statistics</i> <i>Correlation majors/traces</i>	Y	≥2	Y	N	matrix of correlation coefficients and scatterplots
<i>Calculations</i> <i>Statistics</i> <i>Correlation coef patterns</i>	Y	≥3	Y	N	plot of correlation coeff. patterns for each element (Rollinson 1993)
<i>Calculations</i> <i>Statistics</i> <i>Principal components</i>	Y	≥2	Y	N	biplots of principal component analysis (Gabriel 1971)
<i>Calculations</i> <i>Statistics</i> <i>Hierarchical clustering</i>	N	≥2	Y	N	hierarchical clustering dendrogram; multiple methods
<i>Calculations</i> <i>Norms ... Granite mesonorm</i>	N	mjr	N	Y	Q'-ANOR diagram of Streckeisen and Maitre (1979)

multi – combination of more simple plots?; vars – number of numerical variables; stats – statistics involved?; edit – diagram editable inside *GCDkit*?

1.4.1 Plot Settings

Although the specific properties of each plot are either predefined or set by the function call, there are several system-wide options that can be set beforehand.

Available symbols

- 20 symbols, coded by numbers 1–20 (*Plot settings|Show available symbols*)
- letters or other text strings (cannot be combined with symbols above)
- ASCII symbols in range 32–159, coded by numbers
- any Unicode symbol specified by its hexadecimal code (e.g. $-0\times 2642\text{I}$)

Note that for the latter three it may be difficult to identify the true projection spot

Available colours

- 7 basic colours with several shades, coded by numbers 1–49 (*Plot settings|Show available colours*)
- 657 named colours, coded by English name string, see `showColours()`
- any colour in RGB model (8-bit hexadecimal colour code, e.g. $\#FF0000$ is red)
- any colour in RGBA model (the same but with two extra digits for opacity, e.g. $\#FF0000BF$ is red with 75% opacity ($\sim 25\%$ transparency))

Symbols and colours are defined in several ways. First, they may be specified in the input file in columns titled ‘Symbol’ and ‘Colour’. The second option is to auto-assign them during loading according to one of the existing labels, for example, locality. The third possibility is to invoke the *Plot settings* menu, where they can be set according to a chosen label (*Colours by label* and *Symbols by label*) or according to groups (*Symbols/colours by groups*).

Transparency in the range from 0 to 1 can also be defined for each sample in *Plot settings|Set transparency*.

Allied to this is the layout of the plot legend. The legend content is defined together with symbols and colours (obviously). Plotting symbol properties must be pre-defined according to a label (or group); otherwise the legend displays meaningless information. A legend can be added to most plots. If both symbols and colours are based on the same parameter, only one legend appears; otherwise two are drawn, one for symbols and the other for colours. The prepared legend is added to existing plot by *Plot editing|Add...|Legend*.

Some more options controlling the general plot appearance are available in the menu *GCDkit|Options....* For instance, relative plotting symbol size, colour of discriminant boundaries and text annotations are adjusted here.

1.4.2 Single Plot Editing

Single plots can be further manipulated using tools in the *Plot editing* menu.



Only the current plot can be edited, i.e. that labelled ACTIVE in the Title bar. If another plot is created, appropriate places in memory are taken by the new data and the previous plot is not adjustable anymore.

Each plot can be saved to a file (in internal format) and later reloaded including the original data (*Plot editing*|*Save a graph* and *Load a graph*).

Many components of a plot can be edited including title and subtitle as well as axis labels, colours, text and symbol sizes. Table A2.3 lists available tools for adding items to plots, located in the *Plot editing*|*Add...* menu. The last two sit directly under *Plot editing*. Added items can be erased using the *Plot editing*|*Redraw*|*Reset* menu entry.

Table A2.3 Objects that can be added to plots; not all items apply to all plots

Menu entry	Added property
<i>ticks</i>	major and minor ticks for axes
<i>grid lines</i>	dashed grid lines
<i>legend</i>	legend for plotting symbols and colours
<i>reservoirs/minerals</i>	points/lines for predefined reservoirs and minerals
<i>text</i>	text annotation; click centre of its desired position
<i>arrow</i>	arrow; click start and end point
<i>box</i>	box; click opposite corners
<i>linear fit</i>	least-square fit; to all data or each group separately; click to position line label
<i>curve</i>	user-defined line/curve (x–y plots only)
<i>contours by group</i>	group outlines based on probability density estimation
<i>convex hulls by group</i>	polygons outlining each group
<i>Add contours</i>	contours of probability density plot
<i>Filled contour plot</i>	filled contour plot based on counting points density over a regular grid; no extrapolation takes place; meaningful only for large datasets

Another useful tool is zooming (*Plot editing*|*Zoom...*). There are two options—you can adjust the limits of either the x or y axis, or interactively select the rectangular zooming area by clicking its opposite corners. The zoomed area appears in a new window, which should be closed by clicking the OK button therein. If you want to further use it, just put focus on the *R-Console* and press *Esc*.

A further group of tools enables data identification within a plot. Go to *Plot editing*|*Identify points*, and by clicking any symbol in the diagram its name will

show up. The *Select samples* and *Highlight multiple points* selections in turn show (or highlight) points chosen by the standard selection procedure.

1.4.3 *Plates and Plate Editing*

Plates are collections of plots in a single window/on a single sheet. Their charm rests in the fact that plots can be created and edited individually as well as collectively.

Whereas plates can be built automatically, as are, for example, most geotectonic diagrams or all Harker plots, they can also easily be constructed from scratch. Menu entry *Plots|Plate of several plots* defines an empty grid of rows and columns. Right-clicking the context menu *GCDkit plate|Select slot* activates a red rectangle highlighting the “active” slot, which moves together with the cursor. The selection is confirmed with a left-click, and the rectangle colour becomes ochre. Fill the slot with the desired graphics from the *GCDkit plate|Introduce plot* menu option. Several plots are available (*Binary plot*, *Ternary plot*, *Spiderplot* and *Classification diagram*); a particularly convenient technique here is to introduce a previously prepared and saved plot in internal format (*Load a saved graph*).

The existing plate can be further edited, either each plot individually using tools described above (accessed by the *Plot editing* entry in the context menu), or all plots together (*Plate editing*). The latter entry contains several exporting options, tools for axis, plotting symbol and colours editing (and unification) and for text annotations removal.

1.4.4 *Spiderplots*

Apart from the standard multi-element diagram (spiderplot) there are several advanced variants (Sect. 4.2). Instead of individual samples, fields for predefined groups, spider boxplots or spider box and percentile plots can be drawn. Also double-normalized plots are available: once normalized data are re-normalized by the content of one—normally the least incompatible—element, and all the patterns intercept here. Further options, such as combination of shaded fields with individual patterns, can be set up from the command line. See `example(spider)` and `help(spider)`. Normalization data can be inspected and edited in a text file, see this Appendix, Sect. 2.4 for details. The usage of standard spiderplots is discussed in Sect. 3.6. of the main text.

Another useful option is to normalize using a sample chosen from the dataset or average of selected samples.

1.4.5 Classification and Geotectonic Diagrams

Descriptive geochemistry of igneous rocks traditionally employs numerous classification diagrams. Whereas some are easy to implement numerically (i.e. Shand's AN/K–ACN/K diagram), other use empirical or even curved field boundaries and a graphical approach is the only feasible solution.

GCDkit contains a series of Figaro-based classification templates, which can be employed for plotting as well as (automatic) sample classification. The list of available diagrams is accessible from *Plots|Classification...* (the actual possibilities depending on available data). The classification is to be found at *Data handling|Classify...* Results can be appended to `labels` or treated otherwise as described later (Sect. 1.6, this Appendix). Classification may also be used for data grouping (*Data handling|Set groups by... |... diagram*).

Furthermore, *GCDkit* also contains a set of geotectonic diagrams, available from menu *Plots|Geotectonic...* Whereas these may resemble classification plots, there is one crucial difference: geotectonic diagrams are in all cases designed as a hint for geotectonic considerations rather than for authoritative determination of palaeotectonic setting. This is why the option for 'classification' using geotectonic diagrams is (intentionally) disabled. Both types of diagrams are also discussed in the main text (sections 3.4 and 3.5).



Read the original paper. This general rule is particularly important here: each classification diagram has its limits and application rules specified. These guidelines cannot be fully followed by the classification routine, and the results can thus be misleading albeit numerically correct. References for each diagram can be found in *GCDkit* help, or in the file `GCDkit/doc/diagrams.pdf` in your `R library` folder.

1.5 Calculations

Numerous calculation routines are the real core of *GCDkit*. Calculated data are displayed in the *Console* and stored internally (in the variable `results`). From here they can be inspected, exported or appended to data (*GCDkit|Append results to data*), i.e. stored for any subsequent calculations and plotting.

Some calculations are performed automatically during data loading. Depending on the data available in the file, some elemental abundances and basic indexes are computed (K, Ti, P, FeO_i, mg#, Mg#, A/NK, A/CNK, K₂O/Na₂O). All are appended to the main data table `WR`. Majors recalculated to anhydrous basis are stored in `WRanh`, and recast to millications (`milli`; Sect. 2.2.2, main text).

Within the *Calculation* menu are available several normative and related schemes as summarized in Table A2.4. *Calculations|Statistics* offers several variants of descriptive statistics together with graphical presentation.

Table A2.4 Main calculation routines

Required action	Solution
Summary statistics* for one variable	<i>Calculations Statistics... Single variable...</i>
Compare summary statistics* of single variable between groups	<i>Calculations Statistics... Single variable by group</i>
Compare data ranges between groups	<i>Calculations Statistics... Ranges by groups</i>
Summary statistics* for more variables	<i>Calculations Statistics... Majors summary</i>
Compare summary statistics* of more variables respecting groups	<i>Calculations Statistics... Majors summary by group</i>
Correlation coefficients matrix	<i>Calculations Statistics... Correlation: majors (in graphical form)</i>
Principal components	<i>Calculations Statistics... Principal components</i>
CIPW norm	<i>Calculations Norms... CIPW</i>
CIPW norm with hornblende and biotite	<i>Calculations Norms... CIPWhb</i>
Granite mesonorm	<i>Calculations Norms... Granite mesonorm</i>
Catanorm	<i>Calculations Norms... Catanorm</i>
Least-square calculation of modal composition	<i>Calculations Norms... Mode (both constrained and unconstrained variants are calculated)</i>
Niggli's cationic parameters	<i>Calculations Norms... Niggli</i>
Coefficients of De la Roche et al. (1980)	<i>Calculations Norms... De la Roche</i>
Coefficients of Debon and Fort (1983)	<i>Calculations Norms... Debon and Le Fort</i>
Larsen's, Kuno's, Agpaitic indexes	<i>Calculations Norms... Miscellany</i>
Data normalization used for spiderplots	<i>Plots Spider plots...</i>
User-defined, new variable	<i>Calculations Calculate a new variable</i>

*Summary statistics here means number of observations, mean, median, standard deviation, minimum, maximum and quartiles

As already mentioned in Sect. 1.4 of this Appendix, dialogues prompting for a variable selection in course of plot preparation also accept simple formulae. Variables (SiO_2 , La etc.) can be combined with numbers (3, pi), brackets, arithmetic operators (+, -, *, /, ^) and numerical functions (sum, mean, sin etc.).

The same calculation routine can also be called on demand at *Calculations|Calculate a new variable* and the result appended to the internal data. More complicated expressions can be also saved for later use in a text file as R code using *Calculations|Add a new variable to a script*.

1.6 Exporting from *GCDkit*

The system would be of little use without a method to get data and results out of it, either numerical or graphical.

If the dataset was modified within *GCDkit*, for example by merging, subsetting, or direct editing, it is necessary and wise to save it occasionally (yes, the system can crash unexpectedly). The menu entry *GCDkit|Save data* stores the data in *GCDkit* native format (Appendix B, sect. 1.3.1), whereas *GCDkit|Export data table to...* offers several alternative formats (**.html*, **.xls*, **.xlsx*, **.mdb*, **.dbf*). The HTML option is of particular interest, as it features routines for sample and variable selection, computes the sum and rounds off the data if required. This is the best option to obtain a quick and well formatted data table for presentation.

Apart from raw data, each computation as well as many plots produce numerical output, displayed in the *R-Console* and stored in variable `results`. These values can be saved or exported in the same formats as the dataset (*GCDkit|Save results* and *GCDkit|Export results table to...*, respectively). Alternatively, perhaps more handy is to export via the system clipboard (*GCDkit|Copy results to clipboard*).



Do not copy results directly from the console. This is particularly inconvenient, as the output is usually poorly formatted and contains unnecessary symbols. Use one of the exporting options outlined above instead.

Any graphical window may be saved to one of several formats; vector files as well as bitmaps (raster). Both vector and bitmap images can also be transferred via the Windows clipboard. Exporting options are available in the title bar of each graphical window (*File|Save as...*); a somewhat limited set of options is also accessible in the right-click context menu. Moreover, all opened graphical windows can be saved en bloc via *GCDkit|Save all graphics to...* option.



Export to vector graphics for further editing. Using a vector format facilitates further modification of *GCDkit* plots with graphical programs such as *Adobe Illustrator* or *Corel Draw*. Available formats are Windows metafile (**.wmf*), postscript (**.eps*) and Adobe's portable format (**.pdf*), the last one usually giving the best results.

Chapter 2

Under the Bonnet: *GCDkit* Internals

Chapter one introduced the reader into using *GCDkit* with few details of the programme's internal design or binding to the R environment. The dark side of such an approach is obvious—a substantial part of the functionality and flexibility remains hidden. Here we try to go into more detail, explaining the structure of the data, further tools available via the command line and ways to extend the system.

2.1 R Language and *GCDkit*

R language is an open-source project developed in a public, collaborative manner. Apart from the team of core developers, a large community is producing specialized code organized in packages. Both R-core and contributed packages are available from the CRAN repository at cran.r-project.org. *GCDkit* is one such package. However, as it does not follow the strict rules for official packages (most importantly, it is so far Windows only), it is not included in the official repository. The main download hub remains its own home page www.gcdkit.org/download.

The *GCDkit* functions are available through a clickable menu interface or in command line mode. In the former approach, input data and other necessary parameters are supplied to functions via pop-up dialogues. This is user-friendly but tedious and the range of variants is limited. Command line mode on the other hand offers much more flexibility but is more demanding. Advanced users can type commands directly into the *R-Console* or run a plain text file with a *GCDkit* or R script.

To facilitate a user's transition from menu to console approach, *GCDkit* displays the appropriate function in the console (in red) each time a menu is called. This statement is however without used parameters. Many functions do not need any; these can be re-typed in the same form. Otherwise it is necessary to explore the help system (type `?function_name`), which lists the proper syntax, all parameters, detailed description and examples for each function. In particular the abundant examples can provide inspiration for more creative uses of the functions.

Where to find *GCDkit* within Windows folder structure

As for any R package, *GCDkit* files are stored in the `library` folder of the R installation. It resides in the default Windows folder (if not specified otherwise during installation). So, the complete path to *GCDkit* root should be something like:

```
C:\Program Files\R\R-3.1.0\library\GCDkit
```

A working directory containing the data can be set in menu *GCDkit|Options...*

2.2 Data Variables

GCDkit stores the geochemical data in several variables. These can be accessed directly from the *R-Console* or used in batch mode (e.g. in plugins):

- `WR` – matrix with all loaded and appended numerical data, as well as some variables calculated during sample loading (*A/CNK*, *Ti*, *FeOt*...),
- `labels` – a dataframe with the rest of the information. Columns contain all the textual data, as well as plotting attributes ‘*Colour*’, ‘*Symbol*’ and ‘*Size*’,
- `WRanh` – matrix with oxides recalculated to 100 % anhydrous basis,
- `milli` – matrix of molar proportions of the elements (see `?millications`),
- `groups` – vector of group ‘levels’ assigned to each sample (i.e., if groups are defined by locality, vector `groups` contains locality name for each sample),
- `results` – an object (most typically, a matrix) containing the outcome of the last calculation, including the auxiliary data of some plotting functions.

All variables can be accessed and manipulated just like any other R object, for instance `WR[, "SiO2"]` will return a named vector containing the silica contents of your samples. Furthermore, `WR`, `labels`, `WRanh` and `milli` all carry sample IDs as rownames, and the same holds for the `groups` attribute name. Thanks to this the variables can be matched or indexed by sample names.

2.3 System Variables

Moreover, *GCDkit* defines some useful system variables. Vectors `major`, `REE`, `HFSE` and `LILE` contain eponymous species², and can be used as a nickname throughout the system (try `multiple("SiO2", LILE)` as an example). Use of vector ‘`mw`’ containing atomic weights is obvious (try `mw["La"]` or `mw[LILE]`).

Variable	Comment
<code>major</code>	SiO ₂ , TiO ₂ , Al ₂ O ₃ , Fe ₂ O ₃ , FeO, MnO, MgO, CaO, Na ₂ O, K ₂ O, P ₂ O ₅
<code>REE</code>	La, Ce, Pr, Nd, Sm, Eu, Gd, Tb, Dy, Ho, Er, Tm, Yb, Lu
<code>LILE</code>	Rb, Sr, Ba, K, Cs, Li
<code>HFSE</code>	Zr, Hf, Nb, Ta, Ti, La, Ce, Y, Ga, Sc, Th, U
<code>MW</code> , <code>mw</code>	vector of molar/atomic weights of oxides and elements, respectively
<code>mol.wt</code>	matrix of molar weights, number of cations and of O for all oxides
<code>filename</code>	name (including path) of last loaded or appended file
<code>data.dir</code>	path to default data folder
<code>gcdx.dir</code>	path to <i>GCDkit</i> system folder

² NB that these three variables store the list of relevant elements that are *present* in your file.

2.4 Tailoring *GCDkit* to Suit Your Needs

GCDkit includes several built-in datasets used for internal purposes. These are stored in plain text files and can be edited manually, though care should be taken to maintain the formatting.

Data for normalization within spider diagrams are retrieved from a file `spider.data` in the *GCDkit* library root folder (see `gcdx.dir`). Each normalization series is defined in triplet of text lines, with individual elements separated by commas:

```
MORB (Pearce 1996)
Th,Nb,Ce,Zr,Ti,Y
0.2,2.7,10,90,8692.75,30
```

The first line contains the title and reference, the second element names and the third normalizing values. The element order matters as it determines sorting of the spidergram. There is an empty row between the adjacent normalization schemes. As the file `spider.data` is read only when it is needed, the user can add or delete normalization schemes at will using a text editor. See also help to `selectNorm`.

Similar format and location apply to the `reservoir.data` file, which is used by the `Plot editing\Add...|Reservoirs/Minerals` option. However, the elemental order does not matter here, as this function only adds items to an existing plot. The same routine also invokes the file `idealmins.data` to get mineral compositions. The format is tab-delimited table in this case, which may add both rows and columns in units corresponding to the data loaded in *GCDkit* (i.e. wt. % and ppm).

The templates for classification and geotectonic diagrams are also stored as plain text files in the `Diagram` folder of the *GCDkit* root. This allows an R-literate user to explore, edit (translation being the most likely reason) or even create a new template (with a little more effort). Although there is not space to explain the format in detail, it is fairly self-explanatory. In short, the template defines an R list, which is assigned to the variable `sheet`. The boundaries and texts for the plot are each defined as one list item, the item `classf` carries parameters for classification, item `GCDkit` and arguments written in the `sheet` assignment define the parameters determining the plot appearance.

2.5 Plugins

The previous section shows some options to adjust built-in data and templates used for standard *GCDkit* functionality. Users can go further, by creating a plugin to add new functions. In outline, after successfully loading a datafile the system executes any R code (recognized by a suffix of `.r` or `.R`) found in the

\Plugin subdirectory of your *GCDkit* installation. The plugin mechanism thus enables *GCDkit* to be expanded without tweaking or breaking the whole system.

Plugins should include one or more functions that combine R and/or *GCDkit* commands and manipulate any of the geochemical data or system variables (this Appendix, sections 2.2 and 2.3). These functions can be integrated into the menu structure and invoked by other users. By convention, plugins should be called from the *Plugins* menu.

In the Windows version of R, there are two functions for defining the menu structure:

- `winMenuAdd("Plugins/submenu")` – creates a new menu group,
- `winMenuItem("Plugins/submenu", "Name", function())` – defines a new menu item and links it to the corresponding function.

The plugin can also employ dialogue boxes (see help for list of their parameters):

- `winDialog()` – returning value of pressed button, such as ‘Ok’ or ‘No’
- `winDialogString()` – returning entered string,
- `select.list()` – returning one or more selected values,
- `choose.files()` – a file selection dialogue.

A minimalistic plugin can look as follows:

```
newPlugin<-function() {
  myString<-winDialog("yesno",
    "Print available compounds?")
  if (myString=="YES") cat(colnames(WR), "\n")
}
winMenuAdd("Plugins/New")
winMenuItem("Plugins/New", "Run plugin", "newPlugin()")
```



There are some general rules especially important if the new plugin is intended for sharing with other users (which we recommend):

- do integrate the plugin into the appropriate menu, i.e. *Plugins*,
- do not rewrite any existing objects,
- in order to maintain data integrity, do not alter existing *GCDkit* variables directly; create a new variable or use dedicated functions instead,
- use comments in the code to explain its functionality,
- write documentation.

Standard plugins, in the `Plugin` directory, can serve as an inspiration. Further details/hints for plugin programming were given by Janoušek and Moyen (2014).

References

- De la Roche H, Leterrier J, Grandclaude P, Marchal, M (1980) A classification of volcanic and plutonic rocks using R_1R_2 -diagram and major-element analyses—its relationships with current nomenclature. *Chem Geol* 29:183–210
- Debon F, Le Fort P (1983) A chemical–mineralogical classification of common plutonic rocks and associations. *Trans Roy Soc Edinburgh, Earth Sci* 73:135–149
- Gabriel K (1971) The biplot graphic display of matrices with application to principal component analysis. *Biometrika* 58: 453–467
- Janoušek V, Moyen J-F (2014) Mass balance modelling of magmatic processes in *GCDkit*. In: Kumar S, Singh RN (eds) *Modelling of magmatic and allied processes*. Society of Earth Scientists Series, vol 83. Springer, Berlin, pp 225–238
- Pearce JA, Harris NBW, Tindle AG (1984) Trace element discrimination diagrams for the tectonic interpretation of granitic rocks. *J Petrol* 25:956–983
- Rollinson H (1993) *Using geochemical data: evaluation, presentation, interpretation*. Longman, Harlow
- Streckeisen A, Le Maitre R (1979) A chemical approximation to the modal QAPF classification of the igneous rocks. *Neu Jb Mineral, Abh* 136: 169–206

Appendix C

Solving Systems of Linear Algebraic Equations in R

1.1 Linear Algebraic Equation Systems (Single Solution)

Solving sets of linear equations is in fact an inverse of matrix multiplication. If after multiplication of a matrix \overline{A} by a vector \overline{x} :

$$\overline{y} = \overline{A} \times \overline{x} \quad (1.1)$$

Or, in the R syntax (using the operator `%*%`—Table A1.3):

```
> y <- A%*%x
```

only the matrix \overline{A} and vector \overline{y} are known, we can back-calculate the vector \overline{x} using:

```
> x <- solve(A,y)
```

provided that there is exactly the same number of independent equations as variables (i.e. \overline{A} is a square matrix that can be inverted).



Exercise A3.1: Solving a system of linear algebraic equations

- Solve the following set of linear equations:

$$\begin{array}{rclclcl} x & + & 2y & - & 0.7z & = & 21 \\ 3x & + & 0.2y & - & z & = & 24 \\ 0.9x & + & 7y & - & 2z & = & 27 \end{array}$$



```
> A <- matrix(c(1,3,0.9,2,0.2,7,-0.7,-1,-2),3,3)
> A
      [,1] [,2] [,3]
[1,]  1.0  2.0 -0.7
[2,]  3.0  0.2 -1.0
[3,]  0.9  7.0 -2.0
```

```

> y <- c(21, 24, 27)
> x <- solve(A, y)
> x
[1] 30 20 70
> # checking the result
> A%%x
      [,1]
[1,]  21
[2,]  24
[3,]  27

```

1.2 Overdetermined Systems (Unconstrained Least-Square Method)

If there are more independent equations than variables, the system is overdetermined. The matrix $\overline{\mathbf{A}}$ is not square, and thus cannot be inverted. But we can calculate an approximate estimate of the vector $\overline{\mathbf{x}}$ (denoted here $\overline{\mathbf{x}'}$). Defining:

$$\overline{\mathbf{y}'} = \overline{\mathbf{A}} \times \overline{\mathbf{x}'} \quad (1.2)$$

we must find the value of $\overline{\mathbf{x}'}$ such that the computed and real elements of the vector $\overline{\mathbf{y}}$ differ as little as possible. The most common approach is to minimize the sum of the squares of the differences between each element of $\overline{\mathbf{y}'}$ and $\overline{\mathbf{y}}$ (so-called least-square method: Bryan et al. 1969; Albarède and Provost 1977; Albarède 1995):

$$R^2 = \left| \overline{\mathbf{y}'} - \overline{\mathbf{y}} \right|^2 = \min \quad (1.3)$$

It can be demonstrated that the best least-square solution is then:

$$\overline{\mathbf{x}'} = \left(\overline{\mathbf{A}}^T \times \overline{\mathbf{A}} \right)^{-1} \times \overline{\mathbf{A}}^T \times \overline{\mathbf{y}} \quad (1.4)$$

By analogy with Eq. (1.1), $\left(\overline{\mathbf{A}}^T \times \overline{\mathbf{A}} \right)^{-1} \times \overline{\mathbf{A}}^T$ is referred to as the (Moore–Penrose) “pseudo inverse” of matrix $\overline{\mathbf{A}}$ (it serves the same purpose as an inverse).

Albarède (1995) discussed in a detail all the necessary mathematical apparatus that is behind the solution. Janoušek and Moyen (2014) have shown implementation of (unconstrained) least-square method in R and its utilization for solving simple geochemical problems, such as modal calculations or reverse mass-balance modelling of fractional crystallization. The least-squares are implemented by the R function:

lsfit(A, y, intercept = FALSE¹)

The outcome of this function is a list, of which the most interesting is the component `$coefficients`, corresponding to the vector \bar{x}' as defined above, and a component `$residuals` with deviations between the calculated (\bar{y}') and observed (\bar{y}) compositions.

The sum of squares of residuals R^2 [Eq. (1.3)] is an useful quantifier for the goodness of fit. Even though it shows a marked tendency to decrease with increasing number of variables involved in the calculation, as a rule of thumb it should not greatly exceed one. $R^2 \gg 1$ means that the model is not acceptable: the proposed geological hypotheses (i.e. composition of the primitive liquid, nature or composition of the cumulate minerals, or even the process itself) do not explain the observed variation. Note that the error is absolute, and it is therefore always wise to examine the residuals for individual elements or oxides.

1.3 Constrained Least-Square Method

In geochemistry are very often examined some variables that have to fulfil some condition. Most commonly they sum up to a certain value (e.g., unity or 100 %). The ordinary least-square method generally does not produce such normalized solutions, though. Albarède (1995) presented the necessary equations for modified, 'constrained' least squares defining the Lagrange multiplier λ as:

$$\lambda = \frac{1 - \bar{\mathbf{J}}^T \bar{\mathbf{x}}'}{\bar{\mathbf{J}}^T \left(\bar{\mathbf{A}} \times \bar{\mathbf{A}} \right)^{-1} \bar{\mathbf{J}}} \quad (1.5)$$

where $\bar{\mathbf{x}}'$ stands for an ordinary least-square solution ² and $\bar{\mathbf{J}}$ is a vector whose all elements are 1. The constrained least-squares solution is then given by:

$$\hat{\bar{\mathbf{x}}} = \bar{\mathbf{x}}' + \lambda \left(\bar{\mathbf{A}} \times \bar{\mathbf{A}} \right)^{-1} \bar{\mathbf{J}} \quad (1.6)$$

a worked example of least-squares implementation, both unconstrained and constrained, for 'normative' calculations (in wt. %) is given in Exercise 9.4.

¹ Note that the parameter `intercept` needs to be set to `FALSE` for the solution to pass through the origin.

² Obtained by `lsfit` as above.



The so-called generalized mixing problems in igneous or metamorphic geochemistry (including chemical mode computations, magma mixing, liquid line of descent or batch partial melting modelling, end-member calculations and balancing of mineral reactions) are indeed the most commonly solved by the classic least-square techniques (Bryan et al. 1969; Albarède and Provost 1977; Stormer and Nicholls 1978; Le Maitre 1979, 1981). However, these mass-balance problems can be approached also by other minimalization algorithms such as linear programming (Wright and Doherty 1970).

The standard least-square method does not permit constraining the sign of the coefficients of the solution, even when all-positive/all-negative or even mixed signs do not make a petrological sense³. This in fact provides an independent check on the feasibility of the solution. The linear programming, on the other hand, allows much easier forcing all-positive coefficients in the problem. This can be a dubious advantage, however (Rock 1988).

References

- Albarède F (1995) Introduction to geochemical modeling. Cambridge University Press, Cambridge
- Albarède F, Provost A (1977) Petrological and geochemical mass-balance equations: an algorithm for least-square fitting and general error analysis. *Comput and Geosci* 3:309–326
- Bryan WB, Finger LW, Chayes F (1969) Estimating proportions in petrographic mixing equations by least-squares approximation. *Science* 163:926–927
- Janoušek V, Moyen JF (2014) Mass balance modelling of magmatic processes in *GCDkit*. In: Kumar S, Singh RN (eds) Modelling of magmatic and allied processes. Society of Earth Scientists Series, vol 83. Springer, Berlin, pp 225–238
- Le Maitre RW (1979) A new generalised petrological mixing model. *Contrib Mineral Petrol* 71:133–137
- Le Maitre RW (1981) GENMIX—a generalized petrological mixing model program. *Comput and Geosci* 7:229–247
- Rock NMS (1988) Numerical Geology. A source guide, glossary and selective bibliography to geological uses of computers and statistics. Lecture Notes in Earth Sciences, vol 18. Springer, Berlin
- Stormer JC, Nicholls J (1978) XLFRAC: a program for the interactive testing of magmatic differentiation models. *Comput and Geosci* 4:143–159
- Wright TL, Doherty PC (1970) A linear programming and least squares computer method for solving petrologic mixing problems. *Geol Soc Amer Bull* 81:1995–2008

³ But one needs to be aware of the problem of peritectic minerals, for which a negative coefficient is meaningful. See Sect. 6.3.

Index

A

- A/CNK-A/NK, 14
- Accessory minerals, 212
 - allanite, 215
 - apatite, 134
 - exercise*, 150, 216
 - inclusions, 215
 - monazite, 131, 215
 - saturation thermometry, 130, 132, 135, 216
 - solid solutions, 216
 - solubility, 129
 - xenotime, 215
 - zircon, 129, 214, 217, 255, 271
- Activity, 99
- AFC, 117, 163
 - energy constraints, 119, 186, 231
 - exercise*, 173
 - reverse solution, 167
 - software, 119, 168
- Amphibole, 102
- Anatexis. *See* Melting
- Apatite, 134
- Assimilation, 160, 186
- Assimilation and fractional crystallization. *See* AFC
- Atacazo-Ninahuilca Complex, 245

B

- Basic geochemical indexes, 14
- Binary mixing, 159, 186
 - binary isotopic plot, 161
 - concentration vs. isotopes plot, 159
 - equation in x-y plot, 114, 161
 - error propagation, 160
 - exercise*, 148, 169, 171
 - major elements, 78

mixing test (incl. *exercise*), 199

- reverse model, 128, 167
 - exercise*, 175
- trace elements, 114

Binary plot

- constant sum effect, 30
- lever rule, 71
- log–log
 - element ratio, 45
 - fractionation vectors, 202
 - incompatible vs. compatible elements, 195, 250
- mixing, 78
- mixing hyperbola, 114
- mixing test, 199
- two incompatible elements, 198

Biotite, 232

- Bowen's reaction scheme, 1
- Bulk distribution coefficient, 103
 - non constant, 113

C

- Classification diagrams, 34
- Clinopyroxene, 102
- Closure effect. *See* Binary plot, constant sum effect
- Compatibility of elements, 101, 109
 - order of compatibility (incl. *exercise*), 192
- Crystallization, 105
 - batch, 106
 - deep-level, 182
 - equation, 76
 - equilibrium. *See* Batch evolving cumulate, 74

- final liquid composition
 - selection, 206
- fractional, 106
 - exercise*, 85, 86, 87, 141, 142
- fractional, reverse model, 82, 125
 - exercise*, 93, 153
- fractionating mineral
 - identification, 202
 - identification, 195
 - incomplete crystal separation, 75, 120, 181
 - mechanical constraints, 232
 - peritectic phase, 76
 - shallow-level, 181
 - source composition selection, 206
 - terminology, 70, 77
 - worked example, 245
- Cumulate, 69, 71, 182
 - aggregated composition, 108
 - evolving, 74
 - incomplete separation, 75
- D**
- Degree of crystallization, 69
- Descriptive statistics, 18
 - exercise*, 18, 21
- Dilute trace elements. *See* Trace elements
- E**
- Equilibrium, 99, 105, 234
- Essential structural components (ESC), 100, 129. *See also* Accessory minerals
- F**
- Filter pressing, 180
- Fractional crystallization. *See* Crystallization
- Fractionation vectors (incl. *Exercise*), 202
- G**
- Garnet, 102
- GCDkit, 5
 - anomaly plot, 49
 - basic indexes, 16
 - exercise*, 15
- calculation
 - results, further use, 18, 29
- calculations, 329
 - built-in routines, 330
- classification diagrams, 34, 329, 334
- contour plot, 48
- data format, 318
- descriptive statistics, 22, 330
- direct access to data, *exercise*, 12
- documentation, 318
- double-normalized
 - spiderplots, 47
- export data, 331
- export graphics, 331
- export results, 331
- Figaro, 29, 34, 323
- files localization, 332
- geotectonic diagrams, 329
- groups, 22, 23, 40, 322
- help system, 332
- installation, 315
- internal variables, 333
 - `idealmins.data` file, 334
 - labels, 318
 - milli, 17, 329
 - mw, 11
 - `reservoir.data` file, 334
 - results, 329
 - `spider.data` file, 334
 - WR, 318
 - WRanh, 329
- loading data, 319
- merging data, 321
- new variable, 330
- personalization, 334
- plate, 41, 323, 328
- plot, 323
 - adding properties, 327
 - annotation, 29
 - colours, 326
 - contours, 327
 - curve, 327
 - editing, 29, 327
 - legend, 326, 327
 - symbols, 326

- zoom, 327
 - plots available, 325
 - plotted variables specification, 323
 - plugins, 334
 - sample session, 317
 - Saturation plugin, 135
 - spider boxplots, 47
 - spiderplots, 40, 46, 328, 334
 - SrNd plugin, 65, 246
 - stripplot, 50
 - subsetting data, 322
 - user interface, 316, 332
- GCDkit function
- addContours(), 48
 - addResults(), 29
 - annotate(), 29
 - apSaturation(), 135
 - Batchelor(), 17
 - binary(), 28, 325
 - Catanorm(), 17
 - CIPW(), 17
 - classify(), 35
 - cutMy(), 23
 - Debon(), 17
 - figMulti(), 40
 - figRemove(), 40
 - figUser() and similar, 29
 - filledContourFig(), 48
 - groupsByLabel(), 22
 - LaRoche(), 17
 - loadData(), 11, 319
 - Mesonorm(), 17
 - milli(), 17
 - Mode(), 96
 - molecularWeight(), 16
 - multiple(), 32
 - mzSaturation(), 135
 - peterplot(), 49
 - plateCex() and similar, 41
 - plateExtract(), 41
 - plotDiagram(), 34
 - prComp(), 225
 - selectNorm(), 39
 - selectPalette(), 146
 - spider(), 40, 46, 328
 - spider.contour(), 46
 - spider2norm(), 47
 - spiderBoxplot(), 47
 - stripBoxplot(), 50
 - summaryByGroup(), 22
 - summaryRangesByGroup(), 22
 - summarySingleByGroup(), 22
 - ternary(), 34, 325
 - Villaseca(), 17
 - WRComp(), 91
 - zrSaturation(), 135
- Geotectonic diagrams, 35
- H**
- Harker plots, 2
 - exercise, 31
 - Henry's Law, 99, 103
 - Hornblende. *See* Amphibole
 - Hybridization. *See* Mixing
- I**
- Incompatible elements. *See* Compatibility of elements
- Isotopes, 53
- epsilon notation (incl. *Exercise*), 57
 - initial ratio (incl. *Exercise*), 55
 - isochron (incl. *Exercise*), 63
 - mixing, 159
 - model ages, 60
 - exercise, 61, 62
 - parent/daughter ratio, 53
- K**
- Kd. *See* Partition coefficient
- L**
- Lattice strain model, 211
 - Least-square method. *See* Linear equations
 - Leucosome, 183
 - Lever rule, 71
 - Linear equations
 - exact solution, 337
 - exercise, 337
 - least-square method, 82, 338
 - constrained, 339
 - linear programming, 340
 - over-determined system, 338
 - under-determined system, 81
 - Liquid line of descent, 74, 76
 - Liquid remaining, 69

M

Mafic microgranular enclaves (MME), 185, 221
 Magma mixing. *See* Mixing
 Major elements, 67
 Mass balance, 69

- accessory minerals, 214
- equation, 70
- generalized form, 79
- matrix formulation, 72

 Melting, 105

- aggregated, 110
- batch, 110
- batch, reverse model, 127
- crustal anatexis, 183
- disequilibrium, 234
- energy constraints, 231
- equation, 76, 77
- fluxed, 121
- fractional, 110
- fractional with accumulation, 110
- fractional, reverse model, 82
- geological evidence, 183
- identification, 195
- mantle, 184
- melt composition selection, 206
- non-modal, 111
- partial *exercise*, 89, 144
- partial, reverse model
 - exercise*, 94, 154
- peritectic phase, 76, 265
- prograde metamorphism, 265
- progressive, 76
- segregation, 233
- source composition selection, 206
- terminology, 75, 77
- worked example, 261

 Migmatite, 183
 Millications, 16
 Mingling, 185
 Mixing, 105, 114

- binary. *See* Binary mixing
- end-member constraining, 221
- equation, 71
- exercise*, 91
- field evidence, 185
- generalized form, 79

- identification, trace elements, 195
- reverse model, 83

 Mixing hyperbola, 114, 161

- asymptotes, 162

 Modelling

- choosing strategy, 181
- colinearity, 227, 252
- compositional space, 225
- data resources, 3
- element compatibility, 191
- equilibration volume, 234
- internal consistency, 228
- mechanical constraints, 232
- mineral as solid solution, 228, 250
- model constraining, 205
- Monte Carlo check, 254
- phase equilibria, 273
- process identification, 160, 195, 236
- robustness, 254
- software, 3, 208, 273, 320
- system reduction, 227
- thermodynamic constraints, 231

 Monazite, 131
 Multi-element diagram. *See* Spiderplots

N
 Niggli's values, 16
 Normative calculation

- exercise*, 95, 96

 Norms, 17

O
 Olivine, 102, 232

P
 Partial melting. *See* Melting
 Partition coefficient, 101

- calculation, 211
- controlling physical factors, 102
- resources, 211

 Peraluminosity, 14
 Peritectic reactions, 76
 Phase rule, 228

Phlogopite, 205
 Plagioclase, 103
 Principal component analysis, 225

R

Rayleigh's fractionation law, 106

Reverse models, 81

R-function

%% operator, 288
 abline(), 297, 299
 aggregate(), 293
 apply(), 288
 args(), 312
 array(), 287
 as.matrix() and similar, 291
 axis(), 305
 boxplot(), 302
 by(), 293
 c(), 282
 cat(), 309
 cbind(), 288
 colnames(), 288
 contour(), 48, 304
 coplot(), 304
 curve(), 300
 cut(), 292
 data(), 295
 expression(), 306
 factor(), 292
 filled.contour(), 48, 304
 for loop, 310
 function(), 311
 getwd(), 294
 grid(), 300
 help(), 278
 hist(), 303
 identify(), 309
 if-else condition, 310
 is.matrix() and similar, 291
 is.na(), 286
 legend(), 301
 levels(), 292
 lines(), 301
 list(), 290
 lm(), 299
 locator(), 309
 ls(), 281
 lsfit(), 93, 175, 339
 matrix(), 286

ordered(), 292
 pairs(), 302
 palette(), 297
 par(), 296, 298, 305
 parse(), 306
 paste(), 285
 plot(), 295
 points(), 301
 print(), 309
 rbind(), 288
 read.table(), 11, 294
 readClipboard(), 294
 readline(), 309
 rep(), 283
 repeat-break loop, 311
 rm(), 281
 rownames(), 288
 sapply(), 219, 313
 seq(), 283
 setwd(), 294
 solve(), 288, 337
 source(), 280
 strsplit(), 285
 substitute(), 307
 substring(), 285
 summary(), 302
 t(), 288
 table(), 293
 tapply(), 20, 293
 text(), 299
 while loop, 311
 winDialog() and popups, 335
 winMenuAdd(), 335
 write.table(), 295
 writeClipboard(), 295

R-language, 4

array, 282, 286
 batch mode, 280, 309
 Boolean operators, 285
 box-and-whiskers plot, 302
 conditions, 310
 data frame. *See* Matrix
 difference from matrix,
 281, 286
 direct mode, 280
 documentation, 278
 export graphics, 308
 factor, 281, 292
 exercise, 20, 21, 23
 frequency table, 293

- frequency table (incl. *Exercise*), 23
 - function, 282
 - anonymous, 313
 - arguments, 311
 - user-defined, 311
 - graphics, 295
 - graphical parameters, 298
 - high-level, 296
 - low-level, 297
 - histogram, 303
 - installation, 277, 315
 - list, 281, 290
 - load data, 11, 287, 293
 - logical operators, 285
 - loop alternatives. *See* Vectorization
 - loops, 310
 - matrix, 281, 287
 - operations, 287
 - subsetting, 289
 - missing values, 11, 286
 - numerical functions, 284
 - object, 282, 296
 - attributes, 282
 - coercing, 291
 - packages, 332
 - plot, 295
 - annotation, 297, 306
 - creating, 296
 - customization, 305
 - exercise*, 27
 - export, 308
 - interactive functions, 308
 - linear fit, 299
 - parameters, 298
 - save data, 295
 - scripts. *See* Batch mode
 - start Console, 277
 - syntactic rules, 279
 - table-like objects, 286
 - variable assignment, 280
 - vector, 282
 - assignment, 282
 - character, 284
 - logical, 285
 - named, 283
 - regular sequence, 283
 - subsetting, 289
 - substring, 285
 - vectorization, 282, 284, 293, 313
 - working directory, 294
- S**
- Saint-Malo Massif, 261
 - Saturation temperature, 136
 - exercise*, 150
 - Solubility. *See* Accessory minerals
 - Spiderplots, 36
 - exercise*, 38
- T**
- Ternary plot (incl. *Exercise*), 32
 - Trace elements, 67, 101
- V**
- Visualization of data
 - projection, 225
- Z**
- Zircon, 129, 232
 - exercise*, 150